ADVANCED TRANSDUCER TECHNOLOGIES FOR ELECTRICAL CONNECTIONS IN MICROELECTRONIC PACKAGING

SUBMITTED BY

LI HING LEUNG

A THESIS SUBMITTED IN PARTIAL FULFILMENT OF THE REQUIREMENTS FOR THE DEGREE OF DOCTOR OF PHILOSOPHY

AT

DEPARTMENT OF APPLIED PHYSICS

THE HONG KONG POLYTECHNIC UNIVERSITY

JUNE, 2004

Certificate of Originality

I hereby declare that this thesis is my own work and that, to the best of my knowledge and belief, it reproduces no material previously published or written nor material which has been accepted for the award of any other degree or diploma, except where due acknowledgement has been made in the text.

_____ (Signed)

LI Hing Leung (Name of student)

ABSTRACT

Advanced transducer technologies have been developed for making electrical connections in microelectronic packaging industry. This work has focussed on chip level interconnection techniques including wire bonding and thermosonic flip chip bondings. The new transducer designs and technologies developed include:

I) 1-3 Piezocomposite Transducers

Lead zirconate titanate (PZT)/epoxy 1-3 composite rings were used to replace the conventional full PZT rings as the driving elements in wire bonding transducers. The vibration characteristics of 1-3 composite rings were studied and compared to a full PZT ring. The unique feature of suppressing planar resonance modes makes the 1-3 composite rings an attractive alternative to conventional PZT rings. The volume fraction of the 1-3 composite rings was optimized by a finite element method (FEM). Wire bonding transducers were fabricated and characterized. The dynamic behaviours of the transducers were also analyzed by FEM. The 1-3 transducer offers advantages such as purer axial resonance, lower mechanical quality factor and suppression of spurious modes. The composite transducer was installed on a commercial wire bonder for process study. The composite transducer was found to have wider operation windows (>50%) and finer pitch bondings (<10%). In addition, the composite transducer offered a much more consistent bonding results than a conventional PZT transducer.

II) Thermosonic Flip Chip Transducers

Transducers were designed using both the longitudinal and transverse approaches in thermosonic flip chip bonding. The dynamic behaviours of the transducers were modelled

by FEM. Process study was conducted on the two approaches and the bonding defects of both longitudinal and transverse bondings were linked up with the transducer characteristics. It was found that the transverse approach was less susceptible to silicon cratering due to the lower stress induced during bonding. However, due to the insufficient transducer rigidity, it gave rise to more serious chip tilting defect. Both FEM and experimental findings agreed well with this argument. A novel push-pull transducer concept, with multi-support and driving, was proposed to overcome the shortcomings of both longitudinal and transverse transducers. It was found that the new transducer offers superior ultrasonic properties. The novel transducer design has high rigidity to maintain ideal bonding co-planarity for high pin count devices. The transverse vibration can also minimize the silicon cratering. The new transducer concept has been adopted in a commercial flip chip bonder.

III) Multi-frequency Transducers

Methodologies for designing the multi-frequency transducer were demonstrated. The nodal position matching method helps to identify the multi-frequency feature of a conventional transducer. A case study based on a commercial transducer was demonstrated. A new transducer design concept based on balanced wavelength has been developed. The novel design offers advantages of fine pitch bonding using higher frequency (>120 kHz) and robust bonding using a lower frequency (60 kHz). The special structure could allow the transducer to work in its fundamental mode as well as its second harmonics. Both FEM and experimental results showed that the transducer provided good ultrasonic properties at more than one frequencies.

LIST OF PUBLICATIONS

PATENTS:

1. Hing Leung Li, Helen Lai Wa Chan, Kelvin Ming Wai Ng and Peter Choi Kee Liu, "Ultrasonic Transducer", *U.S. Patent*, Filing No: US2004035912, Feb 2004.
2. Jin Hua Hu, Hing Leung LI, Helen Lai Wa Chan, Chung Loong Choy, "Ring-shaped Piezoelectric Transformer Having an Inner and Outer Electrode", *U.S. Patent*, US659104, July 2003

REFERRED TECHNICAL JOURNALS:

1. H.L. Li, H.L.W. Chan and C.L. Choy, "Vibration Characteristics of Piezoceramic Rings", *Ferroelectrics*, Vol. 263, pp. 211-216, 2001.
2. P.W.P. Chu, H.L. Li, H.L.W. Chan, K.M.W. Ng and P.C.K. Liu," Smart Ultrasonic Transducer for Wire-bonding Applications", *Materials Chemistry and Physics*, Vol 75, pp. 95-100, 2002.
3. J.H. Hu, H.L. Li, H.L.W. Chan and C. L. Choy, "A Ring-shaped Piezoelectric Transformer Operating in the Third Symmetric Extensional Vibration Mode", *Sensors and Actuators A*, Vol. 88, pp. 79-86, 2001
4. C.P. Chong, H.L. Li, H.L.W. Chan and P.C.K. Liu, "Study of 1-3 Composite Transducer for Ultrasonic Wirebonding Application", *Ceramics International*, Vol. 30 , pp. 1141-1146, 2004.

5. H.L. Li, C.P. Chong, H.L.W. Chan and P.C.K. Liu, "Finite Element Analysis on 1-3 Piezocomposite Rings for Ultrasonic Transducer Applications", *Ceramics International*, Vol. 30, pp. 1827-1830, 2004.
6. H.L. Li, J.H. Hu and H.L.W. Chan, "Finite Element Analysis on Piezoelectric Ring Transformer", *IEEE Transcations on Ultrasonics, Ferroelectrics, and Freqeuncy Control*, October, 2004.

INTERNATIONAL CONFERENCE PROCEEDINGS:

1. H.L. Li, J.H. Hu and H.L.W. Chan, "Finite Element Analysis on Piezoelectric Ring Transformer", *Proceeding of IEEE Ultrasonics Symposium,* Munich, Germany, Vol 2. pp. 1177-1180, 2002.
2. H. L. Li, H.L.W. Chan, P.C.K. Liu, "Comparison of Bonding Defects for Longitudinal and Transverse Thermosonic Flip-chip", 5th Conference on Electronics Packaging Technology, Singapore, pp. 350-355, 2003.

ACKNOWLEGEMENTS

I would like to express my deepest gratitude to Prof. Helen Lai Wa Chan, my academic supervisor at the Hong Kong Polytechnic University. During the course of my study, Prof. Chan has given me valuable advice and encouragement. Without her kind support and guidance, this work would not have been possible.

I would also like to extend my appreciation to Dr. Peter Chou-Kee Liu, the Chief Technical Officer of ASM Assembly Automation Ltd., who gives me the golden opportunity to devote myself to the packaging industry.

Special thanks are also given to my research colleagues from the ITF project, UIM/29 and the former PZT research team in ASM Assembly Automation Ltd including Dr. Ming-Wai Ng, Mr. Man-Chiu Cheung, Mr. Wai-Yin Ng, Mr. Ching-Hong Yiu, Mr. Chi-Po Chong, Mr. Kwan-Wai Tang, Mr. Wing-Po Chu, Dr. Chun-Hua Xu and Dr. Jun-Hui Hu for all their valuable advices, discussions and ideas.

Thanks are also due to my colleagues in ASM from the Process and Packaging Technology Group including Mr. Charles Pang , Miss Eylen Chung and Dr. Kin-Yik Hung. They have given me valuable supports particularly on the thermosonic flip chip project.

Last but not the least, thanks to my family for their understanding, constant support, and encouragement during the years of my studies.

TABLE OF CONTENTS

LIST OF FIGURE CAPTIONS

LIST OF TABLE CAPTIONS

CHAPTER ONE

INTRODUCTION

1.1 Chip-Level Packaging

Electronic packaging of integrated circuits (ICs) has the ability to establish electrical interconnections for the silicon chips to maintain a suitable operation environment, such that the ICs can function effectively and efficiently. Depending on the manufacturing sequences, electronic packaging can be divided into four interconnection levels. Fig. 1.1 is a schematic diagram showing the hierarchy of electronic packaging [1]. The fundamental or zero-level is the interconnection between different electronic elements such as transistors, resistors, capacitors etc., on the same chip without any packaging. The size of those components is usually in a sub-micron level and this microelectronic circuit is called a “bare die” or “bare chip”. The first level packaging involves mounting, bonding and encapsulating a single or multi-chips to produce an IC chip. Putting the IC modules into a printed circuit board (PCB) will be classified as the second level package. Finally, the third level package is the integration of IC chips into a circuit card or motherboard. As the first level packaging involves the connection between chips and substrates, it is also referred to as chip-level packaging. A typical electronic IC package in chip-level provides four major functions:

1) Provide electrical paths for supplying power to the IC.

2) Provide electrical paths for signal communication.

3) Provide paths for heat dissipation.

4) Provide mechanical supports and protections for the IC.

With the trend of minimization of electronic devices such as mobile phones, the need for smaller and higher density package designs has made the packaging technologies a great challenge for scientists and engineers. Many packaging techniques have been proposed in the past several decades. Nowadays, wire bonding and flip chip assembly are the principal methods of chip-level interconnections in microelectronic packaging industry.

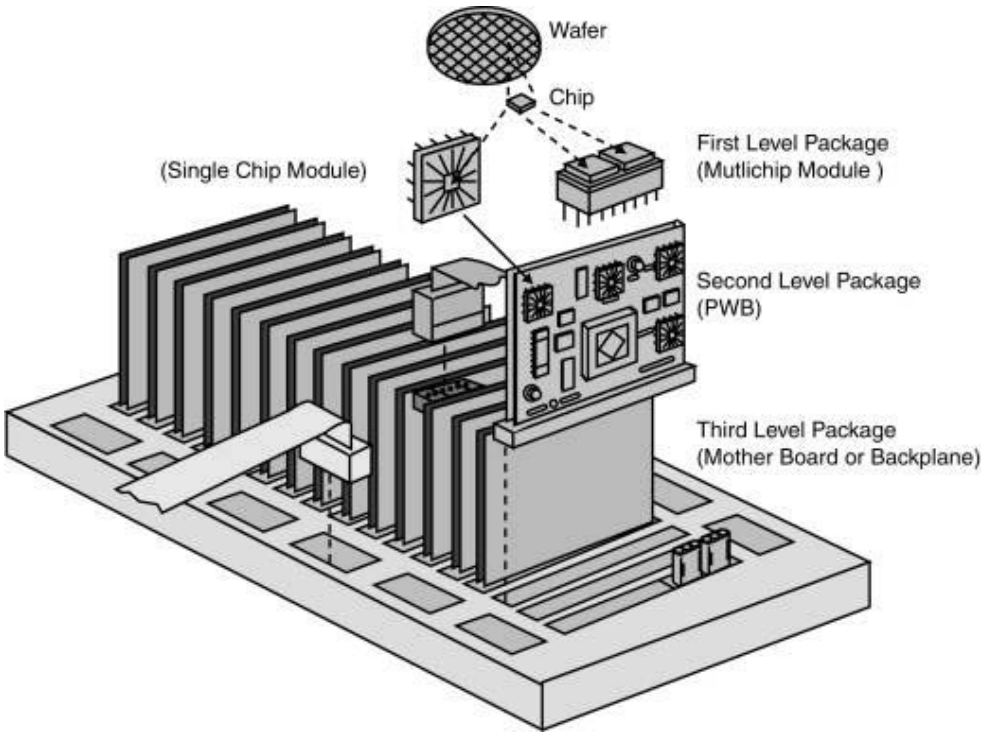

Fig. 1.1 The hierarchy of electronic packaging. [1]

1.1.1 Wire Bonding Assembly

Wire bonding was first developed and proposed by Bell Laboratories in 1957 using the thermocompression method [2]. The improvement obtained by introducing the ultrasonic energy in 1970 had made the wire bonding a considerable successful process [3]. Up to now, wire bonding is still the most dominant interconnection method although other new packaging techniques have been continuously proposed. Wire bonding is the connection of fine metal wires between the IC chip and substrate to provide an electrical connection path. Not all metallurgical combinations can be ultrasonically bonded. Among all the combinations, aluminum to aluminum, gold to gold and aluminum to gold are the most common combinations. Depending on the presence of external heat source, wire bonding can be classified into ultrasonic (US) and thermosonic (TS) bondings [4]. For ultrasonic wire bonding, which is usually performed on aluminum (Al) wire, the bonding tool is a metal (e.g. tungsten) carbide wedge. With the ultrasonic vibration (typically at 60 kHz) of the wedge and a compressive pressure, an intermetallic layer can be formed between the Al wire and the gold layer of the substrate at room temperature. This cold US bonding is also referred to as wedge bonding. When a gold wire (99.9% purity) is to be bonded, an elevated temperature is necessary. Therefore, the bonding is known as thermosonic in the presence of heat. Unlike the wedge bonding, the bonding tool for the thermosonic bonding, called the capillary, is made by ceramic (aluminum oxide). The gold wire is first melted by a high voltage electrical sparking to form a spherical shape. The “ball” is then pressed against the bonding substrate which has been pre-heated to an elevated temperature around 150 to 200 ^{o}C. After applying the ultrasonic energy to the “ball”, a bonding can be formed. Due to the fact that the wire has to be melted to a ball shape before bonding, this technique earns its name as ball bonding. The two types of wire bonding are shown in Fig. 1.2 and Fig. 1.3.

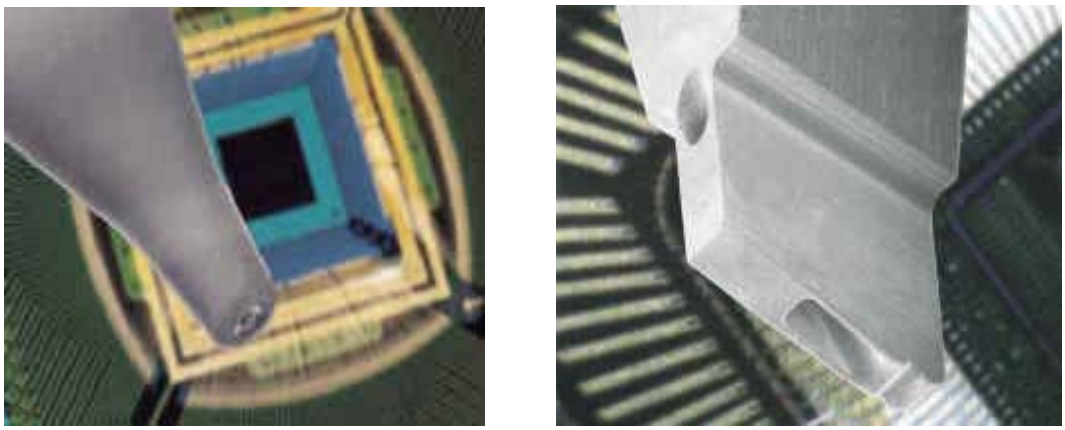

(a) (b)

Fig. 1.2 The bonding tool for (a) ball bonding [5] and (b) wedge bonding. [6]

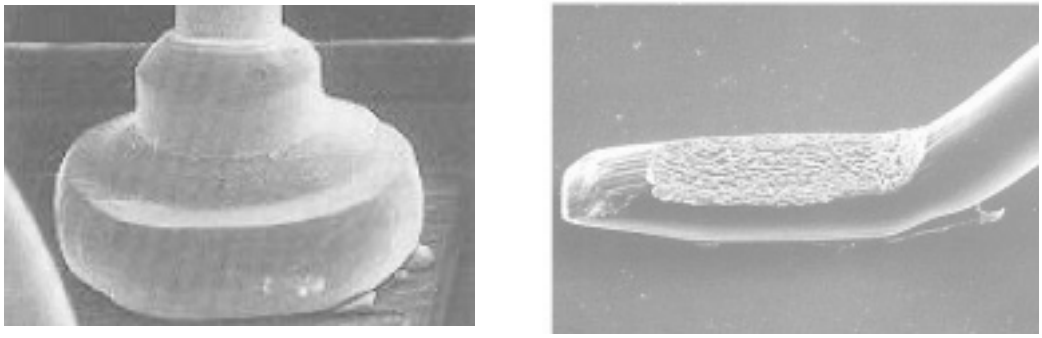

(a) (b)

Fig. 1.3 Two basic forms of wire bond (a) ball and (b) wedge bond. [7]

1.1.2 Flip Chip Bonding Assembly

Flip chip assembly is the direct electrical connection of face-down electronic ICs or chips onto substrates or PCB by means of conductive bumps on the bond pads of the chip [8, 9]. The conductive bumps will serve both as signal and energy interconnection paths as well as supporting elements. Unlike wire bonding, it uses face-up chips with a wire connection to each pad. In addition, the bonded wires will not provide mechanical supports for the chips. As flip chip is a face-down attachment, the chip has to be "flipped" before the

bonding. The flipping mechanism gives this technique the name “flip chip bonding”. The flip chip bonding was first introduced by IBM in the early sixties for their mainframe computers [10]. Since then, the flip chip technique has attracted worldwide attention and started to bloom as one of the major chip scale package methods up to now.

Various flip chip bonding techniques have been proposed and are spreading rapidly. Fig. 1.4 shows the various connection methods for flip chip bondings [11]. It can be divided into two major categories: metal bonding and adhesive contact. In all the techniques using adhesives, such as anisotropic conductive film/paste (ACF/ACP), eustenic solder bump connection (ESC), non-conductive paste (NCP) and stud bump bonding (SBB), as no real metallic joint is formed, it has to make use of heat-hardened resin to hold the chips and maintain electrical contact between the bumps and pads. However, it takes a long time (around 20 seconds) for the resin epoxy to be completely cured. The long cycling time make this technique not production friendly. Furthermore, the electrical connection by contact may induce more noise when compared to a real metallic bond. The control collapsed chip connection (C4) technique which uses solder bumps is an attractive approach. It allows the chip to be automatically aligned by surface tension during the re-flow stage. In addition, this technique has a high productivity rate and is more reliable. However, the disadvantages are obvious that cleaning is required after bonding and the contamination caused by lead based solder is not environmentally friendly. Ultrasonic flip chip however is a fast and clean process which has been successfully applied to bonding of light emitted diode (LED) and surface acoustic wave (SAW) filter which have small number of inputs and outputs (IOs).

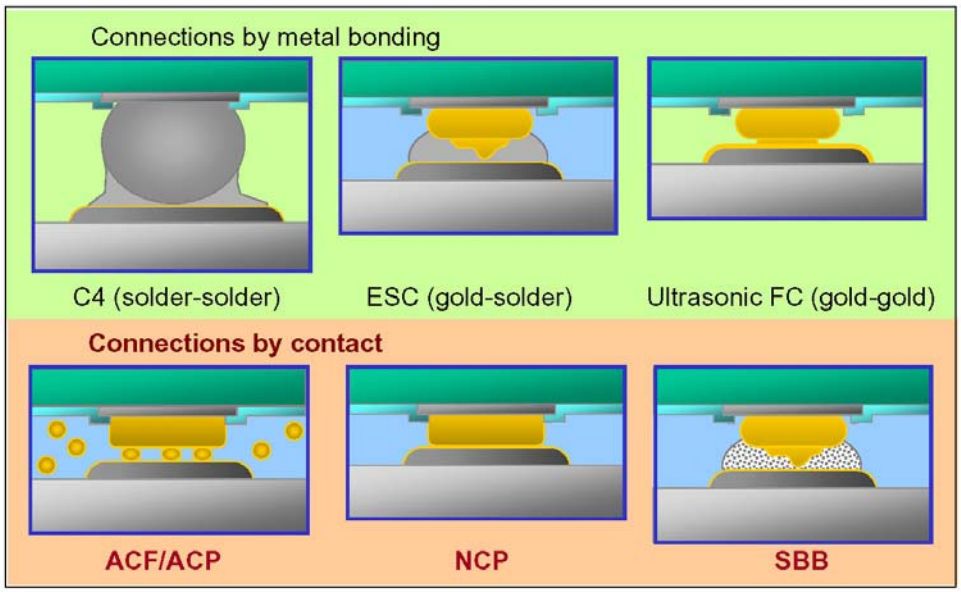

Fig. 1.4 Connection models for flip chip bonding. [11]

1.1.3 Packaging Trends and Challenges

With the great demand on minimization of electronic devices such as cellular phone, IC packages has been driven to become smaller and smaller. In the past twenty years, the package size has been downsized by 10 times from a quad flat package (QFP) to area array flip chip [10]. The IC packaging evolution is shown in Fig. 1.5. The pin-count per chip area has also increased sharply. However, there are also demands for high productivity, low cost, reliable and robust bonding process. The package minimization trend has created great challenges to engineers to further improve the capability of existing machines. Among all the packing techniques, the wire bonding and TS flip chip have similar approaches. Both of them involve true welding by joining the two metallic phases (gold to aluminum or copper to gold) through an intermetallic layer or the same metallic phase (gold to gold or aluminum to aluminum) by material diffusion. In addition, the interconnection of wire or bump is

formed by ultrasonic energy, temperature and pressure. The ultrasonic energy required for the bonding is generated by an ultrasonic transducer which is the heart of the bonder. In order to have a break-through on the current challenges of wire bonding and TS flip chip bonding, it is necessary to find novel transducer designs and technologies. This work is devoted to the development of new transducer technologies to be used in wire bonding and TS flip chip bonding.

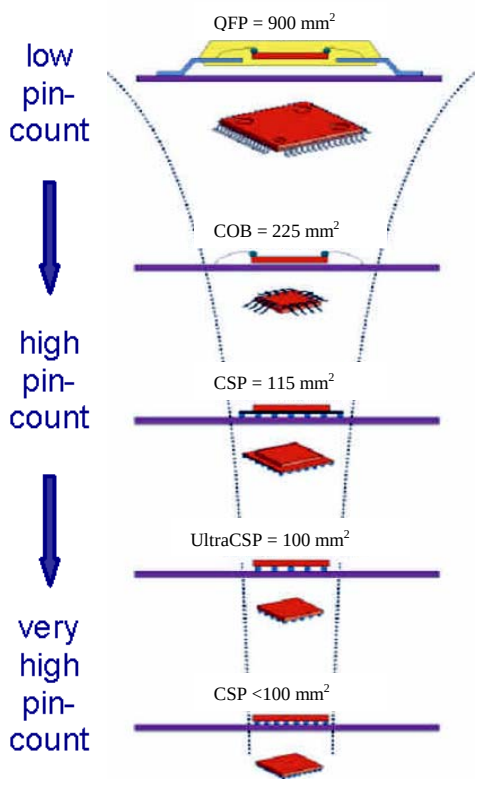

Fig. 1.5 IC packaging evolution. [10]

1.2 Wire Bonding Vs Thermosonic Flip Chip Bonding

The ultrasonic transducer is the most critical component in a wire bonder and a TS flip chip bonder. Performance of the ultrasonic transducer has a major and direct impact on the bonding quality. To understand how the ultrasonic transducer functions in the bonding

system, the process cycle of wire bonding and TS flip chip bondings will be briefly described here.

1.2.1 Wire Bonding Cycle

To understand the role of an ultrasonic transducer during the wire bonding, the process cycle of a ball bonding will be briefly described. Fig. 1.6 shows typical procedures for making a ball bonding wire interconnection with a capillary tool.

1. The gold wire is fed through the hollow capillary and the protruded wire is melted by the electronic flame-off (EFO) sparking. The melted gold wire forms a ball at the capillary tip.
2. The capillary is moved by the wire bonder to the centre of the bond pad and the wire clamp is opened to release the tension force in the wire.
3. The capillary is pressed against the bond pad. Bonding occurs through a combination of plastic deformation and interfacial slipping action between the two materials under the action of pressure, ultrasonic energy and temperature.
4. After the ball is bonded to the chip, the capillary rises and moves to the second target bond pad. The geometry of the wire is controlled by the mechanical motion or the looping.
5. At the second targeted position, the capillary is lowered again to form a bonding under the interaction of pressure, temperature and ultrasonic energy. The capillary deformed the wire against the substrate producing a wedge-shaped impression with a gradual smooth transition of the wire. Therefore, it is known as a stitch bond (second bond) at the substrate.

6. A certain amount of tail bond is left to allow pulling of the wire out of the capillary in preparation of EFO spark for the next bonding cycle.

A wedge bonding cycle is similar to that of a ball bonding except that the capillary is replaced by a wedge. Furthermore, no EFO sparking is required for wedge bonding on Al wires. Fig. 1.7 shows the wire connection for both ball and wedge bonding after the process cycles.

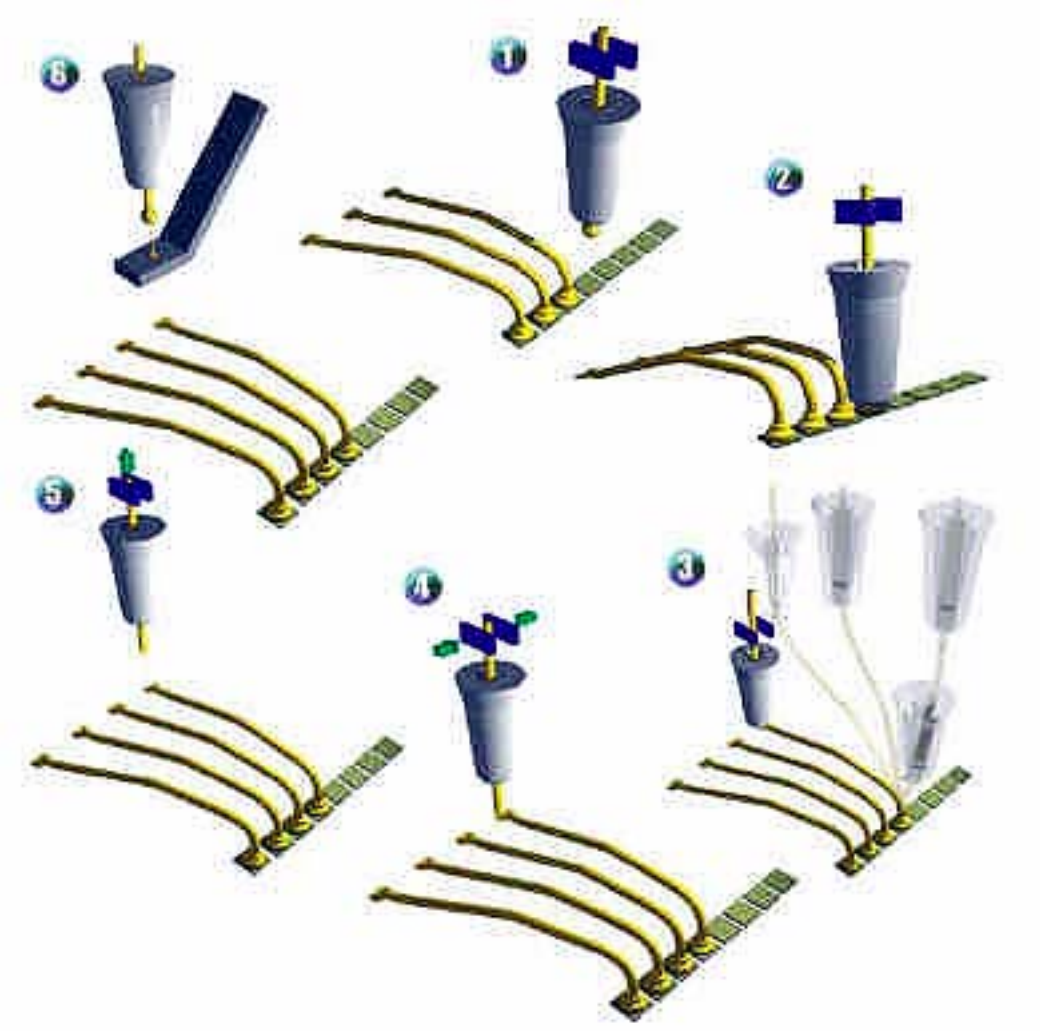

Fig. 1.6 A ball bonding process cycle. [12]

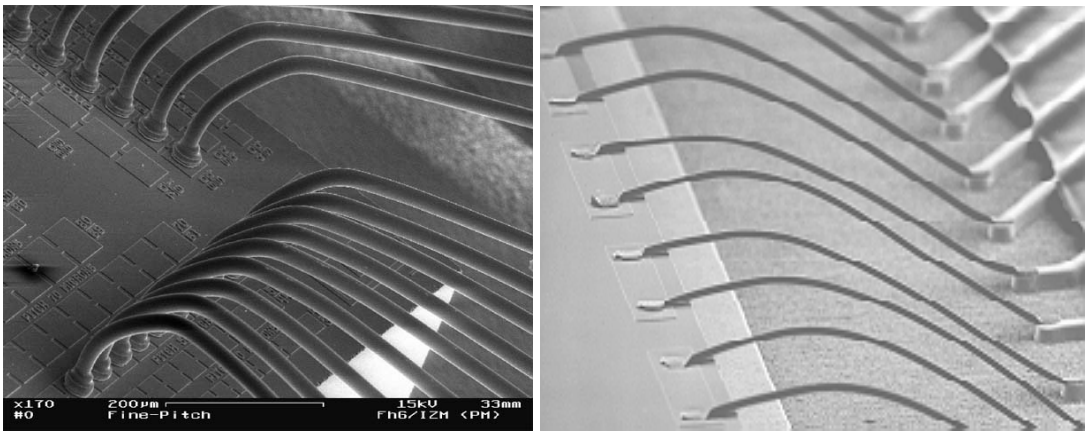

(a) (b)

Fig. 1.7 SEM micrograph of (a) ball bonding and (b) wedge bonding.

1.2.2 Thermosonic Flip Chip Bonding Cycles

When comparing with a wire bonding process, the TS flip chip involves fewer steps as there is no looping requirement. Fig. 1.8 shows typical steps for a TS flip chip bonding process cycle.

1. Bump Bonding

The bump bonding is very similar to a ball bonding process except that no loop will be formed after the gold bump bonding. After the stud bump is formed, the wire will be torn off by the action of the wire clamp immediately. A short tail will be left at the end of the bump after bonding. Fig. 1.9 shows a die with eight gold stud bumps on the periphery.

2. Flip Chip

After the chip has been bumped, the chip will be picked up by a vacuum arm at the upper surface where the bumps were located. The chip will then be flipped upside down and

picked up again by the collet of the flip chip transducer by vacuum suction at the back of the chip. After this flipping process, the chip will be held at the collet tip with the gold bumps facing down. The transducer will then move to a position of the target substrate and the chip will be properly aligned with the bond pads below.

3. Chip Bonding

The transducer will be moved downward until the bumps are in touch with the bond pads. The substrate is pre-heated to an evaluated temperature at around 150 °C. The transducer will be moved further downward to apply the required compressive loading and fired to induce the ultrasonic vibration. The chip bonding can be completed under the action of pressure, ultrasonic energy and temperature.

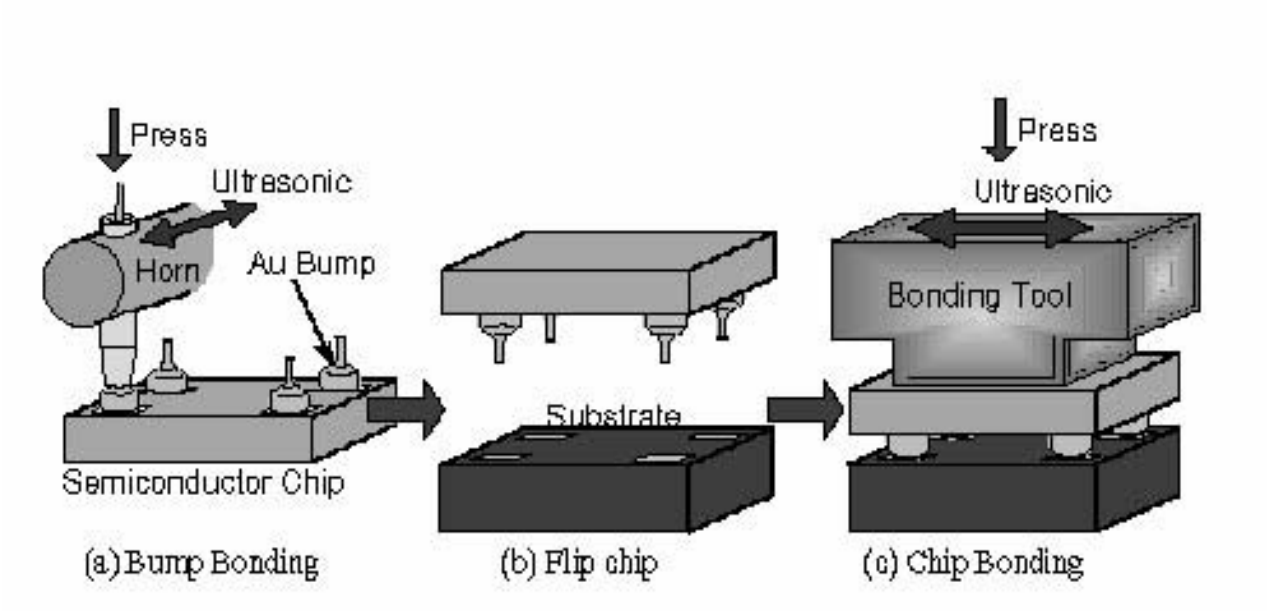

Fig. 1.8 A thermosonic flip chip bonding cycle. [13]

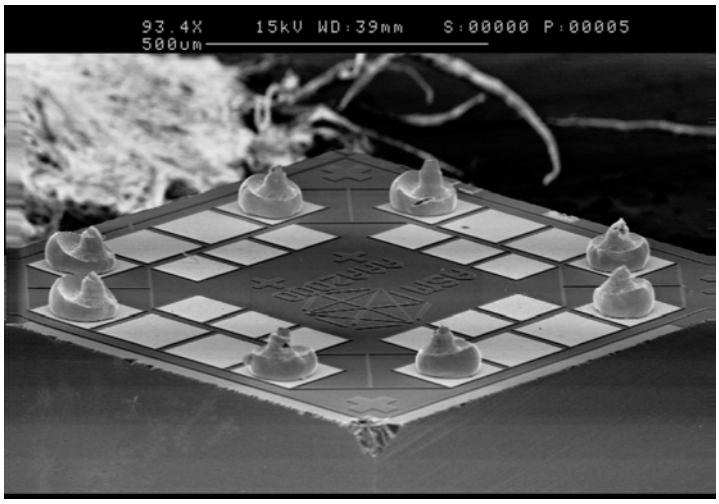

Fig. 1.9 A chip with eight gold stud bumps.

1.3 Ultrasonic Transducers

The ultrasonic transducer is the heart of a wire bonding or a thermosonic flip chip machine. The ultrasonic transducer and the bonding tool together form a mechanical resonant structure. The operation frequency is determined by the dimensions of the ultrasonic transducer and the bonding tool. For most ultrasonic or thermosonic bonding system, the operation frequency is around 60 kHz. It has been reported that higher frequency gives better bondability and lower temperature for thermosonic bonding [14]. However, the drawback for high frequency bonding is that the bonding is much more susceptible to other environmental effects such as material variations. In addition, the high frequency bonding gives narrower process window. The ultrasonic transducer serves two main functions for the bonder machine. First, it converts and transmits the ultrasonic energy in the form of ultrasonic vibration to the bonding specimen through the bonding tool. Second, it applies a bond force to produce an optimized compressive pressure to facilitate

the bonding process. Therefore, an improper design of transducer could lead to unstable ultrasonic vibration and uneven bond force in the bonding system. It is essential to understand the structure and basic design requirements of the ultrasonic transducer in order to obtain high quality bondings.

The ultrasonic transducer consists of three main parts: an ultrasonic driver, an ultrasonic horn and a bonding tool. Fig. 1.10 shows the basic structure of a conventional transducer. The ultrasonic driver is a Langevin-type transducer which has pairs of piezoceramic rings (lead zirconate titante (PZT)) sandwiched by two metal components [15]. The PZT rings are pre-stressed by means of bolt-clamping through a central screw. The PZT is connected electrically in parallel and mechanically in series with thin copper electrodes inserted between each interface. The driver is operating at its fundamental resonance with the total physical length equal to the half wavelength of its resonance mode. Adjoined to the ultrasonic driver is an ultrasonic horn. It usually has a tapered shape with its larger area attached to the driver and tip as the free end. The common shapes for an ultrasonic horn are conical, step and exponential [16]. The geometry of the horn allows it to act as a mechanical amplifier for the ultrasonic vibration such that maximum vibration amplitude occurs at the free end of the horn. A mounting structure usually in form of a flange or a barrel is attached to the horn at its axial vibration nodal position. At the nodal point, the excitation of the mounting structure will be minimized and hence it allows the transducer to be mounted on the bonder machine without disturbing the transducer resonance. Fig.1.11 shows the axial vibration profile of the transducer which indicates the position of PZT stack and the nodal position for the mounting barrel. The bonding tool is located at the maximum vibration location of the horn, usually at the horn tip. The bonding tool is called a wedge and a capillary for wedge bonding and ball bonding system, respectively (Fig. 1.12). For

thermosonic flip chip application, the bonding tool is usually called the collet. Similar to the ultrasonic horn, the bonding tool usually has a fine tip to further amplify the vibration amplitude. Hence, the ultrasonic vibration generated by the driver is amplified and transmitted axially through the horn. This amplified vibration is then transmitted to the horn tip and results in an oscillatory flexural force essentially parallel to the bonding specimens. The flexural vibration, together with the bond force and temperature, form the ultrasonic bond between the wire and the chip.

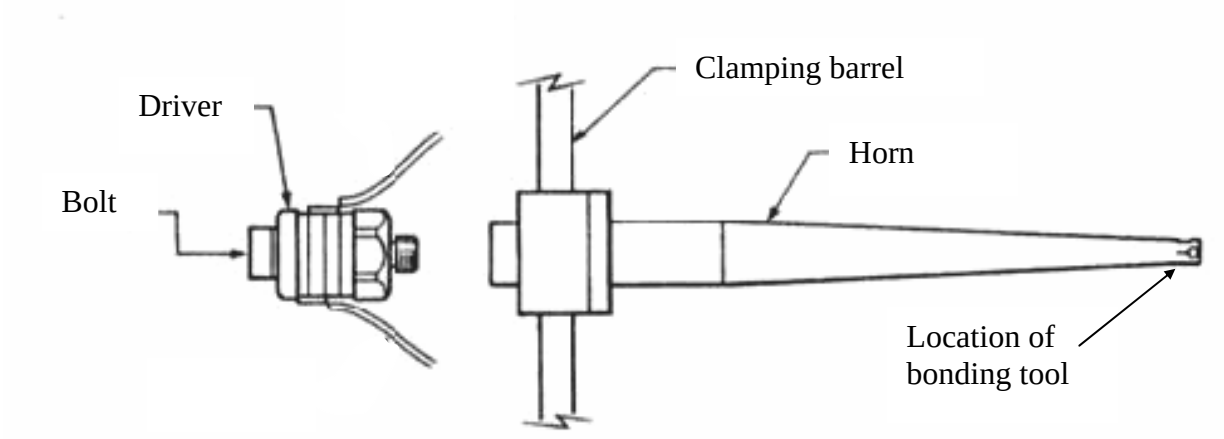

Fig. 1.10. Basic structure of an ultrasonic transducer.

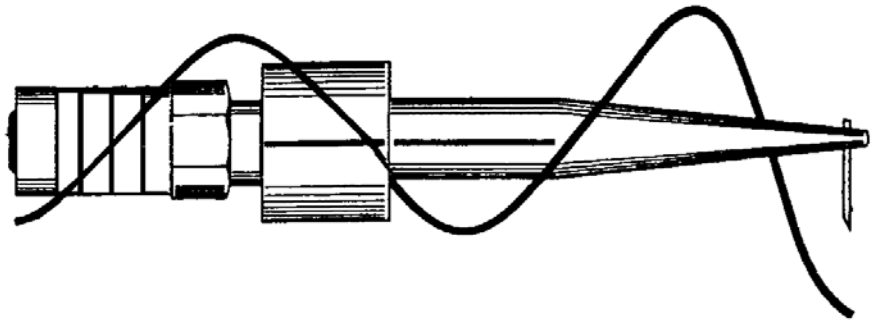

Fig. 1.11 Axial vibration profile of the ultrasonic transducer.

Fig. 1.12 Commercial ultrasonic wire bonding transducers.

1.4 Advanced Transducer Technologies and Designs

In this work, several advanced transducer technologies and designs are proposed and developed. The transducers are mainly designed for the application of wire bonding and thermosonic flip chip bonding. The novel transducer designs are targeted to cope with the challenges ahead in chip-level packaging.

1.4.1 1-3 Composite Transducer

Conventional transducers for ultrasonic wire bonding usually make use of piezoceramics ring (lead zirconate titanate or PZT) as the driving elements [16-19]. Although PZT ring has been used for many years in wire bonding transducers, it is not problem-free. Some critical issues of the conventional PZT transducer are given as follows:

1. Spurious Resonances

The transducer is designed to work at a pre-determined axial resonant mode at a frequency around 60 kHz. However, due to the long and slim structure of the transducer, other high order flexural, torsional or complex modes can also be excited by the strong radial or planar coupling of PZT ring. These unwanted resonances may appear closed or even coupled to the working axial mode and will disturb the ultrasonic energy distribution of the transducer which leads to an unstable bonding.

2. High Mechanical Quality Factor (Q_m)

The mechanical quality factor Q_m is a dimensionless factor that represents the mechanical loss of the transducer. To have a good transducer characteristics such as thermal stability, hard PZT rings with high Q_m (>1500) are usually used in the transducer. The ultimate transducer will then have a high Q_m (~1000) as well. The drawback is that the transducer exhibits a very sharp resonance with narrow bandwidth. Under such a high Q_m operation, the transducer will be very sensitive to external loading. Therefore, it will reduce the robustness of the transducer and result in a smaller process window. In addition, the control system for a high Q_m transducer will be much more demanding.

3. Higher Harmonics Mode Coupling

Due to the strong coupling of PZT rings, higher order harmonics of the operation mode can be excited simultaneously. These higher frequency harmonic modes may couple to other complex modes at high frequency that results in a non-pure excitation. It will not only reduce the bonding energy, but also distort the pure axial vibration loci of the bonding tool.

The non-axial (flexural) vibration of the bonding tool can lead to an increase in bond width which makes it difficult to achieve fine pitch bondings.

In view of the above-mentioned issues, the concept of 1-3 composite transducer has been proposed. The conventional PZT material has been replaced by 1-3 piezocomposite rings [20-22]. The 1-3 composite rings are prepared by a dice-and-filled technique with ultra-high PZT volume fraction (> 0.9). Fig. 1.13 shows the 1-3 piezoceramic composites fabricated by the dice-and-filled method. The 1-3 composite rings are studied and optimized by a finite element method (FEM). The composite transducer with 62 kHz has found to have fewer spurious resonances and a purer axial mode. The composite transducer is installed in a commercial wire bonder for intensive process study. The unique feature of the composite transducer leads to a wider operation window, more robust bonding with a finer pitch bonding.

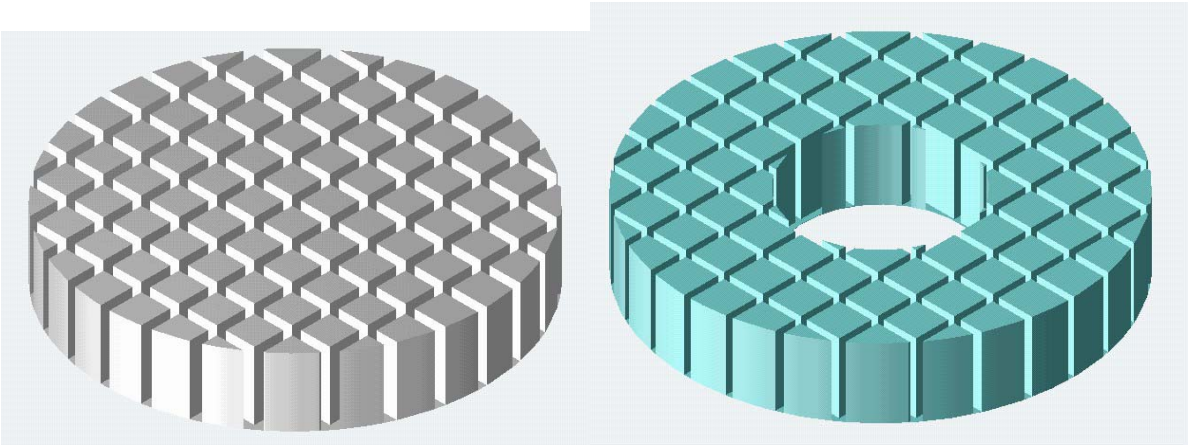

Fig. 1.13 1-3 piezoceramic composite fabricated by the dice-and-filled method.

1.4.2 Thermosonic Flip Chip Transducer

The thermosonic flip chip bonding is a relatively new technique that attracts considerable attention recently. Although flip chip technology using soldering is the dominant process nowadays, the soldering flip chip is not compatible with the conventional wire bonding process. This greatly increases the investment cost on flip chip technology. Therefore, the introduction of ultrasonic energy to flip chip bonding provides an attractive alternative. The new thermosonic flip chip bonding offers several advantages such as simple, clean and lower temperature when compared with thermocompression bonding. Not only it is compatible with the wire bonding process, the elimination of the solder reflow process also makes the thermosonic flip chip technique highly efficient and cost effective. Similar to wire bonding, ultrasonic vibrational energy generated by a piezoelectric transducer is transmitted to the chip through a collet. Together with a compressive force, an intermetallic layer can be formed or material diffusion can happen between the gold bumps and the substrate at an elevated temperature. The thermosonic flip chip bonding involves a lot of gold bumps to be bonded at the same time. Therefore, the transducer used in the TS flip chip transducer must satisfy two basic requirements:

1. Large Vibration Amplitude Output

To facilitate a number of gold bumps to be bonded in a single process, the vibration amplitude of the transducer must be large to deliver enough ultrasonic energy. Although large vibration amplitude can be obtained by increasing the driving power, the excess power may heat up the transducer and reduce the stability of bonding. In the worse case, the heat generated can be high enough to de-pole the PZT ring in the transducer. Therefore, the TS

flip chip transducer should be carefully design to maximize the amplification ratio of the bonding tool.

2. High Rigidity Against Loading

For high IO device, not only a high ultrasonic energy is required, a compressive bond force is also needed. The bond force for a 30 bumps chip can be as high as 3 kg which is around 20 times that of a wire bonding process. The high bond force will deform the transducer and create the bonding planarity problem. A poor co-planarity will lead to non-uniform bondings among the gold bumps. The difference in stand-off height of the bonded gold bumps will lead to the chip tilting problem.

Depending on the direction of the collet vibration, thermosonic flip chip can be divided into transverse and longitudinal modes (Fig. 1.14). In the transverse mode, the collect vibrates in-plane with the chip. However, the collet is moving out-of-plane in the longitudinal bonding. *Tan et al* has successfully demonstrated the flip chip bonding using the longitudinal mode [23]. However, there is lack of researches to compare and explain the difference between the two modes of flip chip bonding. In this work, an attempt has been made to use FEM to analyze the properties of the transducer and stresses generated under ultrasonic vibration and compressive loading. The results have been further verified by experimental data. It provides the evidence that the two different modes may induce different bonding defects : die tilting and silicon cratering in the thermosonic flip chip bonding.

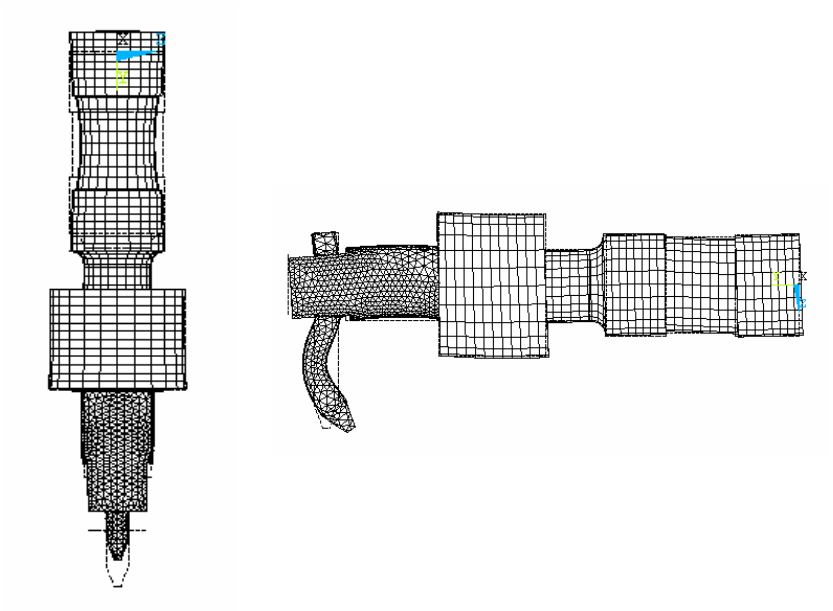

(a) (b)

Fig. 1.14 Thermosonic flip chip transducer for
(a) longitudinal and (b) transverse bonding.

In order to solve the problem encountered by both longitudinal and transverse bondings, a novel transducer concept was proposed for thermosonic TS bonding. As shown in Fig. 1.15, this transducer consists of two sets of driving PZT stacks operated in a push-pull manner. The collet is located in the middle of the transducer and moving with a push-pull motion. The new push-pull transducer has two mounting supports in the middle of the two PZT stacks. In this novel transducer design, the collet tip can retain perfect co-planarity even the transducer is deformed under high load. Due to the push-pull motion of the two PZT stacks, the collet exhibits large vibration amplitude which is twice that of the conventional transducer design. Furthermore, the transverse vibration of the collet makes it less susceptible to silicon cratering when compared with the longitudinal approach. The novel transducer has also been proven experimentally to produce excellent bonding quality.

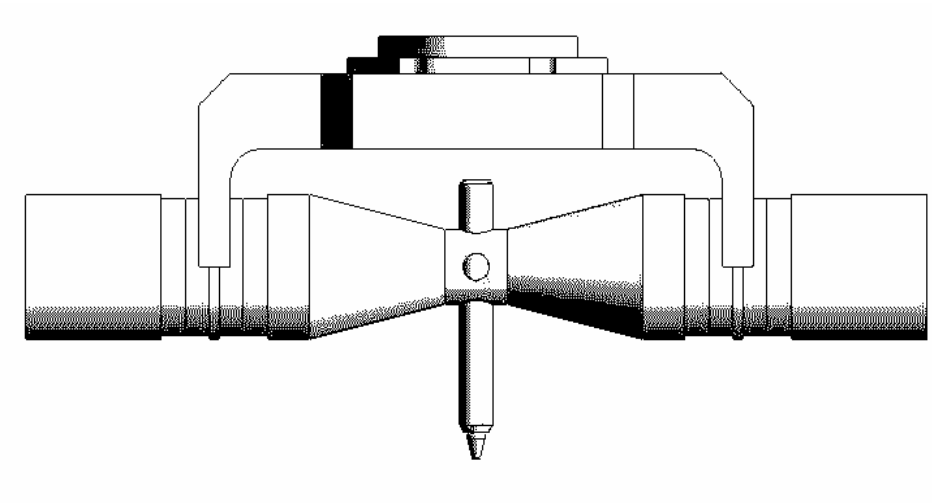

Fig. 1.15 A novel push-pull transducer.

1.4.3 Multi-Frequency Transducer

Most of the conventional wire bonding transducer is operated at around 60 kHz. Higher frequency bonding (above 60 kHz) has recently gained a lot of attention in the microelectronics industry. It offers advantages of fine pitch, shorter bonding time and higher bonding strength [24, 25]. It can also significantly reduce the temperature in thermosonic bonding. However, the use of high frequency system will reduce the operation window of the bonding process. It also requires a very tight material control on the bonding surface to ensure good bondability. The variation of material composition in the bond pad, especially on the substrate, reduces the yields and applications for a high frequency bonding system. Therefore, a multi-frequency wire bonding transducer that can operate at two or more frequencies is highly useful. It allows fine pitch and lower temperature bonding to be made on the die by using high frequency, while a low frequency bonding increases the yield of the bond on the substrate. At its higher harmonic resonance, the transducer can no longer obey the design rules due to the shift of nodal positions. If the mounting position is situated

at a nodal position, substantial ultrasonic energy will be lost from the clamping area. It will result in poor efficiency and stability in bonding. In this study, two methods in designing multi-frequency wire bonding transducer are proposed.

1. Nodal Position Matching Method

As discussed in the previous section, it is important that the mounting structure is located at the axial nodal position of the transducer. Different mode orders will have different nodal positions. However, it is possible for a transducer with two or more axial modes to have a common nodal position for the mounting structure as shown in Fig. 1.16. With this design, the transducer can be free to operate at two or more frequencies without any disturbance by the mounting.

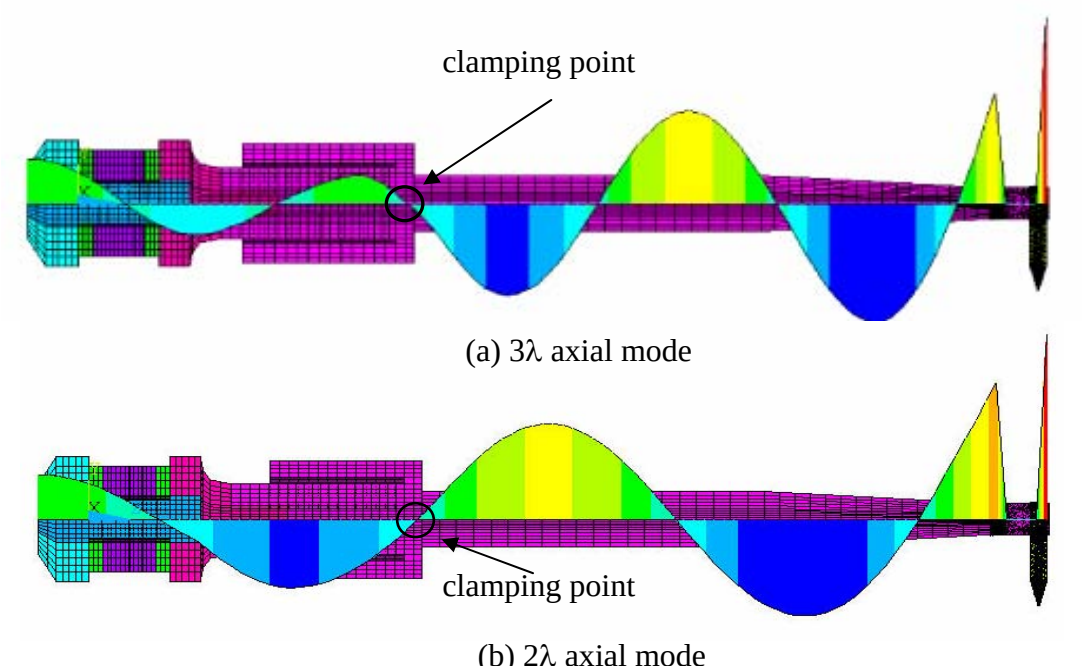

Fig. 1.16 FEM results of a transducer with a common nodal position for mounting at its (a) 3λ axial mode and (b) 2λ axial mode.

2. Balanced Wavelength Design

In the balanced wavelength approach, the driving PZT stacks are located between two metal masses. A mounting flange is located in the middle of the PZT stack. The two metal masses were designed to have similar shape to balance the longitudinal wave profile of the transducer (Fig. 1.17). With such configuration, the transducer can operate at its fundamental resonance having a nodal displacement point at its driving and clamping area. Due to the ultrasonic balance nature, the nodal position will not shift away at its high order harmonic resonance. Therefore, the transducer can operate at two or more frequencies in a wire bonding system.

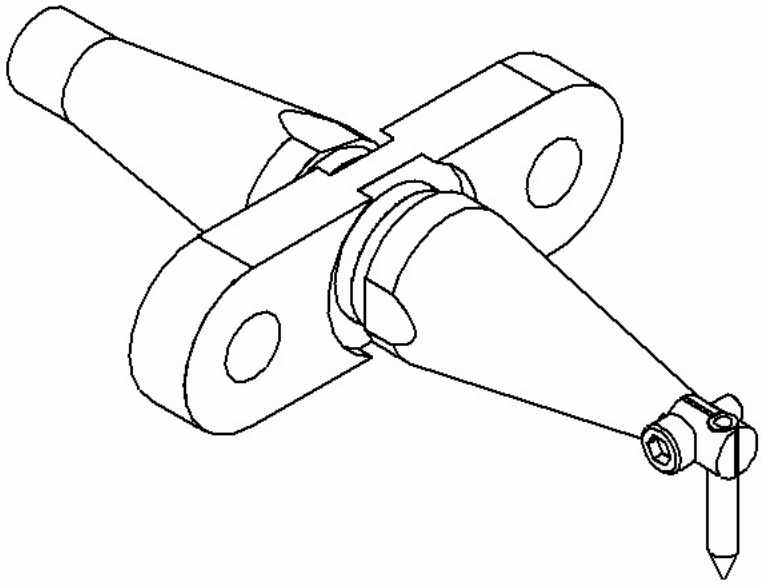

Fig. 1.17 A transducer with the balanced wavelength concept.

1.5 Objectives of Project

This project aims to develop novel transducer designs and cutting-edge technologies to cope with the challenges facing the current wire bonding and thermosonic flip chip bonding assembly. Through studies of these novel transducers, design methodologies and explanations will be provided to the microelectronics package industry which:

1. Facilitate fine pitch, stable and robust bonding through the 1-3 composite technology in the wedge wire bonder.
2. Obtain high performance, high yield and stable bonding through a novel push-pull transducer in the thermosonic flip chip bonder.
3. Exhibit the co-existence of fine pitch and low temperature bonding on die together with high yield and robust bonding on substrate by using multi-frequency transducer in any ultrasonic wire bonder.

1.6 Original Contributions

The present work has made the following original contributions:

1. Optimization guideline to design a 1-3 composite transducer has been given. Experimental verification of 1-3 composite transducer in the application of ultrasonic wedge bonding process. It provides an advanced technology to improve the performance of a wire bonder to achieve a fine pitch, highly reliable and stable bonding, which cannot be possible by a conventional PZT transducer.
2. Assessments on pros and cons for the two major types of thermosonic flip chip transducers: longitudinal and transverse designs. Development of novel push-pull transducer design which can achieve good performance and high yield flip chip bonding without suffering from the shortcomings of either longitudinal or transverse transducer. The new transducer concept has been adopted by a commercial thermosonic flip chip bonder.
3. Methodologies of making multi-frequency transducer were proposed. Multi-frequency transducer with the capability of operating at both high and low frequencies is of great commercial value. Novel transducer design, with the balanced acoustical wavelength concept, has been developed. The transducer prototype shows that it possesses the multi-frequency capability as proven by both FEM and experimental results.

CHAPTER TWO

1-3 PIEZOCOMPOSITE TRANSDUCER

2.1 Literature Reviews

Following the definition of connectivity by *Newnham et al.* [26], a 1-3 composite structure consists of aligned, unidirectional rods or pillars within a 3-dimenional matrix. The definition is based on the fact that there is only one direction of connectivity of rods or pillars that align in the thickness or z-axis (also defined as the 3 axis) along the composite. One typical example as shown in Fig. 1 has active piezoelectric ceramic rods (PZT) or columns embedded in a passive polymer based matrix. The PZT rods are usually in the form of square or circular bars poled in the thickness direction. This type of composite is referred to as 1-3 piezocomposite. The 1-3 piezocomposite offers unique features such as higher transmitting response, lower acoustic impedance, higher sensitivity by its larger electromechanical coupling factor and lower mass over monolithic piezoceramics. These superior properties make the 1-3 piezocomposite being widely used in underwater acoustic devices such as hydrophones [27,28]. Another promising application for 1-3 piezocomposite is as sensing materials in medical ultrasonic transducers [29-31]. By using different piezoceramic volume fraction (ϕ), the transducer can be tailor designed to obtain an acoustic impedance that match

with human tissues. Therefore, the transmission of ultrasonic energy can be maximized without severe reflection due to acoustic impedance mismatch.

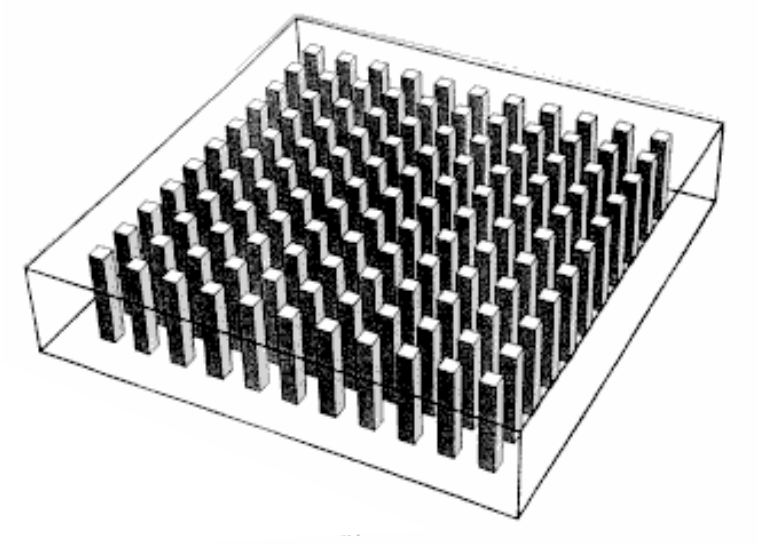

Fig. 2.1 A piezocomposite plate with 1-3 structure [32].

The use of 1-3 composite as sensing elements has been widely reported [33-35]. However, reports on the use of these materials as an actuator are very limited. For the applications of actuators, a very high active ceramic content is essential to retain good actuation performance. *Or et al* has first adopted 1-3 piezocomposite rings as actuating elements in a wire bonding transducer [36]. The 1-3 piezocomposite rings were prepared by a dice-and-filled method with very fine cutting grooves of around 80 μm. By using this technique, composite rings with ϕ greater than 90% can be easily obtained. *Chong et al* has further studied the impact of different ϕ in 1-3 piezocomposite on the performance of wire bonding transducers [37]. The 1-3 transducer offers unique features such as purer axial vibration, reduction in mode coupling and lower mechanical quality factor which gives it a good potential for fine pitch and robust bonding applications. Preliminary bonding results have also shown the fine pitch capability of 1-3 composite transducers. However, there is a lack of a guideline on how to

optimize the 1-3 piezocomposite rings to design the transducer. Most importantly, a detailed process studies on benchmarking the bonding performance of 1-3 composite transducer has not been reported

In this Chapter, guidelines will be given for designing a wire bonding transducer using 1-3 piezocomposite rings and its evaluation will be divided into four major sections.

1. Vibration Characteristics of a PZT Ring

The vibration characteristics of a PZT ring were analyzed by using a finite element method (FEM). The dimensions of the PZT ring were optimized by maximizing the effective electromechanical coupling factor (k_{eff}) of its thickness mode. It helps to obtain the ideal PZT dimensions to maximize the axial excitation of the wire bonding transducer.

2. Optimization of 1-3 Piezocomposite using FEM

The optimized PZT ring was fabricated into 1-3 piezocomposite rings with PZT volume fraction of 0.93 to 0.5 using different number of cuts per direction (cpd) from 5 to 39. Unlike the previous study, the whole 1-3 piezocomposite rings were modelled by FEM. The minimum number of cpd is found such that the composite ring behaves as a homogenous medium. Such findings help to determine the optimized PZT volume fraction to be used for a wire bonding transducer.

3. Characteristics of 1-3 Composite Transducer

A 64 kHz transducer using the optimized 1-3 composite rings were fabricated and studied. The vibration characteristics were also predicted by FEM. The unique features for the 1-3

composite transducer which include less mode coupling and spurious resonances, purer axial excitation and broader bandwidth (lower mechanical quality factor) were characterized.

4. Bonding Process Benchmarking

The 1-3 composite transducer was installed in a commercial wire bonding machine manufactured by ASM. The process windows, fine pitch capability, shear and pull force, heel crack and robustness were compared to that of a convectional PZT ceramic transducer. It gives evidence and correlations between the unique features of 1-3 composite transducer which reveals the advantages during actual bonding.

2.2 Vibration Characteristics of A PZT Ring

Lead zirconate titanate (PZT) rings are widely used in ultrasonic and acoustic applications especially in bolt-clamped Langevin sandwich transducers. The sandwich type driver is the heart of an ultrasonic wire bonding transducer. In the literature, reports on the vibration characteristics of PZT rings are not extensive. In addition, the dynamic characteristics of a ring are very different from that of a solid disc with the same thickness and radius. Therefore, a complete and accurate model of a PZT ring would be very useful in the transducer design. However, several analytical models proposed in the past were based on the assumption that the ring has its thickness (R_t) [38] or wall thickness (W_t) [39] much smaller than the other dimensions. However, at resonances, the ring is vibrated in all three dimensions. Analytical models derived from one-dimensional equations sometimes may not able to predict the dynamic behaviours of a PZT ring with good accuracy. When the ring with R_t approaches to

W_t, the analytical model will no longer be useful. In this section, a commercial FEM code (ANSYS) will be used to analyze the vibration characteristics of a PZT ring of 12.7 mm in diameter. The vibration modes at various resonances are computed and compared with laser vibrometer measurements. The effects of R_t and W_t on the resonance frequencies (F_r) and effective electromechanical coupling factor (k_{eff}) are predicted in order to optimize the dimensions of rings in transducer design.

2.2.1 Vibration Modes of A PZT Ring

A PZT ring used in the design of a Langevin transducer was studied. The Langevin transducer consists of four pieces of PZT rings connected electrically in parallel and mechanically in series. The PZT rings are pre-stressed by two metal plates by means of bolt-clamping. The internal structure of the Langevin transducer and its electrical connection are shown in Fig. 2.2. As the Langevin transducer is designed to vibrate in the axial direction, the excitation of transducer comes from the thickness vibration of each individual PZT ring. Hence, the vibration characteristics of a PZT ring play a significant role in the transducer design. The PZT ring, ASM-PZT8 supplied by ASM, is a hard PZT material with properties similar to PZT-8. The ring has an outer diameter, inner diameter and thickness of 12.7 mm, 5.1 mm and 2.3 mm, respectively. The PZT ring was poled in the thickness direction and covered with sliver electrodes on the two major surfaces. The electrical impedance spectrum was measured with an HP 4194A Gain/Phase impedance analyzer. Five main resonances are observed and they are compared with FEM prediction in Fig. 2.3. The FEM results are harmonic simulation of a PZT ring structure modelled by the three dimensional coupled field elements (SOLID5). The FEM model is shown in Fig. 2.4. Details on FEM of the PZT ring will be given in a later section. The vibration characteristics of its resonance frequency and

k_{eff} of the five modes are summarized Table 2.1. The agreements between experimental measurements and FEM prediction are found to be very good. The k_{eff} is determined by:

$$k_{eff} = \sqrt{\frac{F_a^{\,2} - F_r^{\,2}}{F_a^{\,2}}} \tag{1}$$

where F_r and F_a are the resonance and anti-resonance frequencies, respectively.

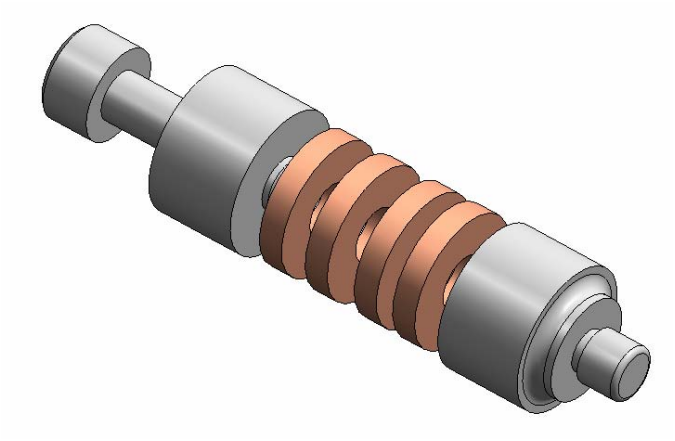

(a)

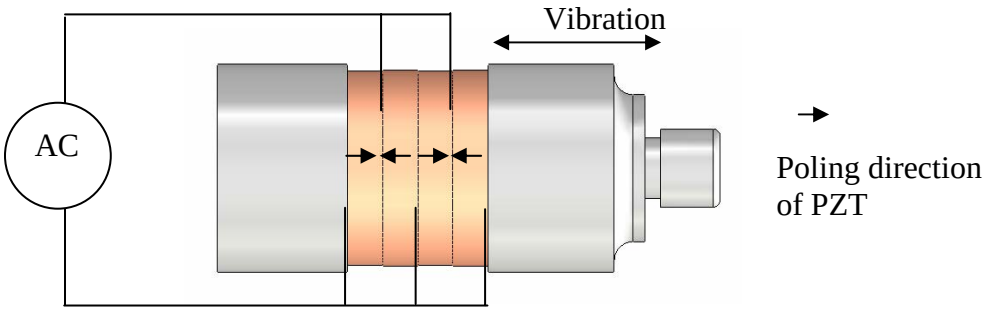

(b)

Fig. 2.2 A Langevin transducer showing its (a) internal structure and (b) electrical connection and vibrational direction.

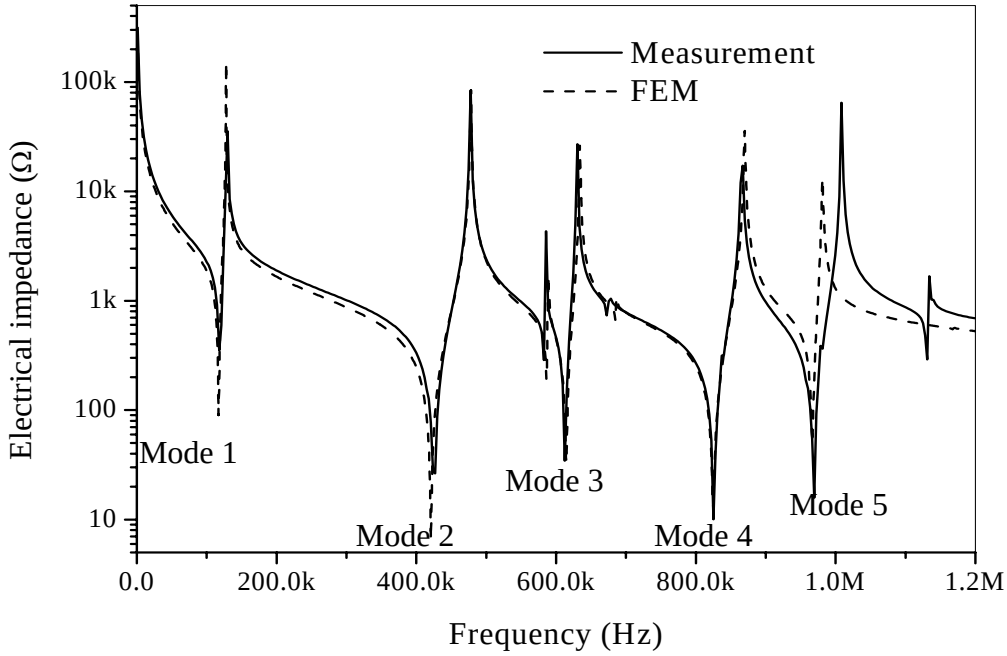

Fig. 2.3 The impedance spectrum of the five major resonances in the frequency domain.

TABLE 2.1 RESONANCE CHARACTERISTICS OF A PZT RING.

		Mode1	**Mode2**	**Mode3**	**Mode4**	**Mode5**
FEM	F_r (kHz)	117.4	421.8	615.0	825.1	967.7
	k_{eff}	0.39	0.47	0.24	0.32	0.20
Experiment	F_r (kHz)	117.9	426.6	612.5	825.3	969.2
	k_{eff}	0.42	0.45	0.24	0.31	0.25

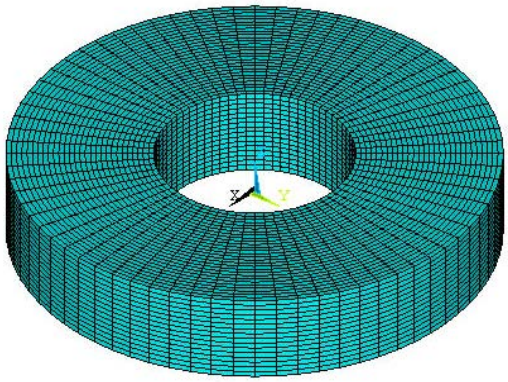

Fig. 2.4 FEM model of a three dimensional PZT ring.

Modes 1 and 2 are sometimes referred to as the first radial mode and wall-thickness mode, respectively. Mode 4 is known as the thickness (piston) mode [40]. The major surfaces are assumed to vibrate as a plane. The thickness mode of a PZT ring is the principal resonance of practical interest in the transducer design. The vibration loci of the radial, wall-thickness and thickness modes are indicated in Fig. 2.5. Mode 3 and mode 5 are complex modes that vibrate in all three directions. For the ring with R_t and W_t of the same order, the vibration modes are found to be more complicated. The impedance and phase spectra measured by the HP impedance analyzer give the resonance properties for each individual mode. However, it provides no information about the mode shape. In order to identify the mode shapes of the ring under various resonances, a Polytec laser vibrometer was used to measure the out-plane displacement of the ring surface along the radial direction as shown in Fig. 2.6 (a). The mode shapes found by FEM and experimental scanning are plotted in Fig. 2.6 (b) – (e). These scannings, together with the mode shape predicted by FEM, allow us to determine the mode shape experimentally.

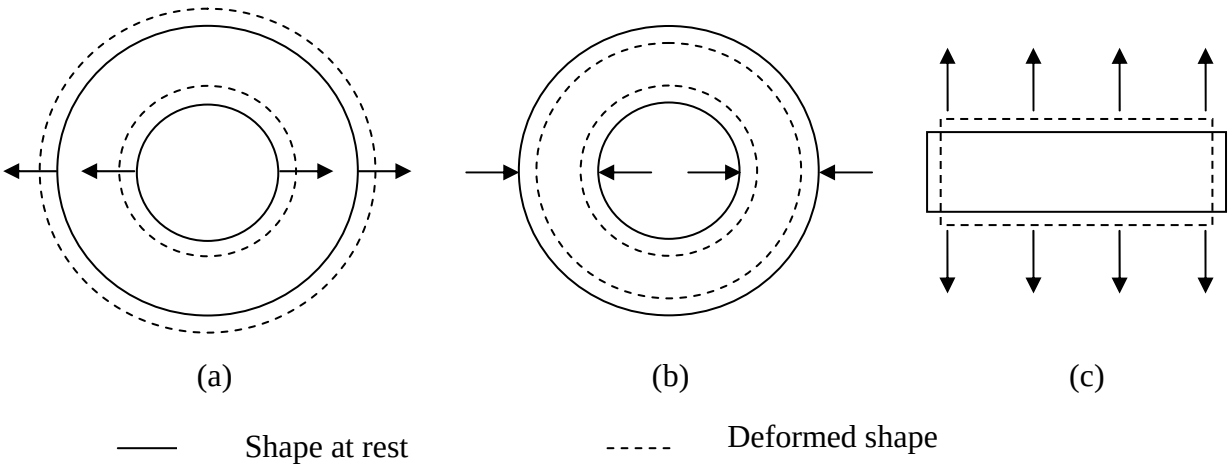

Fig. 2.5 Vibration loci of (a) radial, (b) wall-thickness and (c) thickness modes of a PZT ring.

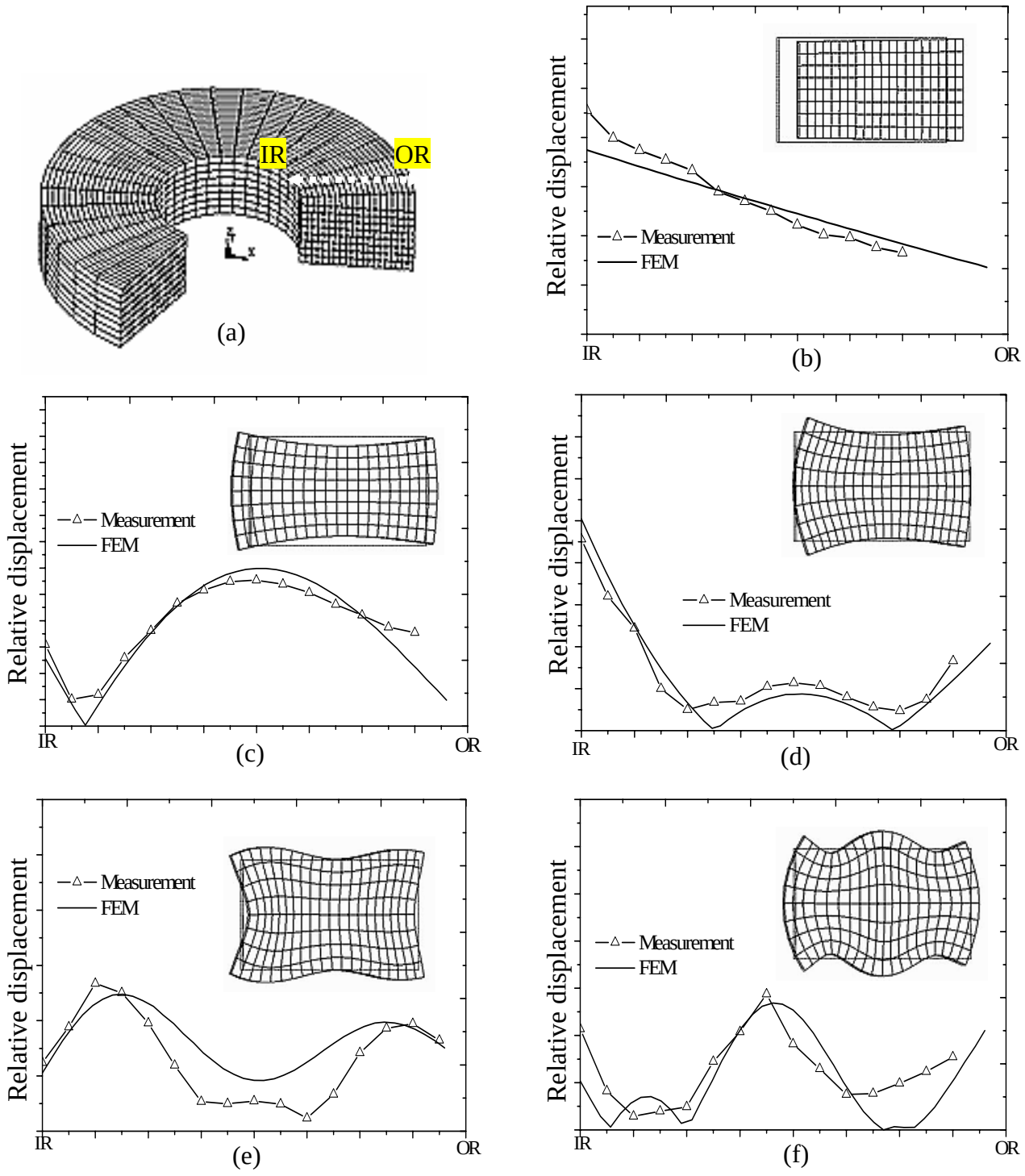

Fig. 2.6 (a) Laser scanning path.

(b) - (f) Out-plane displacement profiles for mode 1-5.

From Fig. 2.6, the complex vibration modes simulated by FEM are confirmed by laser vibrometer measurements. Good agreements are obtained between experimental laser scanning and FEM prediction. The vibration motion in one direction is coupled to that in other direction when R_t is comparable to W_t. For the thickness mode (mode 4), the ring surface is not vibrating with the same amplitude and hence results in a complex vibration profile in all the three directions. The effect on other dimensions should not be neglected in such circumstance. Therefore, being able to predict the variation of vibration characteristics with the ring dimensions is highly desirable for the transducer design.

2.2.2 Optimization of The Dimensions of A PZT Ring for Transducer Design

To understand the effect of dimensions on the vibration characteristics, the resonance frequency F_r and k_{eff} of the ring is modelled as functions of W_t and R_t. The computed F_r and k_{eff} are shown in Fig. 2.7 and Fig. 2.8. In Fig. 2.7, the ring thickness and inner diameter are kept at 2.3 mm and 5.1 mm, respectively. By varying the outer diameter such that the wall thickness varied from 1.5 mm to 6.0 mm, F_r and k_{eff} for modes 1 to 5 are predicted. Similarly, in Fig. 2.8, both inner and outer diameters are fixed, with the ring thickness varied from 1.2 mm to 3.6 mm assuming a constant wall thickness of 4.45 mm. All the resonance frequencies decrease as W_t increases except for the first radial mode. A similar trend is exhibited when R_t increases. Maximum k_{eff} values can be achieved by altering either W_t or R_t. To design a Langevin transducer using PZT rings with an outer diameter of 12.7 mm, W_t and R_t should be set at around 3.8 mm and 2.3 mm, respectively. The dimensions give the ring the largest coupling factor for the thickness mode (mode 4). In the configuration of the Langevin transducer for wire bonding, the whole transducer vibrates in its axial direction which is

corresponding to the thickness excitation of the PZT rings. Therefore, we can maximize the thickness mode coupling to optimize the transducer design.

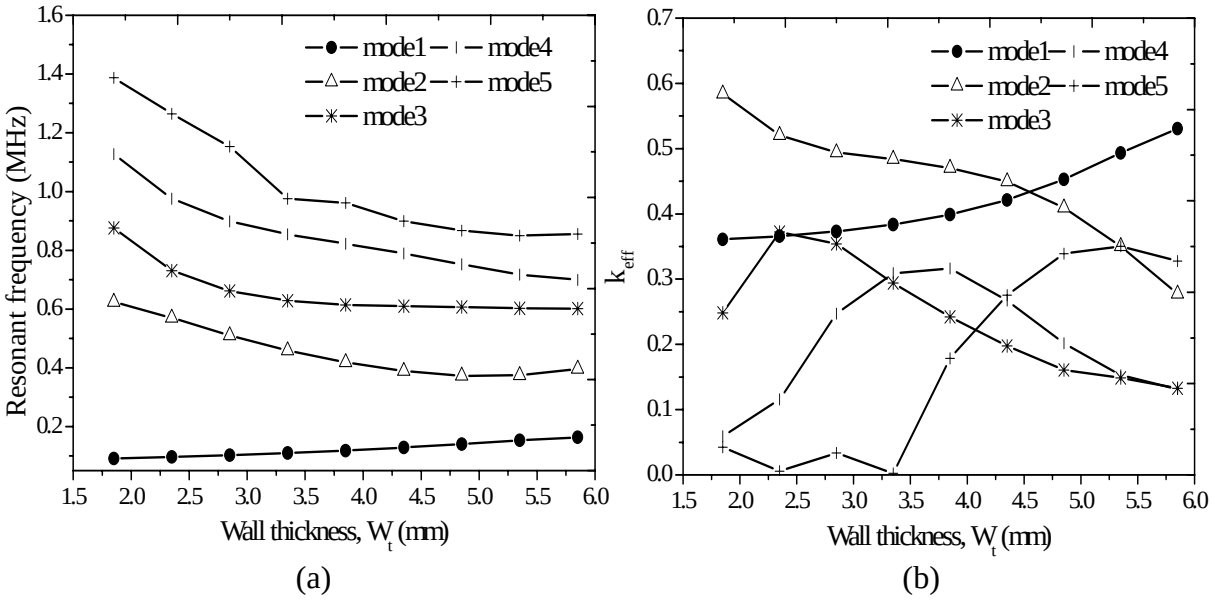

(a) (b)

Fig. 2.7 The variation of (a) F_r and (b) k_{eff} as a function of W_t. (R_t = 2.3 mm)

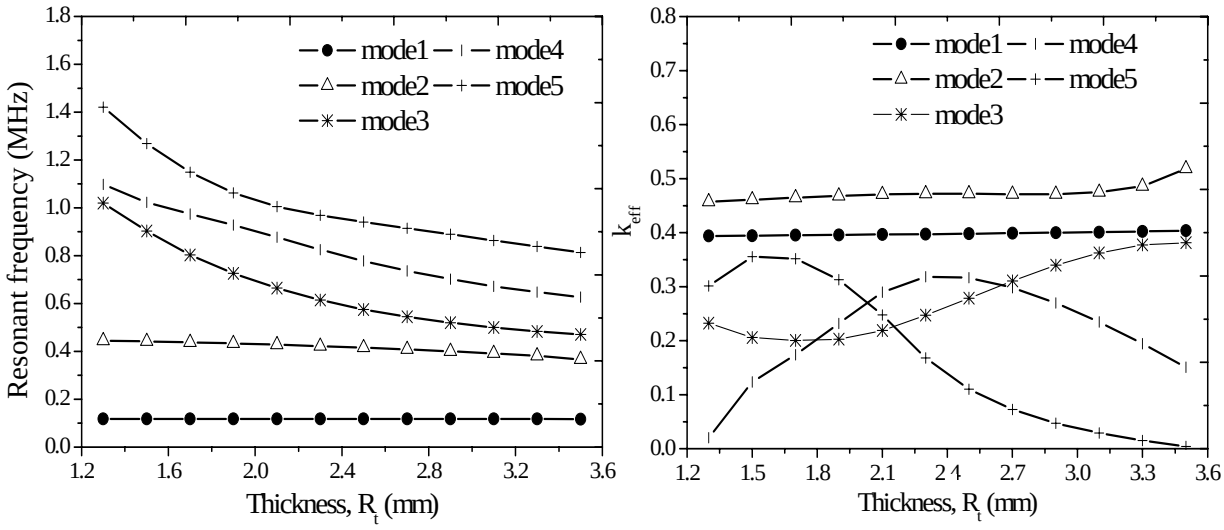

(a) (b)

Fig. 2.8 The variation of (a) F_r and (b) k_{eff} as a function of R_t. (W_t = 4.45 mm)

2.2.3 Summary

The vibration characteristics of a PZT ring from a commercial Langevin transducer is studied. Complex vibration modes are excited as the thickness of ring is comparable to its wall thickness. FEM and laser vibrometer measurements confirmed the mode shapes of the five main resonances. Dimensions of the ring are modelled as a function of R_t and W_t. Optimized dimensions for each individual mode are identified. The result can help to identify the ideal dimensions of the PZT ring used in the transducer design

2.3 Optimization of The Dimensions of a 1-3 Piezocomposite Ring by FEM

Several analytical models have been proposed to predict and simulate the behaviours of 1-3 composites [41-43]. Each of them has either not consider the full set of moduli or has made certain assumptions that limit the application of the theories to general applications. To overcome that, finite element method (FEM) was employed and it is useful to analyze complex problems such as piezoelectric pillar geometries [44-46]. However, the previous FEM studies were mainly based on the assumption that the 1-3 composite has an infinite size when compared with the PZT pillars. Therefore, a unit cell could be accurate enough to represent the whole composite panel. For the 1-3 composite rings in the wire bonding transducers, it was fabricated by the dice-and-till technique [47]. The number of cuts per direction (cpd) has to be limited in order to retain a high PZT volume fraction (>90%) for good transducer properties and reduce the manufacturing costs. However, the number of cpd has to be adequate such that the 1-3 composite ring can be treated as a homogenous medium. In this section, a commercial FEM code, ANSYS, was employed to study the effect of the cpd on the properties of a 1-3 composite ring. Unlike the previous studies, the whole composite

ring was modelled with three-dimensional FEM from 5 cpd to 9 cpd. For composite rings with small number of cpd, the high PZT element aspect ratio (width to height, L/T) makes the previous analytical models no longer accurate enough. With the use of FEM, the dynamic behaviours of such composite rings can be predicted.

2.3.1 Sample Preparation

The 1-3 composite rings were prepared by the dice-and-fill technique. Commercially available PZT-8 materials supplied by ASM were used as the active phase. The passive polymer phase was the Araldite LY5138/HY5138 epoxy (Ciba-Geigy). The materials properties of the ASM PZT-8 and epoxy are listed in Table 2.2. Details of characterization on material properties can be found in reference [37]. The PZT rings have 12.7 mm outer diameter, 5.1 mm inner diameter and 2.3 mm thickness. These are the optimized sizes for usage in transducer as shown in Section 2.2.2. Parallel grooves were cut in the two perpendicular directions on the PZT rings using a Disco DAD321 automatic dicing saw. Very fine grooves (80 μm) could be made on the PZT rings by a thin diamond saw blade. Epoxy was filled into the grooves under the action of vacuum. After curing of the passive epoxy phase, the composite was lapped and polished to remove the excess polymer. Finally, a conductive silver paint was applied on the two major surfaces to serve as the electrodes. The details on 1-3 composite ring fabrication can be found in reference [37]. By varying the numbers of cuts per direction (cpd) from 5 to 39 the composite rings with ceramic volume fraction ϕ ranging from 0.93 to 0.58 could be obtained. The set of 1-3 composite rings with 5 to 39 cpd (ϕ = 0.93, 0.91, 0.88, 0.84, 0.79, 0.75, 0.71, 0.67, 0.63 and 0.58) are shown in Fig. 2.9.

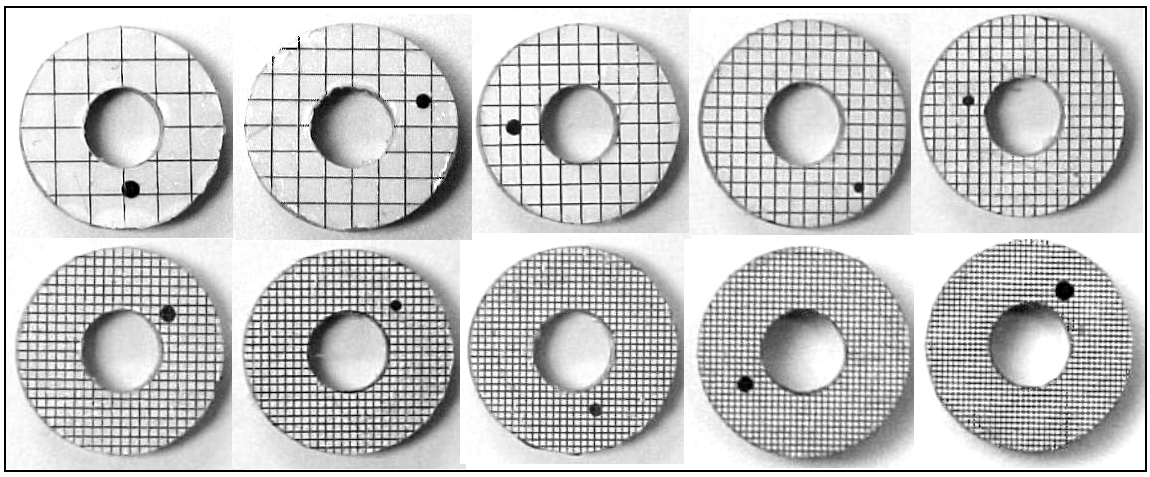

Fig. 2.9 1-3 piezocomposite rings with 5, 7, 9 , 13, 17, 21, 25, 29, 33 and 39 cpd (ϕ = 0.93, 0.91, 0.88, 0.84, 0.79, 0.75, 0.71, 0.67, 0.63 and 0.58). [37]

TABLE 2.2 MATERIAL PROPERTIES FOR ASM-PZT8 AND EPOXY.

Properties	ASM PZT-8	Epoxy
Young's modulus (GPa)	98.6	4.0
Density (kgm^{-3})	7800	1150
Poisson's ratio	0.31	0.36
d_{33} (pC/N)	300	-

2.3.2 Finite Element Analysis

The FEM package, ANSYS, was used for modelling the dynamic behaviours of the composite ring. Unlike the previous study, the composite was modelled as a complete ring rather than a unit cell or using lumped material parameters. It could help to relax the assumption of composite for being a homogenous medium that may not be true for high L/T ratio. Three dimensional coupled-field elements (Solid5), which include both mechanical and electrical degree of freedom (DOF), were used to construct the active PZT phase of the composite. The element matrix is derived from the linear piezoelectric equations [48],

$$\begin{aligned}\{T\} &= [C]\{S\} - [e]\{E\} \\ \{D\} &= [e]^T\{S\} + [\varepsilon]\{E\}\end{aligned} \tag{2}$$

where {T}, {S}, {D} and {E} are the stress, strain, electric flux density and electric field vector, respectively. [C], [e] and [ε] represent the elastic stiffness, piezoelectric and dielectric matrix, respectively.

By the variational principle and finite element discretization, the matrix equation for a single piezoelectric element can be derived as [49]:

$$\begin{bmatrix}[M] & [0] \\ [0] & [0]\end{bmatrix}\begin{Bmatrix}\{u\} \\ \{v\}\end{Bmatrix} + \begin{bmatrix}[C] & [0] \\ [0] & [0]\end{bmatrix}\begin{Bmatrix}\{u\} \\ \{v\}\end{Bmatrix} + \begin{bmatrix}[K] & [K^z] \\ [K^z]^T & [K^d]\end{bmatrix}\begin{Bmatrix}\{u\} \\ \{v\}\end{Bmatrix} = \begin{Bmatrix}\{F\} \\ \{L\}\end{Bmatrix} \tag{3}$$

where {u}, {v}, {F} and {L} are the nodal displacement, nodal electrical potential, structural load and electric load vector. [M], [K], and [K^z] and [K^d] are the structural mass, structural stiffness, piezoelectric coupling and dielectric conductivity matrix, respectively. The coupled finite element matrix equation allows the element to take into account the coupling effect between the mechanical and electrical DOF.

The 3D finite element models were constructed by 8-nodes brick couple field elements. The sliver electrode, typically around 0.05 mm, was neglected in the model because it is much thinner than the thickness of the PZT ring. The equipotential boundary condition was applied to all the nodal points covered by a single electrode. It can simulate the physical conductive behaviours of the silver electrodes. The epoxy width of the composite was set at 80 μm. The thin electrodes were neglected in the FEM. Fig. 2.10 shows 3D FEM models for a 5, 7, 9 and

39 cpd (ϕ = 0.93, 0.91, 0.88 and 0.58, respectively) 1-3 composite rings. The 1-3 composite rings have symmetry from the X-Y plane, a quarter model can be used to simulate the behaviours of the full ring.

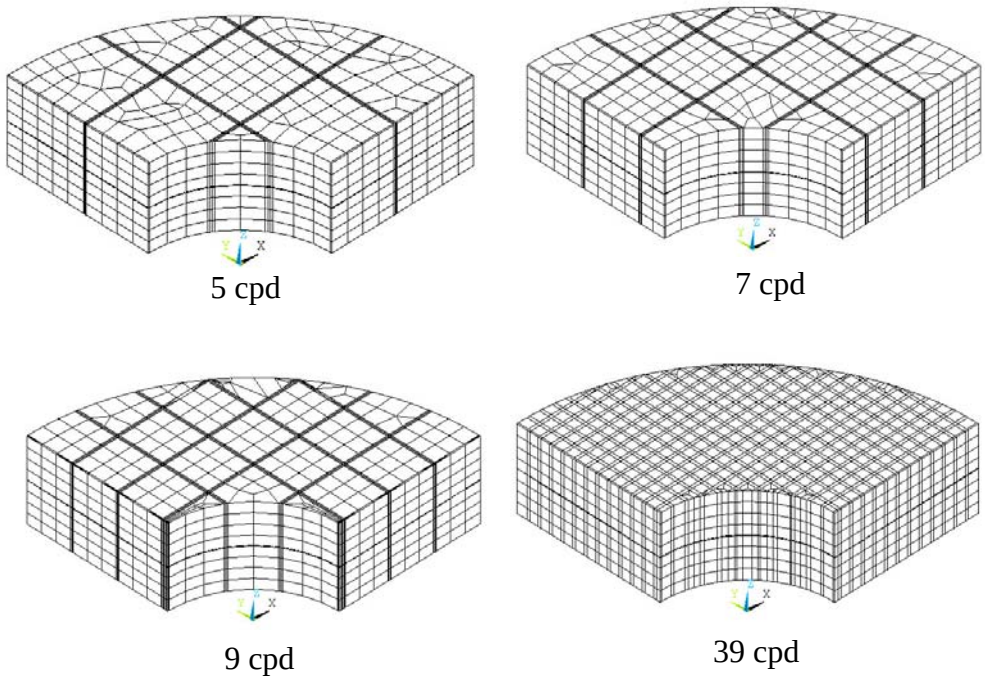

Fig. 2.10 Three dimensional finite element models for the 5, 7, 9 and 39 cpd (ϕ = 0.93, 0.91, 0.88 and 0.58) composite rings.

As the composite has been diced into a number of PZT pillars, a modal analysis would give all the possible resonance modes and hence result in numerous unwanted modes to be simulated. However, most of the resonance modes from a modal analysis may not be excited electrically. In view of that, a harmonic analysis was used instead. The composite models were driven by a voltage signal and the electrical impedance responses were simulated in the frequency domain. The simulated results were compared with the measurement by an HP4194A impedance analyzer in Fig. 2.11.

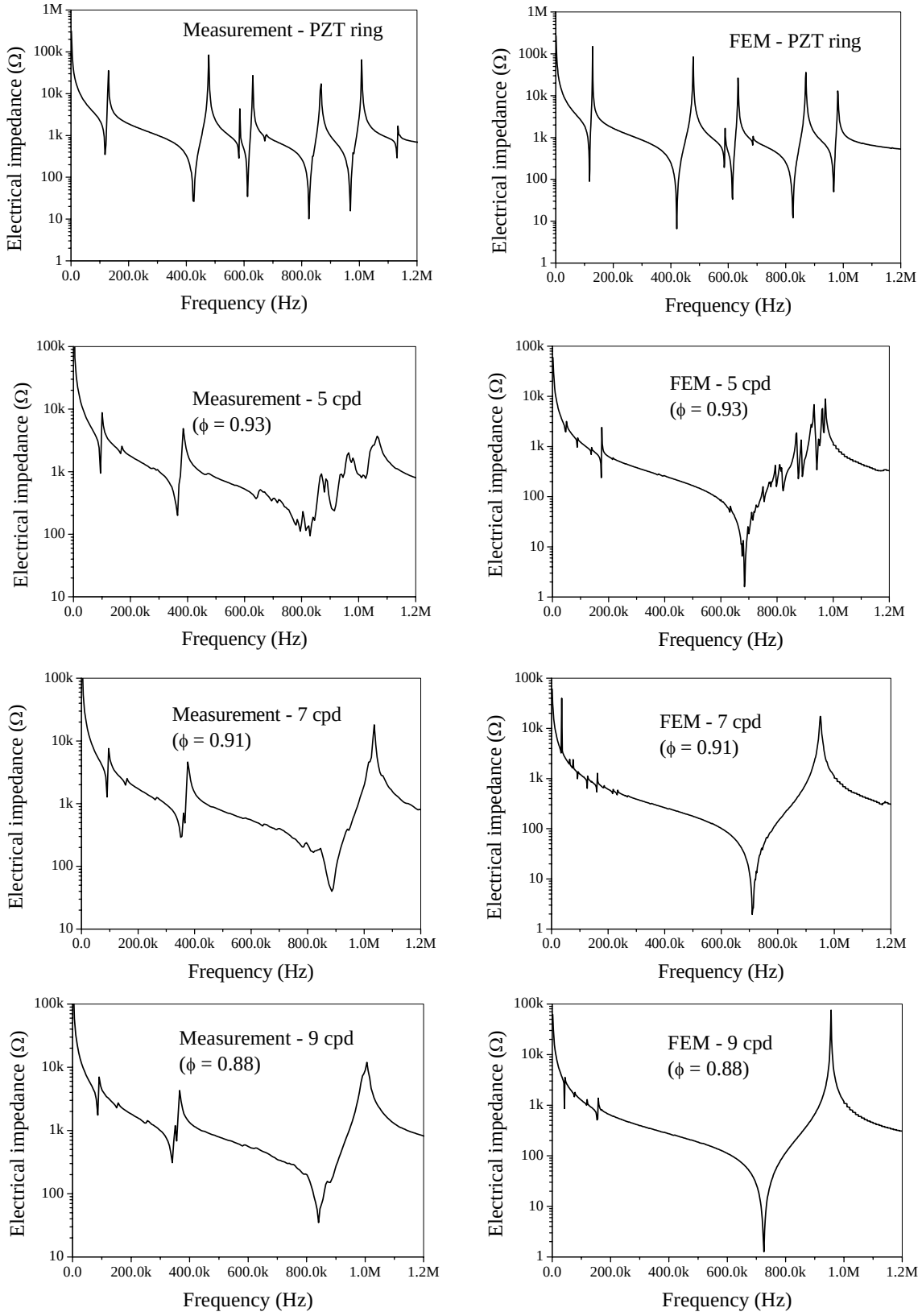

Fig. 2.11 Electrical impedance spectra of the 1-3 composite rings from measurements and FEM.

Theoretically, for an ideal 1-3 composite ring, all the PZT pillars will vibrate in their thickness direction. A single and clean resonance peak can be observed in the frequency domain. From the experimental results, the composite ring with 5 cpd (ϕ = 0.93) has many spurious modes. It indicates that the L/T ratio of 5 cpd composite ring is too large and cannot be treated as a homogenous medium. For 7 or higher cpd ($\phi \leq 0.91$) composite rings, a single resonance is identified at around 850 kHz which is the thickness mode resonance frequency of its PZT pillars. Other planar or radial resonances are greatly suppressed. Similar phenomena can also be found from the FEM analysis. Many spurious modes have been excited in the electrical impedance spectrum of a 5 cpd composite ring. For higher cpd, a single resonance mode is detected. The minimum number of cuts for making a homogenous 1-3 composite ring for above-mentioned dimensions is found to be 7. To minimize the manufacturing costs and maximize the PZT volume fraction, the desirable composite should have 7 cpd and a PZT volume fraction of 0.91.

To examine the vibration mode shape of the 1-3 composite rings, the thickness vibration contours have been plotted in Fig. 2.12. For the 5 cpd composite ring shown in Fig. 2.12 (a), due to the large L/T ratio (0.99), each PZT pillar has its own vibration characteristics. Hence, the whole ring is not purely vibrating in its thickness direction. Other planar and radial modes have coupled together. When the 5 cpd composite rings are used in devices such as a Langevin transducer for wire bonding, those planar and radial modes will excite other unwanted resonances as bending and torsional modes. For 7 cpd composite rings (Fig. 2.12 (b)), all the PZT pillars are moving in the thickness direction. Due to the difference in pillar geometry and boundary condition, each pillar may have different vibration amplitude. However, the vibration amplitude within individual pillar is found to be quite uniform.

Furthermore, each pillar is moving in the same direction with negligible planar or radial activities. These properties are essential for the composite to reduce and suppress undesirable resonances in devices such as a wire bonding transducer. For composite ring with even higher cpd as shown in Fig. 2.12 (c), the PZT pillars is moving uniformly in the same direction despite some with different amplitudes. It is due to the fact that those PZT pillars on the periphery have different boundary conditions and pillar geometries.

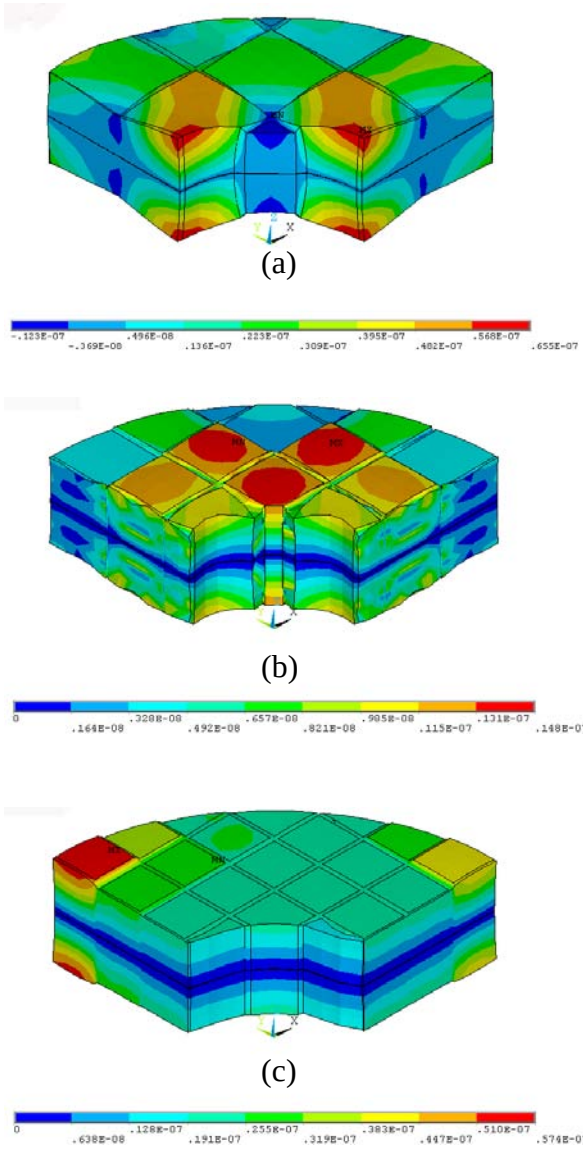

Fig. 2.12 FEM displacement contour in the thickness direction for the (a) 5 cpd (ϕ = 0.93), (b) 7 cpd (ϕ = 0.91) and (c) 9 cpd (ϕ = 0.88) composite ring.

2.3.3 Experimental Verification

To verify the simulated mode shape experimentally, a Polytec laser vibrometer was used to scan the out-plane displacement of the major surface along the radial direction of a PZT ring and a 7 cpd (ϕ = 0.91) composite ring. Both samples were driven with the same input electrical power of 1W. The scanning results are plotted in Fig. 2.13. The vibration profile of both the PZT ring and 7 cpd composite are quite different. The vibration amplitude in the PZT ring is highly non-uniform. Maximum peaks and nodal points co-existed along the scanning path. On the contrary, for a 7 cpd composite, the vibration profile is much flatter and more uniform. No sharp nodal point was found on the scanning path. The maximum difference in vibration amplitude is found to be around 10 nm. It is approximately three times less than that of a PZT ring. Hence, the major surface of the composite is moving in a more uniform way. The uniformity of the thickness vibration causes the composite ring to reduce and suppress lateral and radial modes of a device. It also helps to reduce the mode coupling effect on the thickness mode in the composite devices. In the case of a wire bonding transducer, the use of composite rings can reduce other unwanted lateral vibrations and retain a purer one direction axial resonance mode. It will promote the implementation of fine pitch and high-speed bonding in the wire bonding process.

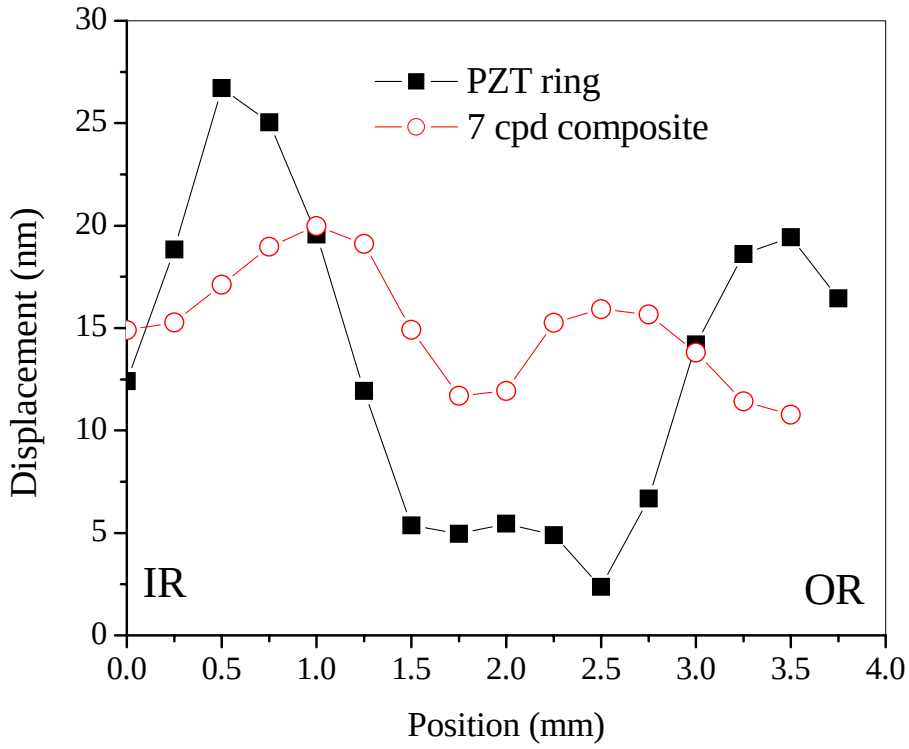

Fig. 2.13 Laser scanning profile for the PZT and 7 cpd (ϕ = 0.91) 1-3 composite ring (IR: inner radius, OR: outer radius of the ring).

2.3.4 Summary

FEM analysis on PZT/epoxy 1-3 composite rings fabricated by a dice-and-fill technique has been reported. The 7 cpd (ϕ = 0.91) composite ring was found to behave as a homogenous medium. The pattern with 7 cuts per direction can maximize the PZT volume fraction and minimize the manufacturing cost. Both FEM and experimental results show that the 1-3 composite rings have uniform thickness vibration mode. It helps to reduce mode coupling effect and suppresses the unwanted lateral vibration modes for devices such as wire bonding transducer.

2.4 1-3 Piezocomposite Transducer

In the design of conventional wire bonding transducer, as the length of the Langevin driver is comparable to the diameter of the ring, therefore, the radial and wall-thickness resonances of the ring may couple with the desired axial mode of the transducer [50]. Moreover, PZT has a high mechanical quality factor Q_m and hence it has a very sharp resonance with limited bandwidth and causes frequency tuning and locking problems in the bonding machine. It can also affect the bonding stability of the whole bonder machine. To alleviate these problems, 1-3 composite rings have been used to suppress mode coupling and maintain a pure axial mode [26]. However, the optimized dimensions and PZT volume fraction have to be found. Therefore, a composite transducer using four ϕ = 0.91 composite rings have been assembled and studied. The commercial FEM code, ANSYS, was used to analyze the vibration characteristics of the composite transducer and compared to experimental results. The characteristics of the composite transducer are compared to that of a conventional PZT transducer assembled using full PZT rings.

2.4.1 Transducer Fabrication

One typical ultrasonic wire bonding transducer operated at 64 kHz is shown in Fig. 2.14. It consists of three main parts, namely, the driver, amplifying horn, and the wedge. Each transducer consists of 4 composite (or PZT) rings. The four rings are connected electrically in parallel and mechanically in series and sandwiched between a front and back metal plate by a pre-stressed screw. The dimensions of the composite ring have an outer diameter of 12.7 mm, inner diameter of 5.1 mm and a thickness of 2.3 mm. By the dice-and-fill method with very fine groove, the composite rings used are optimized to have ϕ = 0.91 (with 7 cuts per

direction, cpd). This is a compromise between cost and performance, as more cuts per direction will increase the cost of fabrication. It has been found that composite rings with ϕ = 0.91 have adequate performance. It is also the minimum cpd that the composite ring behaves as a homogenous medium. Another wire bonding transducer with similar structure using ASM-PZT8 rings as the driving elements has also been fabricated and the performance of the ceramic and composite transducers are evaluated and compared.

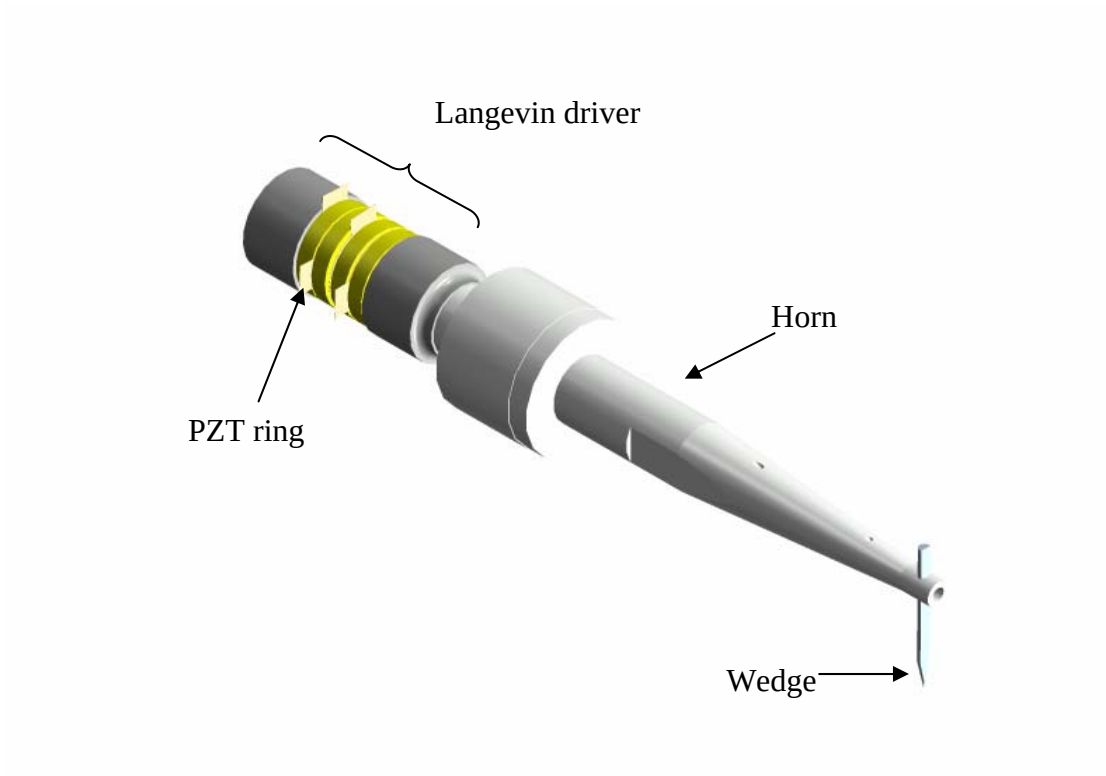

Fig. 2.14 An ultrasonic wire bonding transducer operated at 64 kHz.

2.4.2 Finite Element Model for the Wire Bonding Transducer

The transducer geometry can be described using an axial-symmetry structure along its central axis. However, the installation of the wedge at its horn breaks its symmetry. Therefore, the model of the transducer will be based on a full 360° configuration (i.e. three

dimensional model). Fig. 2.15 shows schematically the 3D finite element model for these transducers. It is noted that the model is common for both transducers, since they have a similar structure. The advantage of using a full model is that all possible resonance modes including both the flexural and axial modes can be found. The material properties of ASM-PZT8 and the metal components are supplied by ASM. The loss factors were not included in the model. Linear and anisotropic properties are assumed for the piezoelectric elements while linear and isotropic properties are used for the metal components. The theoretical background is identical to that described in Section 2.3.2. Coupled field elements (SOLID5) have been used to model the PZT material. The elements are able to couple both mechanical and electrical DOF in a single analysis. It allows the FEM to predict both the resonance and anti-resonance frequencies of the transducer. Therefore, the effective electromechanical coupling factor can also be simulated.

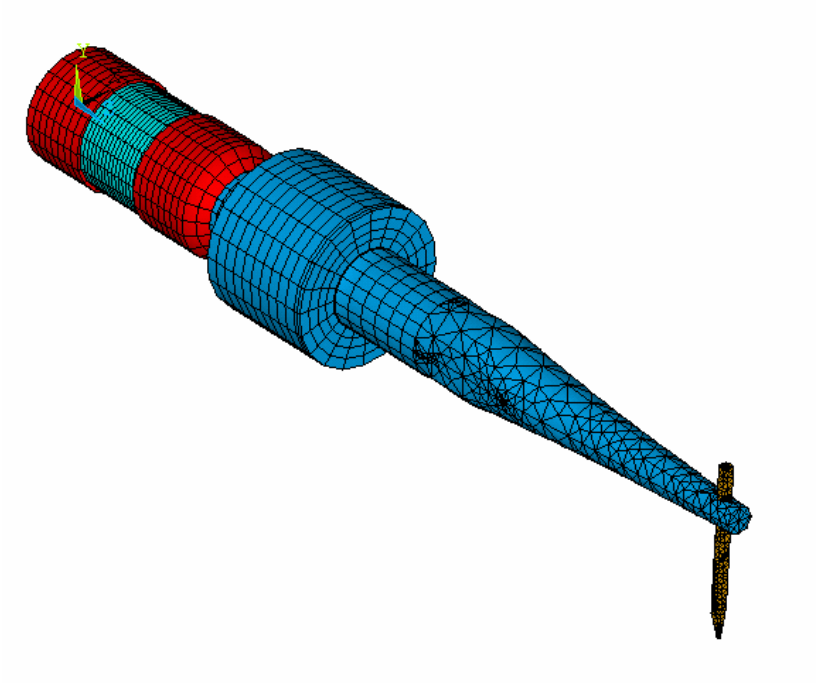

Fig. 2.15 The full 360 degree model of the transducer.

For ease of meshing, the thread of the pre-stressed screw has been ignored. Simplification has been made to some metal components and screws where the thread and threaded bore have been simplified. The ring-shaped copper electrodes used for soldering of lead wires are assumed to be very thin, and they have not been taken into account. All components in the assembly are assumed to have perfect contact and mechanical coupling to each other. The h-type approach is applied to the analysis, and good convergence of the results has been reached by successively increasing the number of solid elements and hence the number of nodes so as to approximate the exact numerical solution to within 5 % for frequencies up to 150 kHz. The lowest 100 natural frequencies and mode shapes of both the composite and PZT transducers have been computed using commercial finite element software package ANSYS.

For resonance frequencies up to 150 kHz, there are a total of 98 and 103 natural modes computed for the composite and PZT transducers, respectively. Among these modes, however, some exhibit very weak electromechanical coupling behaviours ($k_{eff} < 0.05$), especially for those at higher frequencies. These modes could not be excited effectively by the electrical driving signal in practice, so they have been discarded. Due to the lossless system used in FEM, the actual electrical impedances cannot be determined as they have zero ohm at the resonance frequencies and infinite ohm at the anti-resonance frequencies. Moreover, the computed k_{eff} of the composite transducer becomes larger than the real values because the losses in the planar direction of the composite ring have been neglected.

Table 2.3 summarizes these effective modes for the two transducers near the operation frequency. Some of the computed modes were found to be excluded by the electrical boundary conditions and are not observed in the spectrum. The computed mode shapes can be categorized as follows: axial, torsional, and complex flexural modes. The axial operation

mode is found to be 40 and its frequency is 63996 Hz which is in good agreement with the measured values (64 kHz). The operation mode is a 1.5 wavelength axial mode which has a maximum k_{eff} of 0.393 among all 100 modes. The deformed shape and the axial profile is plotted in Fig. 2.16 and Fig. 2.17. Agreed with the transducer design requirement described in Chapter 1, the transducer operates in the axial mode. The axial motion of the horn tip transmits to the wedge and causes the wedge to vibrate in a flexural manner. In Fig. 2.17, it is clearly shown that the mounting barrel is located at its axial nodal point and the axial motion is amplified by the horn profile. Finally, a maximum axial vibration is identified at the horn tip. Moreover, the Langevin driver is vibrating at its fundamental half-wavelength mode. From a physical standpoint, a pure axial excitation produces a front-to-back motion in the axial direction, which in turn, causes the tip of the ultrasonic horn and the wedge to move back and forth axially to generate a large axial displacement. As this motion is essentially in line with the wire to be bonded, hence the axial modes are the most desirable resonance modes.

TABLE 2.3 MODAL RESULTS THE TRANSDUCERS.

Mode No.	**f_a (kHz)**	**f_r (kHz)**	**k_{eff}**	**Mode shape**
36	54387	53873	0.137	1 λ Axial mode
37	54140	54140	0	Torsional mode
38	58494	58076	0.119	Complex mode
39	62685	62685	0	Flexural mode
40	69588	63996	0.393	**1.5 λ Axial mode**
41	65572	65572	0	Complex mode
42	66487	66613	0.062	Flexural mode
43	69297	69297	0	Barrel mode

From the modal analysis , there are several flexural modes and complex modes appear near the operation frequency as listed in Table 2.3 All the mode shapes from 36 to 43 are given in Fig. 2.18. Apart from the desirable operating axial mode, the transducer can vibrate in other complex modes. For example, the flexural mode 39 can make the wedge to vibrate in the left and right direction. Mode 42 indicates that the transducer can also be vibrating in the up-and-down direction. However, not all the modes simulated by the modal analysis can be excited electrically. Some resonances could not be identified in the electrical impedance spectrum. In theory, the modes with k_{eff} equal to zero will not be excited electrically. In practice, however, due to the fact that there is no perfect alignment, all the modes shown in Table 2.3 can have a chance to be excited simultaneously, and the undesirable modes are difficult to eliminate completely. The lateral flexural motions from side to side and the torsional motion would deteriorate the bond quality as a result of diminishing the purity of the axial excitation through the loss of the input energy to other vibrations.

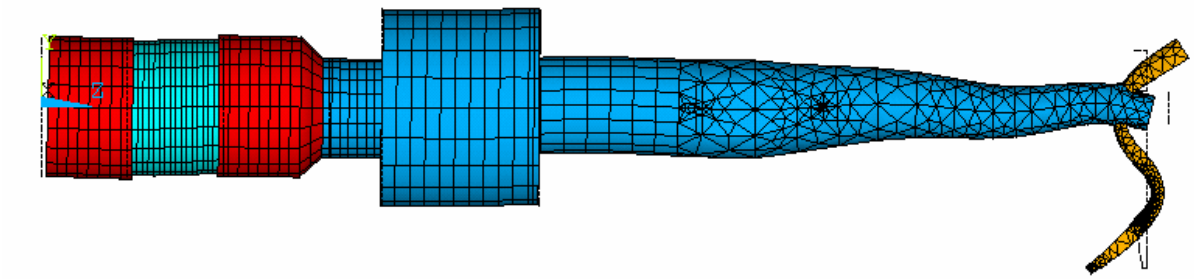

Fig. 2.16 Deformed shape at the operation mode.

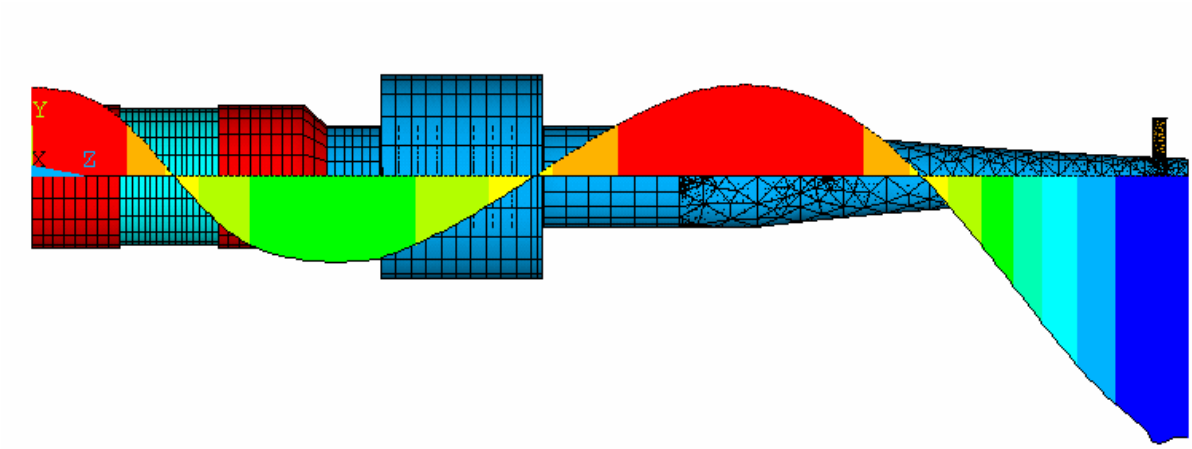

Fig. 2.17 The axial vibration profile at the operation mode.

The resonance of the transducer comes from its excitation by the driving element. For pure PZT ring, due to the strong coupling with other complex modes as discussed in Section 2.2, the flexural, torsional and other complex modes of the transducer can be easily excited simultaneously with the operating axial mode. However, by replacing the PZT rings with 1-3 composite rings, the excitation source of the transducer becomes unidirectional. The other undesirable resonances will not be excited. Therefore, the transducer can retain a pure axial operation mode for the wire bonding applications. The unique features of the 1-3 composite transducer allow it to gain a lot of process capabilities that will be discussed in the coming section.

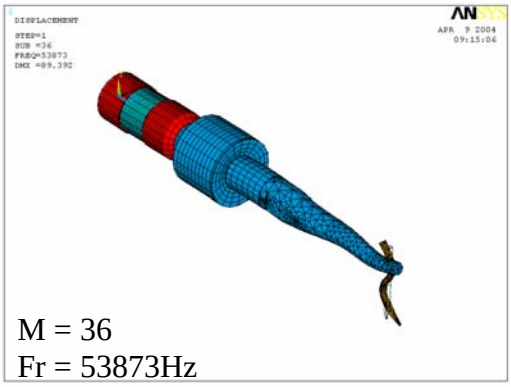

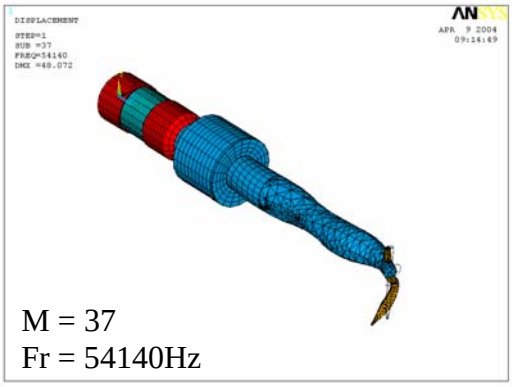

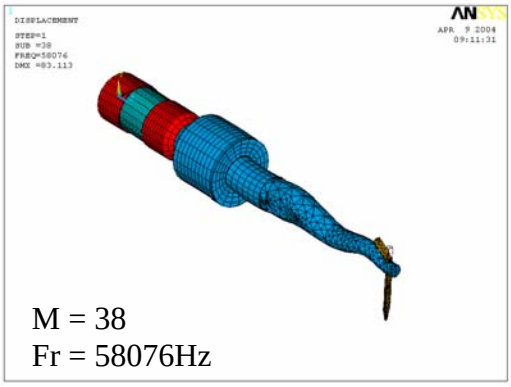

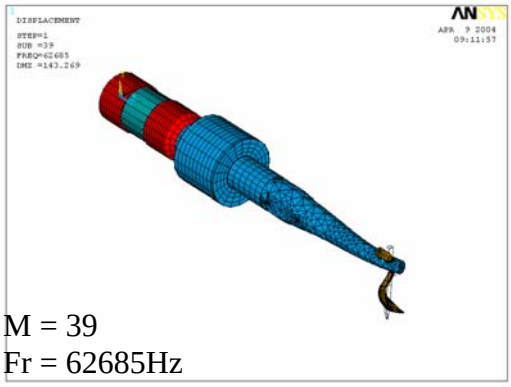

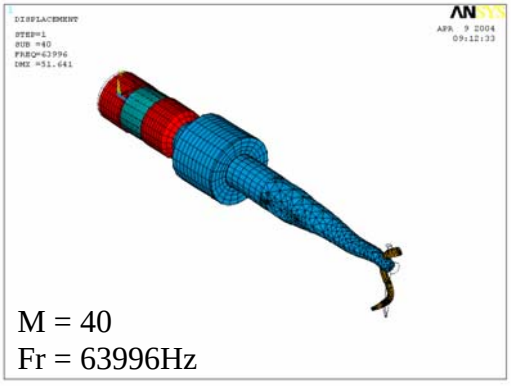

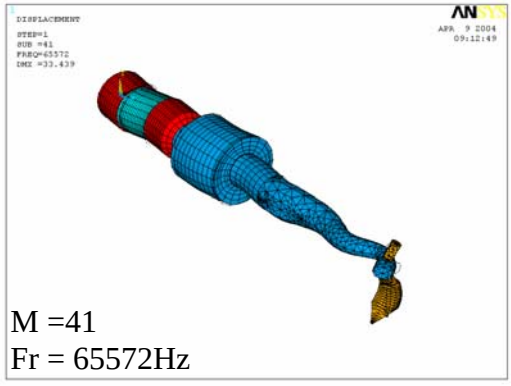

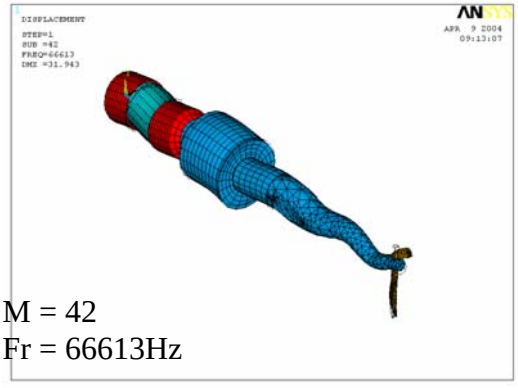

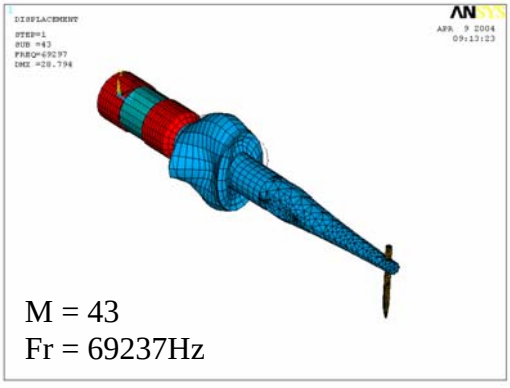

Fig. 2.18 Modal Analysis for all the resonance modes around 64 kHz.

2.4.3 Characteristics of 1-3 Composite Transducer

The 1-3 composite transducer will be characterized and compared with a conventional PZT transducer in this section. The unique features of the 1-3 composite transducer will be highlighted. In the next section, detail process studies will be conducted to link up those unique features to the improvement of bonder machine capabilities.

2.4.3.1 Tool Drop Measurement

The tool drop is measured from the location where the wedge is secured to the wedge tip as shown in Fig. 2.19. The performance of the transducer is highly depended on the tool drop [25]. The tool drop is determined such that the transducer resonance mode matches with that of the wedge. In practice, it is found experimentally that values of the tool drop can affect the impedance and frequency of the transducer. To make a fair benchmarking for the two different types of transducer, it is important to ensure that both types of transducer can share a common tool drop.

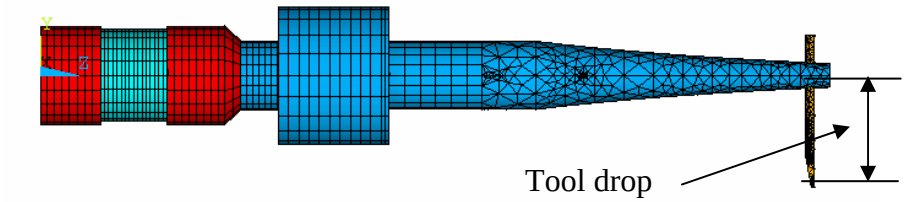

Fig. 2.19 Tool drop of the transducer.

To determine the tool drop for both composite and PZT transducers, the tool drop is varied from 5 mm to 20 mm. The frequency and impedance responses with the tool drop for both transducers are measured and recorded. The electrical impedance and frequency versus the tool drop are shown in Fig. 2.20 and Fig. 2.21, respectively.

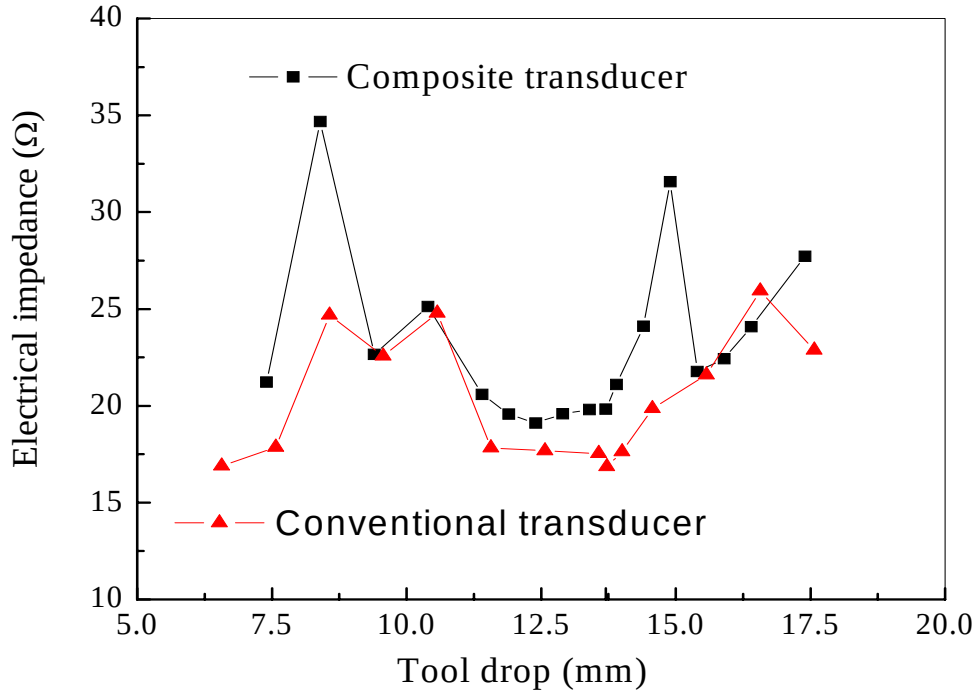

Fig. 2.20 Transducer impedance vs tool drop.

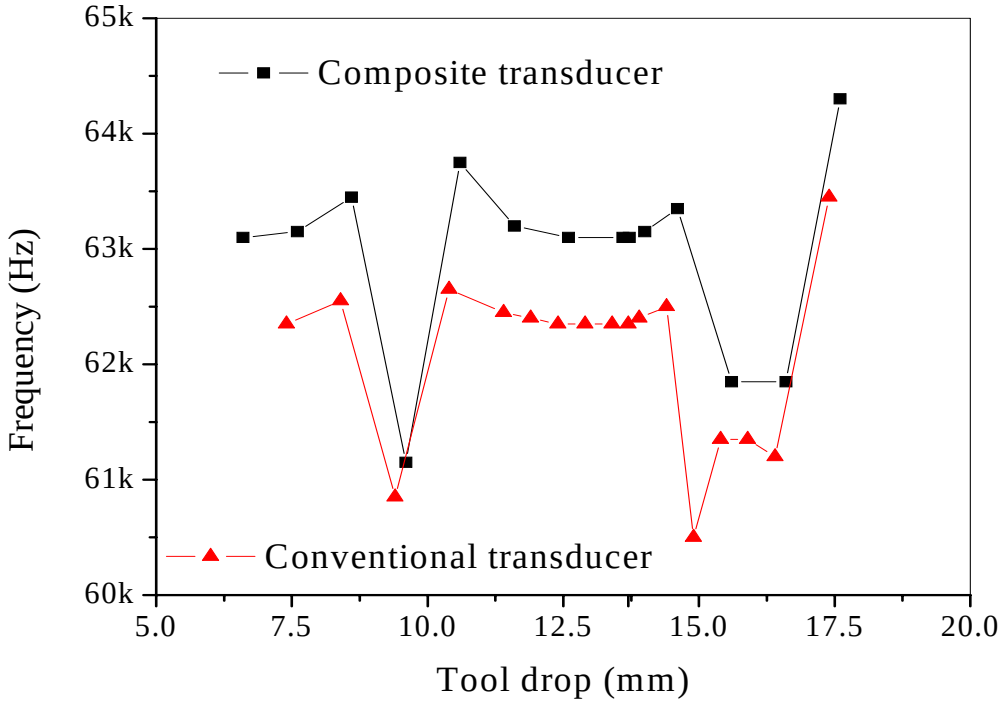

Fig. 2.21 Transducer frequency vs tool drop.

From Fig. 2.20 and Fig. 2.11, the transducer properties have a stable range when the tool drop equals to 10.5 to 14.0 mm. The behaviour of both transducer exhibits similar trend for both frequency and impedance. According to the specification of the PZT transducer, the nominal tool drop is 13.7 mm which can also be suitable for the composite as well. Therefore, both of the transducer will use the same tool drop for the subsequent characterization and process studies.

2.4.3.2 Electrical Characteristics

The impedance and phase spectra of the composite and PZT transducers up to 600 kHz are shown in Fig. 2.22. In the conventional PZT transducer (Fig. 2.22(b)), the strongest resonance at around 64 kHz is identified as the second axial mode, which is the designated working mode of the transducer with the length of the horn equals to one longitudinal wavelength. Together with the fundamental half wavelength of the Langevin driver, the whole transducer is operating in its 1.5λ longitudinal resonance. The first and third axial modes are found at 50.8 kHz and 76.0 kHz, respectively. For frequencies ranging from 100 to 600 kHz, the conventional PZT transducer (Fig. 2.22(b)) has very complicated resonance characteristics with many resonance peaks. In fact, when this transducer is used in bonding, the non-axial and spurious resonance modes, especially those with frequencies very close to the working axial mode or equal to its higher frequency harmonics, are likely to be excited simultaneously. Therefore, the beauty of the composite transducer is that it can suppress very high frequency mode of the transducer. It allows the transducer to be free from the influence of high frequency harmonics of the operation mode.

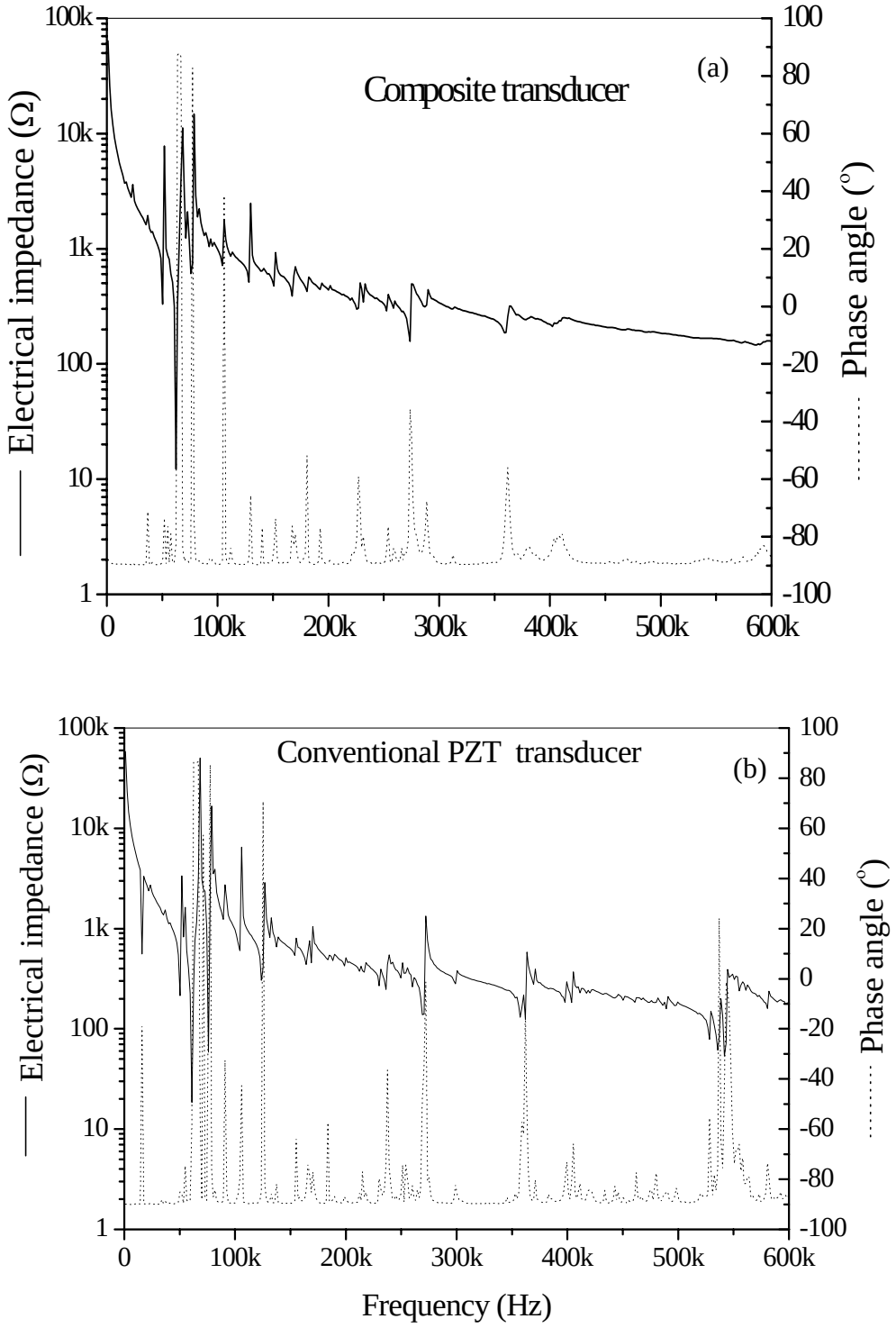

Fig. 2.22 Electrical impedance and phase spectra of

(a) composite and (b) conventional PZT transducer. [37]

From Fig. 2.22 (a), the designated working mode of the composite transducer with 7 cpd (ϕ = 0.91) composite rings is found at 62.8 kHz. The first and third axial modes are found at 51.2 kHz and 76.0 kHz, respectively. No other prominent resonance is observed although some weak higher order modes can still be found in the frequency range of 150 to 600 kHz. The high frequency modes have been suppressed by the use of 1-3 composite rings. The impedance spectrum is essentially pure in that the axial modes are strengthened by suppressing any non-axial and spurious modes.

Apart from the high frequency modes being reduced, the spurious response around the operation mode can also be suppressed. Those spurious modes are the complex or flexural modes predicted by the FEM. However, for the conventional PZT transducer, due to the misalignment of the mechanical parts or assembly process, the electrical spectrum is very susceptible to spurious resonances. Those spurious modes can affect the ultrasonic properties of the transducer which is highly undesirable. By making use of a pure unidirectional excitation of 1-3 composite rings, the spurious peaks can be easily removed.

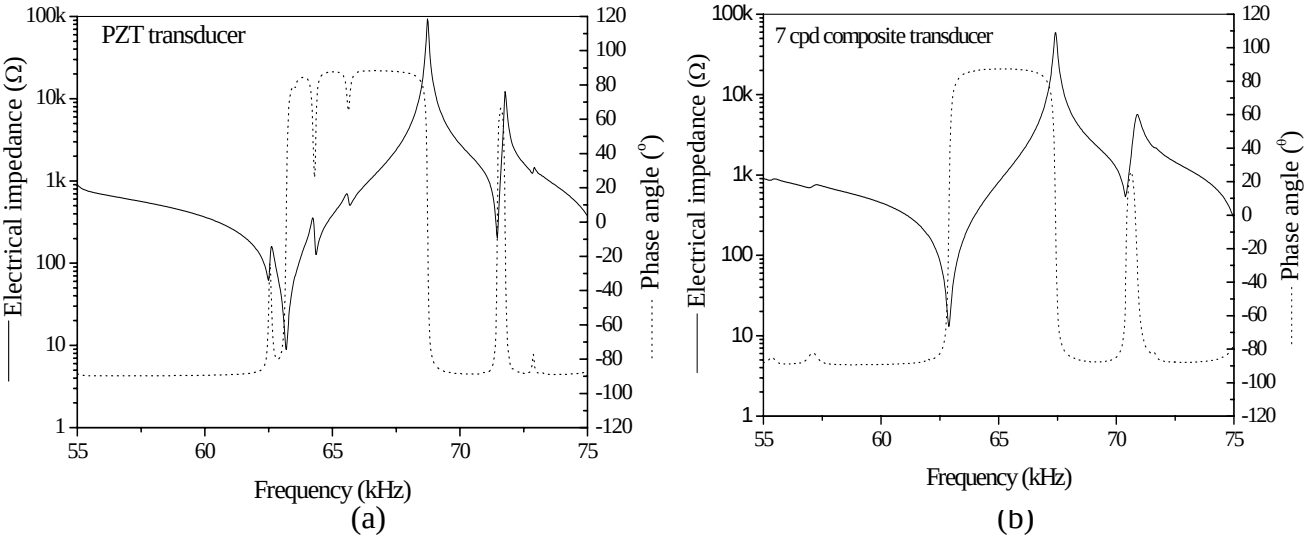

Fig. 2.23 Electrical impedance and phase spectra near the operation mode of the (a) PZT and (b) composite transducer.

2.4.3.3 Vibration Amplitude

The vibration amplitude in this section referred to the vibration displacement in the wedge tip which is one of the key characteristics of the transducer. It determines how efficient the transducer is in converting electrical energy to mechanical vibration in the wire bonding process. The vibration displacement is measured by a Polytec laser vibrometer. Both axial and lateral displacements of the wedge have been measured as illustrated in Fig. 2.24.

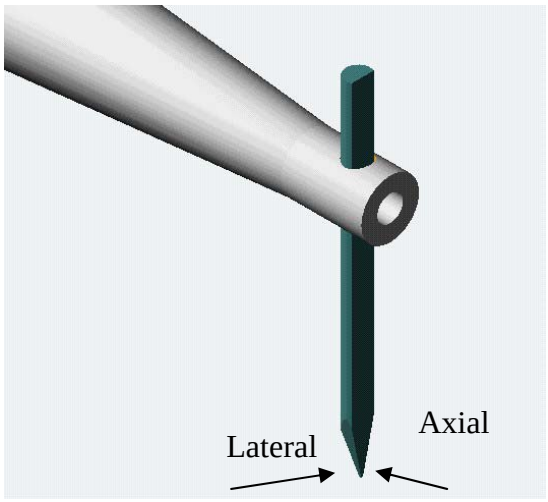

Fig. 2.24 Laser vibrometer measurement of the wedge.

Fig. 2.25 shows the laser vibrometer measurement results for both types of transducer. From Fig. 2.25(a), the axial vibration amplitude of the composite and conventional PZT transducer is very similar. It means that both of them can function with similar efficiency during the bonding. However, the composite has a much smaller lateral vibration than that of a conventional PZT transducer. It is evident that the composite has a purer axial mode and no other resonance is coupled with the operation mode. Therefore, the lateral vibration induced by other spurious modes has been greatly reduced and it is 3 times lower for the composite.

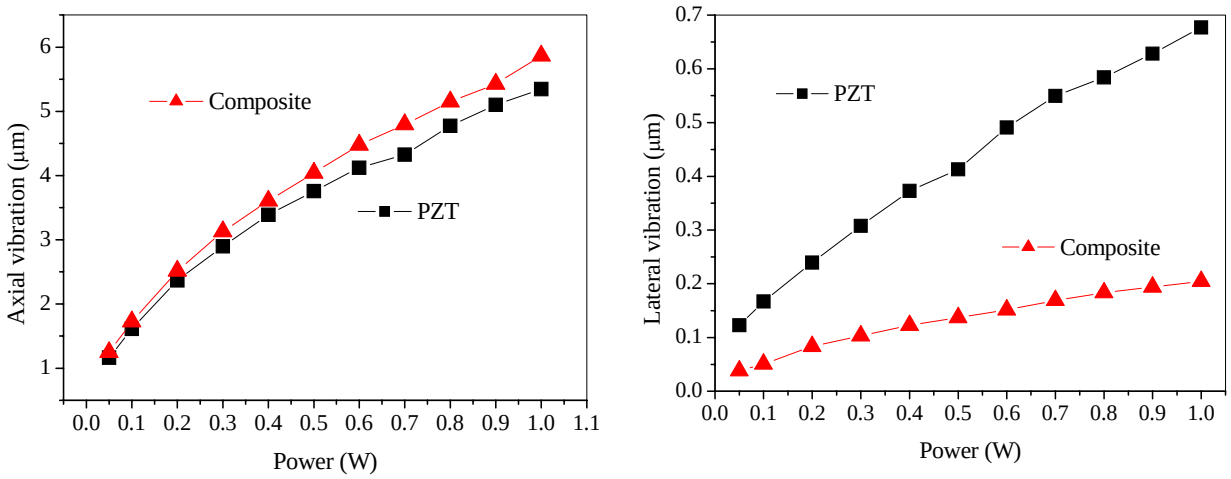

(a) (b)

Fig. 2.25 Vibration amplitudes along the (a) axial and (b) lateral direction.

2.4.3.4 *Transducer Response by FFT*

A typical axial vibration response waveform of the composite transducer is shown in Fig. 2.26. The composite transducer has a rise and fall time of voltage ~40% shorter than that of the PZT transducer, which indicates that it is heavily damped. This result agrees with previous findings that Q_m of the composite transducer is lower than that of the conventional one. Furthermore, shortening of the rise and fall time of the voltage can correspondingly increase the effective bonding time during the wire bonding process. For a constant effective bonding time, the complete bonding process can be accomplished in a shorter time if a composite transducer is used. Hence, there is an advantage in using the composite transducer in high speed bonding. By applying a fast Fourier transform (FFT) to the steady-state portion of the displacement waveform, the corresponding displacement amplitude spectrum (in dBm) can be obtained. By the FFT analysis, it is seen from Fig. 2.27 that the excitation of other frequency components, including higher order harmonics and sub-harmonics to the fundamental, are comparatively insignificant in the composite transducer as their amplitude

are about –40 dBm lower. The purity of axial excitation is ~94.2 % for the composite transducer but only ~90.6 % for the conventional PZT transducer, reflecting again the low mode coupling nature of the composite transducers. These observations are also in good agreement with those observed from the impedance and phase spectra.

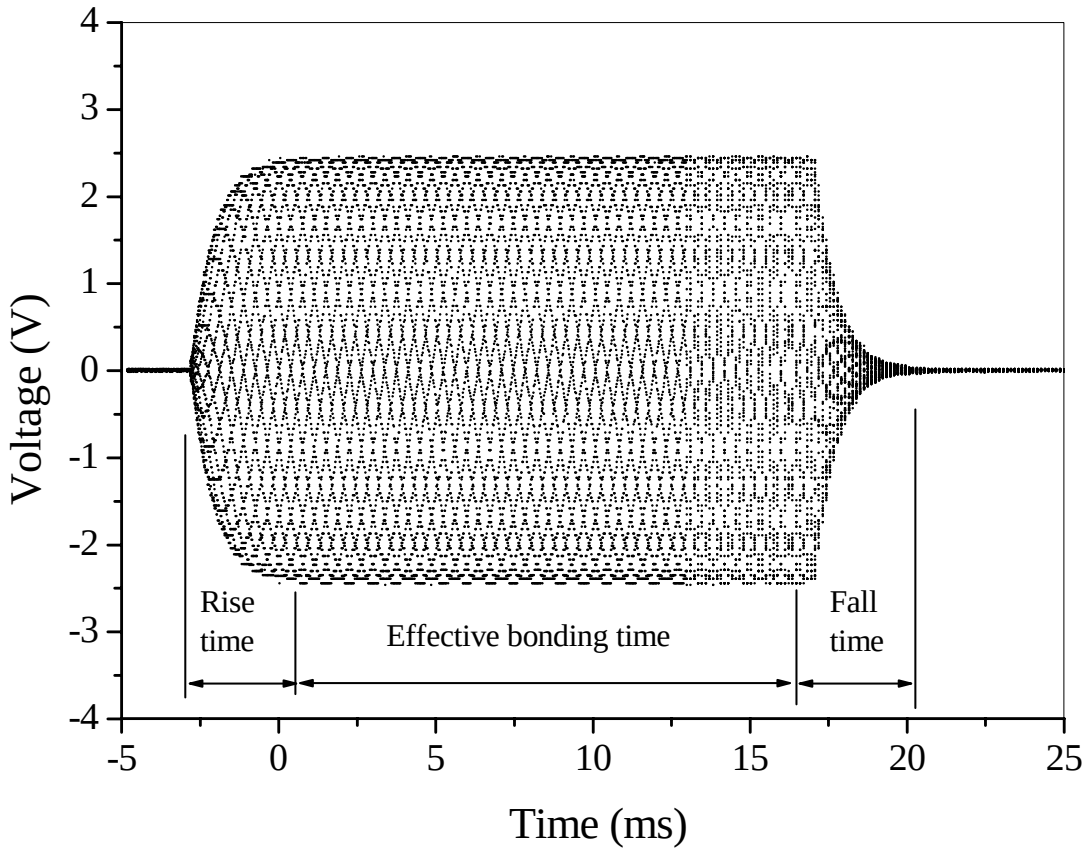

Fig. 2.26 A typical ultrasonic vibration signal of the transducer. [37]

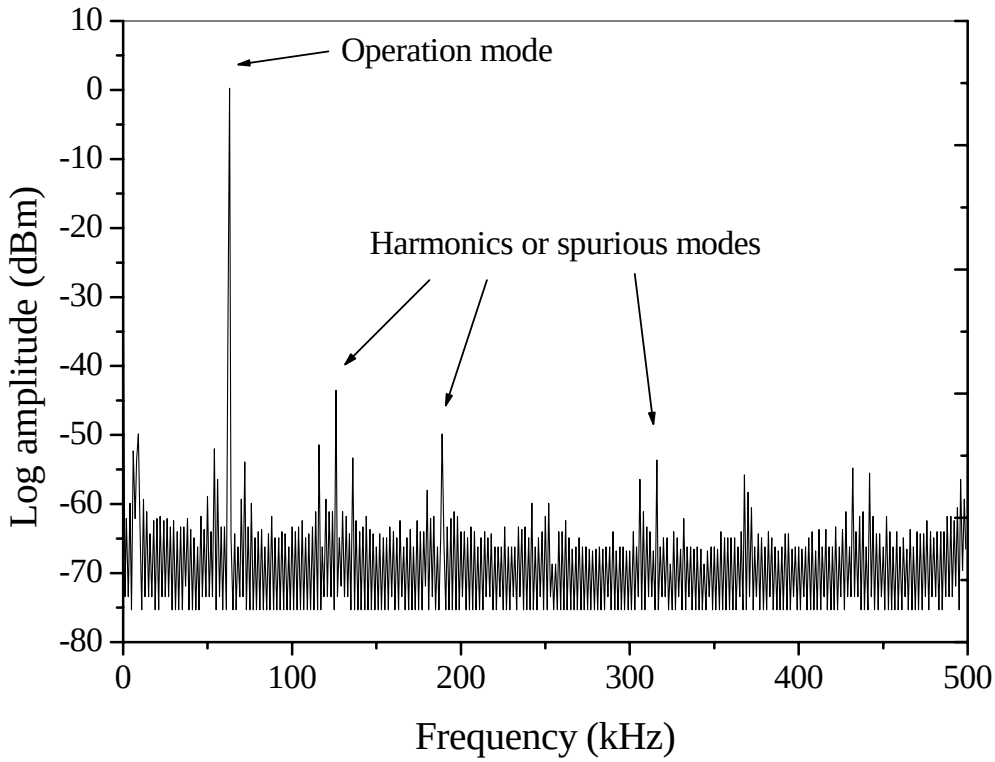

Fig. 2.27 FFT result of the ultrasonic vibration signal from the composite transducer. [37]

2.4.4 Summary

A summary of the characteristics of both composite and conventional PZT transducers from the work together with the findings in [37] are listed in Table 2.4. Due to the effect of polymer damping, the measured Q_m of the composite transducer (with ϕ =0.91) at the working axial mode is around 611. The conventional PZT transducer, in contrast, has Q_m ~ 1084 which is 77% higher and thus exhibiting a sharper resonance. Under a lower Q_m operation, the composite transducer will be more adaptable to various types of bonding surfaces, and can provide a reliable working platform for implementing fine pitch bonding. The F/S ratio which is the ratio of the longitudinal to lateral displacement amplitudes at the wedge tip can be used as a measure of the purity of the axial vibration. The composite transducer has a

larger F/S ratio and will facilitate fine pitch bonding. In a ceramic transducer, due to the presence of higher frequency harmonics in the driving voltage, higher harmonic vibration are excited and the measured waveform at the wedge tip is deformed due to these complex vibrations. In a composite transducer the harmonics content of the vibration is expected to be greatly reduced.

TABLE 2.4 SUMMARY OF COMPOSITE AND CONVENTIONAL PZT TRANSDUCER CHARACTERISTICS. [37]

Transducer type	**ASM-PZT8**	**ϕ= 0.91 Composite**
Resonance frequency, f_r (kHz)	64.25	62.8
Impedance, Z_m (Ω)	6.69	11.35
Mechanical quality factor, Q_m	1084	611
Electromechanical coupling factor, k_{eff}	0.378	0.361
Average vibration amplitude at:		
Horn end, Front (μm)	0.788	0.788
Wedge tip, Front (μm)	1.614	1.723
Wedge tip, Side (μm)	0.167	0.051
F / S ratio	9.66	33.98
Average rise time, t_r (ms)	3.0	1.6
Average fall time, t_f (ms)	3.0	2.0
Purity by FFT (%)	90.6	94.2

2.5 Process Studies

In the previous section, the composite transducer has been shown to offer superior and unique features over the conventional full ceramic transducer. In this section, detailed process studies to assess the advantages of the composite transducer in actual bonding are presented. The bonding performance will be benchmarked against the conventional PZT transducer.

2.5.1 Test Vehicles

- ***Bonder Machine*** – A commercial wedge bonder, AB520A (Fig. 2.28) by ASM Assembly Automation Ltd., has been used in the study. It is an automatic ultrasonic wedge bonder for bonding of chip-on-board (COB), multi-die and light emitting diode (LED) devices. The maximum speed is 5 wires/second.

Fig. 2.28 An ASM AB520A automatic wedge bonder.

- ***Bonding Specimens*** – The specimen used in the process study is ASM printed circuit board (PCB) testing die. It consists of two silicon chips with aluminum bond pads that attached to a gold coated PCB by die bonding (Fig. 2.29).

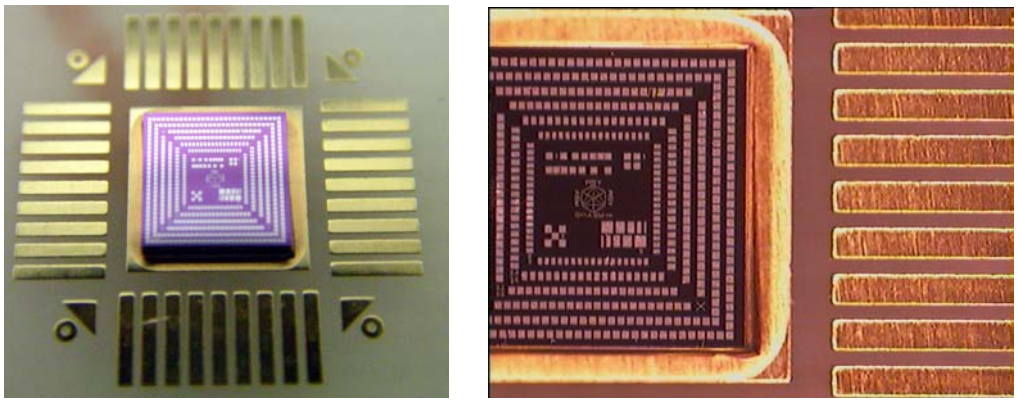

Fig. 2.29 ASM Testing PCB.

- ***Bonding Tool*** – The bonding wedge is from Gaiser Ltd. with model number 2130-2025. The bonding tool is made by tungsten carbide (WC) which is designed for 64 kHz operation (Fig. 2.30).

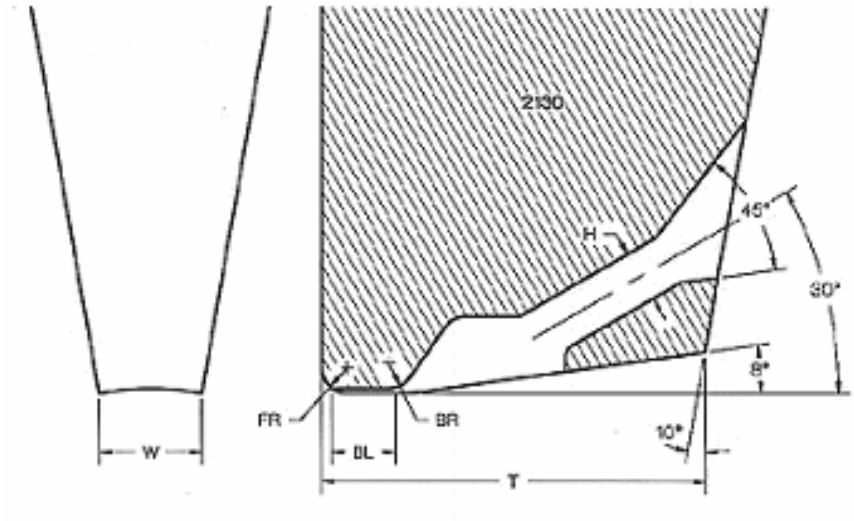

SERIES Dash Number	H in./µ ±.0002/5µ	BL in./µ ±.0002/5µ	W in./µ ±.0002/5µ	FR in./µ ±.0002/5µ	BR in./µ ±.0002/5µ	T in./µ ±.0005/13µ
2025	.0020 / 51	.0025 / 64	.0040 / 102	.0010 / 25	.0010 / 25	.0150 / 381

Fig. 2.30 Gaiser bonding wedge.

- ***Bond Wire*** – The wire used in the study is aluminum alloy wire (99% Al and 1% Si) purchased from Tanaka Ltd.. The diameter of the wire is 1.25 mil (55 μm).

2.5.2 Bonding Evaluation

- ***Pull Test***

The wire bond pull test is the most universally accepted method for controlling the quality of the wire bonding process. It is a destructive test to evaluate the tensile strength of a bond wire. This test gives important information for evaluating bonding quality and reliability. However, the pull results are strongly dependent on the geometry for the wire looping and normalization is needed to give absolute values of wire tensile strength by

$$F_1 = \frac{F\cos(\theta_2 - \beta)}{\sin(\theta_1 + \theta_2)}; F_2 = \frac{F\cos(\theta_1 + \beta)}{\sin(\theta_1 + \theta_2)} \quad (4)$$

where β is the pull angle, which is positive when the pull direction is deviated from the first bond (bond 1 is Al wire bonded to an Al bond pad on the die). F_1 is the component of force acting along the wire at bond 1, F_2 along the wire at the second bond (bond 2 is Al wire bonded to a Au bond pad on the PCB substrate). θ_1 and θ_2 are the wire angles of the two bonds, which can be easily calculated based on the hook attachment position, and the hook heights from the two bonds. A schematic diagram of wire pull test is shown in Fig. 2.31.

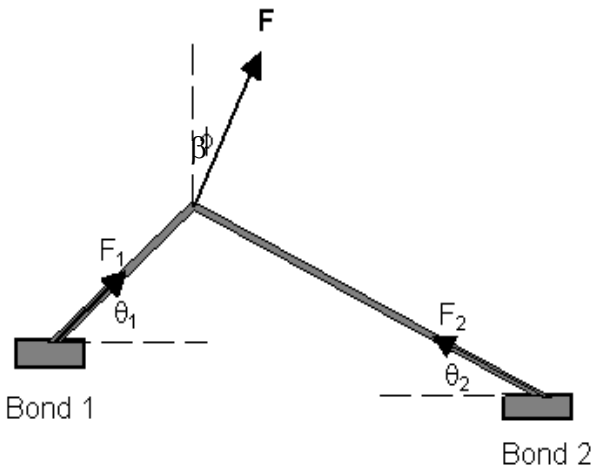

Fig. 2. 31 A schematic diagram of the pull test.

After the destructive pull test, the wire will be broken at its weakest point. Normally, the wire will either break at its heel or its bonding interface. In case that the wire is broken at its heel and leaves a portion of wire on the bonding specimen, it is referred to as a good bond. It has ensured that the bonding has sufficient strength and good electrical connection. If the whole wire has been removed after the pull test, and leaving only a bonding mark on the specimen, the case is referred to as a peel-off bond which is classified as a disqualified bond. (Fig. 2.32)

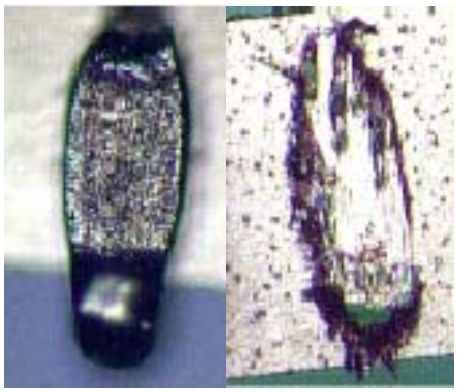

Fig. 2.32 Typical failure modes after pull test –

a good bond (LHS) and a peel-off bond (RHS).

- ***Shear Test***

Although pull test is the primary method for bonding evaluation, it fails in determining the real strength of the bonding interface. The reason is that a large interfacial welded area is formed after the bond has fully matured, and the bond width is often around 10 times larger than the wire diameter. The pull test often causes the wire to break at its weakest point usually at the transition (often referred to as the heel of the wire) of the bond. Thus, it gives no information on how strong does the wire stick on the bonding sample. Therefore, to determine the actual bonding strength, a shear test is necessary. In addition, a shear test can help to examine the cratering problems which normally cannot be found by a pull test. A commercial shear test machine, Dage 4000, used in the study is shown in Fig. 2.33.

Fig. 2.33 The shear test machine - Dage 4000.

- ***Bond Width***

The bond width is the degree of wire deformation after the bond formation. The measurement of bond width can be done using a high magnification projector or a microscope. The measurement of bond width is usually given as the factor of the original wire diameter (D). For example, a 1.6 D bond width for a 1.25 mil (50 μm) Al wire is corresponding to 2 mil (1.6 x 1.25 mil) actual bond deformation.

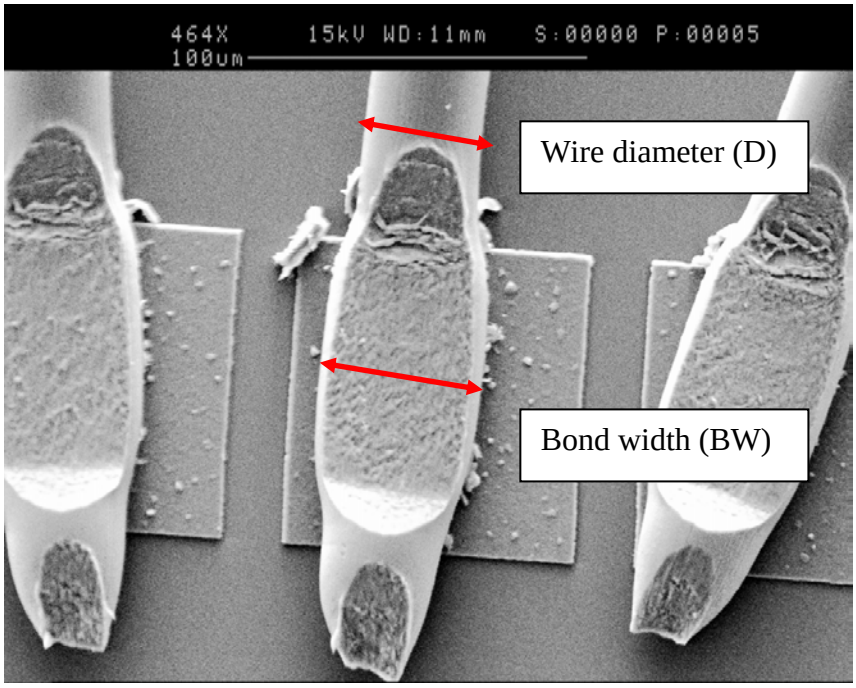

Fig. 2.34 Definition of bond width.

2.5.3 Process Windows

The process window or the operation window refers to a specific range in which the parameters can be set and a stable bonding process can be achieved. The process window depends on two major factors: the bonder machine conditions and transducer performances. The process window is highly influenced by the capabilities of the wire bonder such as the bonding speed, the control of bond force and ultrasonic energy, and the loop control and the stability of mechanical motions. The performance of the transducer also plays a significant role in determining the size of the process window. A stable and high performance transducer can widen the window which enables the bonder machine to be tuned and set-up more easily. Moreover, it will significantly increase the capability of the wire bonder to handle various types of bonding samples and increase the robustness of the machine. Therefore, a large process window is one of the most desirable and important characteristics for present commercial wire bonder. In this work, a commercial automatic wire bonder AB520A from ASM has been used as the testing platform to evaluate the process windows for a commercial full ceramic and a 7 cpd (ϕ = 0.91) composite transducer. To eliminate the influence caused by the wire bonder, the following procedures have been followed:

- ***Adding long delay time before bonding*** – Adding a long delay time before ultrasonic firing to the transducer ensures that all the mechanical vibrations have been settled before bonding. It can reduce the impact of mechanical motion and bonding speed of the wire bonder.

- ***Using parallel straight wires with the same length*** – It can reduce the impact on the looping by bonding wires with the simplest form of loop. To further reduce the noise from the wire bonder, only parallel and straight wires with a length of 2 mm will be bonded.

- ***Using the same bonder for both ceramic and composite transducer*** – It can reduce the difference in force and electronic control between two different machines.

By following the above-mentioned procedures, the process windows determined by this study will only reflect the actual capability of the transducers.

.

2.5.3.1 First Bond Process Window

The definition of the process window is based on the bond width that can be achieved in the interaction between the bond force and the ultrasonic bond power. To minimize the variation of other factors, such as measurement errors, bonding contamination, a large number of bonding samples, 150 bonded wires, were made for the bond width measurement. The post-bond inspection function of ASM wire bonder can allow the measurement of bond width in a large scale automatically. The average 1st bond width contour formed using the composite transducer and a conventional PZT transducer are shown in Fig. 2.35 (a) and (b) , respectively.

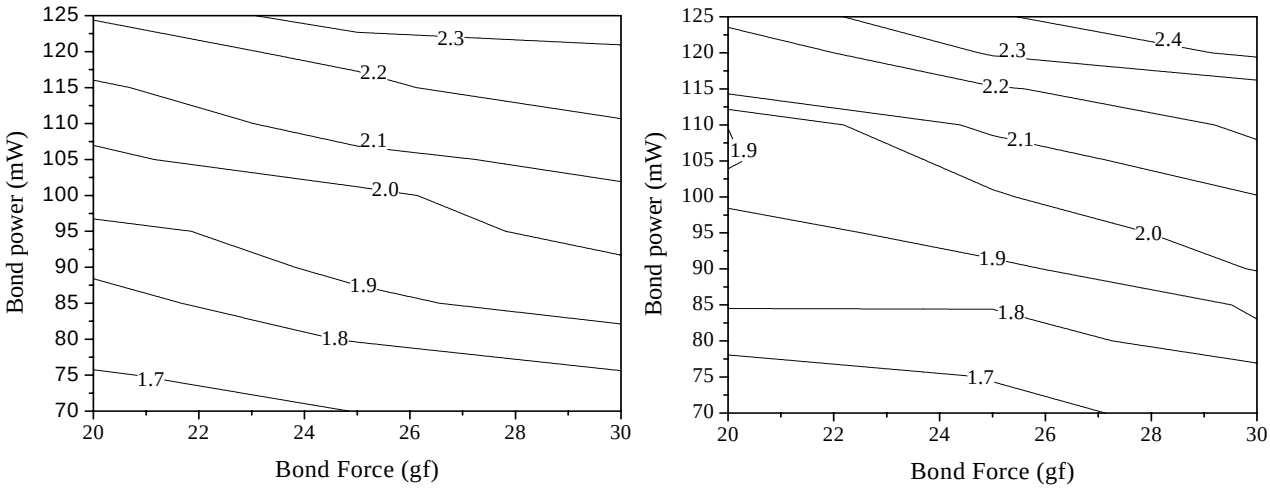

Fig. 2.35 First bond width contour plot of bonds formed using the (a) composite and (b) conventional PZT transducer.

The average bond width of both conventional and composite transducers exhibits the same trend. The average bond width increases as the ultrasonic bond power increase. The same observation has also been found on the bond force. For higher bond power, more ultrasonic energy is applied to the bonded wire and hence it facilitates the ultrasonic softening of the wire. The wire will exhibit a larger deformation under the same bond force. Similarly, even under the same ultrasonic energy, a higher bond force could squeeze the wire further and results in an increase of bond width. From the average bond width contours, they show the combined effect of how the bond power and bond force change the bond width.

In real applications, the average bond width contour does not equal to the process window of the transducer. The wire bonding technique requires an extremely reliable process and a

commercial wire bonder will need to have a bond yield of above 99.9%. The average bond width process windows can only provide the trend of interaction between the bond force and ultrasonic power. It cannot reflect the actual process capability of the transducer. As the data contour only gives an average value of the testing results for 150 wires. In extreme cases, the maximum or minimum bond width can be very different from the average value given by the process contour. For example, the average bond width of the composite transducer at the bond force of 25 g and an ultrasonic power of 105 mW is 2.0 mil. However, the maximum bond width can be as high as 2.4 mil within the 150 wires. Given the maximum allowable bond width to be 2.3 mil, the pair of the bonding parameters still falls outside the window. Therefore, the plot of process windows that takes into account the statistical estimation will be more meaningful and representative.

In actual cases, the width of a bonded wire should be as small as possible provided that it is sticking. The maximum value of the bond width will be the criteria to determine if the particular bonding parameter is within the bonding window. However, in the large scale of bonding samples, the window will be highly susceptible to any one of abnormal bonds if only maximum value is considered. Hence, the process windows that use the maximum bond width as the criterion may be misleading. To overcome the dependency on only one single bonding point, the statistical technique can be implemented. The process windows are plotted as the average bond width plus three times its standard deviation. By using the statistical technique, the process window will be more related to the real applications.

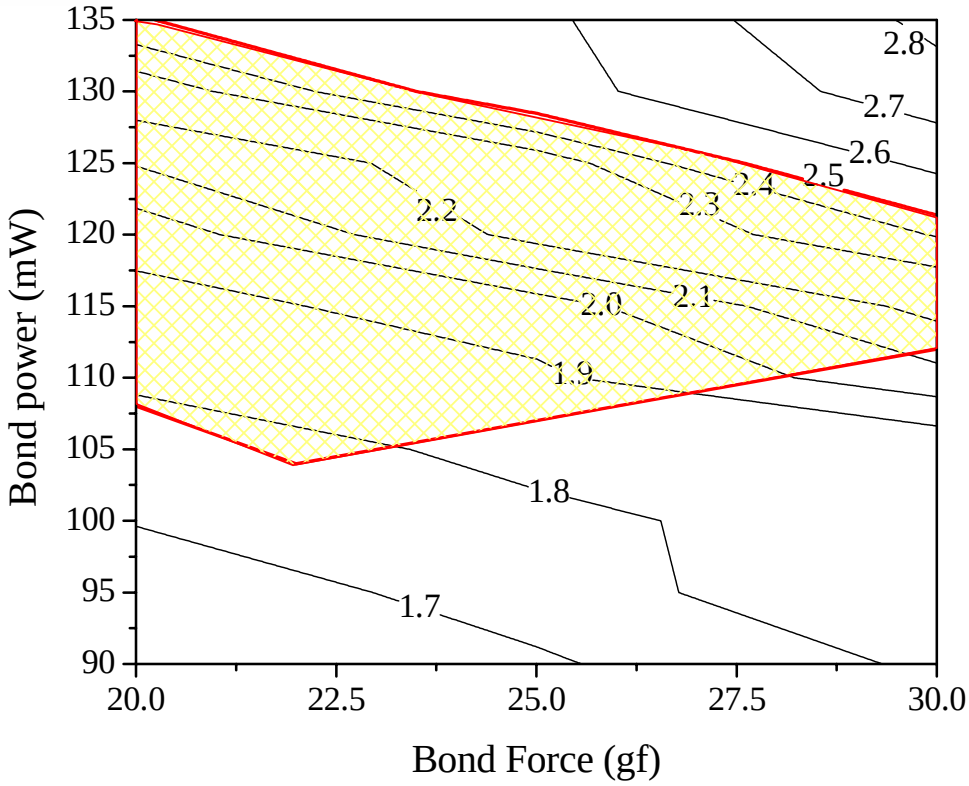

Fig. 2.36 First bond process window of the composite transducer.

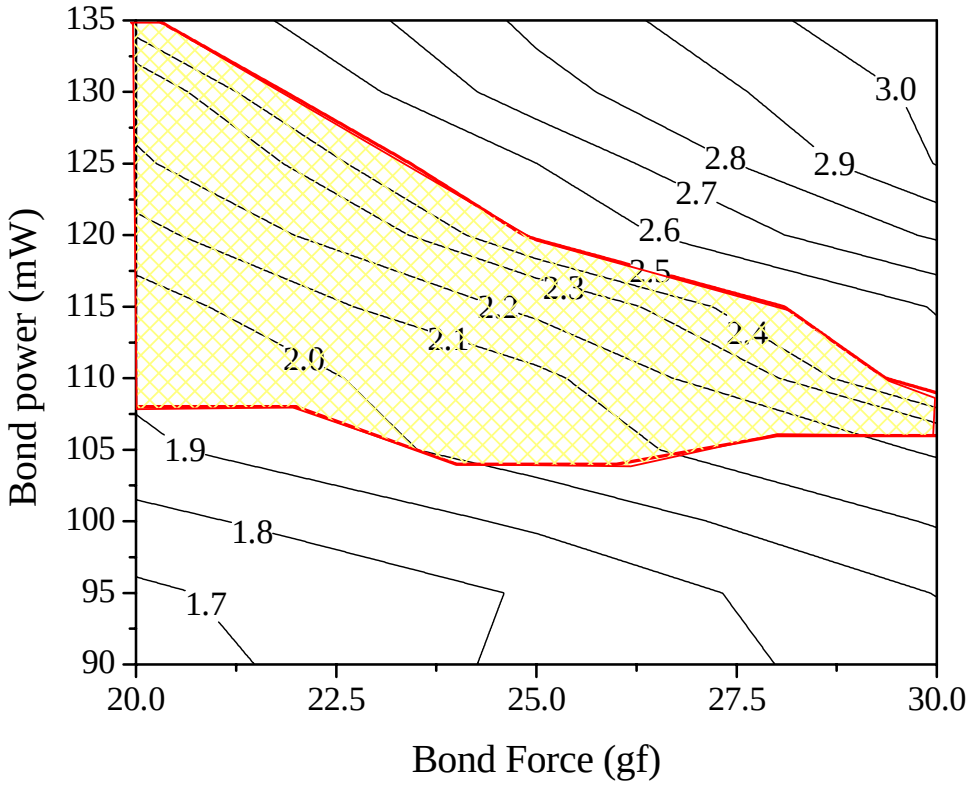

Fig. 2.37 First bond process window of the conventional PZT transducer.

The process windows based on the statistical variation of the first bond for both composite and ceramic transducer are shown in Fig. 2.36 and Fig. 2.37. The windows exhibit similar trend. The bond width increases with either an increase in bond force or ultrasonic power. For the bonder machine AB520A, the maximum allowable bond width for the 1st bond is 2.5 mil (where 1 mil = 25.4 μm). Therefore, the upper boundary of the bond width should be set at 2.5 mil. Although the deformation of the bonded wire should be as small as possible, insufficient bond deformation may cause sticking problem. Therefore, the lower boundary of the windows will be the minimum sticking bond width. The minimum sticking bond width is found by pulling a large number of the wires by a tweezer and ensure portion of the wire left on the bonding specimens. The tweezer pull method is a very common practice for the industry to quickly check the sticking condition. The sticking line is constructed by tweezer pull of a total number of 1500 wires (99.93% confidence level) of each data point and none of a non-stick wire could be detected. The process windows of bond width are therefore the area bounded by the 2.5 mil bond width contour line and the minimum sticking bond width. The process windows are highlighted in Fig. 2.36 and Fig. 2.37. When comparing the size of the process windows of the 1st bond width, the composite transducer has a total area of 155 units which is 7 % larger than that of a full ceramic transducer. In addition, the minimum bond width that can be achieved for the composite transducer is around 1.78 mil at a bond force of 22 g and ultrasonic power of 105 mW. However, the same condition for the conventional PZT transducer will be 20 g bond force and 108 mW ultrasonic power. The bond width is 1.9 mil which is around 10% large than the composite transducer. It gives evidence that the composite transducer gives more consistent and finer-pitch bonding at the 1st bond.

2.5.3.2 Second Bond Process Window

The material control of the die is usually much better than that of the PCB substrate. Therefore, the difference of the process windows of composite and conventional PZT transducer would not be too much. During the bonding on the PCB (2nd bond), due to the material variation, a robust transducer is highly desirable. The evaluation of process windows on 2nd bond will therefore give more information on the transducer performance. The bonding for the 2nd bond window evaluation will be identical to the 1st bond. The average bond width contours by average 150 wires for each data point are given in Fig. 2.38. Similar to the 1st bond, the application of bond force and ultrasonic power will increase the wire deformation as explained before. When compared to the 1st bond, the 2nd bond is very sensitive to the bonding parameters. It can tell from the fact that the contour lines are more closely packed in the 2nd bond. Therefore, the adjustment of 2nd bonding parameter is usually more challenging. In some worst case, the process window may not exist.

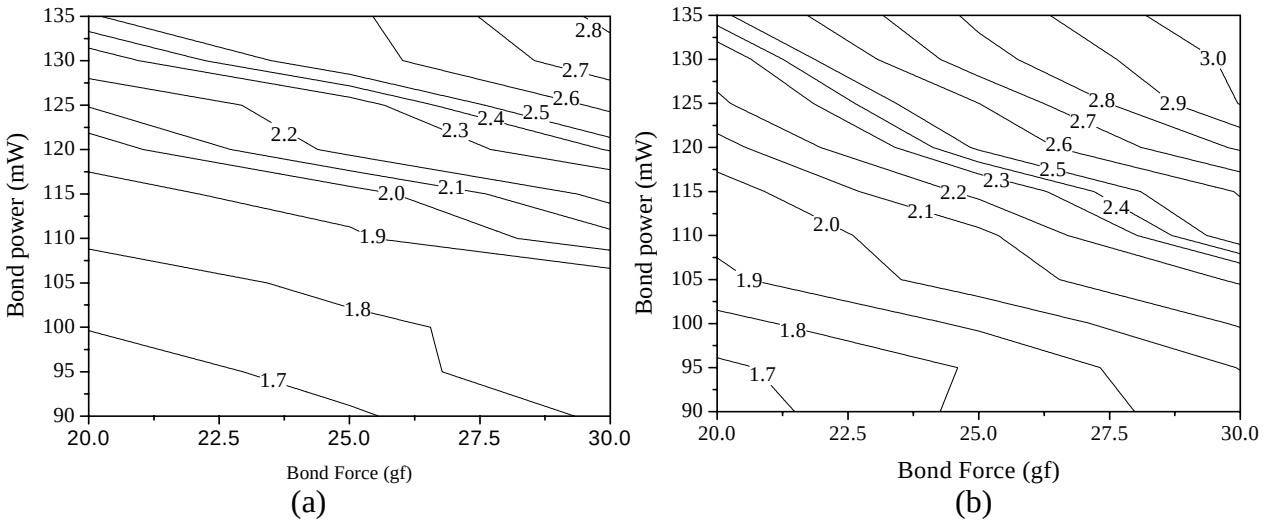

Fig. 2.38 Second bond width contour plot for bonds formed using the (a) composite and (b) conventional PZT transducer.

Similarly, the process windows for both composite and conventional PZT transducer will be determined by adding 3 times the standard deviation on each corresponding data point. The process windows for the composite and conventional PZT transducer are shown in Fig. 2.39 and Fig. 2.40, respectively. The 2nd bond process window is generally smaller. At the higher bond force region ($>$27 g), no process window can be found. The PCB for this test is not suitable for using high bond force. The window size measured for the composite transducer is 68 units and for the conventional PZT transducer is 32 units. Therefore, the composite offers a window which is 47% larger than the ceramic transducer.

The composite transducer has a lower mechanical quality factor such that it gives larger bandwidth. The larger bandwidth makes the transducer more stable and less susceptible to external variation. It can tell by the 2nd bonding windows on which the gold pads on PCB substrate has a much larger material variation. The material variation seems to have less impact on the composite transducer. By using the composite transducer, the wire bonder has improvements on the bonding capability particularly in the bond width of 2nd bond. Not only the composite transducer make the machine easier for tuning and setup, it also offers a more robust bonding and less sensitive to external variations. It is more useful for handling of various kinds of bonding specimens. It can also help the advanced wire bonder to approach a "perfect" (100%) bonding yield.

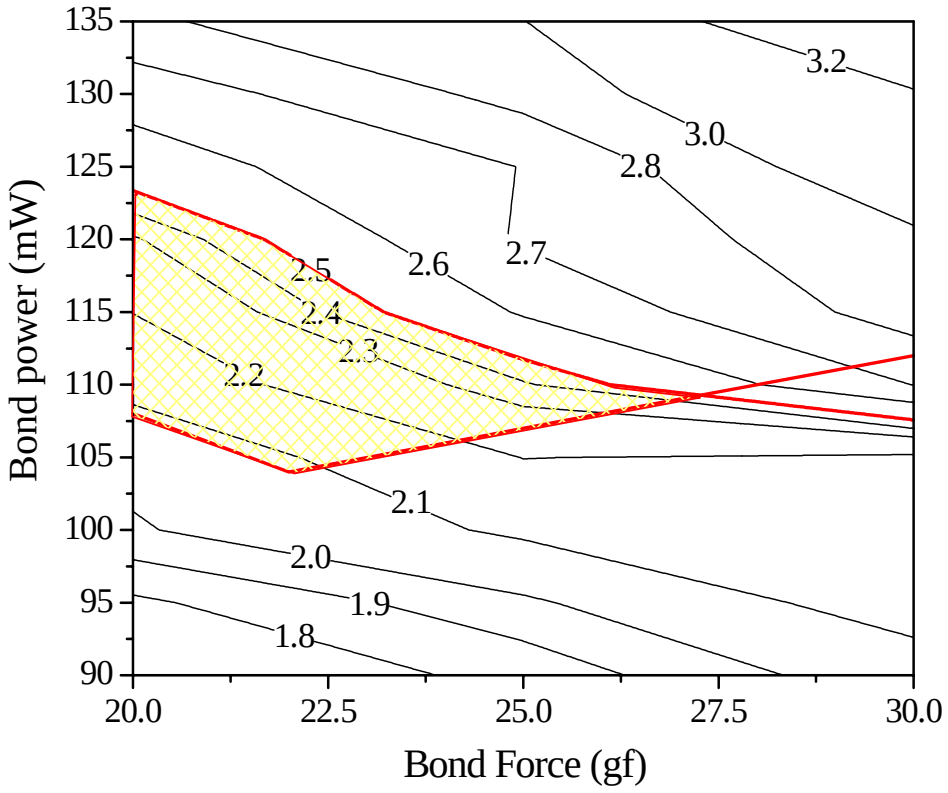

Fig. 2.39 Second bond process window of the composite transducer.

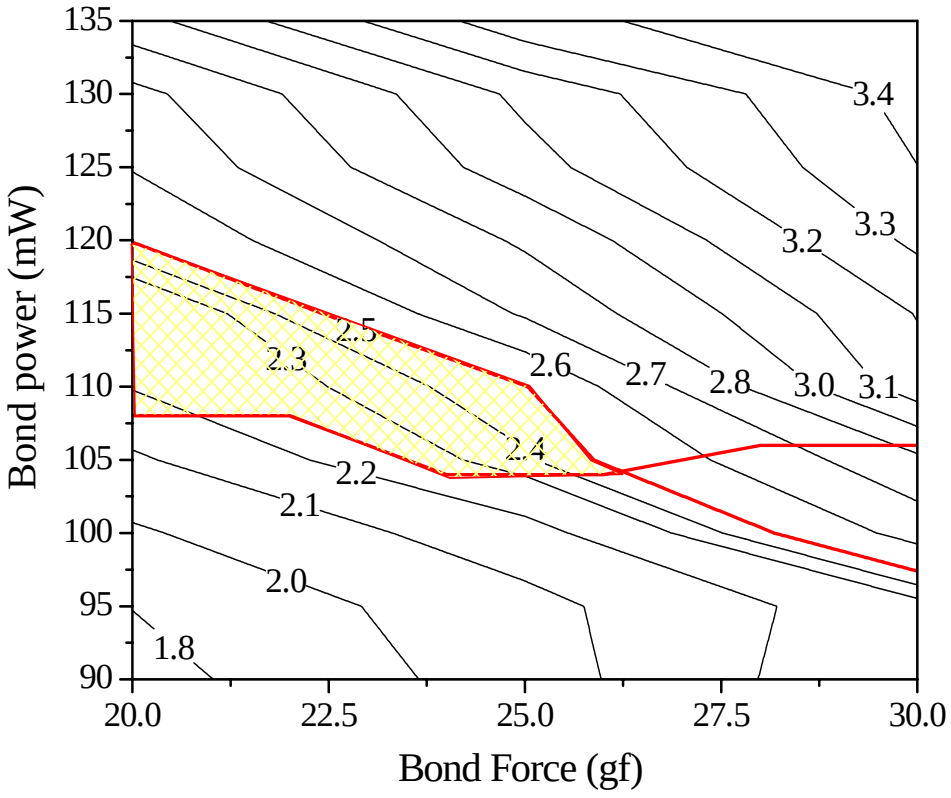

Fig. 2.40 Second bond process window of the PZT transducer.

2.5.4 Wire Pull Performance

The wire pull test is the most common technique to evaluate the wire bonding process. It gives valuable information such as the pull force and the sticking condition of the wire. The pull force is important in the sense that the wire has to sustain certain force during the post bonding processing such as encapsulation. If the wire exhibits a small pull force, it may break during the flowing of epoxy. Moreover, the sticking condition can also be examined by the pull test. A desirable bonded wire will break at its weakest point, usually at the bond heel, after the destructive pull test. The significance of the sticking is to ensure sufficient intermetallic layer (Au-to-Al bonding) or material diffusion (Au-to-Au bonding) to be formed. The intermetallic layer or diffusion is essential for good electrical contact between the wire and bonding pad.

The pull force is plotted against the wire deformation by varying the ultrasonic power. The bond force and bond time are fixed at 18 g and 20 ms. As the die has a better material control, the pull force will be focussed on the 1st bond. Each data point contains the average pull force of 20 wires at different bond widths and pull force. The pull position is biased to the 1st bond location and therefore the wire can be either peeled off at the 1st bond or broken at the 1st bond heel. The pull test results for the composite and conventional PZT transducers are plotted in Fig. 2.41 and Fig. 2.42, respectively.

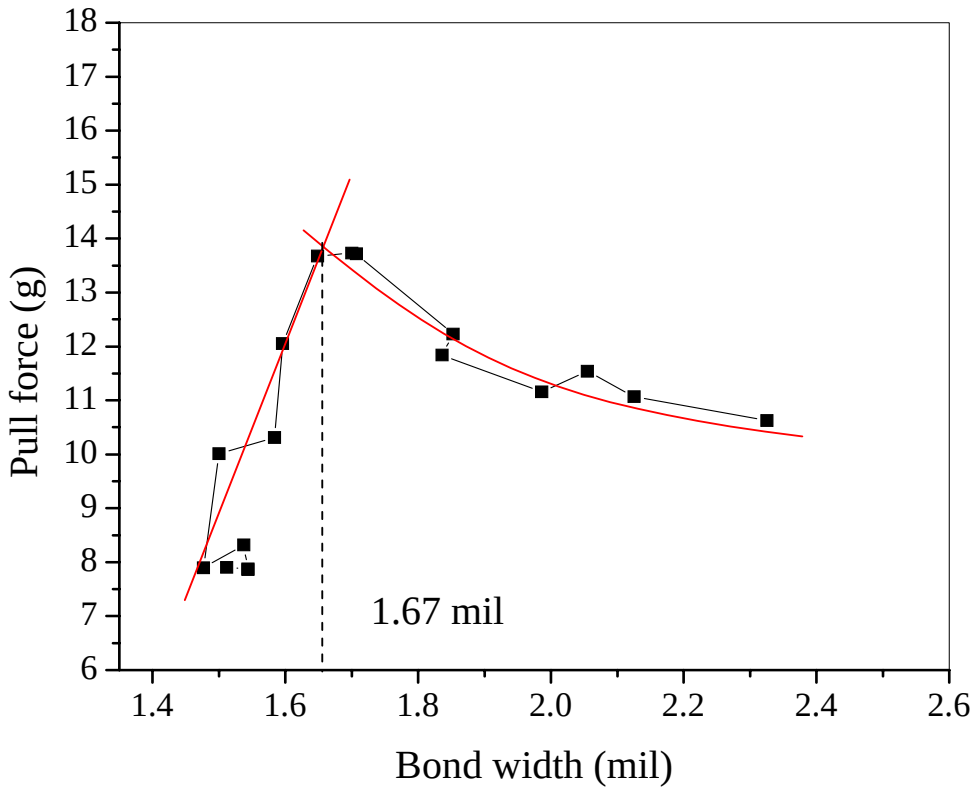

Fig. 2.41 Pull force vs bond width for the composite transducer.

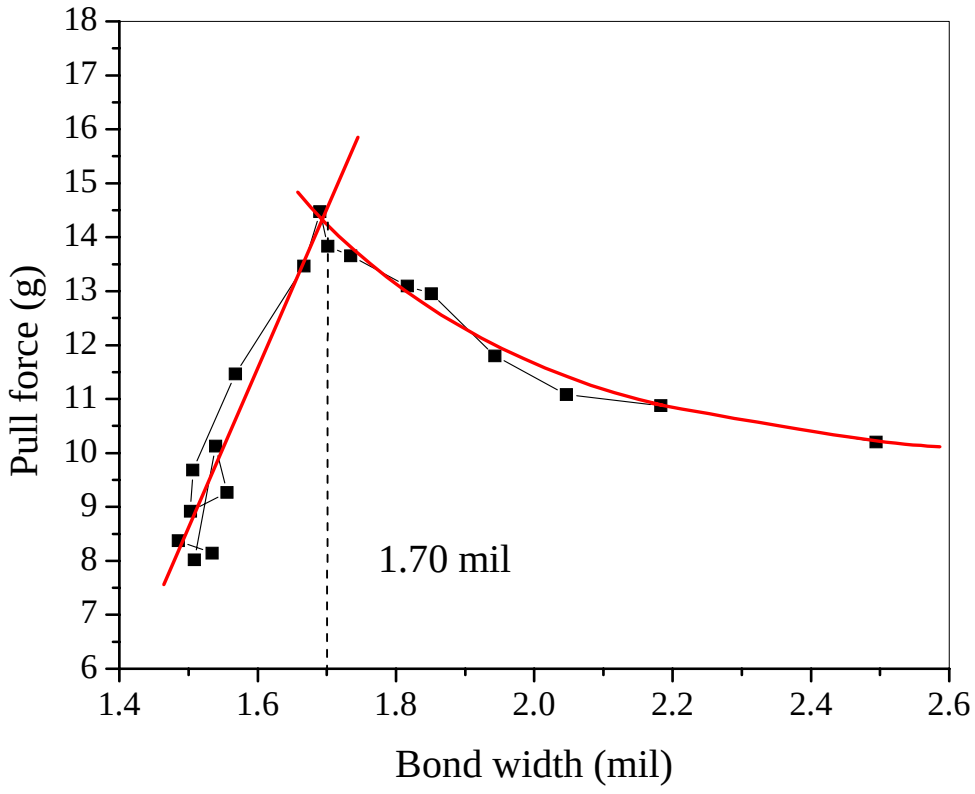

Fig. 2.42 Pull force vs bond width for the PZT transducer.

The pull force for both transducers first increases to a maximum and start to drops gradually. The maximum pull force achieved for both transducers is around 14.5 g at which the composite transducer has an average bond width at 1.67 mil. The conventional PZT transducer gives maximum pull force at 1.70 mil. In the graphs, the data have been fitted to two curves. The first monotonically increasing curve represents the strength of the interfacial bonding strength between the wire and the silicon die. When the ultrasonic power increases, more energy is applied to facilitate the ultrasonic joints. Not only the strength of the bonding interface increases, but also the bond width increases to allow more area to be bonded. Therefore, the pull force monotonically increases with the ultrasonic power. However, at this stage, the interfacial strength is still lower than the failure strength of the wire heel. The interface will be peeled off during the destructive pull tests. The curve is an index on the ultrasonic bonding formation between the wire and bond pad.

When the ultrasonic power is further increased, the deformation of the wire will also be increased. The gain of bond width will on one hand enhance the interfacial bonding strength. On the other hand, the heel crack will become more severe and lower the breaking load of the wire. Therefore, the wire will be broken at its heel for large wire deformation. It is still referred to as the sticking condition. The second monotonically decreasing curve represents the pull force of the heel condition of the wire. As bond width increases, the larger deformation will weaken the heel and results in lower pull force. As a result, the second curve is totally independent of the bonding interfacial condition. Whereas, it reflects the strength of the wire at its heel. At the intersection of the two curves, it is the ideal working location of the wire bonding process. It gives the finest pitch that can fulfill the sticking condition. The pull force of the wire also reaches its maximum value.

For evaluation on fine pitch capability, the bond width at the ideal position should be compared. For the composite transducer, the ideal bond width is 1.67 mil. It is around 2% smaller than the conventional PZT transducer which has an ideal bond width of 1.70 mil. Therefore, the fine pitch capability is only slightly better for the composite transducer. Both transducers can achieve maximum pull force of around 14.5 g for a 1.25 mil diameter aluminum wire.

Although the composite has only slight improvement on the fine pitch applications, it offers other advantage for less heel damage after bonding. By inserting more data point on the second monotonically decreasing curves from the pull tests, it can be found that the composite transducer gives a slight higher pull force against bond width graph at the sticking region. The results are plotted in Fig. 2.43. The composite transducer has a pull force curve at the upper-right position when compare with a conventional PZT transducer. Therefore, at a given wire deformation, the composite transducer has a higher pull force than a conventional PZT transducer in the heel broken condition. From the SEM micrograph in Fig. 2.44 and Fig. 2.45, the heel crack for a conventional PZT transducer is more severe. The serious heel crack will weaken the pull force even under the same bond width. The heel condition for the composite has lesser scrap from the wedge due to the elimination of sideway and other unwanted motions.

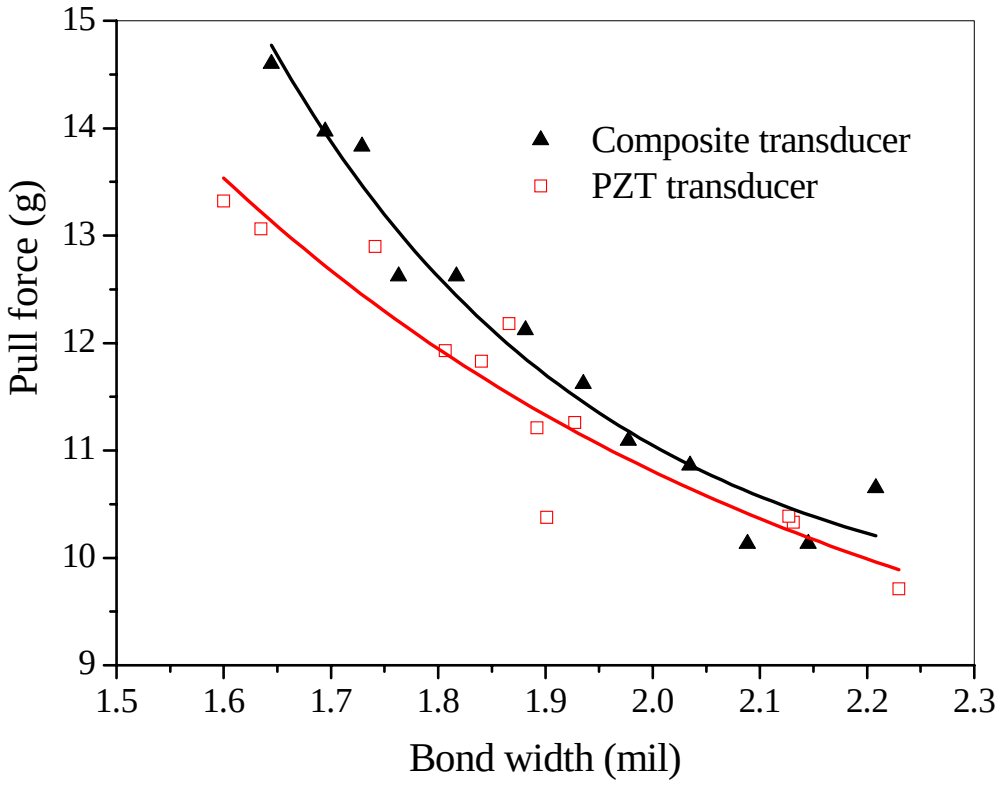

Fig. 2.43 Pull force under the sticking region for the

(a) composite and (b) conventional PZT transducer.

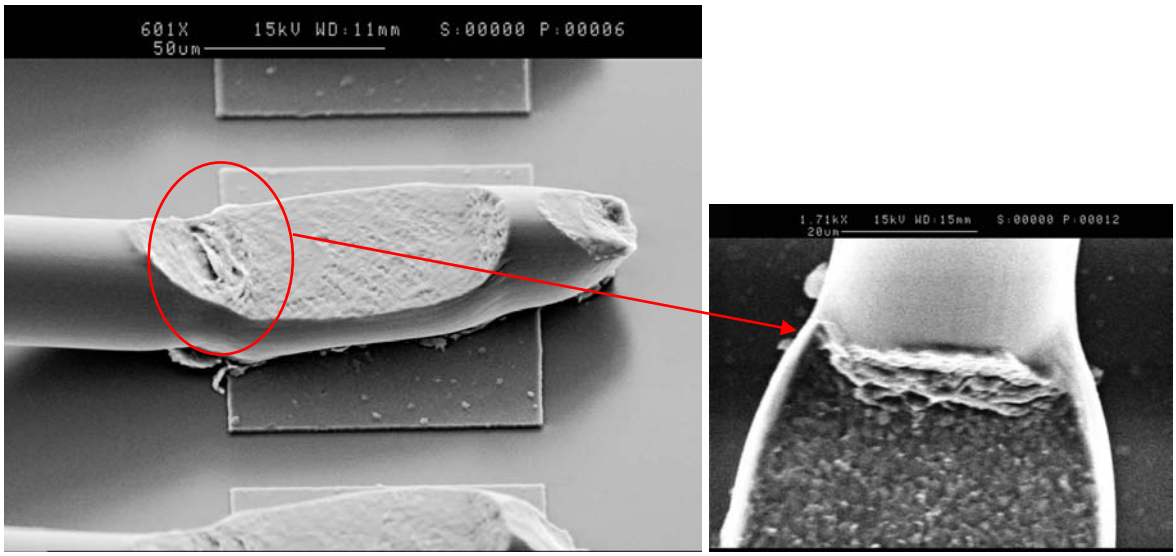

Fig. 2.44 Heel crack condition of the bond formed by the composite transducer.

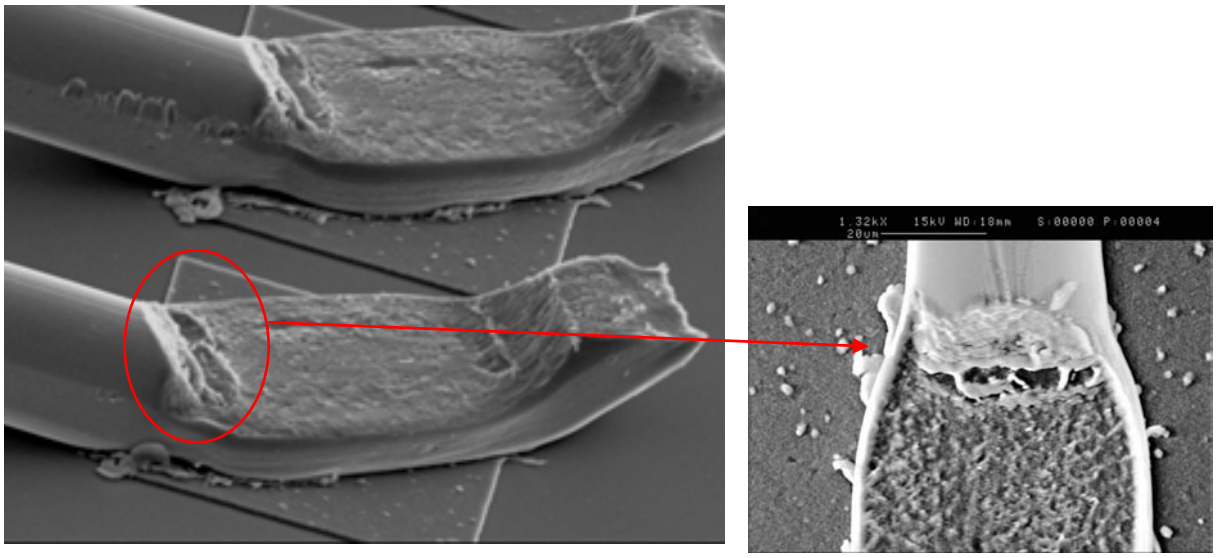

Fig. 2.45 Heel crack condition of the bond formed by the conventional PZT transducer.

2.5.5 Shear Test Performance

The shear test is used mostly for ball bonds, it is not widely used in wedge bonds. The reason is that the geometry of the ball bonds enables the shear test to be done more easily. However, for large aluminum wire (1.25 mil or above), the interfacial strength can also be successfully evaluated by the shear test method. In a shear test, a shear tool has been set 2 μm above the substrate. The shear tool will be moved at a constant speed through the bonded wire. A precision load cell connected to the shear tool can give accurate shear loading of the bonded sample. Similarly, the shear test is conducted on the 1st bond due to its better material consistency. Each data point is obtained by the average of 20 wires. The shear test results are plotted in Fig. 2.46.

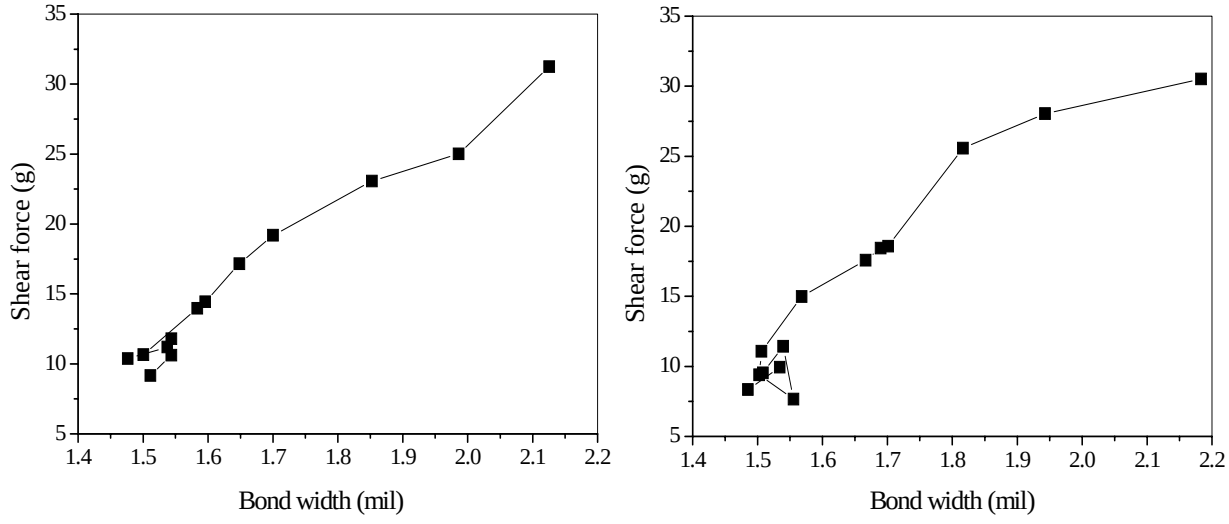

Fig. 2.46 Shear test results for the (a) composite and (b) conventional PZT transducer.

The shear force increases with the bond width. The increase of shear force comes from two areas – (1) the increase in contact area results in a gain in bond width and (a) the increase in interfacial strength results in an increase of ultrasonic energy. The lower limit for the load cell is around 10 g. Therefore, the shear force below 10 g cannot be accurately detected. Both types of transducer give very similar results. No significant difference can be found between two types of transducers. The finding agrees with the pull test results that the composite transducer offers similar interfacial bonding strength.

2.5.6 Bonding Consistency

Theoretically, the same bond width should be able to repeat under the same bonding parameters such as bond force, ultrasonic power and bond time. However, during the real bonding applications, due to the variation of bond pad material, mechanical vibration of the machine, the stability of transducer, etc, the actual bond width will fall into a certain range. The range of bond width should be controlled to as narrow as possible in order to achieve fine pitch and high yield bondings. Nevertheless, a consistency in bonding can also widen the process windows. To achieve a consistency in bonding, a robust transducer is essential. To evaluate the robustness of the transducer, a large number of bond width is measured to evaluate the bond width at the same bonding parameters. The bonding parameters are selected based on the optimized settings from the previous process windows as shown in Table 2.5. However, the bonding parameters are further fine-tuned to fit the actual bonding requirements.

TABLE 2.5 BONDING PARAMETERS FOR THE CONSISTENCY TESTS.

	Composite transducer		Conventional PZT transducer	
Parameters	Force (g)	Power (mW)	Force (g)	Power (mW)
1st bond	22	110	20	110
2nd bond	22	105	20	115

A total number of 10 testing PCB are used to evaluate a single bonding parameter. After counting on the measurement yield loss by the post-bond inspection of ASM bonder, the number of measurements for each setting is around 1300 to 1500. The populations of the bond width for both 1st and 2nd bonds are plotted in Fig 2.47 and Fig. 2.48. The results are further fitted to a Gaussian distribution. From the 1st bond consistency, the SD of bond width for the composite transducer is 0.061 mil which shows an 18% improvement when compared to the conventional PZT transducer with 0.074 mil for 1st bond width SD. The mean bond width is found to be 1.79 mil by using the composite transducer. The reduction in the value of mean bond width and its reduced SD will increase the fine pitch capability of the composite transducer. For the conventional PZT transducer the mean 1st bond width has to be 1.98 mil in order to have good bonding performance. It is noted that the requirement of fine pitch capability is mostly focussed on the 1st bond. Agreed with the pull test results, the composite transducer offers better fine pitch handling capability. By the using composite transducer, a 9.6% reduction of average 1st bond width can be achieved by using 1.25 mil aluminum wire. For the 2nd bond, the improvement in the consistency is more obvious. The SD of 2nd bond width has been reduced from 0.148 mil to 0.08 mil after using the composite

transducer. The improvement of SD is 46%. The great reduction on SD allows the composite to perform stable bonding with relatively lower bond width. Bonding consistency tests are summarized in Table 2.6

TABLE 2.6 SUMMARY ON THE BONDING CONSISTENCY TESTS.

	Composite transducer				**Conventional PZT transducer**			
Bond width	Max. (mil)	Min. (mil)	Mean (mil)	S.D (mil)	Max. (mil)	Min. (mil)	Mean (mil)	S.D (mil)
1st bond	2.06	1.60	1.79	0.061	2.18	1.76	1.98	0.074
2nd bond	2.12	1.43	1.72	0.080	2.22	1.39	1.83	0.148

The wider bandwidth and lower mechanical quality factor of composite greatly improve the robustness and stability of the composite transducer. When compared with a conventional PZT transducer, the application of 1-3 composite in the wire bonding transducer can improve the bonding stability. When there is a large material variation of the bond pad, the composite transducer has demonstrated the bonding consistency by it robustness. A stability of bonding can also improve the fine pitch capability and widen the process windows.

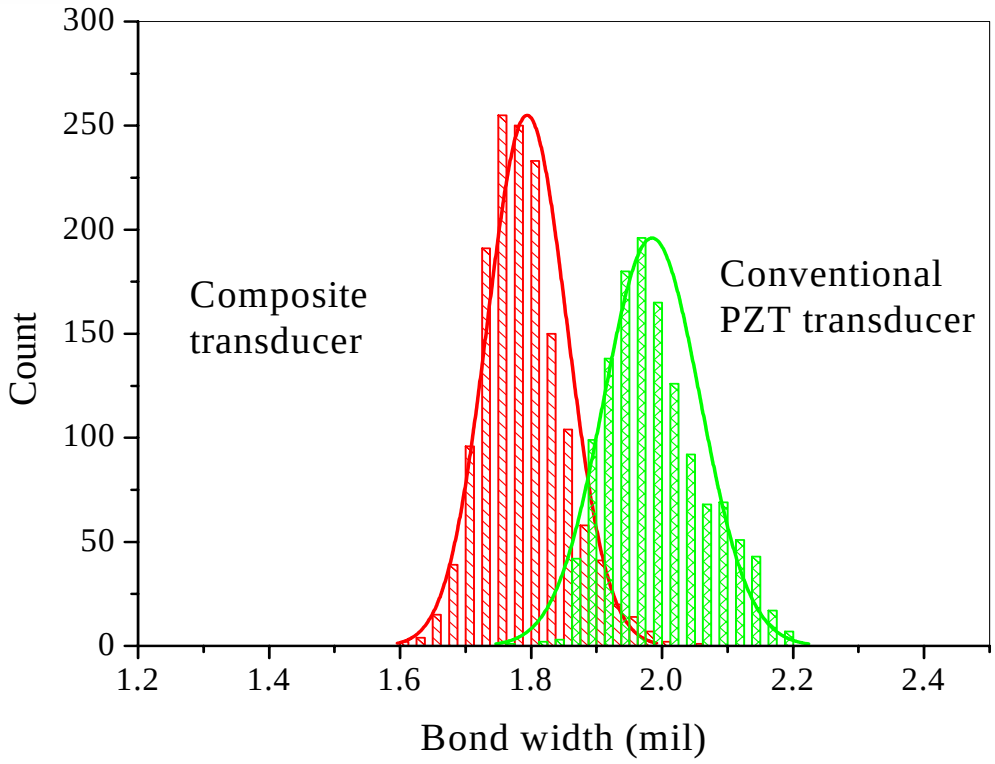

Fig. 2.47 First bond width distribution.

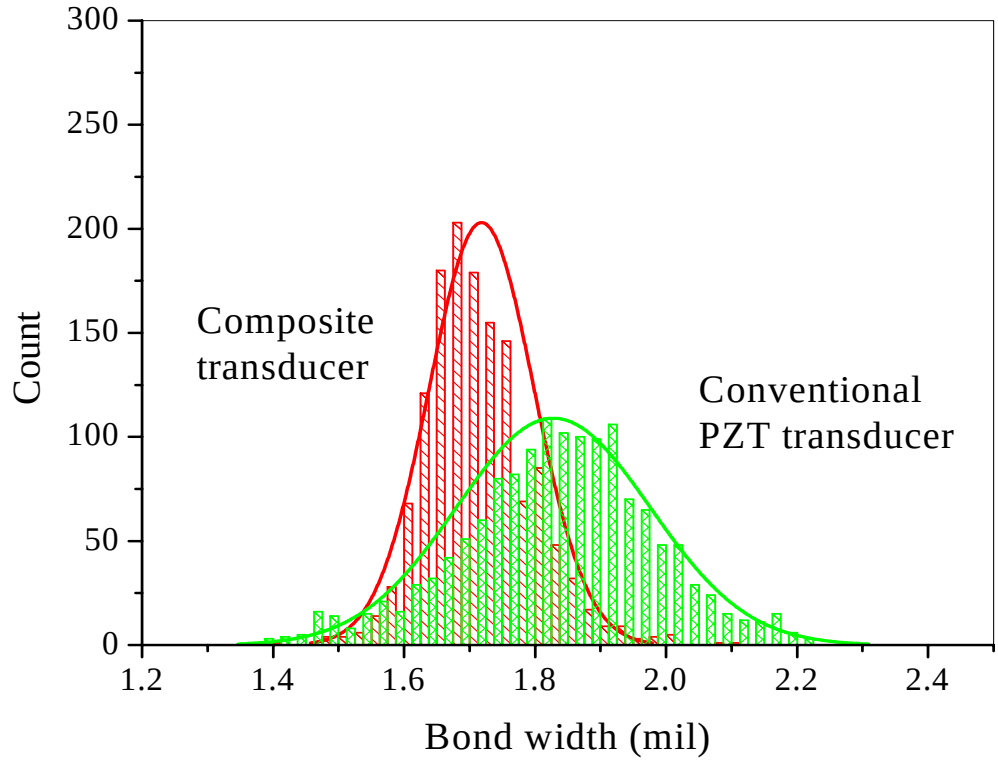

Fig. 2.48 Second bond width distribution.

2.5.7 Summary

According to the process studies on the benchmarking of two different types of transducer, the results are summarized in Table 2.7. The composite technology used in wire bonding transducer for a wedge aluminum bonder offers 4 major advantages:

- Large process windows for both 1st and 2nd bond – The wire bonder can be more easily tuned up and it also allows the bonder to handle different bonding materials.
- Fine pitch capability – Both process windows and pull test indicate the composite transducer can achieve finer bond width. It is a great benefit for the minimization of IC chips for high IO devices.
- Higher bonding consistency – It increases the robustness of the bonder machine and also can benefit the bonding yield.
- Less heel crack – It not only benefits the pull force, but also helps to reduce wire damage on the looping process.

TABLE 2.7 SUMMARY ON THE BONDING PERFORMANCE OF COMPOSITE AND CONVENTIONAL PZT TRANSDUCER.

		Composite	Conventional
Process windows	1st bond (units)	155	145
	2nd bond (units)	68	46
Fine pitch capability on 1st bond	Windows (mil)	1.78	1.90
	Pull force (mil)	1.67	1.70
Bonding consistency	1st bond SD (mil)	0.061	0.074
	2nd bond SD (mil)	0.08	0.148
Heel damage		slight	severe

2.6 Summary and Conclusions

In Chapter 2, a complete study on composite transducer technology used in wire bonding has been conducted. 1-3 piezocomposite rings fabricated by the dice-and-fill method, were used to replace the conventional PZT rings in the Langevin driver of the transducer. The cutting edge composite technology has made a positive impact on the current transducer design. It makes a break-through on the traditional and near-perfect wire bonding technology. Therefore, the 1-3 composite transducer has a great benefit to the microelectronic package industry.

The design and evaluation of the 1-3 composite transducer technology on wire bonding has been summarized as follows. First, the vibration characteristics of PZT ring was reported.

By studying the PZT ring, we can identify the optimized dimensions for the transducer design. These optimized dimensions can further be applied to the 1-3 composite ring. Second, the characteristics of 1-3 composite ring have also been studied. The FEM was adopted as the composite ring made by the dice-and-fill method has a very large PZT pillar aspect ratio and analytical approach is no longer accurate enough for the analysis. The fabrication of 1-3 composite ring was optimized by compromising cost and performance. Then, based on the optimization, a wire bonding transducer with 7 cpd (ϕ = 0.91) was fabricated. The composite transducer was characterized and benchmarked against a conventional PZT transducer. Finally, detailed process studies were conducted by comparing the bonding performance between the composite and conventional PZT transducers.

The results show that the composite transducer offers several advantages on actual bonding applications. It includes larger process windows, better fine pitch capability, higher bonding consistency and less heel crack. All those advantages are unique for the novel composite transducer and not easy to achieve in the conventional one. It is not hard to imagine that the use of 1-3 composite rings on the transducer will provide a huge practical benefit in the industry.

.

CHAPTER THREE

THERMOSONIC FLIP CHIP TRANSDUCERS

3.1 Introduction to Thermosonic Flip Chip

Due to the demand and the fast growing of smaller, faster and cheaper electronic devices, the wire bonding technology has been pushed to denser and denser packing. Nowadays, the wire bonding technology has almost reached its limit for fine pitch and high input and output (IO) density applications. Even though with the composite technology, it becomes a very challenging task for bonding wires with pitch less than 35 μm. Flip chip packaging has become an alternative technology of choice for high IO and clock speed devices. One of the most attractive features of flip chip bonding is its minimal interconnection length between the chip and substrate. It can significantly reduce the electrical inductance that is particularly desirable for high clock speed devices [51]. Moreover, the IOs in the form of bumps can be spread over the whole chip surface to form an area array (Fig. 3.1). It allows a much higher IO density to be achieved. The capability of bonding all the IOs within one single step also makes the flip chip approach a cost effective choice.

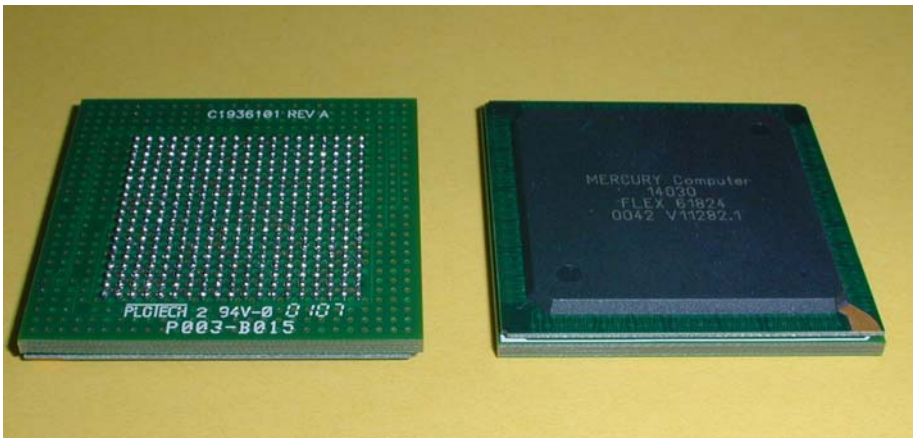

Fig. 3.1. A flip chip ball grid array (BGA) package. [52]

Flip chip techniques have been spreading rapidly in the last few decades. Various connection methods have been proposed. Among all the flip chip methods, the thermosonic (TS) flip chip approach has attracted a lot of attention recently. The process of TS flip chip can be considered as a modified method from the conventional wire bonding technique. Ultrasonic energy is applied to facilitate the bonding process through an ultrasonic transducer. The major difference from wire bonding is that the TS flip chip performs several to several hundred bondings at the same time. Depending on the vibration locus of the bonding tool, the TS flip chip can be divided into two approaches, namely the transverse and longitudinal flip chip. Fig. 3.2 illustrates the configuration of both transverse and longitudinal flip chip bondings. Most conventional wire bonding is done by transverse bonding. The bonding tool vibrates in-plane with the bonding sample. The sliding motion of the chip generates frictional shear force within the bumps. However, in the longitudinal bonding, the tool vibrates out-of-plane with respect to the chip and creating a hammering action. The bumps will then be subjected to an uniaxial compressive force.

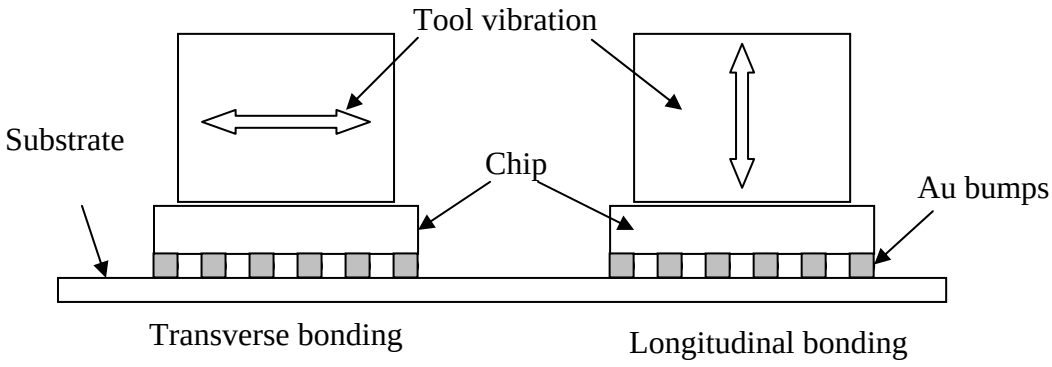

Fig. 3.2 Schematic diagram for transverse and longitudinal flip chip bondings.

Kang at el has done one of the pioneer work to demonstrate the idea of thermosonic flip chip bonding with both modelling and experimental methods in 1995 [53]. He has estimated, by using energy method, that the length and mass of the tool has a critical impact on the flip chip system. In 1997, *McLaren et al* has developed the TS flip chip process for the assembly of a smart pixel array using an 8 x 8 IOs device [54]. The process development was based on a transverse transducer. It involved the formation of an intermetallic layer or material diffusion between the gold bumps and the bonding substrate. The idea of longitudinal bonding in TS flip chip was first proposed by *Tan* in 1998 [55]. The longitudinal flip chip is believed to offer better mechanical rigidity over the transverse system [55, 56]. Therefore, it has an advantage of maintaining perfect co-planarity especially during high IOs bonding. Recently, the TS flip chip on the assembly of surface acoustic wave (SAW) devices has been reported [57]. The reliability of the TS flip chip process has also been assessed.

In this Chapter, transducers for both transverse and longitudinal flip chip bondings have been designed and developed. The transducers were modelled and analyzed by FEM. The

characteristics of both types of transducer were compared. The pros and cons for the two flip chip approaches were assessed. It was found that longitudinal bonding gives high rigidity and can maintain perfect co-planarity under high bond force. However, the hammering motion makes it more susceptible to silicon cratering defect. The findings have been further verified by both FEM and experimental results. A novel push-pull transducer concept was proposed and developed. It consists of multi-supporting and multi-driving PZT stacks. The new transducer gives superior ultrasonic properties and ideal co-planarity despite of the value of the bond force applied. The transverse vibration of the bonding tool is also less susceptible to cratering problem. The new transducer concept has been adopted by a commercial flip chip bonder from ASM.

3.1.1. Why Choose the Thermosonic Flip Chip?

The TS flip chip process is a modification of a conventional wire bonding process. The development cost can be greatly reduced. Apart from that, other unique advantages are the main reason to drive peoples' attentions to the TS flip chip method. When compared with other flip chip technologies, the TS method offers the following advantages:

I) *Reduce Process Cycle Time*

When compared with the anisotropic conductive film (ACF) and solder reflow process, the TS flip chip allows the bonding to be maturely formed at a much shorter time. Typical bonding time for TS flip chip ranges from 0.5 s to 1.5 s, however, it takes several minutes for adhesive to be cured or solder to be reflowed in other flip chip techniques.

II) Lower Bonding Temperature

The introduction of ultrasonic energy has also significantly reduced the temperature required. A typical re-flow temperature is 220 °C and it is around two times higher than that of a TS process. Normal TS flip chip uses only 100 to 150 °C. For high frequency TS flip chip bonding developed recently, the assembly temperature can even be reduced to 60° [14]. The reduction of bonding temperature allows more choices for the assembly substrates.

III) Reliable Intermetallic Joints

The TS flip chip involves intermetallic joints of aluminum/gold system or material diffusion of gold/gold system. It is a true metallic joint which is more reliable and has lower inductance when compared with the adhesive joints by ACF.

IV) Lower Assembly Pressure

The TS flip chip requires a lower bond force (~100 g per bump) than the other methods. Less compressive bond force reduces the chance of bonding defects such as cratering to occur.

V) Fluxless and lead-free

TS flip chip is a clean process as no flux is required. The using of gold stud bump is also a lead-free assembly process.

3.1.2 Thermosonic Flip Chip Method

The TS flip chip process consists of three major steps: gold bump bonding, chip flipping and chip bonding. Each process plays a significant role in the TS flip chip and will be briefly described. The gold stud bonding is usually done by a commercial gold wire ball bonder or gold stud bumping bonder in advance. It is classified as a pre-flip-chip

process. The quality of the gold stud bumps can directly affect the bonding performance. Therefore, for the completeness of the thesis, it should not be omitted.

3.1.2.1 Gold stud bump bonding

Unlike wire bonding, the flip chip interconnection is made in the form of bumps. One of the obvious advantages of the bump connection is the reduction in interconnection length. Typical length for wire bonding is around 1 mm. However, a typical bump height might be only 50 μm which is 20 times shorter. The shorter interconnection gives lower electrical inductance and allows the electrical signal to be transmitted with less lost and lower the power requirements. Bump connections being widely used today is a lead-tin (Pb-Sn) solder bumps. The most famous of these solder bumps process is IBM's C4. Variation of the C4's processes has dominated the flip chip market nowadays. The call for need on lead-free processes has shifted the focus to other bumping material. One of alternatives is the gold bump connection. Not only gold bump is environmental friendly, but also gold offers better conductivity over solder bump. Gold has a conductivity of 2.19 $\mu\Omega$-cm which is 10 times high than the lead alloys. The use of gold bumps allows the chip to be bonded ultrasonically. The formation of gold stud bump is similar to a gold wire ball bonding. A typical shape of a gold bump is shown in Fig 3.3(a). A tail will be left at the top of the bump. The tail length must be controlled with high consistency. Sometimes, the tail or bump height can be kept in consistency by pressing and pre-deforming the bumps. This process is referred to as coining and a coined bump is shown in Fig 3.3 (b).

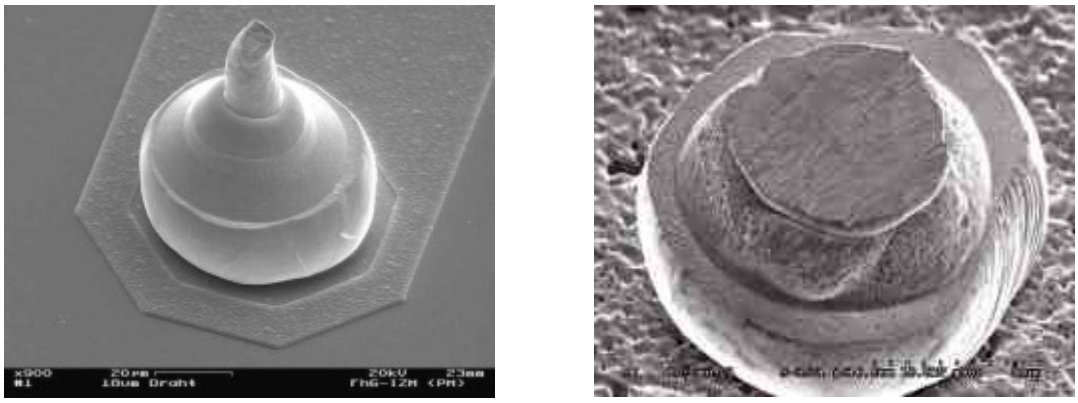

(a) (b)

Fig. 3.3 A typical gold bump (a) before and (b) after coining.

.

3.1.2.2 Chip Flipping

The chip after bumping will have all its joints facing upward. After the whole wafer has been fully bumped, it will be diced into very small units. Each unit or chip has several IOs that form a device. The diced chips will be placed on a sticky wafer tape. To pick a small chip up, an injector pin will push upwards from the backside of the die to dislodge the die from the wafer tape. Such pin usually has a smooth, highly-polished taper and a small angle, allowing gentle penetration of the wafer tape with very little tape disturbance. After dislodging the wafer tape, a pick-up arm is used to lift up the chip under the action of vacuum. After the chip has separated from the wafer tape and lifted up by the pick-up arm, the arm will flip upside down. The flipping of the die from a face-up position to a face-down position gives rise to the name "flip chip bonding" for such process. After flipping, the chip will have all its bumps facing down. The collet will move to the position of the pick-up arm. The chip can be transferred from the pick-up arm to the collet by vacuum suction again. To allow the pick up motion by vacuum, the collet has to be hollow in

structure. After the chip has been transferred to the collet, all the bumps will then be facing down. The collet will align with the circuitry of the substrate and be ready for flip chip bonding. The whole flipping process has been illustrated in Fig. 3.4.

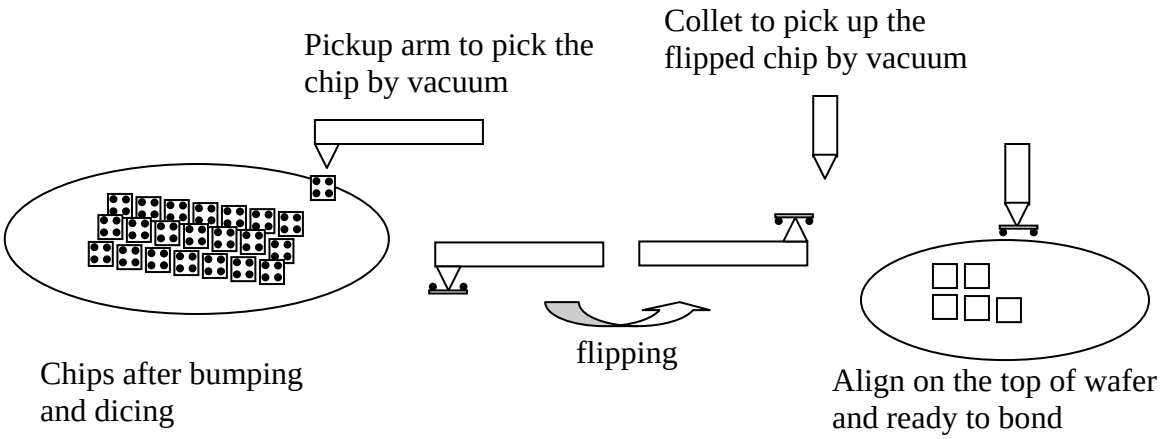

Fig. 3.4 Schematic diagram for the flipping process.

3.1.2.3 *Chip Bonding*

The chip bonding is similar among all the thermosonic bonding process. It involves thermal energy, compressive pressure and ultrasonic energy. The thermal energy, like all the wire bonding, is applied under the bonding substrate. A hot plate is located under the substrate and provides an evaluated temperature at around 120 ºC to 180 ºC. The collet will be pressed against the chip and given the necessary bonding pressure. A typical bond force of TS flip chip process is around 100 gram per bump. However, the actual bond force will also depend on the size and geometry of the bumps. The hardness of gold bump material also plays a significant role in the bond force level. Ultrasonic energy is used to facilitate the TS process and reduce the temperature used. The ultrasonic frequency is commonly used at around 60 kHz, although some researches have been conducted for

higher frequency bonding. By introducing the ultrasonic energy, the temperature can be reduced from several hundred degree to around 100 ºC. The reduction of temperature allows the TS process to cover more types of devices, especially for those with lower transition temperature. The ultrasonic vibration can be applied either transverse or longitudinal to the device through the collet. The method of vibration is determined by the transducer design. Fig. 3.5(a) shows a SAW filter bonded with the TS process. The Au bumps were deformed after the TS process and a cross-sectional view has been shown in Fig. 3.5 (b)

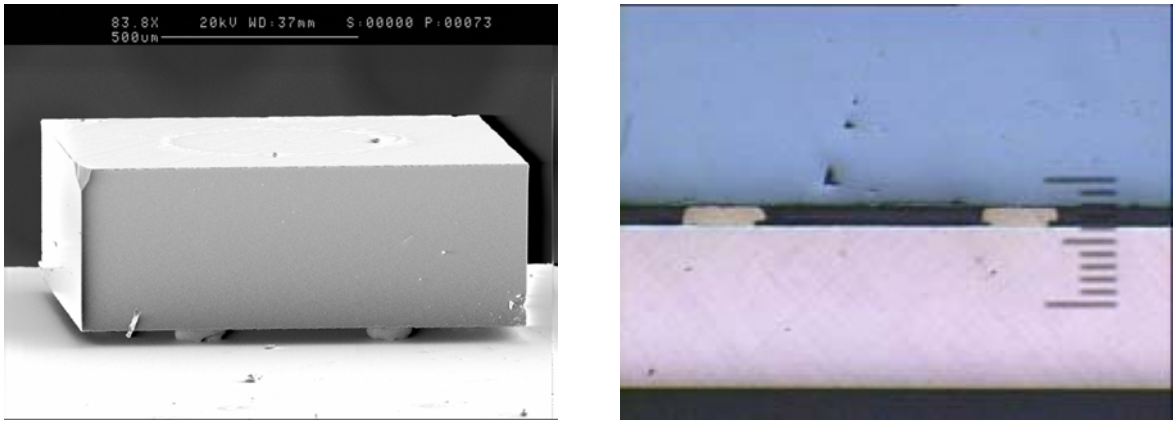

(a) (b)

Fig. 3.5 (a) A SAW filter device bonded by TS process and (b) a cross-sectional view of the bonded sample.

3.2 Ultrasonic Flip Chip Transducers

The design of an ultrasonic flip chip transducer is very similar to that of a wire bonding transducer. It shares the same basic design requirements as previously mentioned. It consists of a Langevin type of driver, a mechanical amplifying horn and a bonding tool.

For the current TS flip chip market, the transducer frequency commonly used is around 60 kHz, although some studies has been made on higher frequency flip chip bonding [14]. In this section, 62 kHz flip chip transducers will be designed for both transverse and longitudinal bonding. The Langevin driver has the same design as the 62 kHz wedge wire bonding transducer which the dimensions of PZT ring have been optimized as discussed in Chapter 2. As a shorter transducer length will make the future bond head design easier, the wavelength of the horn will be reduced from a full longitudinal wavelength (λ) to half wavelength (0.5λ). The reduction in horn length also helps to improve mechanical rigidity of the transducer because of less cantilever deformation. The whole transducer, together with the driver and horn, will add up to a complete one wavelength resonance mode. The design concept is shown in Fig 3.6. For flip chip transducers, the exponential horn profile will be removed and replaced by a step horn design. The step horn can also serve as a mechanical amplifier to increase the vibration at the horn tip.

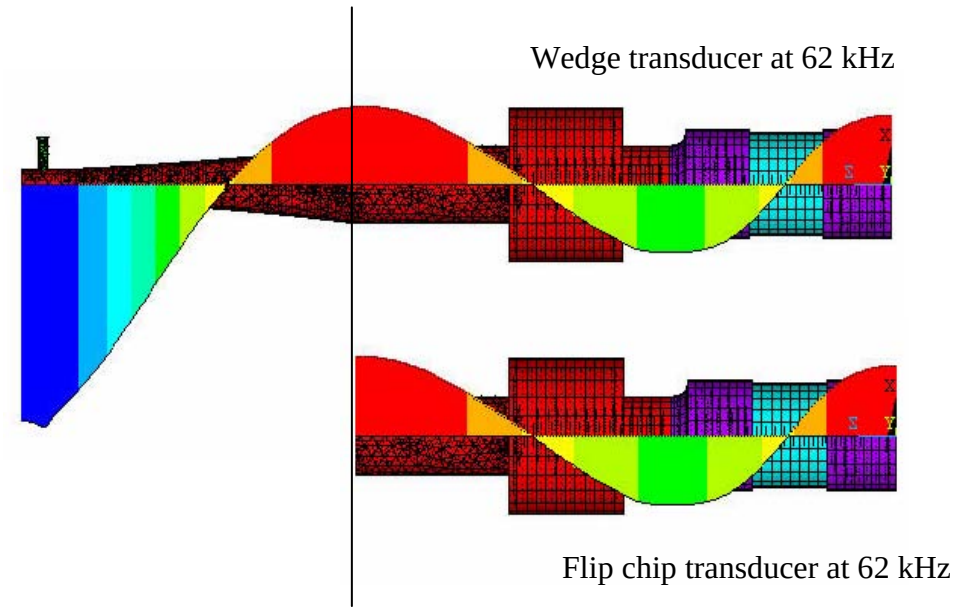

Fig. 3.6 Design concept for a 62 kHz flip chip transducer.

The transducer can be designed to operate in either transverse or longitudinal modes. It is done by proper installation of the bonding tool. The bonding tool, named as collet, for the TS flip chip bonding is a hollow stainless steel tube with tungsten carbide tight fitted at its tip. The collet has a diameter of 3.125 mm and the total length of 26 mm and 14 mm for the transverse and longitudinal transducer, respectively. Due to the need of bonding different sample sizes, the tungsten carbide collet tip will be tailored design for each die. A collet for the transverse transducer is shown in Fig 3.7. The collet is hollow in structure to allow the pick up of die at the collet tip by vacuum.

Fig. 3.7 A collet for transverse flip chip bonding (Diameter: 3.125 mm, Length: 26 mm).

Similar to wire bonding transducer, the collet has to be installed at the horn tip where the vibration amplitude is a maximum. For the transverse mode, the collet will be fastened perpendicular to the transducer similar to a wedge or capillary. The axial vibration of the transducer will turn into a flexural mode of the collet. Therefore, the flexural vibration of the collet transmits transversely into the bonding sample. For the longitudinal mode, the collet will be installed co-axially with the transducer. The collet will vibrate in phase with the transducer and the ultrasonic energy is transmitted longitudinally. The axial vibration

will form a hammering action during the longitudinal bonding. To connect to a vacuum pump, a connection polymer tube can be attached to the collet end for the transverse transducer. However, it is not the case in the longitudinal one. A longitudinal horn has to be hollow in structure with an extra vacuum connecter that extends from the body of horn. The dragrams of both transverse and longitudinal transducer are shown in Fig. 3.8

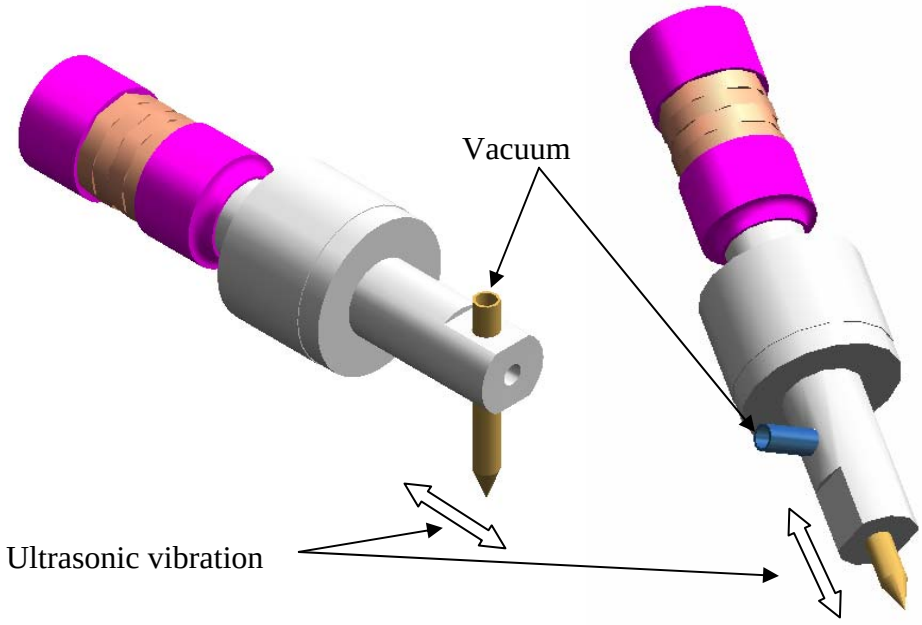

Fig. 3.8 62 kHz flip chip transducer for (a) transverse and (b) longitudinal bonding.

3.2.1 FEM of Flip Chip Transducers

Although the flip chip transducer design is based on a wire bonding transducer, the dynamic behaviours can have great difference. FEM was employed to model and analyze the transducer designs. Commercial FEM package, ANSYS, was used again for the modelling. Similar to that described in Chapter 2, three dimensional models were built and couple-field elements (SOLID 5) were also used for the piezoelectric elements. For the FEM models, the same assumptions as Chapter 2 were also applied. The thin copper electrodes were excluded and perfect coupling between each interface was assumed. For the longitudinal transducer, the vacuum tube was ignored in the model. The differences between the transverse and longitudinal transducer arise from the geometry of the collet and the method of collet mounting. For the transverse one, the collet length is 26 mm which is much longer and it is mounted perpendicular to the transducer. The long collet allows it to vibrate in the flexural mode that matches with the 62 kHz transducer system. However, for the longitudinal one, the collet is mounted and aligned with the transducer and the extension of the collet should be minimal in order not to disturb the axial vibration mode of the transducer. The FEM models for the transverse and longitudinal transducer are shown in Fig 3.9 and Fig 3.10, respectively. The difference in collet mounting is illustrated in Fig. 3.9 (b) and Fig. 3.10 (b).

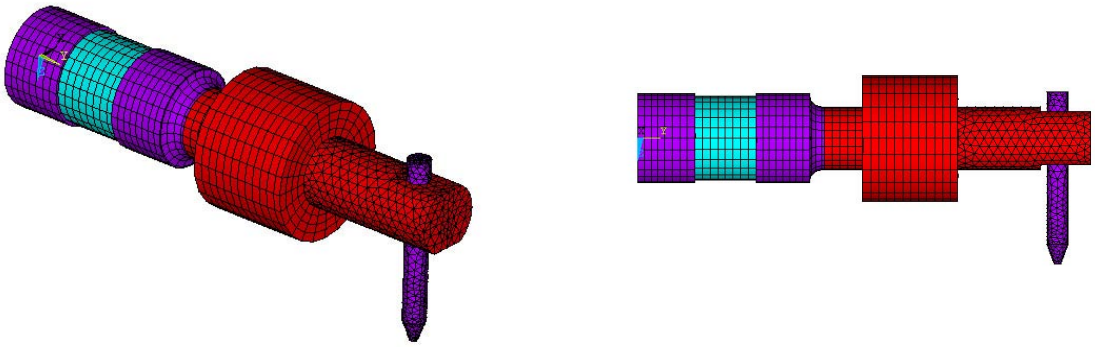

(a) (b)

Fig. 3.9 Finite element model of the transverse transducer (a) 3D view and (b) plane view.

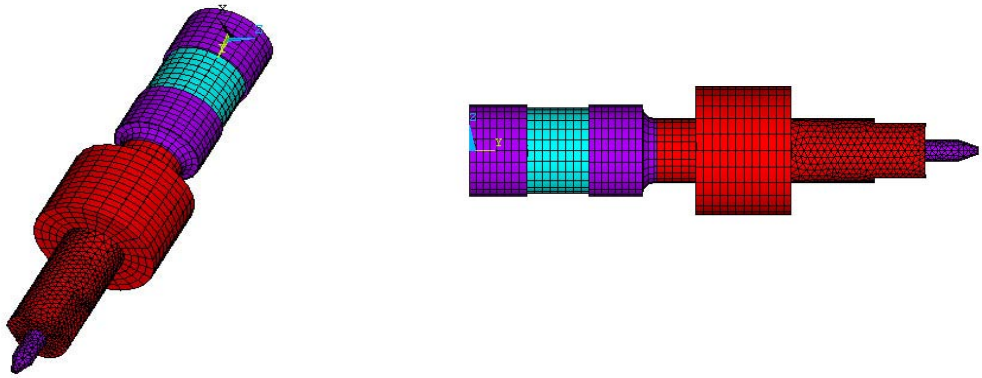

(a) (b)

Fig. 3.10 Finite element model of the longitudinal transducer (a) 3D view and (b) plane view.

Modal analyses were carried out on the two types of transducer. Due to the plane symmetry, one half of the model can be used to represent the whole transducer. Although some of the resonance modes would be suppressed, the operation mode will not be altered. By making used of the coupled field element (SOLID5 in ANSYS), it is possible to determine both resonance (F_r) and anti-resonance (F_a) frequencies. The effective electromechanical coupling factor (k_{eff}) can also be found by using equation (1) in Section 2.2.1. Table 3.1 lists out 10 resonance modes closed to the operation frequency. The

operation modes are found to be 62698 Hz and 60669 Hz for the transverse and longitudinal transducer, respectively. The k_{eff} of the operation modes are found to be a maximum among all the resonance modes.

TABLE 3.1 MODAL ANALYSIS RESULTS.

	Transverse Transducer		**Longitudinal Transducer**	
Mode	**F_r (Hz)**	**k_{eff}**	**F_r (Hz)**	**k_{eff}**
11	34127	0.06	36669	0.08
12	35559	0.	37079	0
13	48394	0.09	53098	0.15
14	53269	0.18	58753	0
15	59384	0	***60669***	***0.401***
16	***62698***	***0.423***	66368	0
17	66387	0	69087	0.05
18	69136	0.06	72939	0
19	72911	0.02	87005	0
20	82509	0.02	90382	0.02

Fig. 3.11 shows the mode shapes of the operation modes and its adjacent resonances. It was found that more flexural or complex modes were excited by the transverse transducer. The long collet at the horn tip breaks the symmetry of the transverse transducer. Therefore, more complex modes including flexural mode of the collet (mode 14), flexural mode of the horn (mode 15) and the barrel mode (mode 16) could be excited. For the longitudinal transducer, it has an axial symmetry structure. The vibration mode would be simpler and cleaner. Although flexural modes for the collet and transducer can also be found, most k_{eff} of these modes are found to be zero. The zero k_{eff} modes will not be excited electrically. The longitudinal transducer, therefore, exhibit a purer axial vibration.

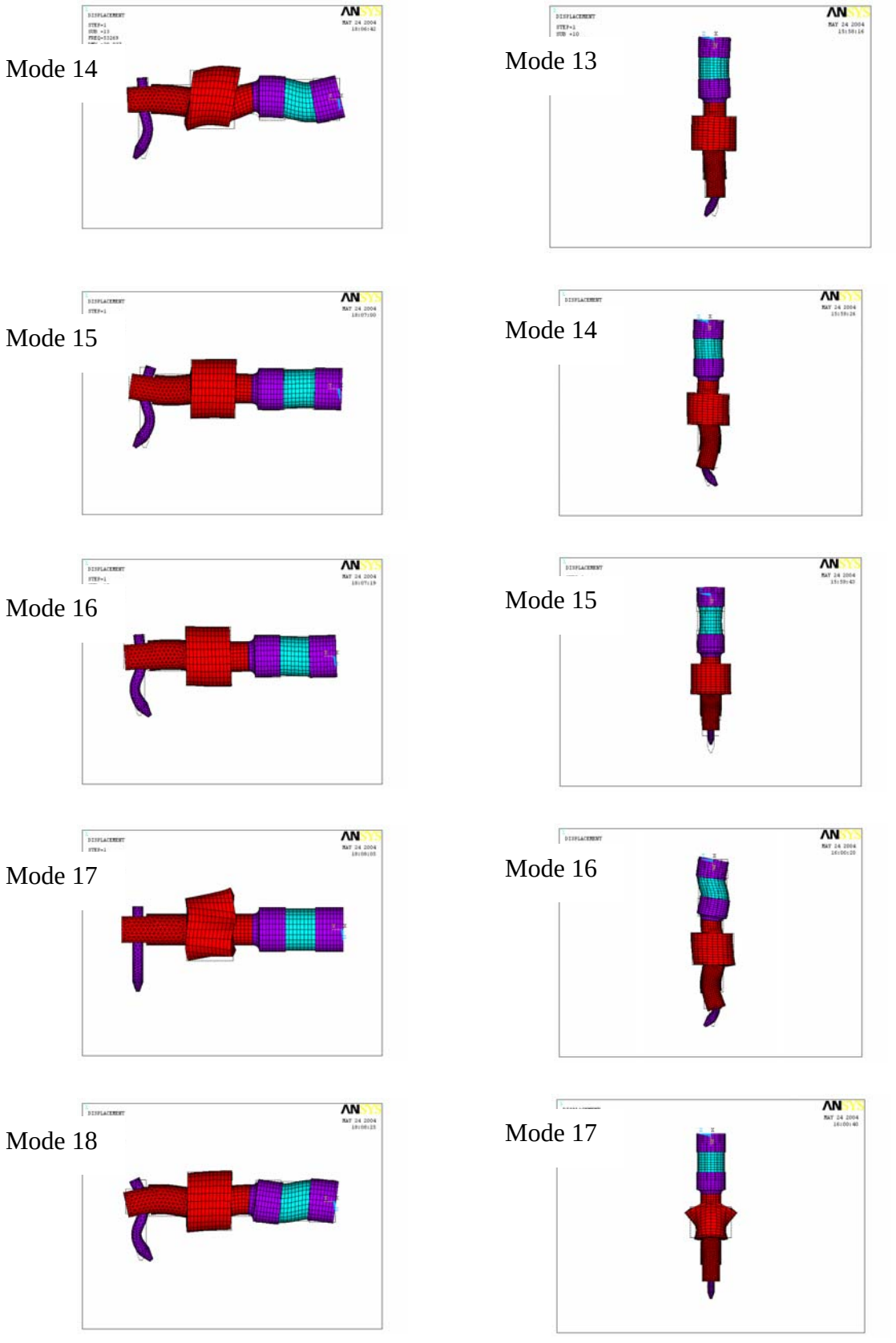

Fig. 3.11 Modal analysis results for transverse (LHS) and longitudinal (RHS) transducers.

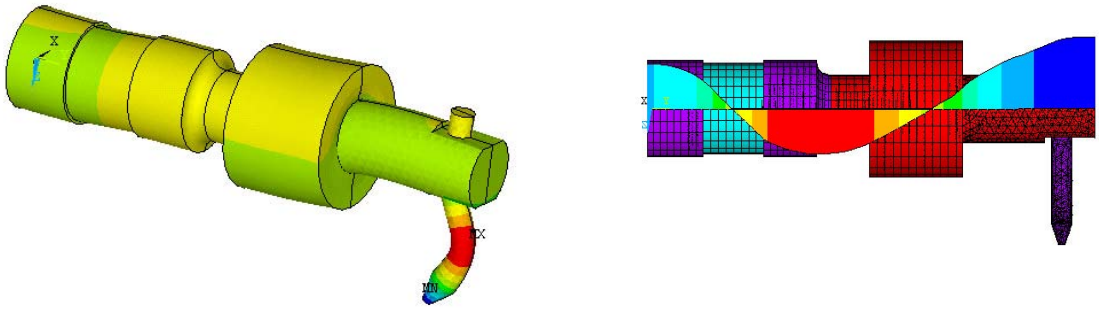

Fig. 3.12 Operation mode of transverse transducer (a) axial contour and (b) axial profile.

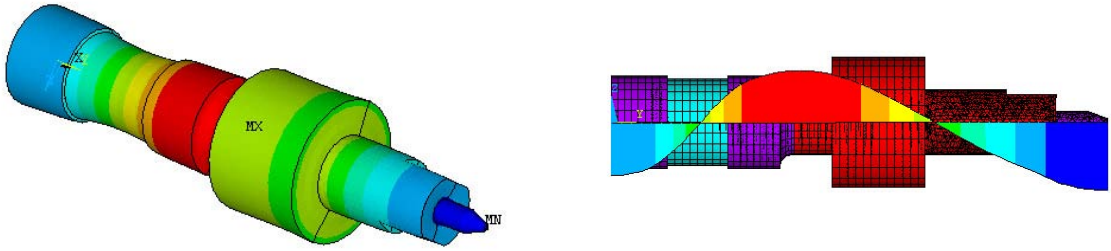

(a) (b)

Fig. 3.13 Operation mode of longitudinal transducer (a) axial contour and (b) axial profile.

Fig. 3.12 and Fig. 3.13 show the operation modes of the two types of transducers. From the deformed shape and axial contour plot shown in Fig 3.12 (a), the axial motion of the transducer converts to the flexural mode of the collet. The ultrasonic vibration is amplified and maximized at the collet tip. The whole transducer is operated at a one wavelength resonance as shown in Fig 3.12(b). Similar findings can also be observed for the longitudinal transducer. The deformed and contour plot in Fig. 3.13 (a) indicates that the

longitudinal transducer has a purer operation mode. And, the operation mode also has a full wavelength resonance (Fig. 3.13 (b)). For both transducer designs, the nodal point is located at the barrel position. Although there is a little deviation of the nodal position for the transverse type, it will not affect the actual function of the transducer.

3.2.2 Characteristics of Flip Chip Transducers

Based on the previous FEM results, prototypes were fabricated for both types of transducer. The Langevin type of driver consists of 4 PZT rings (ASM PZT-8). The dimensions of the PZT ring have been optimized for the 62 kHz transducer design in Chapter 2. The transducer horns have been re-designed according to the FEM results and the horn material is 7075 Aluminum alloy. The photos for the transducer prototypes are shown in Fig. 3.14. For the transverse type flip chip transducer, it has a step horn design with the collet fixed at the horn tip. As the collet is hollow in structure, a plastic tube can be attached to the collet end for vacuum suction (Fig. 3.14 (a)). However, the collet end is inserted into the transducer for the longitudinal type, an extra vacuum connector has to be extended from the horn body as shown in Fig. 3.14 (b). The vacuum connector has been designed so that it has minimal impact on the transducer performance. Unlike the transverse transducer, the plastic tube does not have to attach at the collet end where there is large vibration amplitude, the attachment of plastic tube has negligible change on transducer impedance for the longitudinal design.

(a) (b)

Fig. 3.14 Flip chip transducer prototypes for (a) transverse and (b) longitudinal bonding.

3.2.2.1 Tool Drops of Transducers

The transducer characteristics are highly dependent on the tool positions. *Kang et al* has reported that random mode change could happen if a suitable tool drop has not been used for a flip chip transducer [58]. And, the random mode change will lead to a sharp increase in impedance and affect the bonding performance. The definition of tool drop, which has been stated in Chapter 2, is the length of the collet end to the bottom of horn tip as shown in Fig. 2.19. The collet used for the flip chip transducer is supplied by Semicon Tool Co. Ltd. The collet has a diameter of 3.175 mm and a total length of 26 mm and 14 mm for the transverse and longitudinal transducers, respectively. The collet is made by stainless steel with a tight-fitted tungsten carbide tip.

Fig 3.15 shows how the transducer resonant frequency and impedance vary with tool drop for the transverse design. The transducer should work in the region of minimum transducer impedance and stable frequency. By varying the tool drop, it was found that transducer impedance could change from a minimum of 10 Ω to as high as 40 Ω. At the high impedance region, there is also a sharp change in the transducer frequency. This phenomenon is the so-called random mode change. A tool drop should be chosen to avoid mode change. Therefore, a tool drop should be set either longer than 16.5 mm or between 13 mm to 14.5 mm. To leave room for the plastic vacuum tube attachment, a tool drop of 14.5 mm has been used. At a tool drop of 14.5 mm, the transverse transducer has an impedance of 12.2 Ω and a frequency of 63.2 kHz. The tool drop characteristics of the longitudinal transducer are quite different from the transverse one as illustrated in Fig. 3.16. The transducer impedance increases as the tool drop increases and a drop in transducer frequency is also observed. The frequency change indicates the random mode change. However, it does not occur as sharp as the transverse design. Therefore, the longitudinal transducer is less sensitive to the variation of tool drop which makes it more robustness in terms of using collets with different die size. Although the transducer impedance reduces as the tool drop, it has to maintain a suitable working clearance. Therefore, a tool drop of 8 mm has been chosen just before the frequency starts to drop. A transducer impedance and frequency for the longitudinal design are 13.5 Ω and 61 kHz, respectively.

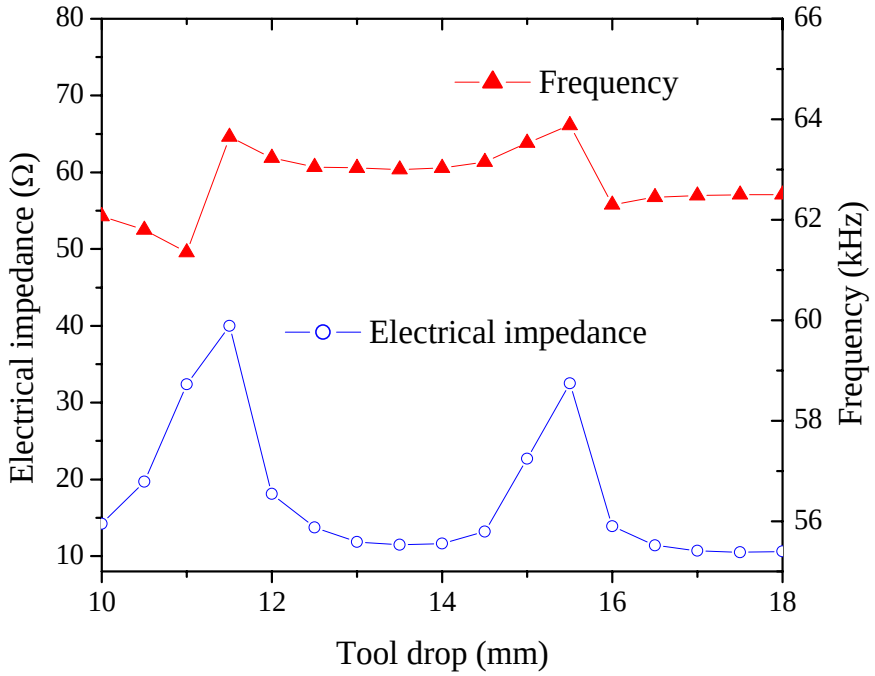

Fig. 3.15 Transverse transducer characteristics vs tool drop.

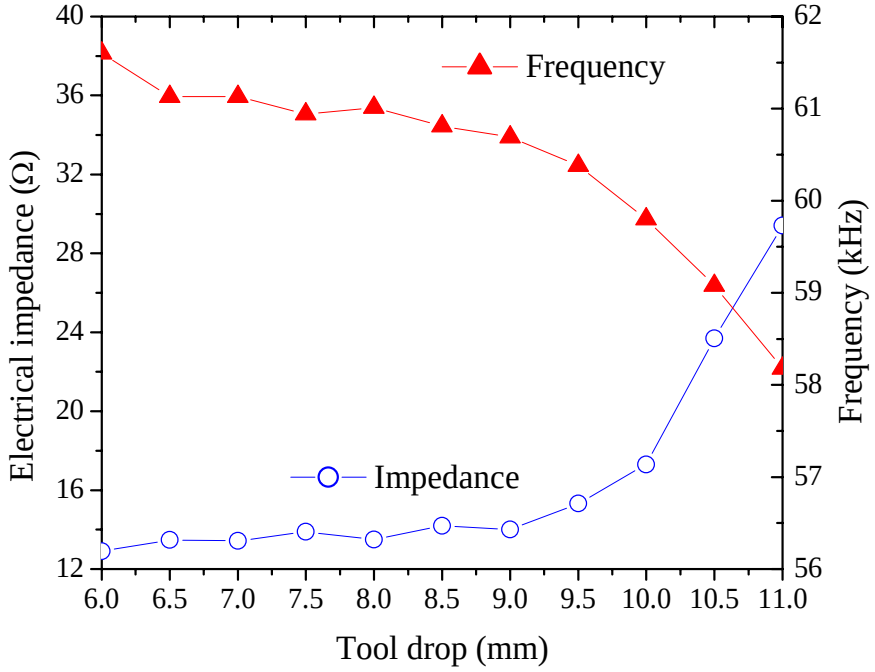

Fig. 3.16 Longitudinal transducer characteristics vs tool drop.

3.2.2.2 Electrical Characteristics

After the optimized tool drop has been determined, the electrical properties of the transducers are characterized. The transducer impedance spectrum has been recorded using an HP 4194A gain/phase impedance analyzer and plotted in Fig 3.17. No other strong resonance can be found in the frequency range and the designed operation mode has the strongest coupling factor. The electrical impedance spectrum indicates that the transducers have stable and good resonance characteristics. The electrical properties for both transducers are summarized in Table 3.2. The measurement results are compared with the FEM prediction. Good agreement has been obtained.

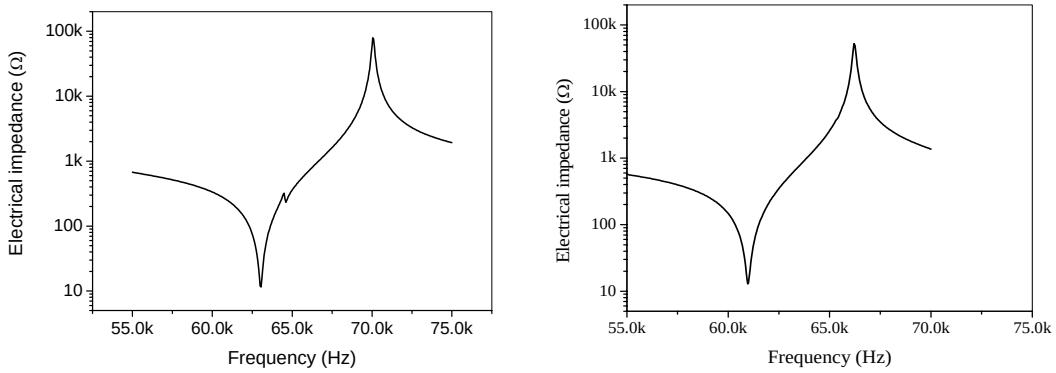

(a) (b)

Fig. 3.17 Electrical impedance spectrum of (a) transverse and (b) longitudinal transducer.

TABLE 3.2 SUMMARY ON ELECTRICAL CHARACTERISTICS.

	Transverse Type		Longitudinal Type	
	Measurement	FEM	Measurement	FEM
F_r (kHz)	63.2	62.7	61.0	60.7
F_a (kHz)	70.1	69.2	66.4	67.2
k_{eff}	0.44	0.42	0.40	0.43
Z (Ω)	12.2	-	13.5	-
Q_m	556	-	604	-

3.2.2.3 Vibration Amplitude

The vibration amplitudes at the collet tip were measured by a Polytec laser vibrometer. As the two types of transducer vibrate in different directions, the flexural displacement of the transverse transducer will be compared with the axial displacement of the longitudinal transducer at their collet tips. The measurement results are plotted in Fig. 3.18. The two types of transducer have similar vibration amplitudes as both shared the basic driver and horn design. However, the flexural amplification of the collet in the transverse transducer makes its vibration slightly higher. At high power, however, both transducers show similar vibration amplitude. It can be explained that the longer and massive transverse collet leads to a faster saturation in vibration amplitude than the vibration in the axial direction.

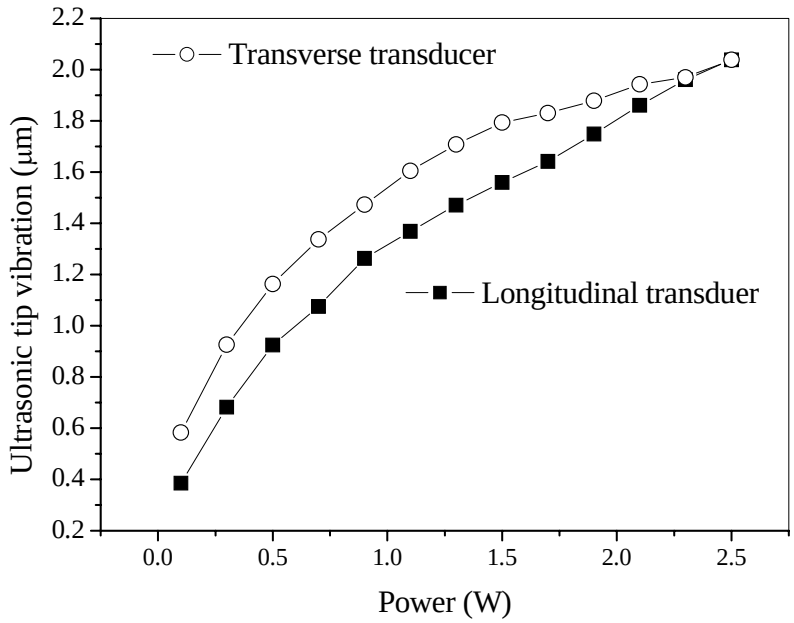

Fig 3.18 Comparison on collet tip vibration of longitudinal and transverse transducers.

The flexural vibration profile for the transverse type is also scanned and shown in Fig. 3.19. As the laser vibrometer cannot tell the vibration direction, only the absolute vibration amplitude is plotted. The whole collet vibrates in a 1.5 wavelength flexural mode. The tapered collet tip serves as a mechanical amplifier similar to the profile of the horn. This results show how the transducer vibration turns into a flexural vibration of the collet. However, for the longitudinal vibration, similar scan to find the axial vibration profile cannot be carried out.

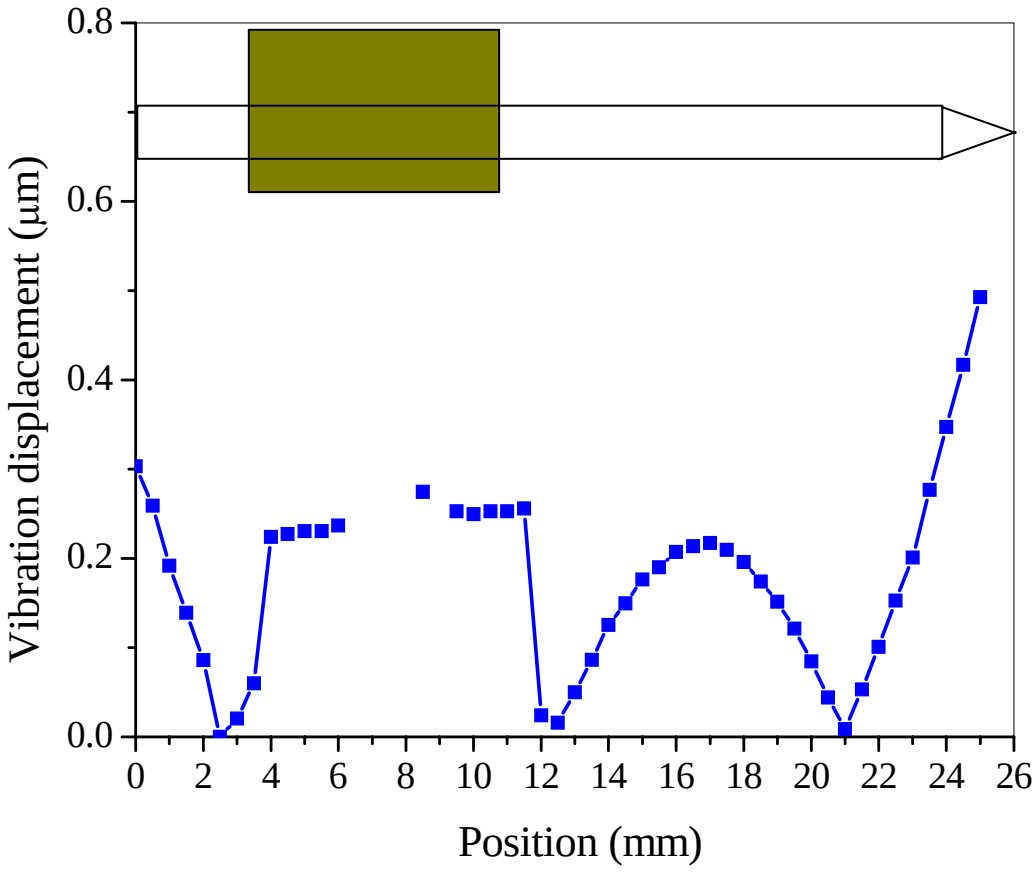

Fig. 3.19 Collet vibration profile for the transverse transducer.

3.3 Testing Vehicles

In this section, the testing vehicles including the test die, substrate and a test platform will be briefly described. With the test platform, simple bonding evaluation will be possible. However, unlike a real bonding machine, the flipping process has to be done manually. It may affect the bonding performance to some extent. In the course of work, two types of bonding defects, die tilting and silicon cratering, will be compared for the two types of transducers. The test jig, however, when carefully tuned, is effective for examining and evaluating the flip chip processes on the two types of bonding defects.

3.3.1 Test Die

The bonding specimens used in the study is ASM 2000 test die. The die size is 1 mm x 1 mm with a thickness of 350 μm. The ASM 2000 test die has 8 gold bumps on the periphery. The gold bumps are bonded by a commercial gold bumping machine, Hummingbird. The transducer frequency for the bumping is around 138 kHz. The wire for the gold stud bumps is GBE model purchased from Tanaka Ltd. A top view of the ASM 2000 test die with 8 gold bumps is shown in Fig. 3.20

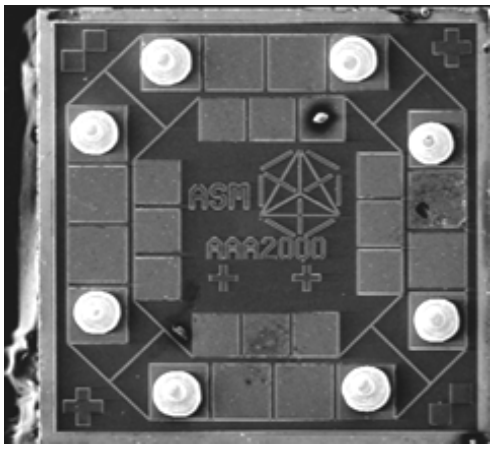

Fig. 3.20 ASM 2000 test die with 8 gold bumps.

By carefully tuning the bumping parameters, the bumps can be formed in a consistent geometry. During the bumping process, the bump size and the tail length has to be controlled very precisely. The ball size and tail length can directly affect the subsequent flip chip bonding performance. The bump shape is shown in Fig. 3.20. The bump is similar to that of a ball bonded joint except that the connection wire is no longer needed. The wire will be broken at its heel and leave a small portion (tail) at the top of the bump. A typical shape of a gold stud bump is shown in Fig. 3.21. The bumping results are summarized in Table 3.3

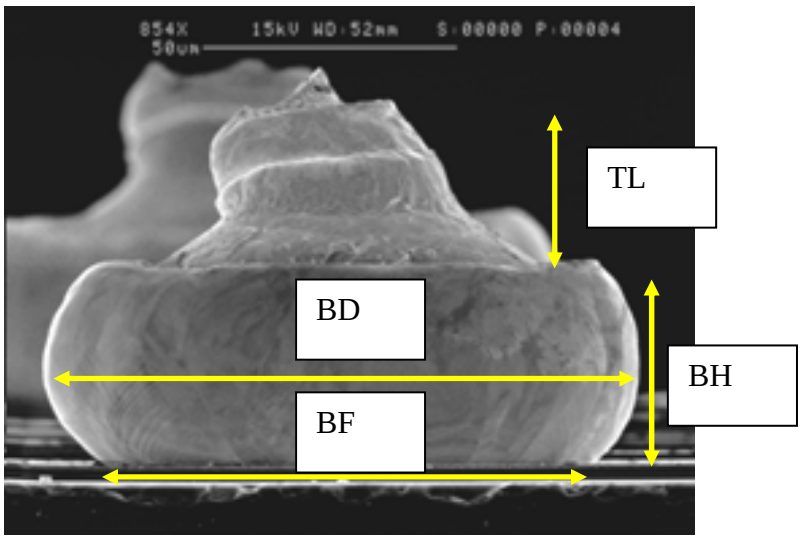

Fig. 3.21 Bump shape on the test die.

TABLE 3.3 SUMMARY ON BUMP DIMENSIONS.

Ball diameter, BD (μm)	Ball footprint BF (μm)	Tail length TL (μm)	Ball height BH (μm)
115 - 120	85 - 100	30 - 33	42 - 48

3.3.2 Bonding Substrate

After the bumping process, the test dies are ready for the flip chip bonding. The substrate for the flip chip bonding in the present study is a silver-plated leadframe (L/F) supplied by ASM. The copper L/F is fabricated by the etching process with silver plated by electroplating. A typical L/F is shown in Fig. 3.22. By cross-section inspection, the thickness of the silver plate on the Cu L/F is found to be around 8 μm on average as shown in Fig. 3.23.

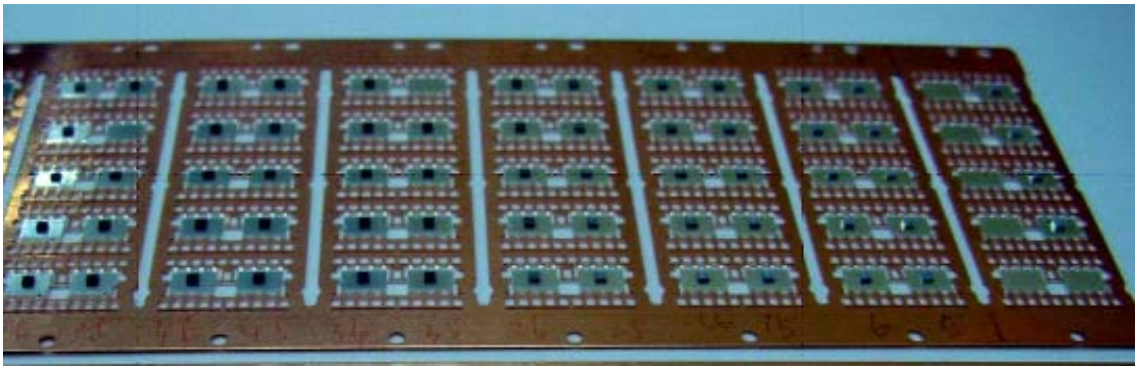

Fig. 3.22 A leadframe substrate for thermosonic flip chip.

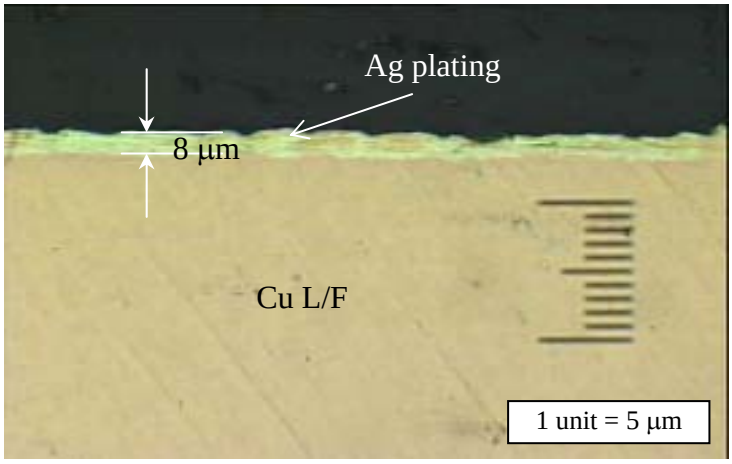

Fig. 3.23 Cross-section of the leadframe.

3.3.3 Test Jig

A test jig has been designed for bonding evaluation. The schematic diagram for the test jig is shown in Fig. 3.24. The transducer has been clamped at its barrel by a bracket. The clamping location has been designed to minimize the impedance change on the transducer. The bracket, together with the transducer, is fixed on a computer-control Z-axis slider. The slider can be programmed to move up and down with high accuracy and repeatability. The resolution of the slider is 1 μm. The bonding co-planarity can be adjusted by the mechanical clearance of the test platform. Between the bracket and the slider table, there is a set of springs to give the required bond force. More springs can be added if a larger bond force is required. Right under the collet, there is a hot plate supported on a stage. The hot plate contains a heater to provide a high temperature environment. A thermocouple has been connected to the hot plate and feedback to a thermo-controller for temperature adjustment and control. The maximum temperature of the current setup is 250 ^{o}C.

The bonding substrate, silver-plated L/F, was placed on top of the hot plate. The L/F is further secured by a mechanical clamp to prevent any motion during bonding. The L/F will heat up within a few seconds because it is very thin with good thermal conductivity. During the bonding test, the chip is placed under the collet with the bumps facing down. Due to the action of vacuum, the die is secured at the collet tip. By moving the slider downward, the bond force can be controlled by the stiffness of the set of springs. The downward displacement of the test rig has been pre-calibrated with a standard force sensor. A linear relation is observed for the force below 5 kg (Fig. 3.25). Higher force can be applied by either adding more springs or replacing springs with higher stiffness. After the

required bond force has been applied against the bonding samples, the transducer is fired by the ultrasonic energy source.

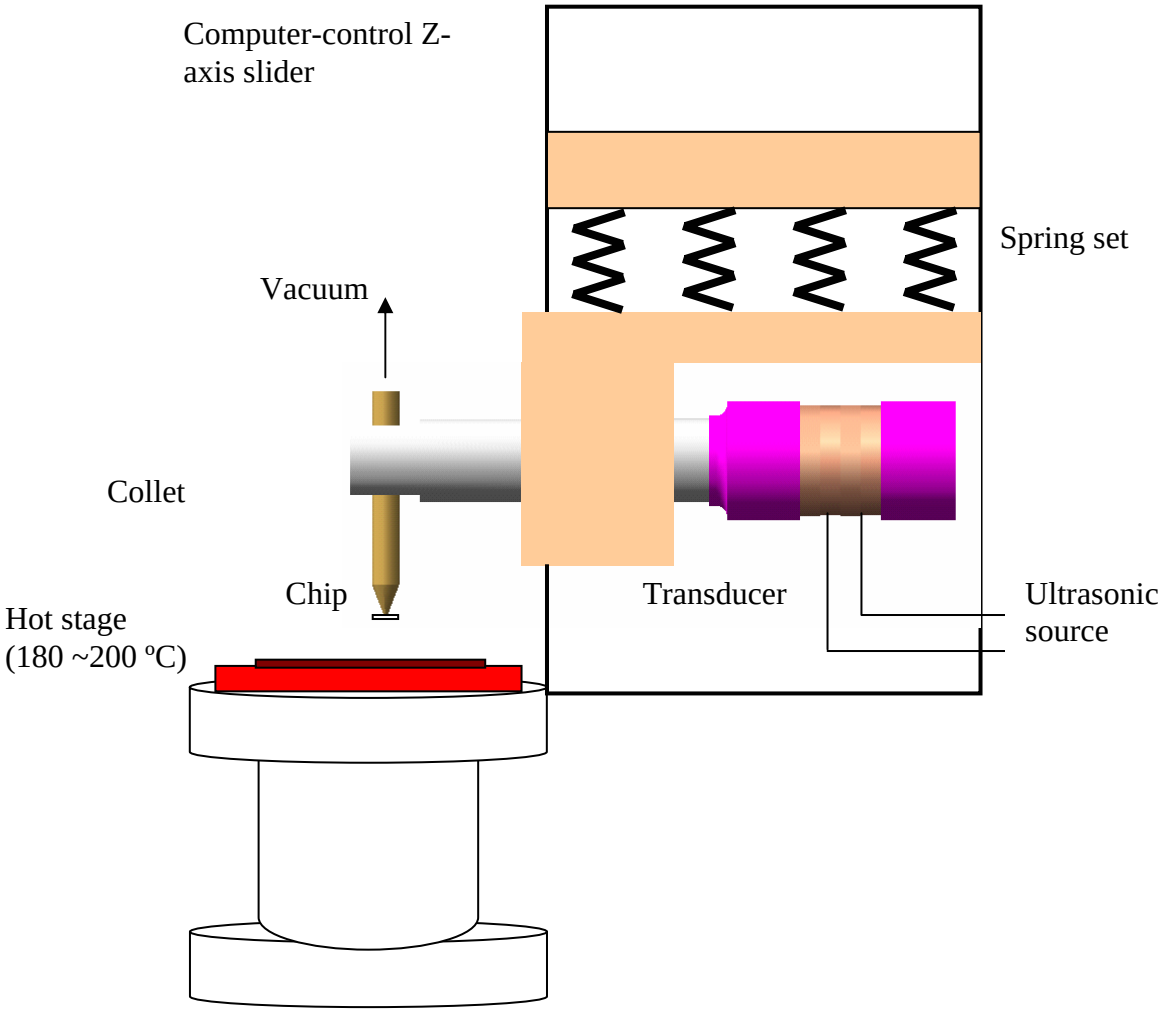

Fig. 3.24 Schematic diagram of the test platform.

The ultrasonic source is a commercial ultrasonic generator board (USG) fabricated by ASM. The USG board has a sophisticated phase lock loop (PLL) control such that the USG will keep track of any resonant frequency change. It is able to drive the transducer at its zero phase position which is its resonant frequency during the bonding process. Apart from phase locking, constant power or constant current mode is also possible.

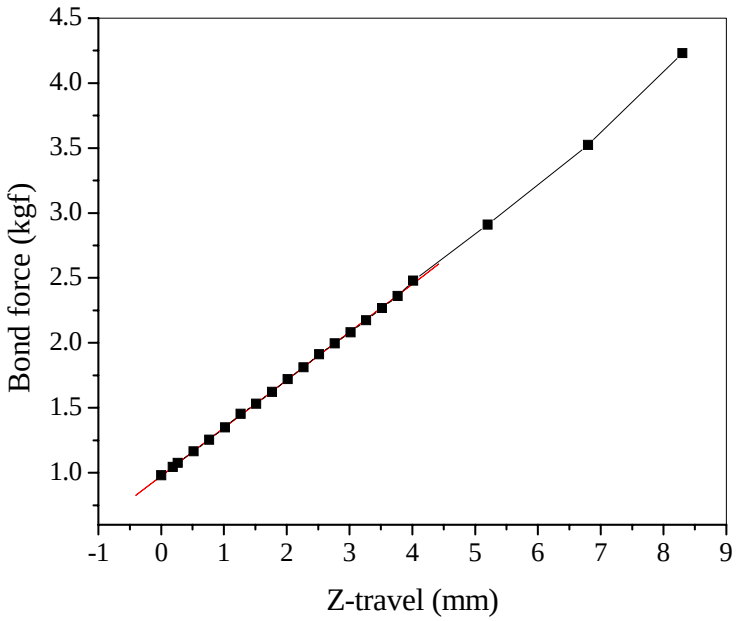

Fig. 3.25 The bond force vs Z-travel for the test platform.

Fig. 3.26 and Fig 3.27 show the photographs of the bonding platform for both transverse and longitudinal transducers. As shown in Fig. 3.26, the L/F are clamped on the hot plate. On the top of the photo, the spring set is used to apply the required bond force. A plastic tube is attached at the collet end which is connected to a vacuum pump. The transverse transducer is held by the bracket that has been mounted on the Z-slider table. For the longitudinal transducer set-up shown in Fig. 3.27, only one adaptor is needed to add on the test jig. The longitudinal transducer is secured on the adaptor and then mounted to the transducer bracket. To convert from transverse to longitudinal bonding, only the Z-level and the co-planarity have to be re-adjusted.

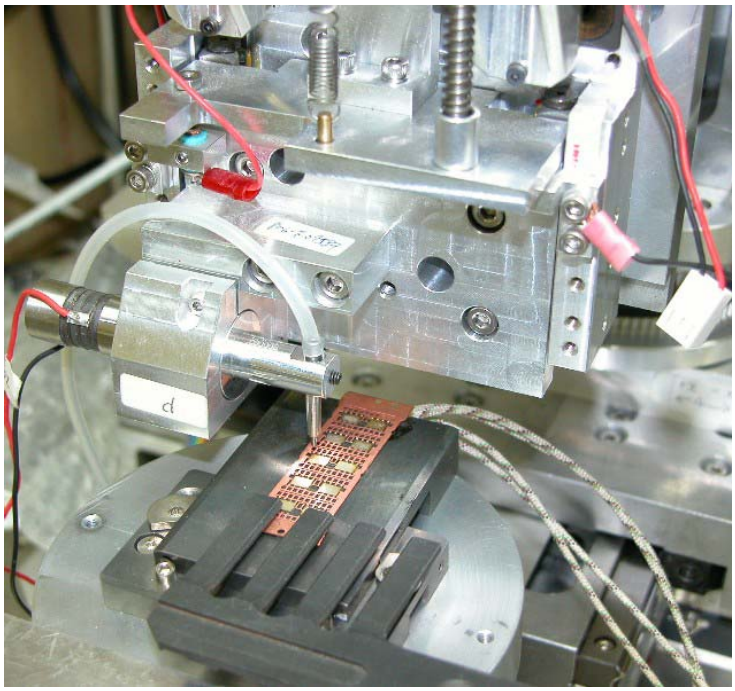

Fig. 3.26 Bonding jig for transverse transducer.

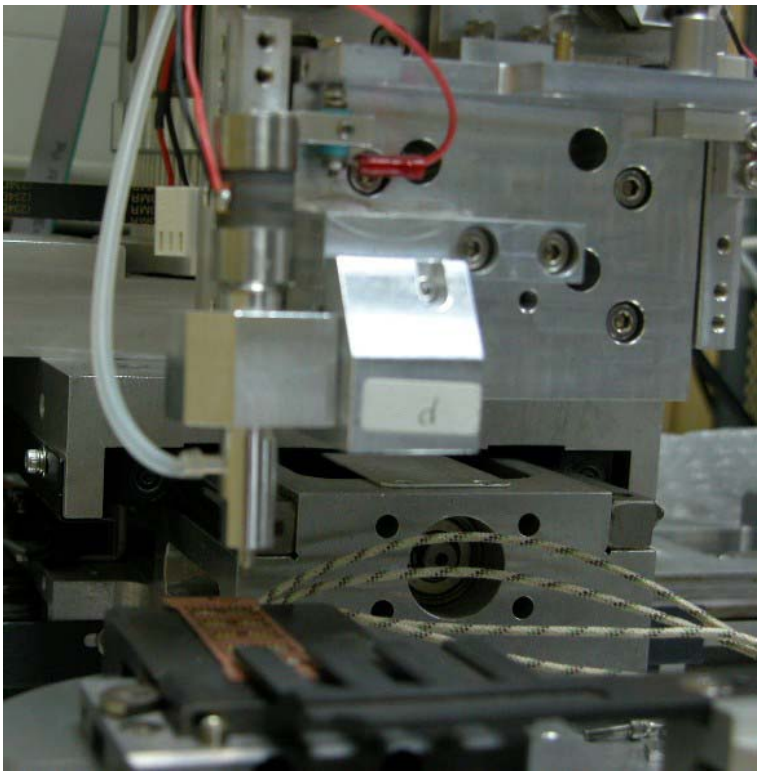

Fig. 3.27 Bonding jig for longitudinal transducer.

3.4 Bonding Defects

In this section, two common defects: chip tilting and silicon cratering were compared for the two types of thermosonic flip-chip bonding. Finite element analysis (FEM) using ANSYS was used to study the effect of rigidity of transducer and the stress induced on the silicon layer during bonding. It was found from both simulation and experiments that the deformation of the transverse transducer under a loading contribute to the chip tilting defect. For longitudinal bonding, the collet can maintain a perfect planarity even under high loading and hence eliminate the tilting problem. Actual vibration amplitudes of both types of transducers were measured by laser vibrometers at different ultrasonic power and loadings. The measurement data were fed into the FEM, together with the compressive loading, to study the stress generated at the silicon layer. Using the maximum principal stress criterion, the stress level induced by longitudinal bonding was found to be higher than that of the transverse mode. A maximum stress of 1.2 GPa occurs at a bond force of 200 gf per bump and an ultrasonic power at 2 W for the longitudinal mode which is 20 % higher than the transverse mode. Silicon cratering was also observed from experiment in the longitudinal bonding but not in the transverse mode. It matches with our FEM prediction that longitudinal bonding induces higher stress level at the silicon layer and hence it is more susceptible to silicon cratering.

3.4.1 Chip Tilting

Chip tilting resulted in a non-uniform bonding between the gold bumps. One of the main causes of the chip tilting defect is due to an improper alignment of the machine. It leads to a poor coplanarity between the collet surface and chip as indicated in Fig. 3.28(a) .

Therefore, a non-uniform pressure is applied across the chip and also on each individual gold bump. As the compressive loading facilitates the thermosonic bonding, there will be "over-bonded" at the gold bumps with higher compressive stress and "under-bonded" with lower stress. The chip will incline with a tilt angle θ with respect to the horizontal plane after bonding. The chip tilting defect is shown in Fig. 3.28 (b). For a poor machine alignment, it can sometimes be solved by carefully adjusting the bond level. However, the chip tilting defect may also be casused by the insufficient rigidity of the transducer. During the thermosonic flip chip bonding, both ultrasonic energy and compressive force are applied through the transducer and collet. The deformation of the transducer under high bond force can produce the above-mentioned tilting defect.

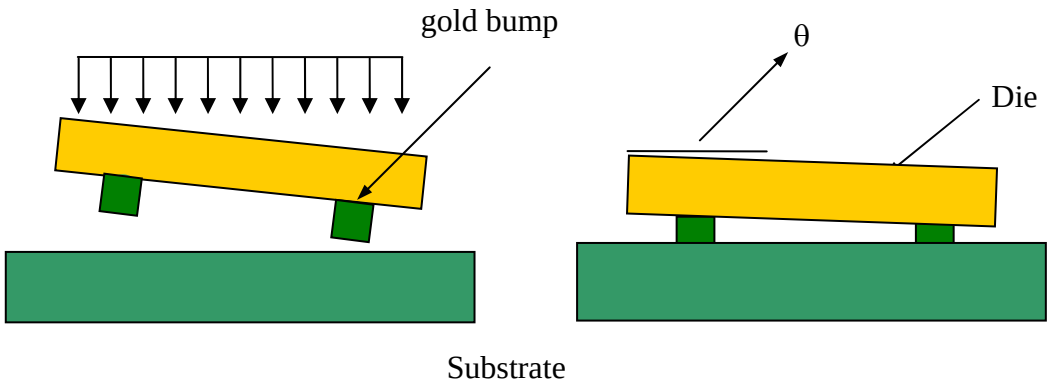

Fig. 3.28 (a) Die tilting caused by poor co-planarity and (b) an inclined chip with tilt angle.

A FEM analysis has been performed to study the transducer deformation under a static bonding. The static force is applied against the collet tip to simulate the transducer under loading. The deformed shapes of the transducers from the FEM results are shown in Fig. 3.29. In the longitudinal mode, the bond force is applied co-axially with respect to the central axis of the transducer. Even though the transducer deforms, the collet surface can be kept perfectly perpedicular to the transducer until buckling occurs. However, the

buckling limit of the structure is ususally far beyond the actual applied force. As a result, the longitudinal approach can maintain a uniform pressure across the chip during bonding. In the transverse transducer, the applied bond force can lead to a bending of the transducer horn. The bending can give rise to the incline angle between the collet tip and the chip surface. It will result in the chip tilting defect shown in Fig. 3.28 (a). Fig. 3.30 shows the FEM results of the collet incline angle against the applied static loading. The longitudinal mode can maintain a zero angle at all bond force. However, for the transverse mode, the incline angle of collet is proportional to the bond force. The existing of incline angle implies a non-uniform bonding pressure and eventually leads to the chip tilting defect.

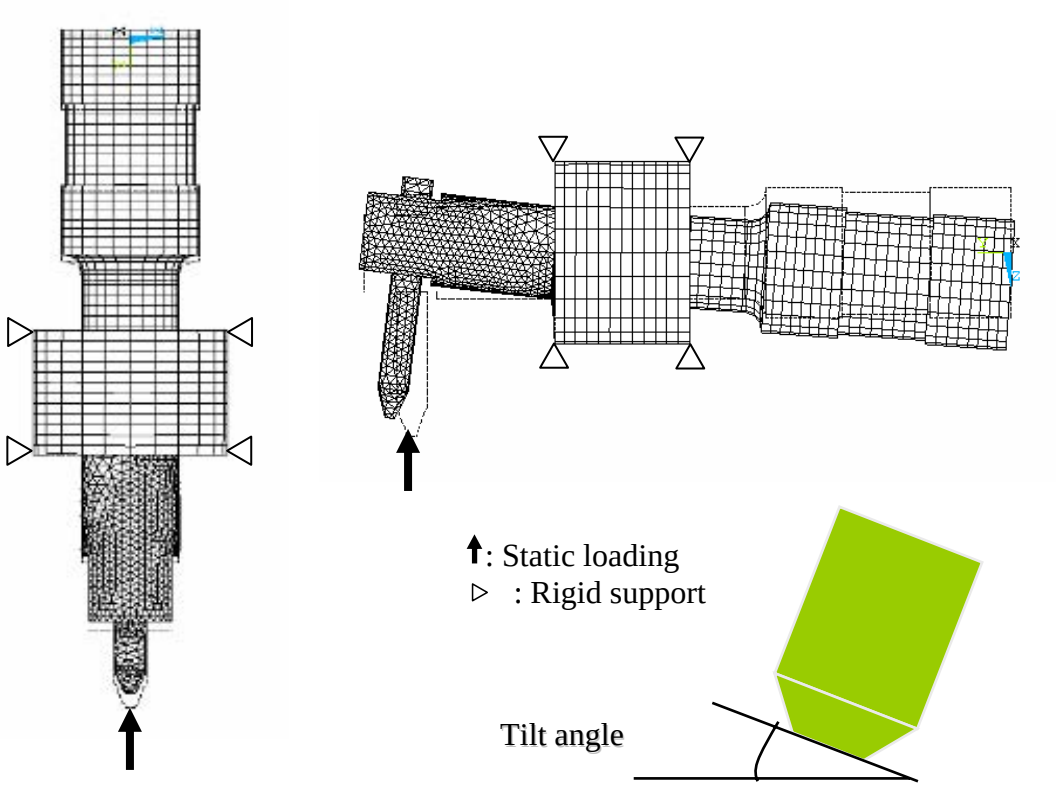

Fig. 3.29 FEM simulation of deformed shape of transducer under a static loading.

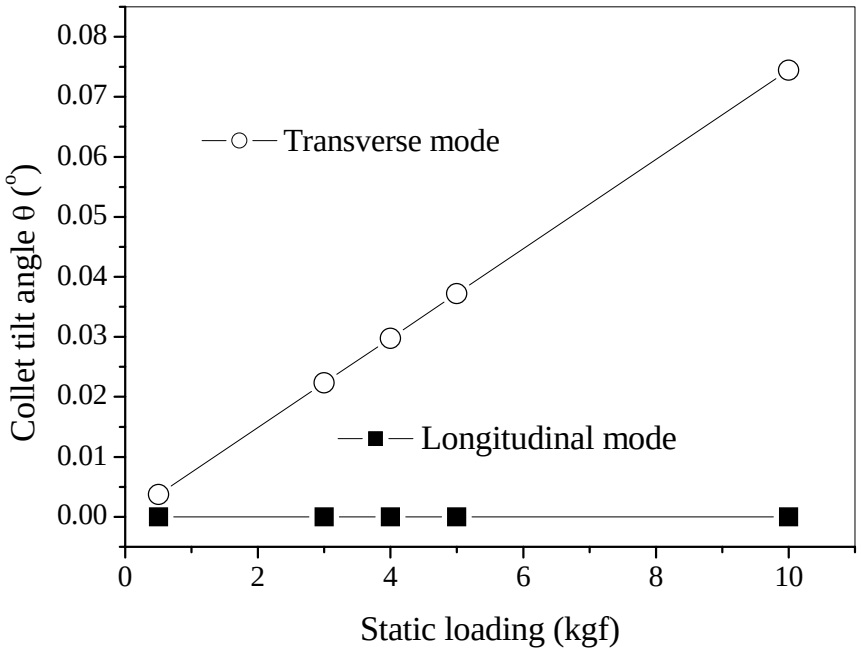

Fig. 3.30 FEM simulation of the collet tilting under a static loading.

.

To verify the effect of the bond force on the tilting problem, an ASM test die of 1 mm x 1 mm silicon chip with 8 gold bumps on the periphery was pressed against a silver-plated leadflame (L/F) substrate under various force up to 10 kgf. The substrate was heated at 120 ^{o}C. No ultrasonic energy was applied so that the change in bump height was only due to the compressive loading. The pressed silicon chip was held for 10 seconds to facilicate the attachment on the L/F even without an ultrasonic energy. The chip tilt angle was measured and plotted in Fig. 3.31. For the transverse mode transducer, the tilt angle increases as the bond force increases. However, the tilt angle can maintain a constant level up to 10 kgf for the longitudinal mode. It matches with the trend predicted by the FEM simulation. For the present 8-bump silicon chips, the typical bond force is normally under 2 kgf. The tilt angle between transverse and longitudinal bonding does not have

significant difference. However, as the number of IOs increases, a huge bond force even greater than 10 kgf may be required. The tilting problem of the transverse bonding will dramatically affect the bonding stability and yield. For high IOs devices, the longitudinal mode offers a better choice in terms of eliminating the chip tilting defect on the thermosonic bonding. It is because the longitudinal transducer provide a better rigidity to maintain a good coplanarity between the bonding surfaces and hence eliminates the tilt defect.

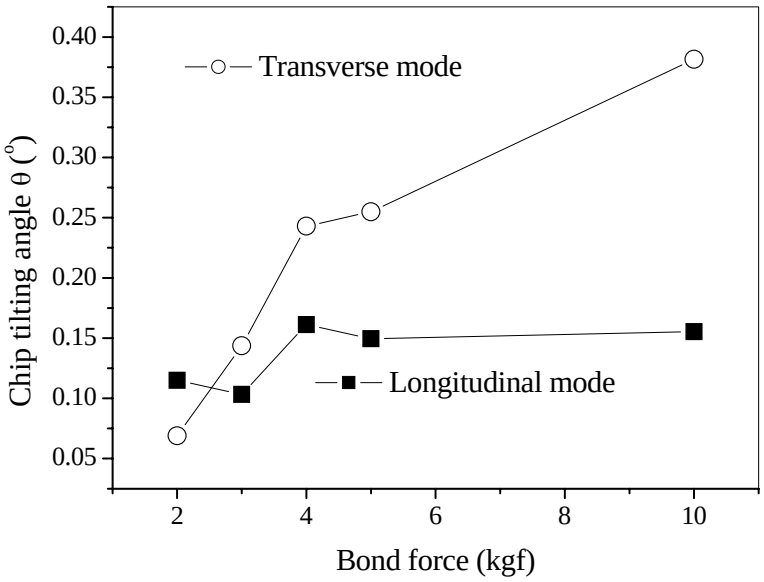

Fig. 3.31 The chip tilt angle under a static bond force (without ultrasonic energy applied).

3.4.2 Silicon Cratering

Silicon cratering is one of the common defects in thermosonic bonding. It is the damage of silicon chip after bonding. In some severe cases, part of the silicon can be "torn-off" after a destructive test. Many researches have been conducted to study cratering in the past. [59-60] The actual cause of silicon cratering is very complicated and has not yet been

fully understood. However, it is believed that excessive ultrasonic power and bond force are the main causes of cratering. In this Section, a finite element method is used to study the stresses induced on the silicon layer under a compressive loading and ultrasonic vibration. A three (3D) dimensional FEM has been built to study the stresses generated on the silicon and gold interface. The FEM model is shown in Fig. 3.32 and the materials properties found from data books are listed in Table 3.4.

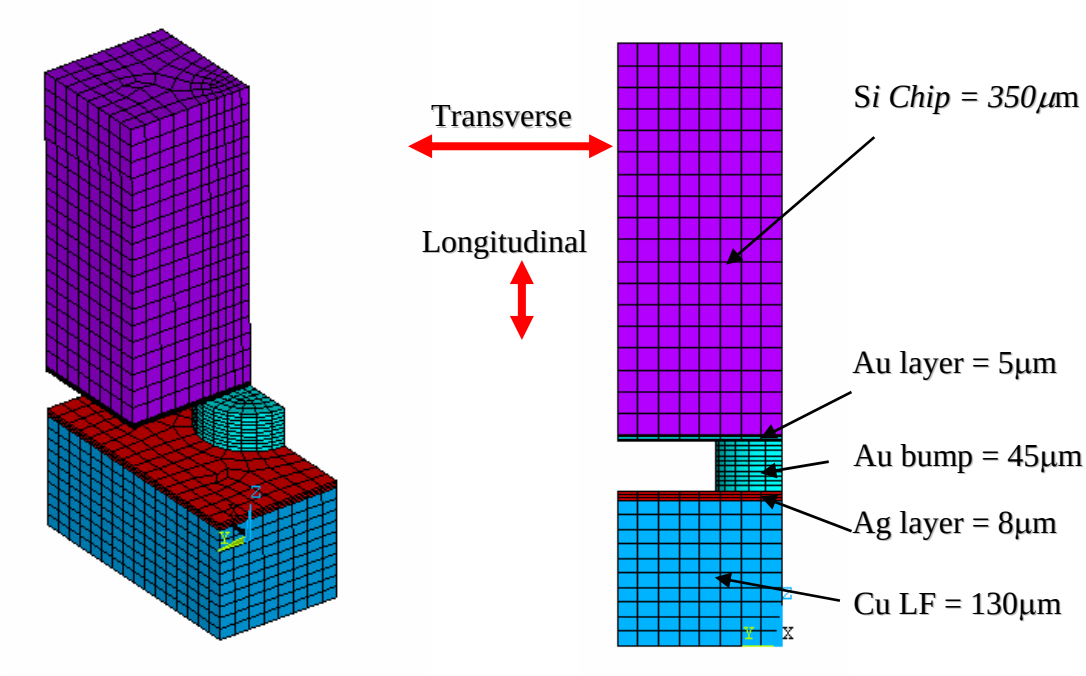

Fig. 3.32 Finite element model of a gold bump between a silicon chip and silver-plated leadframe.

TABLE 3.4 MATERIAL PROPERTIES USED IN FEM.

	Modulus (GPa)	Possion's ratio	Density (kg/m^3)
Gold	78.0	0.44	19300
Silver	76.0	0.40	10491
Silicon	131.0	0.22	2329
Copper	113.0	0.36	8800

In order to apply a proper loading to the FEM, the actual vibration amplitude of both transverse and longitudinal transducers were measured under a loaded condition. The collet was pressed against a silicon chip up to 5 kgf. The collet tip vibration was measured by a laser vibrometer up to 2 W. The experimental set up is shown in Fig. 3.33. A Polytec out-plane vibrometer is used to measure the vibration amplitide under loading. For the longitudinal mode, the vibration has to be measured by an in-plane vibrometer from Polytec instead. From the measurement results shown in Fig. 3.34, the collet vibration of the two transducers show different behaviours. The vibration of the longitudinal transducer is more stable with the loading. It can be explained by the fact that the axial vibration of the collet has a higher force factor than that of a flexural mode. Therefore, the force generated by the longitudinal transducer is higher and the vibration amplitude is less susceptible to the change of external loading. The ultrasonic displacement measured at each power setting and the bond force were put into the FEM analysis. In the FEM model, we made an assumption that the skipping and slipping motion between the collet surface and the silicon are negligible. Therefore, the vibration of the collet tip is equal to the vibration of the silicon chip during the thermosonic bonding. The displacement, together with a static bond force, was applied transversely and longitudinally to the silicon chip to

simulate the bonding condition of transverse and longitudinal bondings, respectively. The stresses induced in the silicon and gold layer interface were found and analyzed.

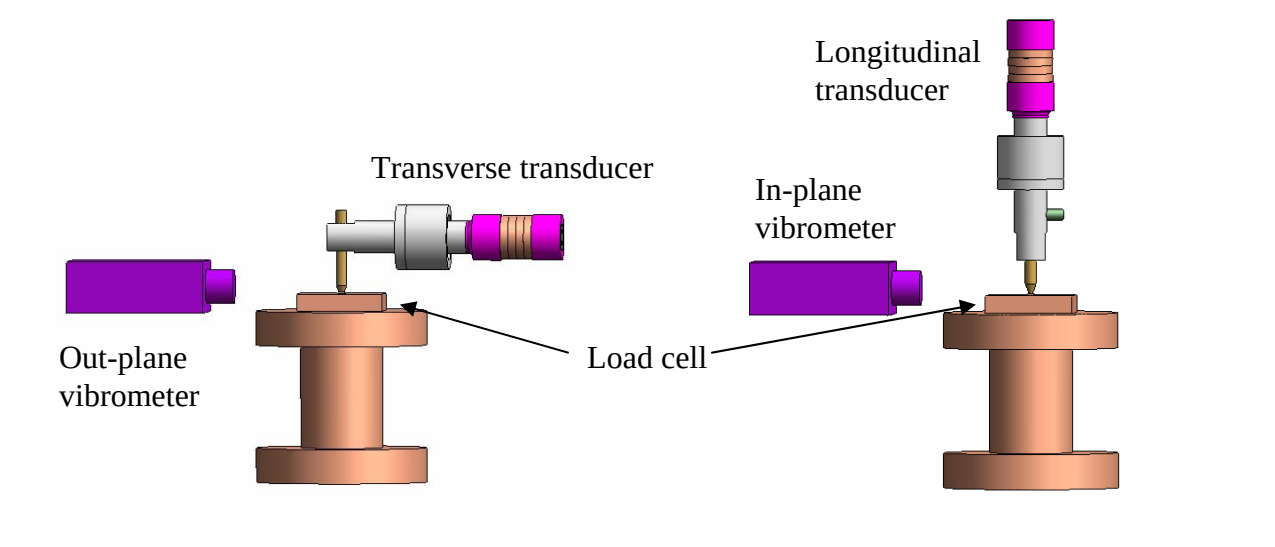

Fig. 3.33 Experimental set-up for laser vibrometer measurements.

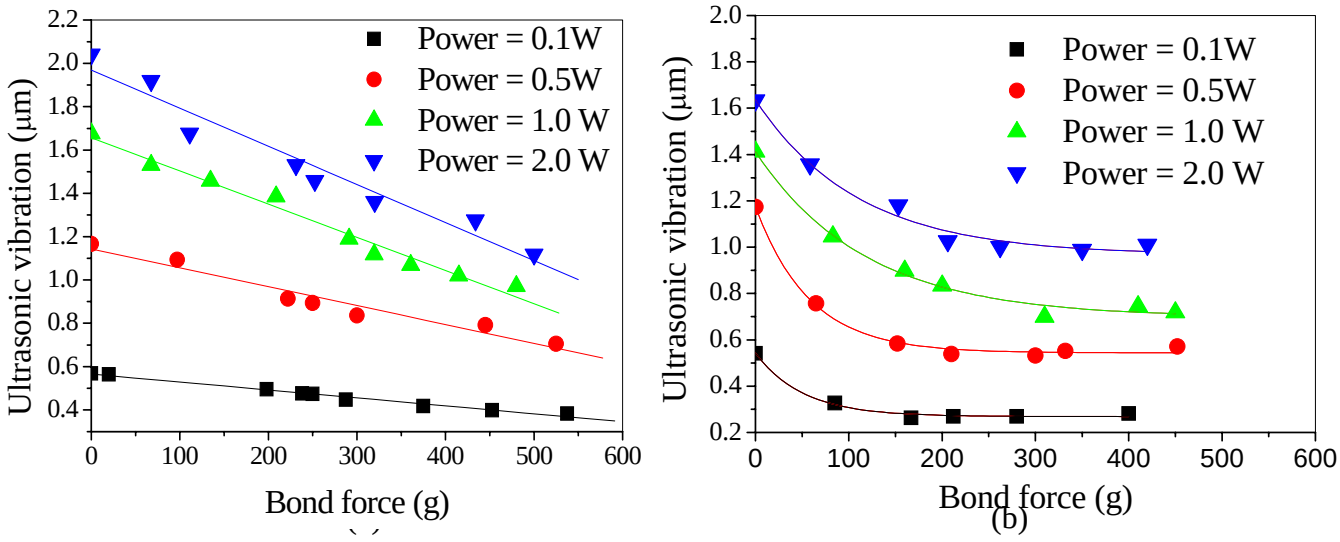

Fig.3.34 The collet displacement amplitude under loading for (a) transverse and (b) longitudinal mode.

3.4.3 Failure Analysis

Many well-recognized failure theories have been proposed in the past, including maximum distortion energy, maximum shear and maximum principal stress. The maximum principal stress theory states that fracture of brittle materials occurs when at least one of the principal stresses is equal to the failure stress in a simple uniaxial test of the material [61]. The failure criterion from the maximum principal theory is:

$$Max|\,\sigma_1,\sigma_2,\sigma_3|\,=\sigma_{fail} \qquad (5)$$

where σ_1 ,σ_2, σ_3 are the three principal stresses and σ_{fail} is the failure stress of the material. For the case of thermosonic bonding, the maximum principal stress is found to be σ_3 for all cases. For brittle materials such as silicon, there will be little or even no plastic deformation. The failure stress will be equal to the ultimate stress.

Fig. 3.35 shows the principal stress contours for the transverse and longitudinal bonding induced by 1 μm ultrasonic displacement and 100 gf per bump. The actual bond power for 1 μm displacement can be found in the laser vibrometer measurement results in Fig. 3.34. The estimated ultrasonic power would be 0.5 W and 1 W for the transverse and longitudinal bonding, repectively. For the transverse bonding, a 1 μm transverse harmonic displacement and a 100 gram compressive bond force were applied to the FEM. The steady state stress contour is plotted in Fig. 3.35(a). For the transverse case, due to the transverse displacemnet, shear deformation as well as compressive deformation were identified. By the interaction between shear and compressive stresses, the maximum prncipal stress occurs at the silicon layer right under the edge of the gold bump. For the

longitudinal bonding, both bond force and displacement were applied in the same direction. As all the loadings were uniaxial, only compressive deformation was observed. The princpal stress contour was plotted in Fig. 3.35 (b). Similarly, the maximum princpal stress is also identified at the silicon interface right under the edge of the gold bump. From the maximium princpal stress theory, silicon failure occurs if the stress induced is larger than $\sigma_{fail.}$ Similarly, the maximum stress induced can be found at different ultrasonic bond power and bond force.

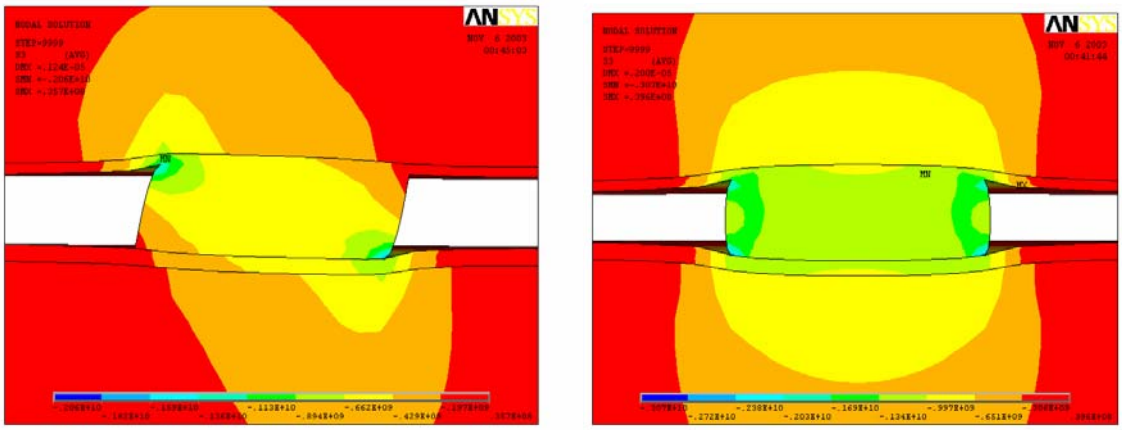

(a) (b)

Fig. 3.35 Principal stress contours for (a) transverse and (b) longitudinal bonding at an ultrasonic displacement of 1 μm and bond force of 100 gf per bump.

Fig. 3.36 shows the FEM results on the interaction between the maximum principal stress between the ultrasonic power and the bond force per bump for both transverse and longitudinal bonding. The maximum ultrasonic power is set at 2 W and maximum bond force is also limited to 500 gf per bump. For both bonding modes, the maximum principal stress of the silicon and gold interface occurs right under the edge of the gold bump as shown in Fig. 3.35. The stress also increases as the bond force and ultrasonic power

increases. For higher ultrasonic power, the longitudinal bonding generated a greater stress level than the transverse bonding. The maximum stress of longitudinal bonding can be as high as 1.2 GPa which occurred at a bond force of 200 gf per bump and an ultrasonic power of 2 W. The stress level is 20% higher than that of the transverse bonding. From a previous study by *P. Stepin* [62], the failure stress of silicon can range from 0.2 GPa to 2 GPa. The stress level calculated by FEM is sufficient to cause silicon cratering. To verify the cratering defect experimentally, thermosonic bonding was performed at an ultrasonic power of 2 W and bond force of 200 gf per bump on a 1 mm x 1 mm chip with 8 gold bumps. Shear tests were performed on the 20 bonding samples. The fracture surface was examined by the scanning electron microsocope (SEM). No cratering was found on all 160 gold bumps for transverse bonding. However, 3 samples from the longitudinal bonding have silicon cratering. Fig. 3.37 (a) shows a fracture surface with silicon cratering for the longitudinal bonding. The silicon chip was damage during the thermosonic bonding and a portion of silicon has been removed after shear test. Fig. 3.37 (b) shows a typical fracture surface of the transverse bonding under the same bonding conditions. No cratering was found. The bonding results indicated that the higher induced stress makes the longitudinal bonding more susceptible to the silicon cratering defect.

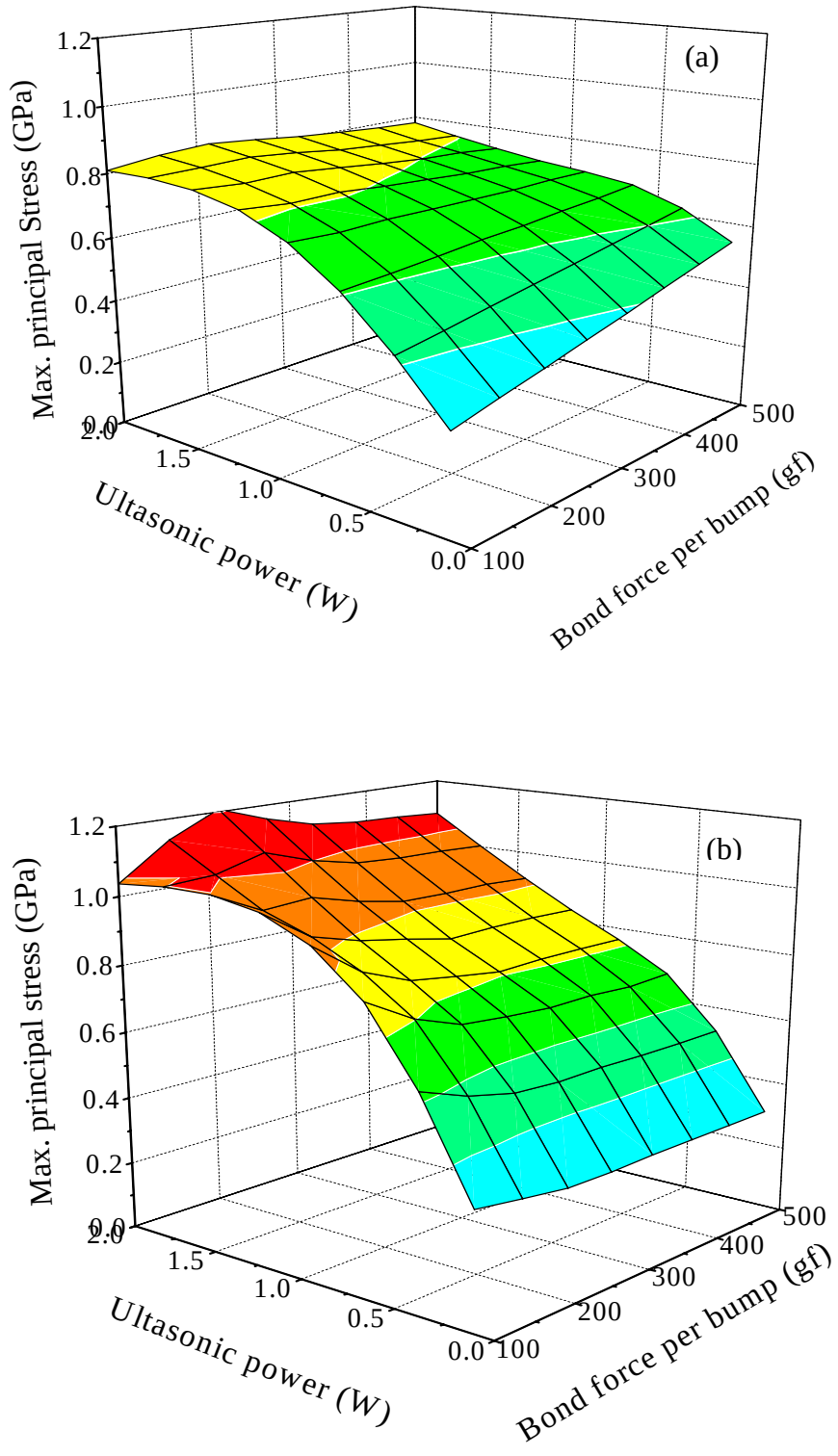

Fig. 3.36 Variation of the maximum principal stress, ultrasonic power and bond force per bump for (a) transverse and (b) longitudinal bonding.

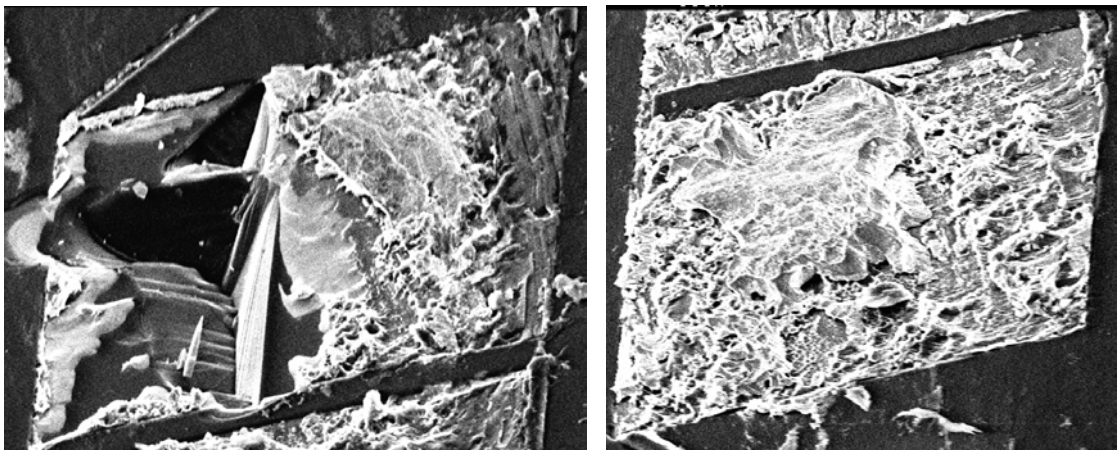

(a) (b)

Fig. 3.37 (a) Fracture surface showing cratering defect for a longitudinal bonding and (b) fracture surface for a typical transverse bonding.

3.5 Novel Push-pull Flip Chip Transducer

As both the transverse and longitudinal approaches have their own advantages and shortcoming, they cannot meet the requirements of the demanding thermosonic flip chip market. A novel transducer design is proposed to tackle the disadvantages of both TS flip chip transducer designs. The novel transducer offers the attractive features such as high ultrasonic displacement, perfect bonding co-planarity under high bond force, transverse displacement with minimal up-and-down (hammering) motion and minimization of rotary inertia, etc. The new transducer design concept has been adopted in a commercial thermosonic flip chip bonder in ASM and promising bonding performance has been identified.

3.5.1 Design Concept

Unlike conventional transducers, the novel dual driving transducer has two piezoelectric driving sources, that is the transducer consists of two Langevin drivers. The two Langevin drivers have been arranged to operate in an opposite phase. When one set of Langevin transducer expands, the other will contract. It contributes to a push-pull motion in the transducer. The push-pull action can be synchronized by a proper arrangement on the poling direction of the two Langevin stacks. Consider two Langevin drivers connected together with the PZT poling direction configuration in Fig. 3.38, with the electrical connection as indicated, one set of PZT stack will expand while the other contract. At resonance, the whole transducer will operate at a full wavelength mode to produce the push-pull motion. This structure builds up the fundamental idea of the novel transducer design. The mounting of the transducer must be on the axial displacement nodal point. From the displacement profile, the two nodal locations are in the middle of the two PZT stacks. Unlike conventional transducers, there will be two mounting supports. The dual support will enhance the transducer rigidity and maintain perfect co-planarity which will be discussed later.

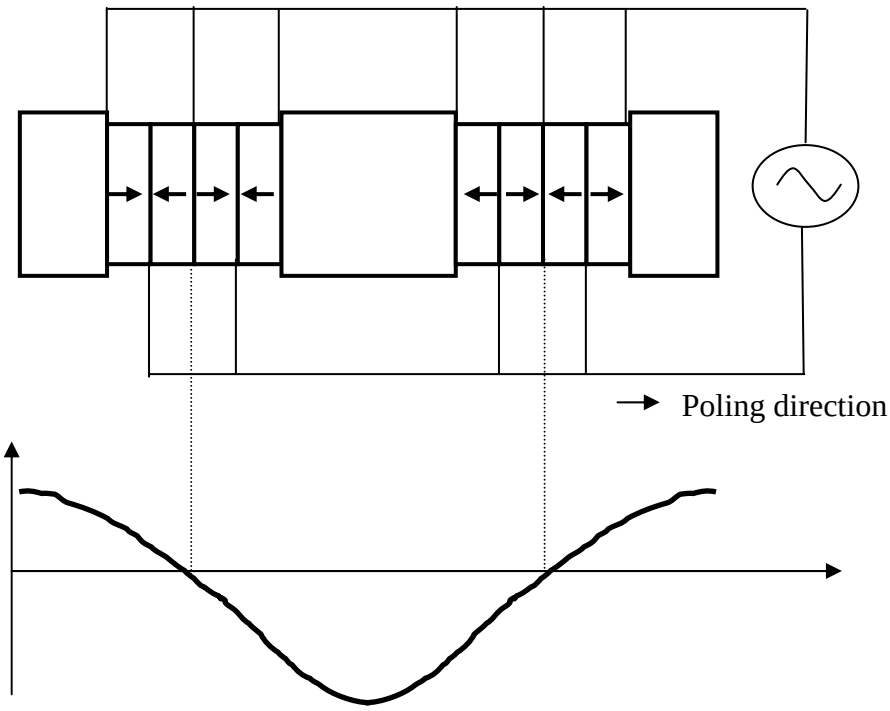

Fig. 3.38 Working principle of the novel transducer.

The new transducer prototype is shown in Fig. 3.39. It consists of two Langevin stacks and each PZT stack consists of 4 PZT rings with the poling direction arranged as shown in Fig. 3.38. There are two mounting flanges in the middle of each PZT Langevin stack. The two mounting flanges were linked to form the transducer bracket. The transducer is designed to operate at around 60 kHz. Therefore, the PZT rings have 12.7 mm outer diameter, 5.1 mm inner diameter and 2.3 mm thickness which follow the dimensions optimized for the transducer design. The transducer horn is bi-conical shape and located in between the two PZT stacks. The bi-conical shape allows the mechanical amplification of the ultrasonic displacement induced from each of the driving stack. Therefore, the maximum displacement location of the transducer will be in the middle where the collet is located. The tool drop of transducer has been tuned similar to the transverse transducer as

discussed in the previous section. However, due to the machine limitation on the spacing, the collet length has to be increased to 32.0 mm for the new transducer design.

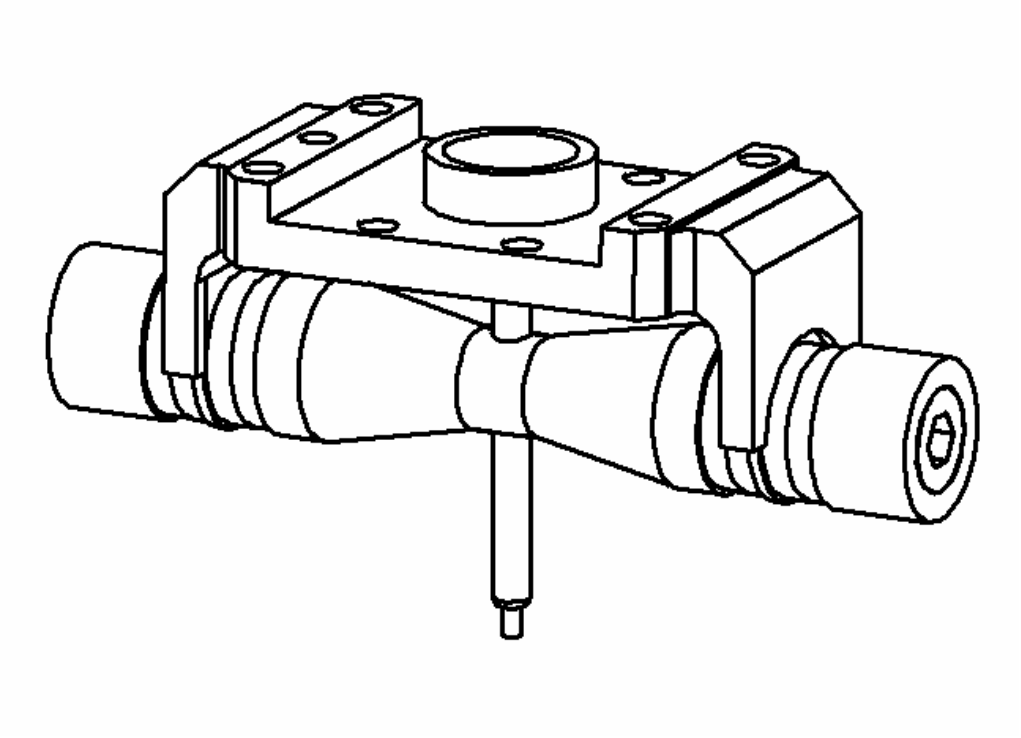

Fig. 3.39 The new push-pull flip chip transducer.

3.5.2 Finite Element Model

To understand the new design concept, a FEM was conducted to study the dynamic behaviours of the transducer prototype. Again, ANSYS will be used as the computational tool. Three dimensional FEM were performed to determine the vibration mode shape of the transducer at its operation frequency. As coupled-field elements, SOLID5, were used to build the PZT parts, it is possible to find both the resonance and anti-resonance frequencies. Similarly, perfect boundary interface is assumed and fine details for the transducer have been neglected. As the transducer has one symmetric plane and only the axial mode is concerned, one half of model with symmetry boundary conditions can be

used to represent the full model. The FEM model for the new transducer design is shown in Fig. 3.40.

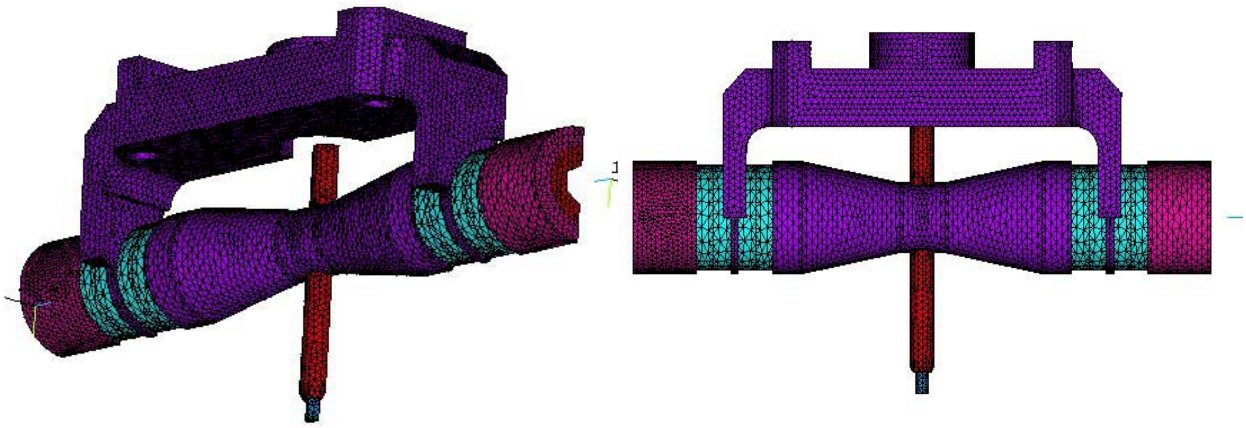

Fig. 3.40 Three dimensional model of the push-pull transducer
(a) isometric view and (b) plane view.

The majority of the transducer parts are made from aluminum alloy, Al-7075, including the bi-conical horn and the transducer bracket. The back plates of two Langevin stacks are stainless steel. The collet, purchased from Semicon Tool Ltd, is a hollow stainless steel body with a tungsten carbide tip. The diameter of the collet is 3.125 mm with a total length of 32.0 mm. Due to the complexity of the structure, higher order elements, 10-node tetrahedral solid elements and coupled-field elements were used. Symmetric boundary condition was applied at the plane of symmetry. Four ASM PZT8 rings with the optimized dimensions were used to construct the Langevin driver at each side. Fig. 3.41 shows the modal analysis results of the transducer and excitable mode shapes near 60 kHz and the details are listed in Table 3.5.

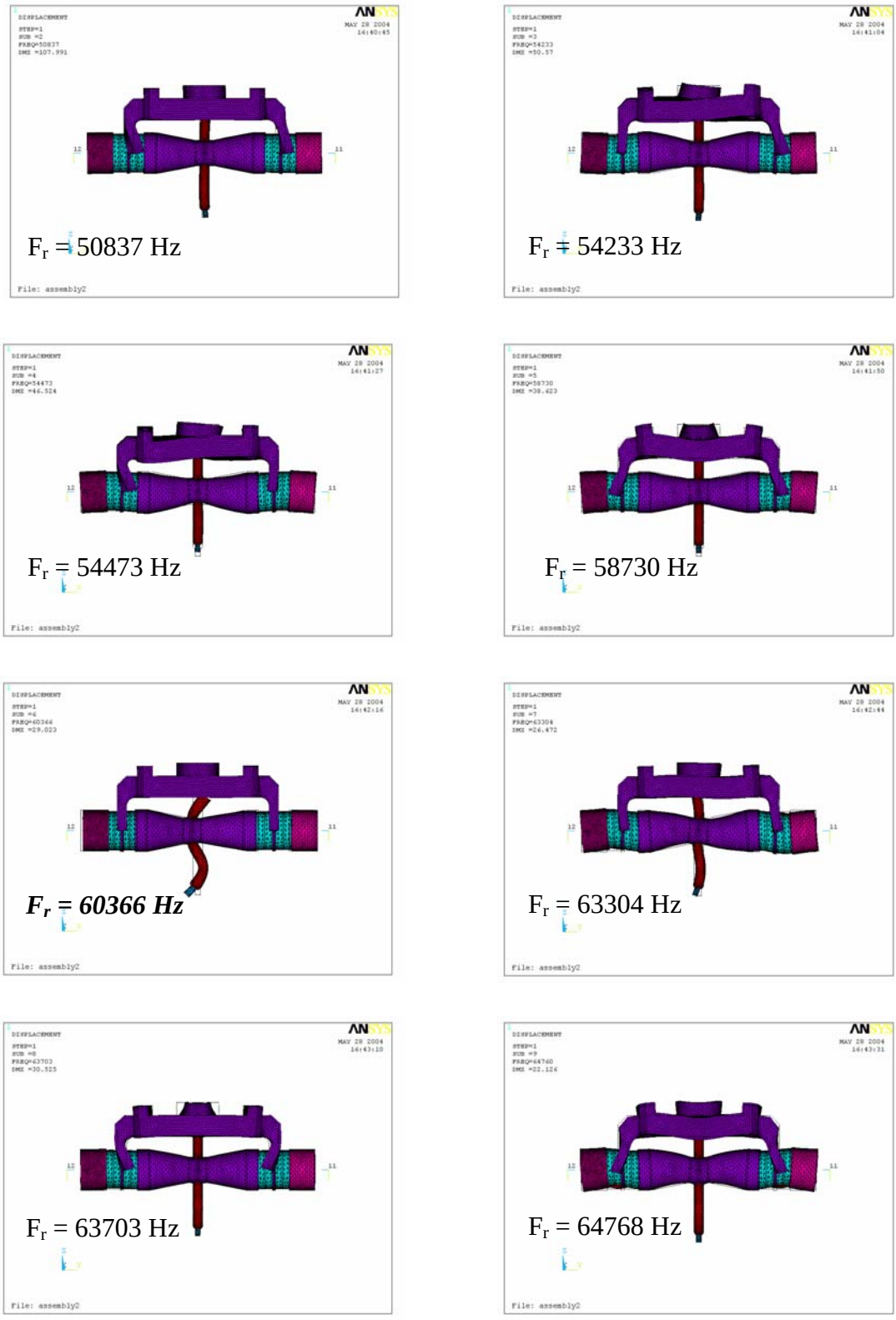

Fig. 3.41 Modal analysis of the push-pull transducer.

TABLE 3.5 MODAL ANALYSIS RESULTS NEAR 60 kHz.

Mode	F_r (kHz)	k_{eff}	Mode shape
1	50837	0	bracket mode
2	54233	0	bracket mode
3	54473	0	bracket mode
4	58730	0	bracket mode
5	60366	0.42	Axial mode
6	63304	0.09	Flexural mode
7	63703	0	bracket mode
8	64768	0.02	Hammering mode

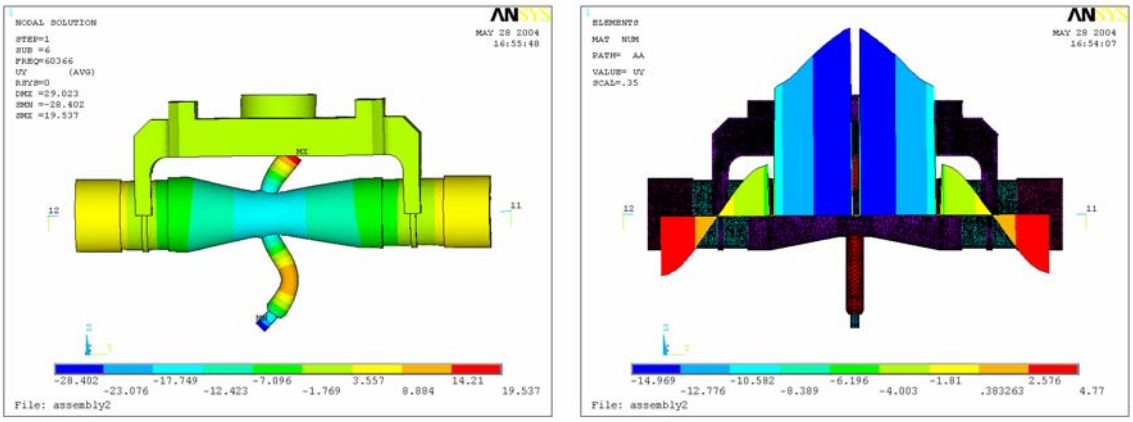

(a) (b)

Fig. 3.42 (a) Axial contour deformed shape and
(b) axial profile against the operation mode at 60366 Hz.

From the modal analysis, most of the modes simulated come from the complex structure of the transducer bracket. The operating axial mode is found to be 60366 Hz which has a largest k_{eff} of 0.42 among all the modes. Some other resonances, like a flexural mode and hammering mode, can also be found. However, those spurious resonances have very small coupling. The axial displacement contour of the operation mode is shown in Fig. 3.42 (a). It indicates that the bi-conical horn vibrates axially and maximum vibration is located in the middle. The collet is also vibrating transversely. The axial profile is plotted in Fig.

3.42 (b). The curve is discrete because some portion is hollow in structure. However, it can be clearly observed that the mounting locations are at the nodal displacement positions of the transducer.

One of the advantages of the novel design comes from the self-adjustment on the bonding co-planarity under a high bond force. Due to the balanced structure, both sides of the transducer will have the same degree of deformation under loading. The balanced structure allows the transducer to keep a perfect co-planarity even under deformation. A static analysis was performed on the new design. The deformation shape and Z contour under a static bond force of 1 kg is plotted in Fig. 3.43. Under a 1 kg bond force, there is 2.02 μm collet deformation in the Z-direction. However, by the beauty of the balanced design, the collet tip maintains a perfect co-planarity even subject to severe deformation. The structural design has solved the co-planarity issue encountered by the transverse design.

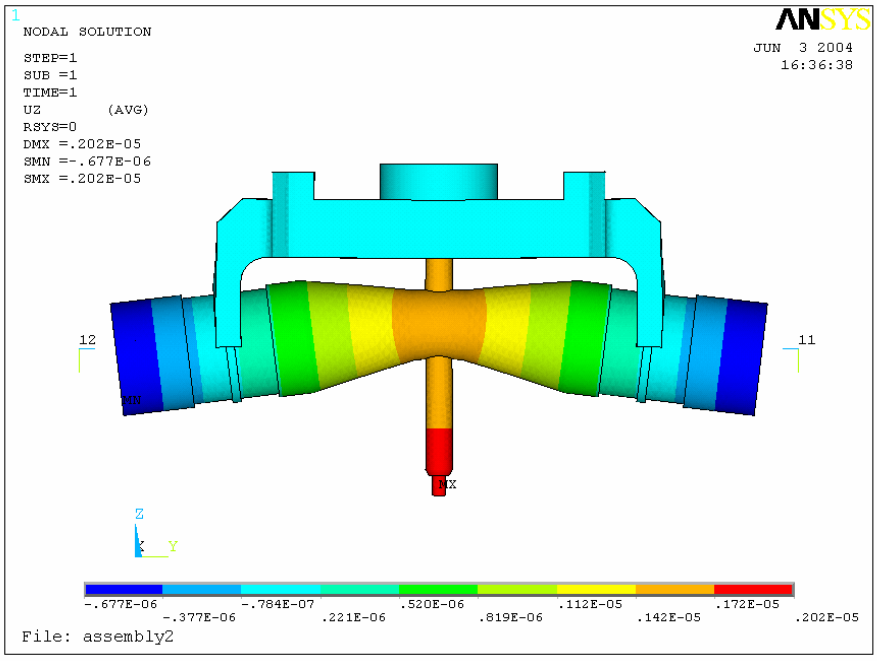

Fig. 3.43 Static deformation under 1 kg bond force.

3.5.3 Transducer Characteristics

Transducer prototype of the new design has been made by using ASM PZT8 rings. The photograph is shown in Fig. 3.44. The lead wires are connected to the required push-pull motion. Similar to the previous prototypes, the new transducer has also been characterized by its tool drop characteristics, electrical properties and vibration amplitude. Due to the geometry of the transducer and the bond head clearance, a longer collet has to be used. The collet length has been increased from 26 mm to 32 mm. However, the diameter of the collet has not been changed.

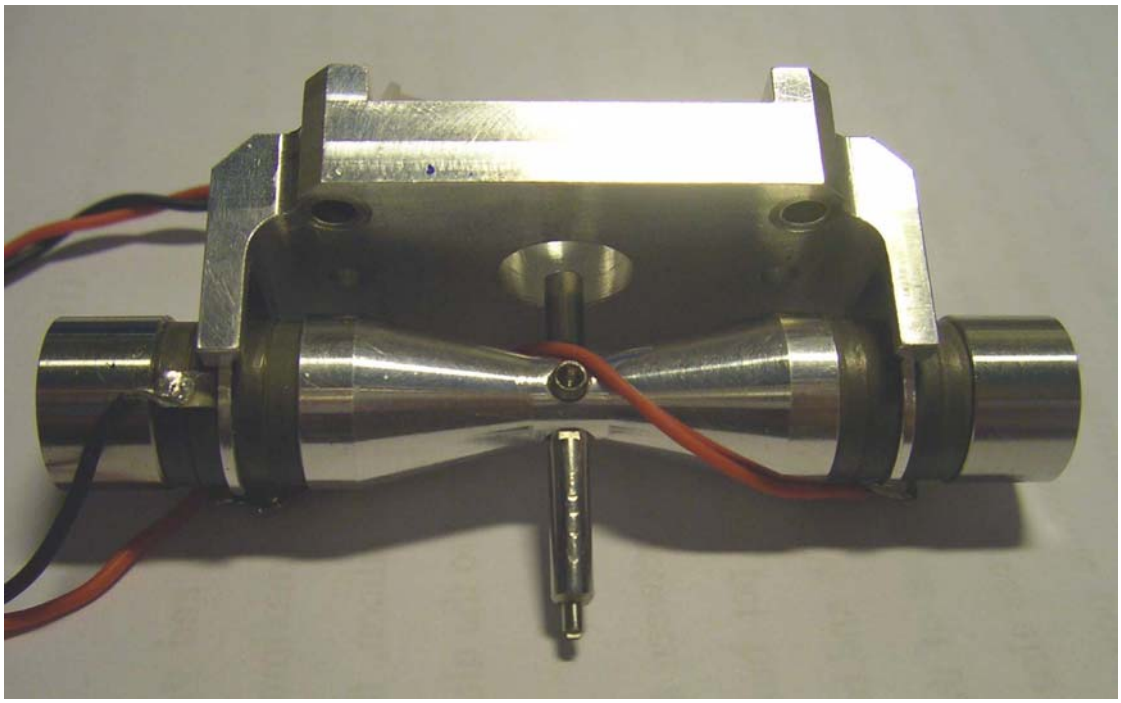

Fig. 3.44 The new push-pull transducer.

3.5.3.1 Tool Drop Characteristics

Similar to the transverse type design, the tool drop determines the characteristics of transducer. The tool drop has the same definition that it is the distance measured from the collet tip to the bottom of the horn. The characteristics of the transducer were measurement by a HP 4194A gain/phase impedance analyzer at different tool drop. The impedance and frequency against the tool drop is plotted in Fig. 3.45. Due to the machine requirement, the tool drop cannot be shorter than 15 mm. From tool drop range from 15.0 mm to 18 mm, both frequency and impedance are almost constant. When the tool drop exceeds 19 mm, a sharp change of frequency has been observed. It indicates that a random mode change occurs. Fig. 3.46 illustrates how the random mode change affects the electrical impedance spectrum of the transducer. Therefore, a tool drop of 17.0 mm has been used for the new type of transducer.

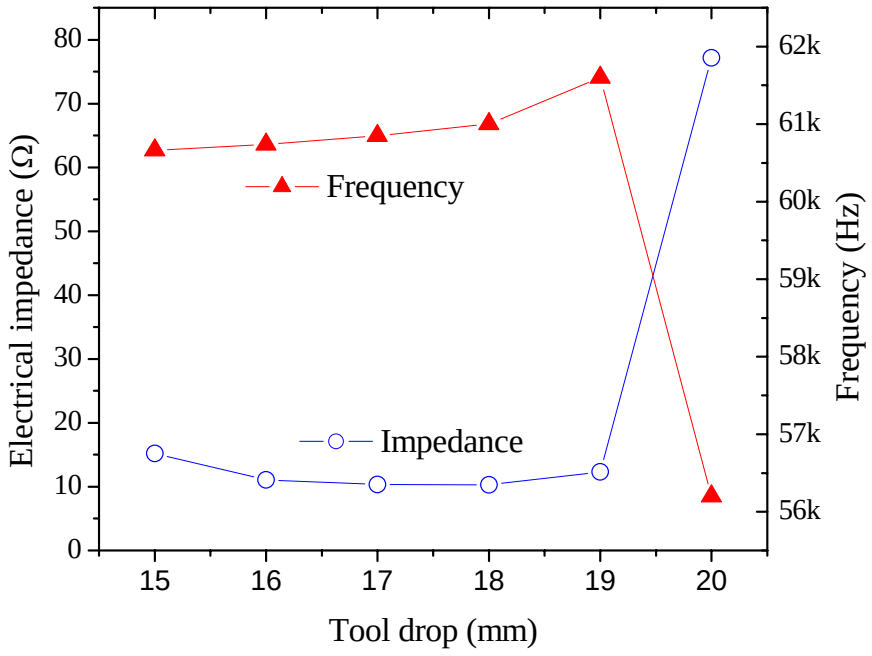

Fig. 3.45 Impedance and frequency vs tool drop for the novel transducer.

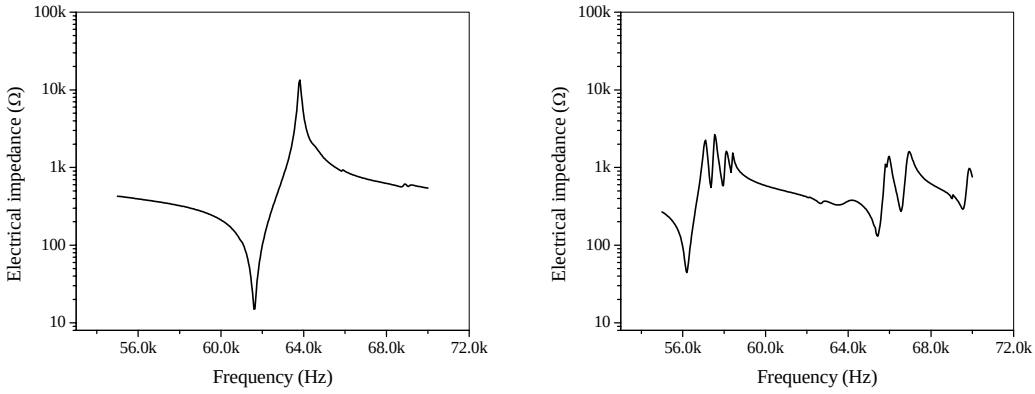

Fig. 3.46 Random mode change of the electrical impedance spectrum for a tool drop of (a) 19 mm and (b) 20 mm.

3.5.3.2 Electrical Properties

The transducer was characterized at an optimized tool drop of 17 mm at which the impedance was a minimum. Further, the transducer characteristics must be stable near the optimized tool drop. The electrical impedance spectrum measured by the impedance analyzer is shown in Fig. 3.47. At the optimized tool drop, the transducer has a clean electrical impedance spectrum and is free from other spurious resonance. An impedance of 11.2 Ω and a frequency of 61.2 kHz were measured in the new transducer. A summary of the transducer characteristics is listed in Table 3.6 and FEM results are also used for comparison. The electromechanical coupling factor predicted by the FEM is 0.32 which is slightly greater than the measurement result. Due to the complexity of the transducer, some energy has been lost to the joining interface between components. The energy loss reduces the actual energy conversion efficiency of the system and hence a smaller k_{eff} has been obtained.

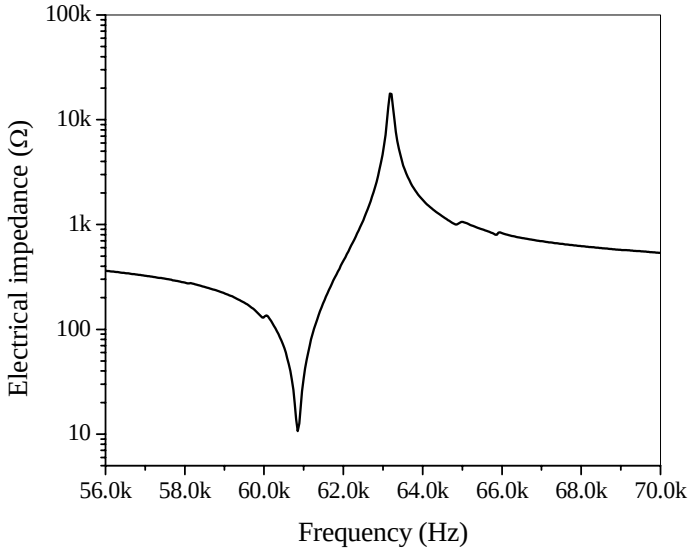

Fig. 3.47 Electrical impedance spectrum at the optimized tool drop (17 mm).

TABLE 3.6 SUMMARY ON THE ELECTRICAL CHARACTERISTICS.

	Measurement	FEM
F_r (kHz)	61.2	60.6
k_{eff}	0.28	0.32
Z (Ω)	11.2	-
Q_m	545	-

3.5.3.3 Vibration Amplitude

The vibration amplitude of the collet tip was measured by the Polytec laser vibrometer. The results are shown in Fig. 3.48. The new transducer has high vibration amplitude which is around double that of a transverse or longitudinal one. In the push-pull design, there are two Langevin drivers that synchronized the pull and push motion. Either one of the Langevin driver has the same amount of PZT rings as that of a transverse or longitudinal transducer. Therefore, due to the synchronization of the anti-phase motion,

the action of the two Langevin drivers has a summation effect on the vibration amplitude. As a result, the novel push-pull design offers superior vibration output. The high vibration is a very desirable feature for flip chip applications of high IO (> 100 pin counts) devices. Due to the double in the number of PZT rings, the new transducer has better power handling capability. For the transverse or longitudinal one, the power input will be saturated at around 3 W due to the high impedance at high power. However, by doubling the number of PZT rings in the new design, the transducer has increased the power input limit and an input power up to 5 W is possible.

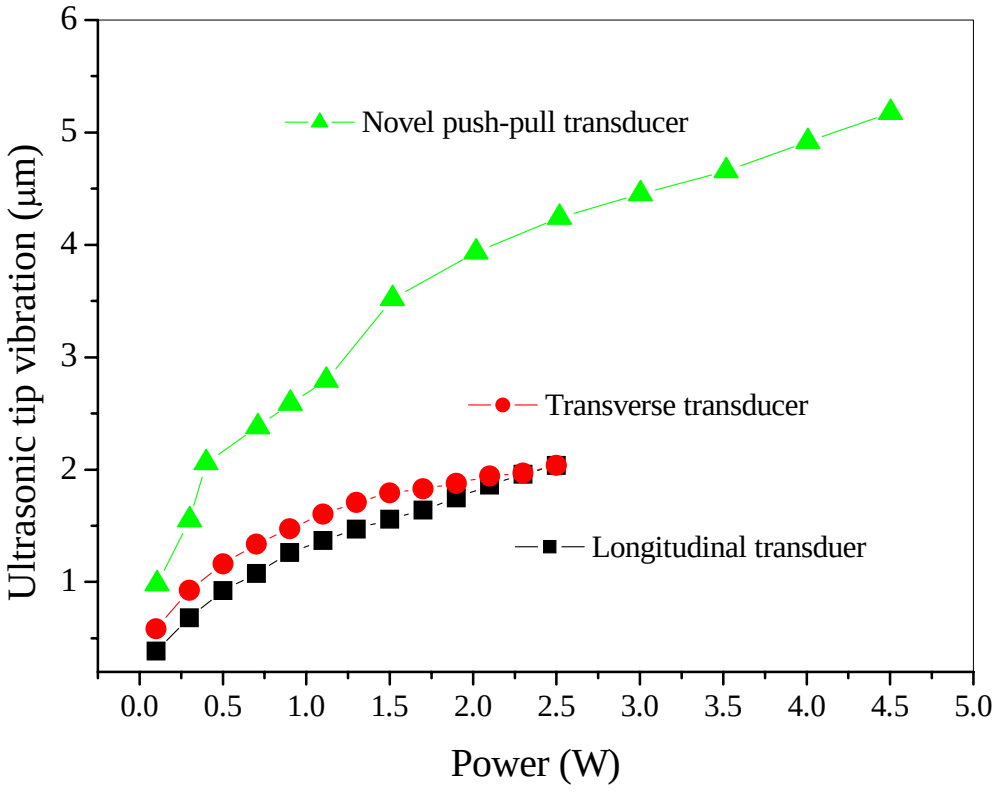

Fig. 3.48 Comparison on collet tip vibration for the novel push-pull design with the transverse and longitudinal transducers.

3.5.4 Bonding Performance

The new transducer was installed in a commercial TS flip chip bonder, AD900-TS, from ASM. The AD900-TS is a high speed production machine with the capability to handle thermosonic flip chip bonding applications. Fig. 3.49 shows the novel push-pull transducer on the AD900-TS bond head. The transducer takes the advantage of its balanced structure such that the rotary inertia can be minimized by aligning the rotary axis with the centre of gravity of the transducer.

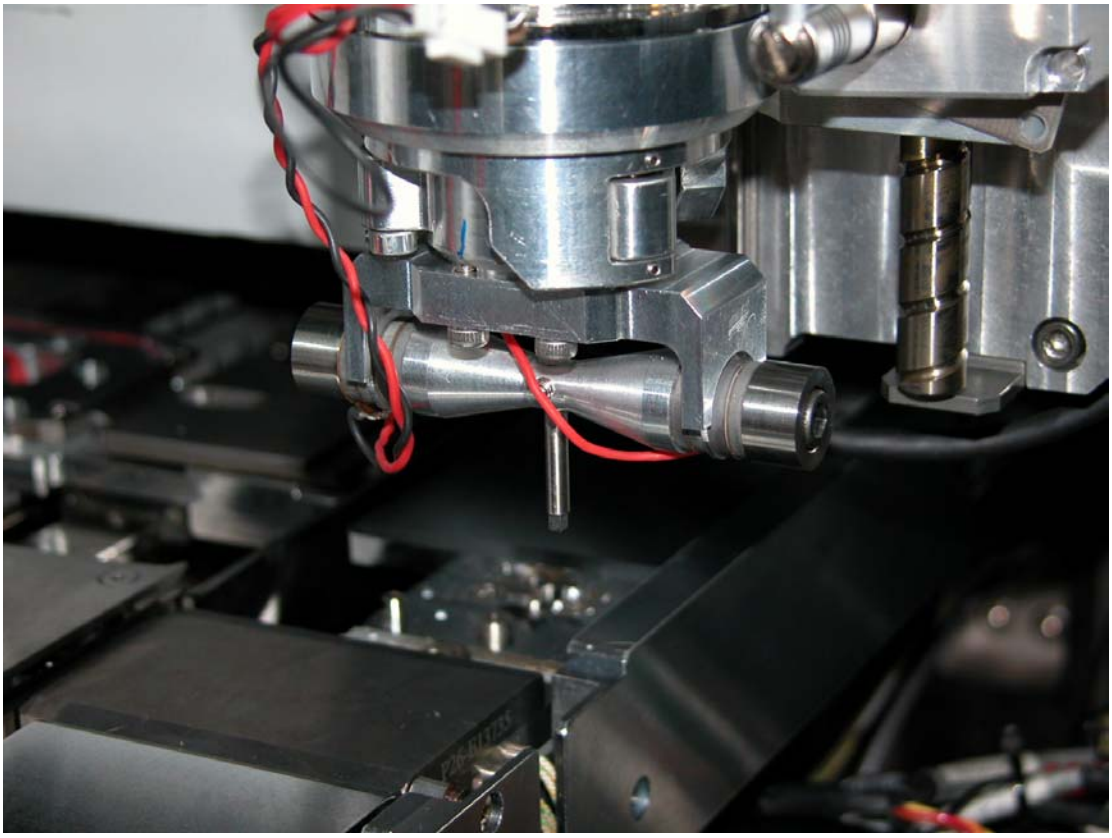

Fig. 3.49 Novel push-pull type transducer installed on an ASM commercial flip chip bonder.

By using the ASM test die 2000, with 8 gold bumps on the periphery, bonding tests can be performed on the LF substrate. The bond force used in the study is 1 kg which amounts to 125 gram per bump. The temperature was kept at 120 °C. After bonding, shear tests were conducted to examine the bonding shear strength. The stand off height of the bonded samples were also measured. The stand off height is defined as the average height of the gold bumps after thermosonic bonding. The stand off height can be easily measured under an optical microscope. The results under 1 kg bond force and a temperature of 120 °C are plotted in Fig. 3.50.

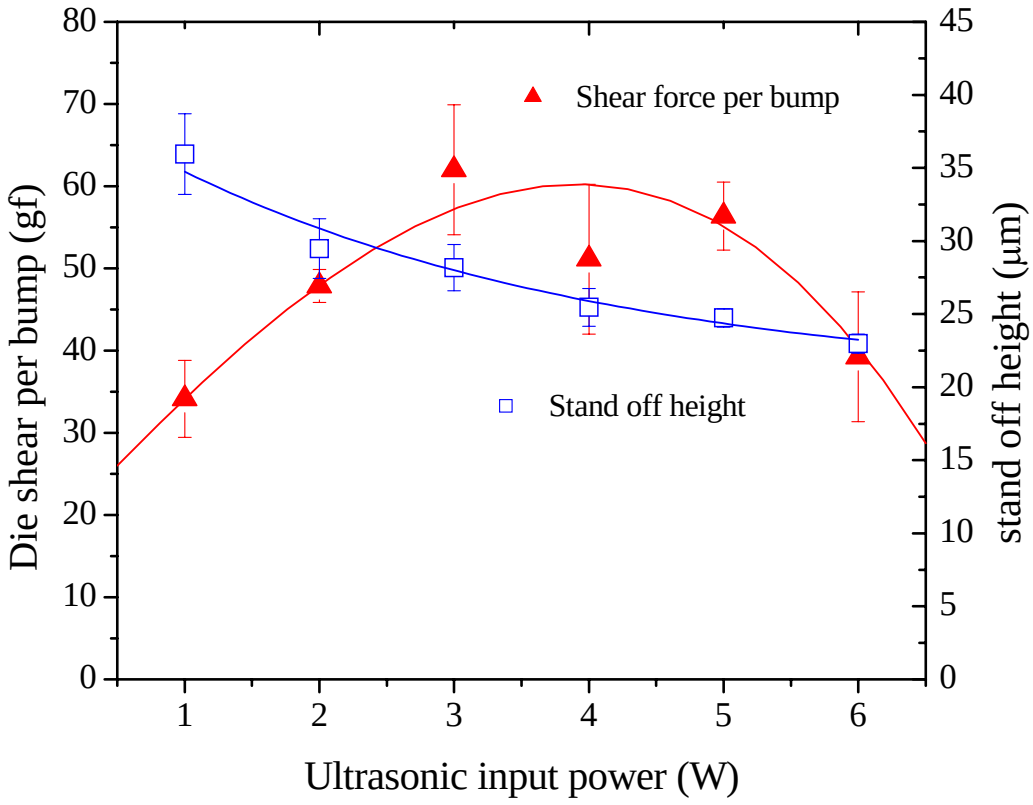

Fig. 3.50 Bonding results of the novel transducer under 1 kg bond force and a temperature of 120 °C.

Fig. 3.50 shows the bonding results of ASM test die at an ultrasonic power up to 6 W. When the bond power increases, the gold bumps will exhibit more deformation. The bump height will drop from 36 μm to 23 μm when the power increases from 1 W to 6 W. The stand off height will therefore reduce as the power increases and starts to saturate beyond 6 W. The shear strength increases as the power increases up to a maximum at around 3 W. Maximum shear strength of 62 grams per bump can be achieved. When the power is further increased, the shear strength starts to drop. The drop of shear strength can be explained by the fact that cratering occurs under excessive ultrasonic power. Therefore, the die will crack in the silicon layer rather than at the bonding interface. When more power is applied, more cracks will be induced and the shear strength is reduced.

After bonding, the die is removed from the substrate by an etching process. It is possible as the electrode pad of the die is an aluminum layer. By using sodium hydroxide (NaOH), the aluminum layer can be dissolved while the gold bumps are unaffected. After etching, Au bumps are left on the L/F substrate as shown in Fig. 3.51. There is no cracking on the corresponding die pad.

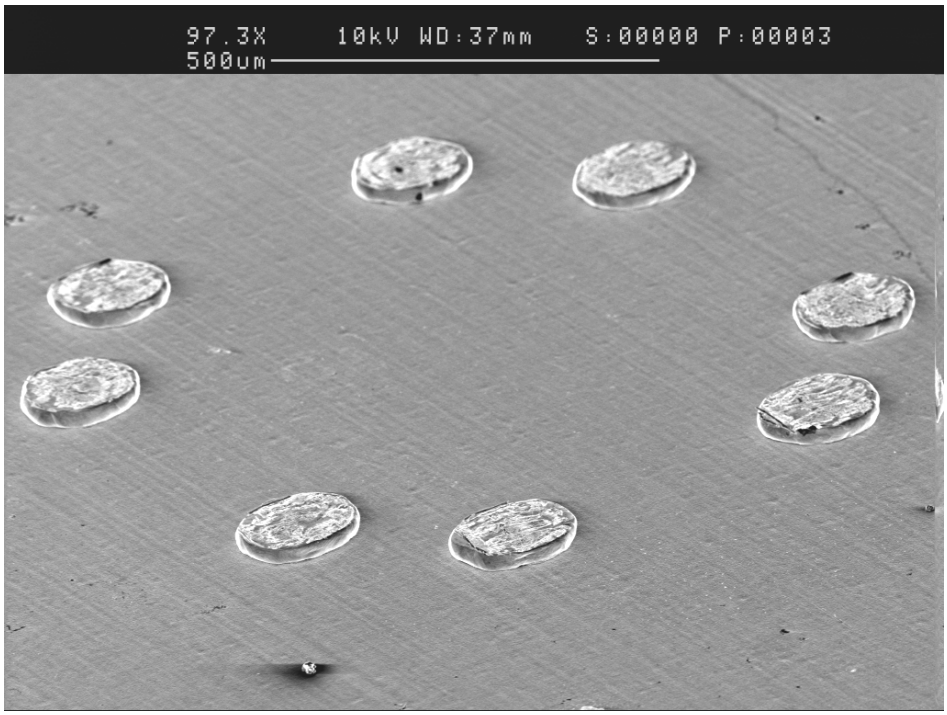

Fig. 3.51 Gold bumps on the substrate after removing the die by etching.

The removal of die making the measurement of gold bumps deformation easier. Fig. 3.52 shows the deformation in the bumps after bonding. It can be seen that the bumps deformed into an elliptical shape after bonding. Along the direction of ultrasonic vibration, the diameter of the bumps becomes larger while the other diameter keeps almost constant in spite of the power input. Fig. 3.53 shows the maximum bump diameter measured in the direction of ultrasonic vibration and the stand off height against the power. The diameter reflects the ball deformation which matches the change in the stand off height. When the power exceeds the optimized power of 3 W, the deformation of bumps starts to saturate. Further increase of the ultrasonic power may only induce bonding defect such as silicon cratering and reduce the shear strength.

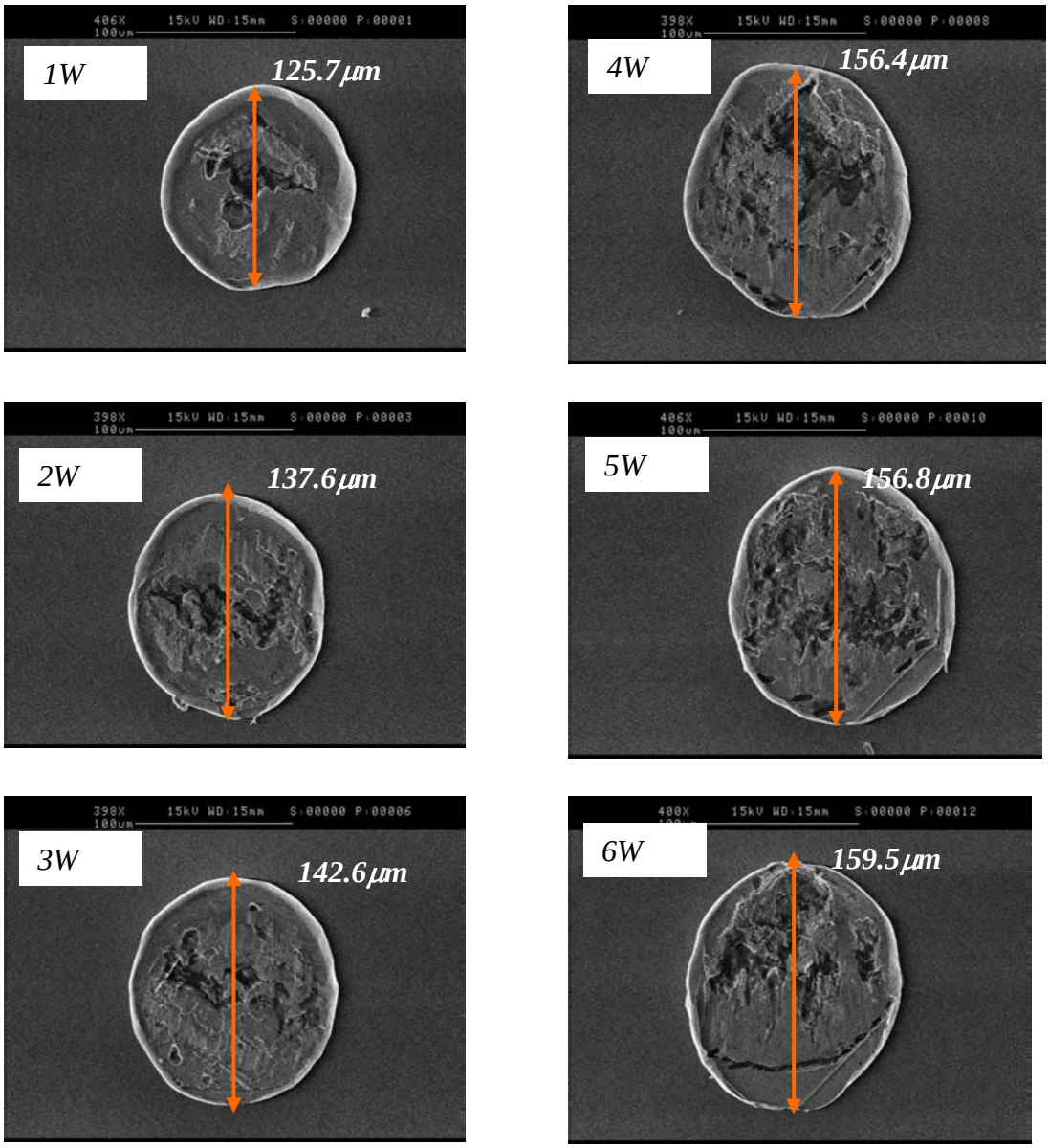

Fig. 3.52 Bonding deformation after bonding – bump diameter are measured in the direction of ultrasonic vibration.

The tilt angle of the die can be measured by the maximum difference in bump heights among the 8 bumps. The die tilt results at 3 W are shown in Fig. 3.54. An average of 2.38m deg tilting angle can be achieved which is comparable to the longitudinal approach.

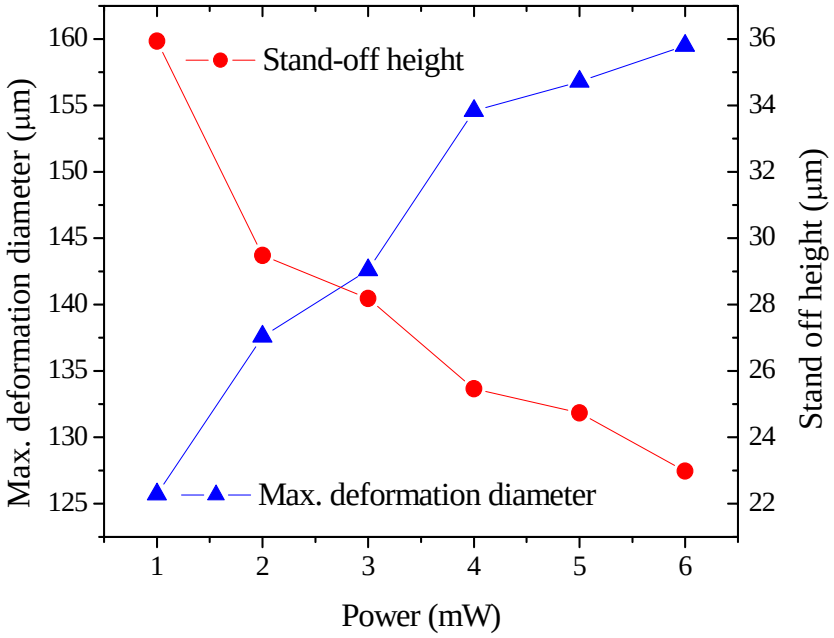

Fig. 3.53 Maximum deformation bump diameter and stand off height vs bond power.

(Bond force = 125 g per bump and temperature = 120 °C).

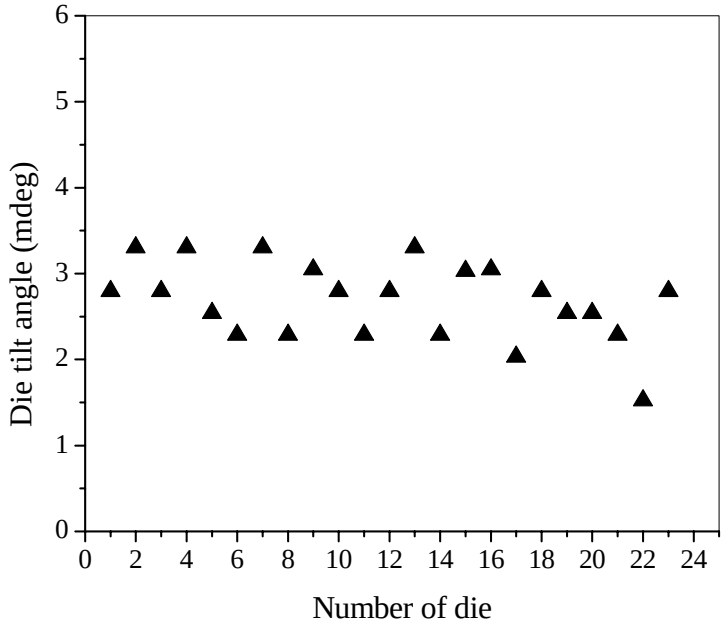

Fig. 3.54 Die tilting results for the push-pull transducer.

(Bond power = 3 W, bond force = 125 g per bump and temperature = 120 °C).

3.6 Summary

I) 60 kHz transducers were designed for both transverse and longitudinal thermosonic flip chip bonding. The design of flip chip transducers were based on finite element approaches. Three dimensional FEM was conducted to analyze the transducer characteristics. Good agreements were obtain between the FEM and experimental characterization.

II) A test rig was designed to conduct thermosonic flip chip bonding for both transverse and longitudinal transducers. The test rig can be used to identify the bonding defects between two approaches. Through both FEM analysis and experimental evidence, it was concluded that the transverse transducer does not have enough mechanical rigidity for high bond force. This could lead to the die tilting problem. In contrast, the longitudinal transducer is free from the tilting issue. However, the hammering motion (out-of-plane displacement) will induce higher stress concentration during longitudinal bonding. The high stress makes the longitudinal process more susceptible to silicon cratering defect.

III) A novel transducer design has been proposed which can overcome the shortcomings of both transverse and longitudinal bondings. The new push-pull transducer offers perfect co-planarity and pure transverse ultrasonic vibration. The new design idea has been adopted by a commercial flip chip bonder, AD900-TS, from ASM. Process study shows that the new transducer can achieve good bonding performance and is free from the bonding defects of die tilting and silicon cratering.

CHAPTER FOUR

MULTI-FREQUENCY TRANSDUCERS

4.1 Introduction

Ultrasonic energy was first introduced to the wire bonding process in the early 1970s [63-65]. The use of ultrasonic energy has successfully reduced the bonding temperature to around 200 °C which is only half the temperature of the thermocompression process without ultrasound. When the wire bonding technique was further developed in the 1990s, almost all the wire bonders were equipped with a 60 kHz transducer system. With the appropriate transducer dimensions, control electronic circuitries and the proven bonding stability, the 60 kHz system is a well-recognized and standardized system in the IC industry. Up to now, many commercial wire bonders in the market are still using 60 kHz transducer frequency. Other frequencies, ranged from 25 kHz to 780 kHz, have been reported for welding wires ultrasonically [66-70]. In the past decade, researches in high frequency wire bonding has been a very active topic. The use of higher frequency in ultrasonic bonding has been proven to have a number of advantages such as lower temperature bonding, shorter bonding time, enhancement of bonding strength, etc. However, the frequencies beyond 100 kHz require several modifications to the bonding process. Dedicated, well-designed electronic control systems are essential for making

effective and high quality bonds at higher frequencies. These make the high frequency bonding more susceptible to external disturbances. Therefore, the robustness and bonding window will be reduced when using high frequency bonding. In the practical point of view, the bonding frequency will reach a limit such that the bonding yield will be affected at extremely high frequency. With the development of transducer design and electronic systems, commercial wire bonders can now perform ultrasonic bonding in the range of 120 kHz to 140 kHz with yield greater than 99.99%. With further improvement of machine capability, frequencies higher than 140 kHz will be expected to come to the market in the near future.

4.1.1 High Frequency Bonding Phenomena

With the evidence that high frequency bonding reduces the temperature required, it is obvious that the introduction of ultrasonic energy substitutes the thermal energy. It is possible to explain that based on phonon generation [71]. A phonon is a quantum of vibrational energy in the lattice of atoms. With the action of thermal energy or acoustical energy, phonons can be generated. As more phonons will be scattered and generated at high frequency acoustical vibration from the transducer, it facilitates the movement of dislocation in the bonding material and hence leads to an ultrasonic softening. The ultrasonic softening of metal is an essential phenomenon to start an ultrasonic bonding. With higher acoustical vibration energy at higher frequency, the dislocation in the material will be simulated by the increasing amount of phonons. The increased reactivity at higher frequency because of metal softening will diminish the temperature required during the wire bonding process.

4.1.2 Advantages and Disadvantages of High Frequency Bonding

Based on the literature of high frequency bonding, the pros and cons are briefly discussed and summarized. From a previous research conducted by ESEC and Texas Instruments [72], gold wire bonding at ambient temperature has been demonstrated by a 240 kHz transducer system. The low or even room temperature bonding allows the choice of organic substrates such as BGA or smart cards to be possible for ultrasonic bonding. Similar findings have also been published from other research groups. [71, 73]. The shear strength has been reported to show a 25% increase when compared to a 60 kHz bonding process. The enhancement of bonding strength provides advantages for the fine pitch applications. Smaller deformation in the wire at high frequency can produce equivalent shear strength similar to a large bond width bonded at low frequency. The reduction of wire deformation allows fine pitch bonding (less than 40 μm pitch) to be possible. Another implication of bonding enhancement at high frequency is that the bonding could be achieved in a shorter period of time when compared to the low frequency process. The reduction in bond time is one of the most critical concerns for high speed wire bonder nowadays. However, the process windows for higher frequency bonding are usually narrower [74]. The narrow process windows make the high frequency bonding more susceptible to external factors such as material variation, cleanness of bond pad, vibration of the machine, etc. Any one of that can reduce the high frequency bonding yield significantly. The situation has become even worse at the second bond on PCB substrate. The PCB substrate usually has a less precise material control. Therefore, the robustness of high frequency bonding is not as high as the standard 60 kHz system. It has been also reported that for sensitive material, the low frequency bonding gives better yield and offers more stable bonding results. Therefore, the high frequency and low frequency ultrasonic

bondings have their respective advantages and disadvantages. The choice of the transducer frequency will therefore depend on the actual applications.

4.1.3 Multi-frequency Bonding

The reason for multi-frequency bonding is that it can make use of the advantages for both high frequency and low frequency bondings. Fine pitch applications are mainly required at the bond pitch of the die and not on the substrate. The minimization of chip for high IO density devices presents a great challenge for the wire bonding technique. Bonding pitch of less then 40 μm can only be achieved using higher frequency process. However, the high frequency bonding also reduced the yield on the substrate where fine pitch has not been required. For the second bond on the substrate, a low frequency bonding will be more desirable. A multi-frequency transducer that can operate at both high and low frequencies will then be very useful for wire bonding. It can achieve fine pitch and lower temperature 1st bond on the die using high frequency, at the same time it can improve the robustness and yield of the 2nd bond on the substrate by using a lower frequency bonding. Fig. 4.1 shows how the multi-frequency bonding can benefit the wire bonding process.

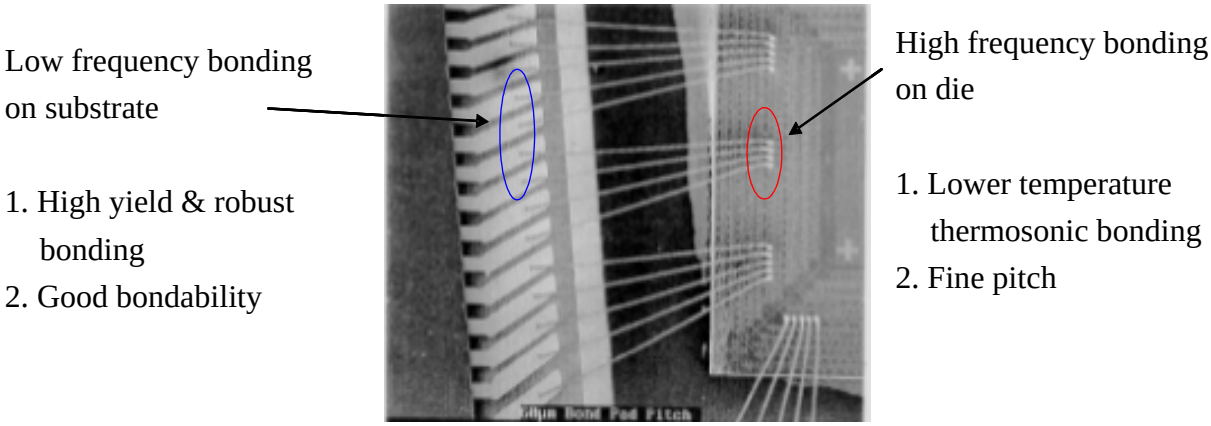

Fig. 4.1 A photo to illustrate the benefit of multi-frequency bonding.

4.2 Nodal Position Matching Method

To design the multi-frequency transducer in wire bonding, several design criteria have to be considered. One of the most important criteria of basic transducer design is that the mounting, either in the form of flange or barrel, has to be located at the axial nodal position. The axial displacement profile for a typical 64 kHz wedge transducer is shown in Fig. 4.2. From the axial displacement distribution, the barrel is attached to the transducer at its nodal point. The significance is very obvious. Provided that the transducer mounting has shifted away from the zero displacement location, the ultrasonic energy generated from the Langevin driver can drain into the mounting structure. It is likely to excite the resonances of the mounting structure with frequency near the transducer operation frequency. Therefore, when the transducer has been clamped or mounted on other supporting structure, a drastic increase of impedance will happen. The high impedance indicates that ultrasonic energy has been lost to other structures rather than retained inside the transducer. The circumstance can sometimes be detrimental. Not only the lost of ultrasonic energy affects the stability of transducer power output, but also the structural resonance of the bonder can be excited and causes a dramatic drop in the bonding yield. That is why other axial resonances, which do not have a nodal point at the mounting position, cannot be used in the ultrasonic bonding process. In the nodal position matching approach, we will derive a methodology to examine the bundle of axial resonances excited in the frequency domain. With fulfilment of some basic criteria, it can be proven that, apart from the designated operation mode, there are other resonances that can perform the ultrasonic bonding with good results. A case study on a commercial ball bonding transducer will be demonstrated to show how the multi-frequency ability can be optimized.

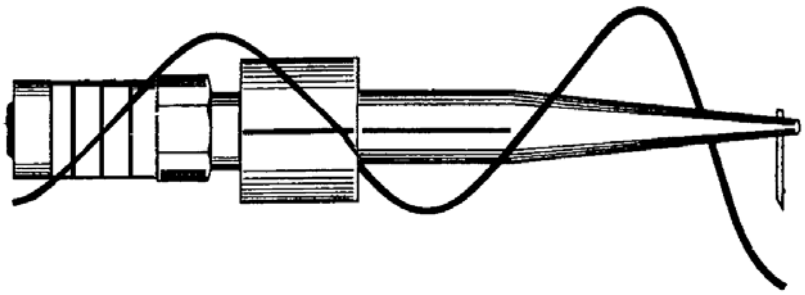

Fig. 4.2 An axial profile showing the mounting nodal position.

4.2.1 Transducer Characteristics

Consider a commercial ball bonding transducer (Uthe BS512L) as shown in Fig. 4.3, according to the manufacturer's specification, the transducer is designed to work at a frequency around 136.8 kHz. In theory, this commercial transducer can only be operated at a single frequency specified by the manufacturer. If it is desired to use a different frequency for bonding operation, then it is necessary to replace the transducer with a different design for that designated frequency. However, using the nodal position matching method that utilizes both FEM analysis and experimental verification, it can be proven that this commercially available transducer has more than one frequencies that meet the transducer design criteria. Furthermore, the transducer has found to have good ultrasonic properties in more than one resonance modes. And, it has been proven by FEM and experimental methods that the transducer can be multi-mode and can perform wire bonding operations at different frequencies.

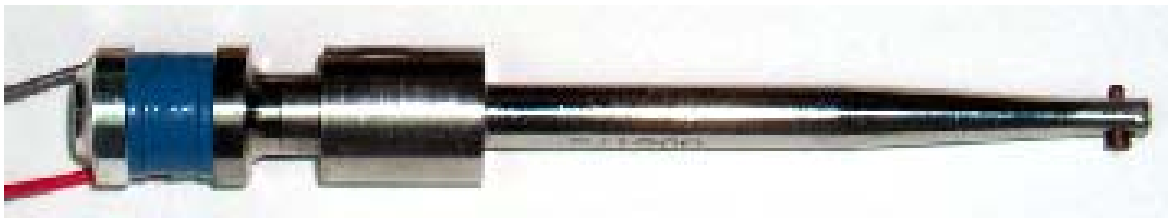

Fig. 4.3 A commercial wire bonding transducer from Uthe.

Consider the electrical impedance spectrum of the transducer from 20 kHz to 200 kHz obtained by the HP 4149A impedance analyzer, a bundle of resonance modes can be identified. The operation mode was found at 136.8 kHz with the lowest impedance of around 9 Ω. Apart from the designated operation mode at 136.8 kHz, there are a number of resonances with strong electromechanical coupling. Some of them are axial modes of different orders and some are undesirable complex modes such as torsional or bending modes of the transducer. However, by merely observing the electrical impedance spectrum, there is no way to identify the mode shape of each individual resonance. The electrical impedance signature gives no information on the vibration mode of the transducer. It can only provide the information of the electromechanical coupling factor and the lost factor are determined by the anti-resonance frequency and impedance, respectively. Therefore, an analysis of the vibration characteristics of the transducer is necessary and can be performed by using ANSYS, or other commercial FEM package. Such modelling enables the modes of vibration which can be excited in a given frequency range to be determined and to accurately characterize the corresponding mode shapes and vibration amplitudes.

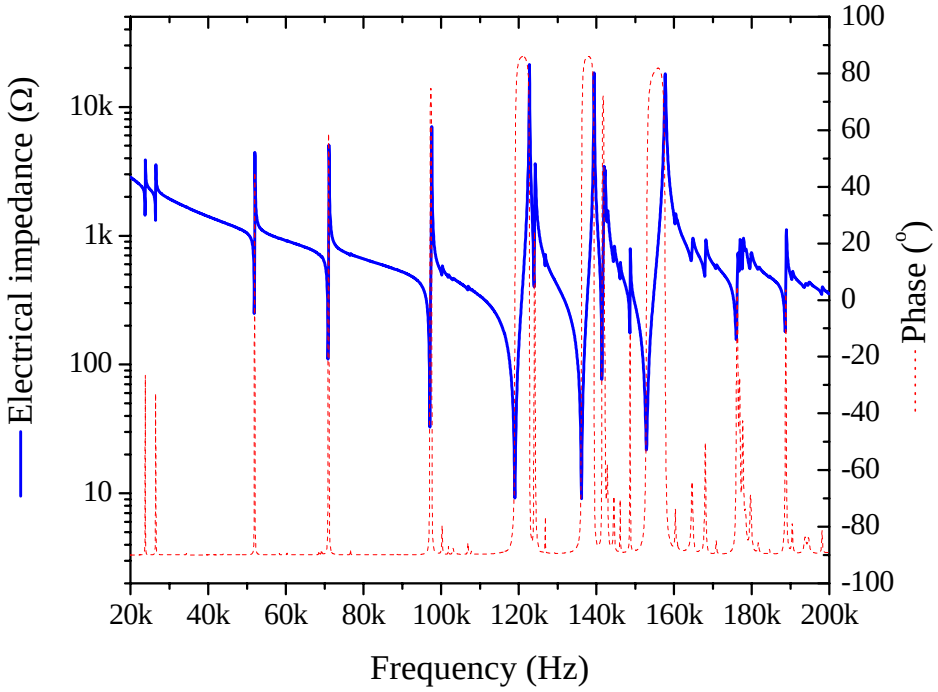

Fig. 4.4 Electrical impedance and phase spectra for the BS512L Uthe transducer.

4.2.2 Finite Element Model

To identify the mode shapes of the transducer in its frequency domain, a modal analysis was performed. A full three dimensional finite element model was constructed such that all possible resonances can be simulated. Similar to the previous simulation, some assumption has been made on the mode. All the interfaces are perfectly joined and small features or fillets are neglected. Initially solid 3D elements with 8 nodes were used to construct the majority of the models, except for the fine detail of the transducer tip. However, due to the complexity of the structure, high order solid elements with 20 nodes have to be used instead. Again, coupled field elements (SOLID 5) were used to model the PZT rings for the transducer. The full 3D model is shown in Fig. 4.5.

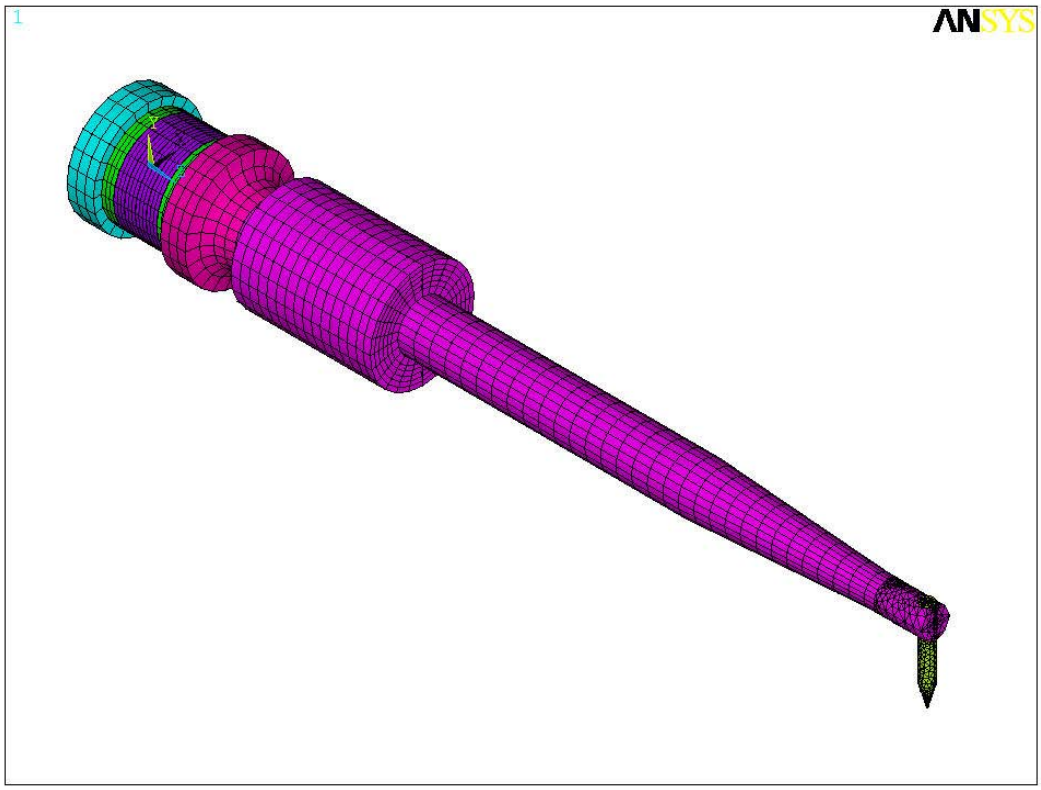

Fig. 4.5 The full three dimensional finite element model of the Uthe B5SL17 transducer.

With the use of coupled field analysis from ANSYS, both resonance and anti-resonance frequencies can be simulated. The first 50 allowable modes calculated from the modal analysis are summarized in Table 4.1. Some of these modes have the same or nearly the same frequency for both resonance and anti-resonance. It indicates that those resonance modes cannot be excited electrically and therefore, it will not be observed in the electrical impedance spectrum. By using the FEM analysis, all the axial resonances of the transducer can be determined up to 200 kHz. The axial modes are high-lighted in Table 4.1. There are all together 8 axial modes being identified up to 200 kHz. The designated operation mode from the manufacturer is found to be the 6^{th} axial mode with a frequency of 136.67 kHz.

TABLE 4.1 MODAL ANALYSIS RESULTS OF THE FIRST 50 MODES.

Mode	F_a (Hz)	F_r (Hz)	k_{eff}	Mode	F_a (Hz)	F_r (Hz)	k_{eff}
4	2543.7	2543.7	0.00	28	115460	115460	0.00
5	6355.1	6355.1	0.00	29	116970	116960	0.01
6	10925	10925	0.00	***30***	***123570***	***122110***	**0.15**
7	16827	16827	0.00	31	125590	124730	0.12
8	19959	19959	0.00	32	132230	132080	0.05
9	***24034***	***24015***	**0.04**	33	132920	132920	0.00
10	26130	26122	0.02	***34***	***138460***	***136650***	**0.16**
11	32575	32572	0.01	35	143830	141810	0.17
12	***36594***	***36474***	***0.08***	36	146570	145930	0.09
13	41292	41292	0.00	37	149580	147270	0.18
14	44488	44488	0.00	38	149870	149870	0.00
15	51614	51614	0.00	***39***	***157070***	***156100***	**0.11**
16	59144	59121	0.03	40	161910	160890	0.11
17	62870	62870	0.00	41	162910	162580	0.06
18	***79334***	***78704***	**0.13**	42	164700	164490	0.05
19	80613	80611	0.01	43	165210	165210	0.00
20	81168	81168	0.00	44	174360	174290	0.03
21	81577	81577	0.00	45	175760	175580	0.05
22	96583	96091	0.10	46	177550	177550	0.00
23	***97222***	***96948***	**0.08**	47	178660	178640	0.01
24	104120	104120	0.00	48	180640	180640	0.00
25	108040	108040	0.00	***49***	***186950***	***186040***	**0.10**
26	109350	109350	0.00	50	188920	188910	0.01
27	113160	113160	0.00				

The axial displacement profiles of all the axial modes are plotted in Fig. 4.6. It is found that the transducer has its fundamental axial mode, with half-wavelength resonance, at around 24 kHz. At each high order axial mode, there will be an increment of half wavelength and a 4λ axial resonance is found at 189.9 kHz. The operation mode, at 136.67 kHz, is found to be the 3λ axial mode. The mounting barrel was located right at the axial nodal position. However, it is interesting to note that besides this operation mode, the 2λ axial mode at 96.9 kHz also has a nodal point located at this mounting position.

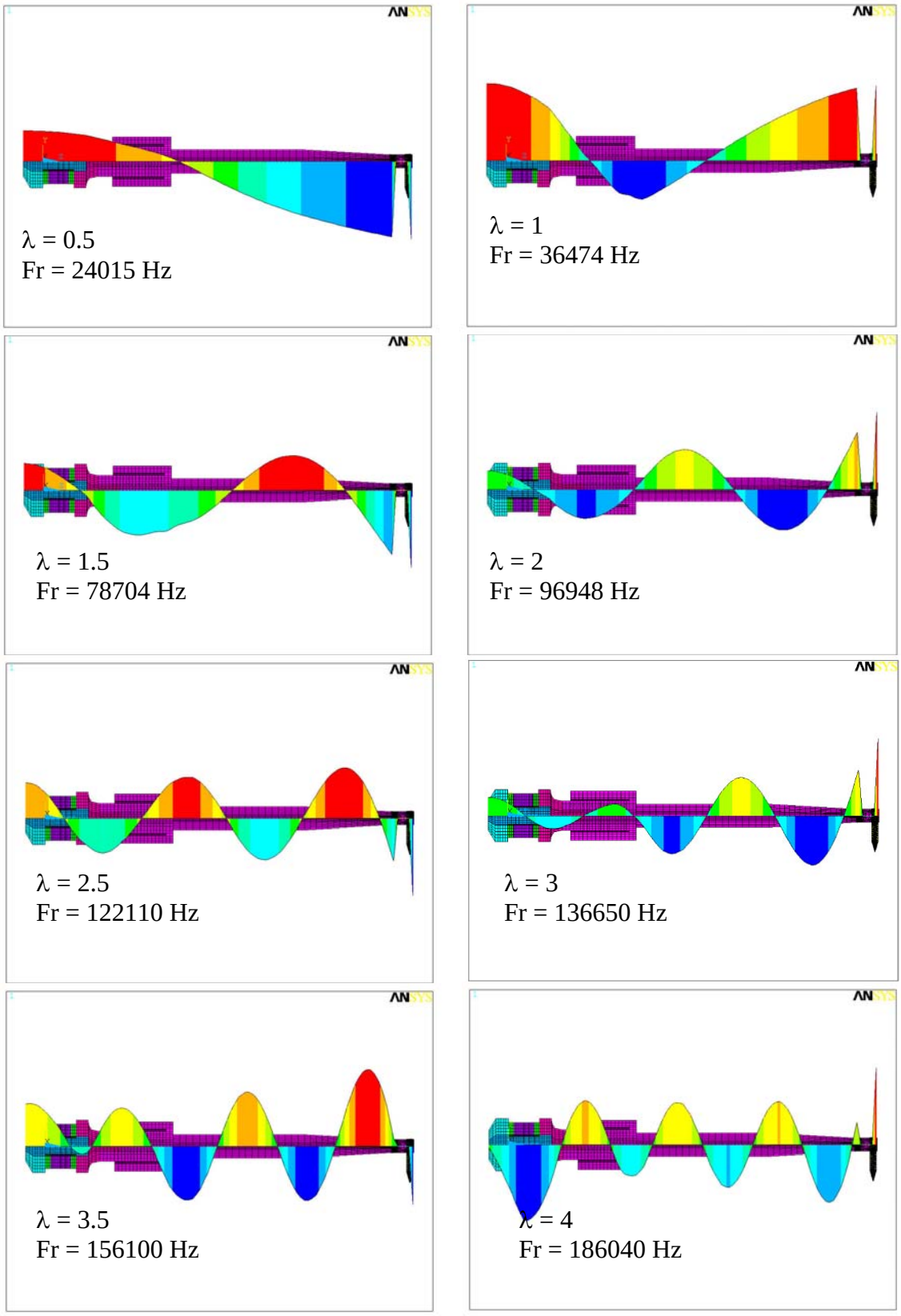

Fig. 4.6 Modal analysis results showing all the axial mode profiles.

The axial displacement profiles for both 2λ and 3λ axial modes are plotted and compared in Fig. 4.7. It is found that both resonances have a common nodal position where the barrel is attached. And, both resonances have an amplification of vibration amplitude near the horn tip where the capillary is located. The driving location of the 2λ mode is not located exactly at the nodal position of the driver and this will lead to an increase in the transducer impedance and reduction in the electromechanical coupling factor. However, provided that the transducer impedance can be maintained at a reasonable level, less than 40 Ω in practice, the transducer can still be operated in the 2λ mode. The only drawback is that a slight greater power has to be input to compensate for the high impedance and low coupling factor. A summary on the measurement and FEM prediction of all the axial modes are given in Table 4.2.

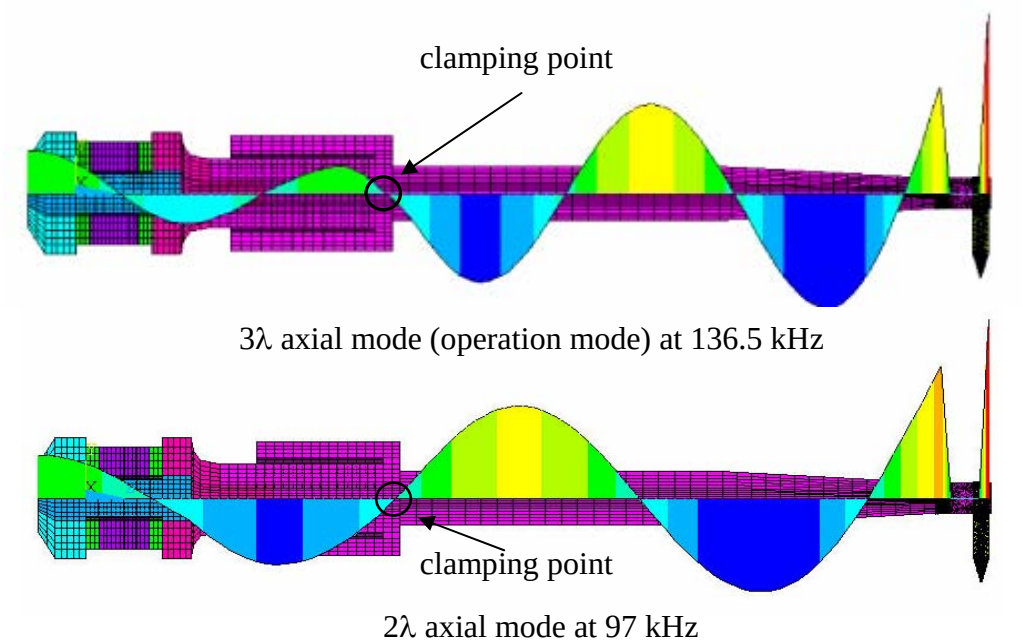

Fig. 4.7 The FEM results of axial displacement profiles for both 2 and 3 wavelength modes.

The merge in the nodal position of the two resonance modes gives the transducer the ability to operate at more than one frequencies. At both resonance frequencies of 136.5 kHz and 97 kHz, the transducer can be mounted without disturbing the ultrasonic properties. However, more experiments have to be carried out to further support that claim. A laser displacement measurement has been performed to verify the nodal position experimentally.

TABLE 4.2 SUMMAY ON THE AXIAL MODE CHARACTERISTICS.

	FEM			Experiment		
Mode	**F_a (Hz)**	**F_r (Hz)**	**k_{eff}**	**F_a (Hz)**	**F_r (Hz)**	**k_{eff}**
0.5 λ	24015	24034	0.04	23850	23750	0.09
1 λ	59144	59121	0.03	52050	52190	0.07
1.5 λ	79334	78704	0.13	71150	70900	0.08
2 λ	***97222***	***96948***	***0.08***	***97600***	***97100***	***0.10***
2.5 λ	123570	122110	0.15	122750	11900	0.25
3 λ	***138460***	***136650***	***0.16***	***139400***	***136150***	***0.21***
3.5 λ	157070	156100	0.11	157750	152900	0.25
4 λ	186950	186040	0.10	188950	188650	0.06

4.2.3 Experimental Verification

To verify the nodal position experimentally, an in-plane laser vibrometer LSV-065-306F from Polytec was used to scan the axial displacement profile along the transducer horn. The barrel of the transducer was removed in order to determine the nodal location more accurately. In addition, the horn surface has to be polished to a mirror finishing in order to give better reflection response which can improve the stability of the laser vibrometer signal. Fig. 4.8(a) shows the photo of the transducer with the barrel removed

during the laser vibrometer measurement. Due to the highly polishing horn surface, a stable vibrometer signal can be obtained as shown in Fig. 4.8 (b).

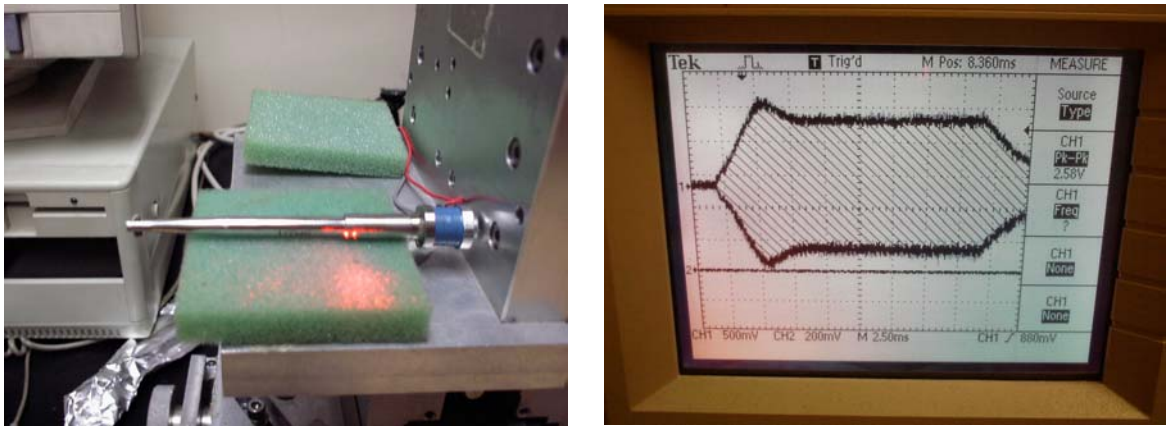

(a) (b)

Fig. 4.8 (a) In-plane laser scanning on the transducer with the barrel removed and (b) a typical stable laser vibrometer signal.

By using the in-plane laser scanning, the axial vibration profile can be found experimentally. The scanning results of the 3λ and 2λ modes are plotted in Fig. 4.9. Two orthogonal directions, with respect to the capillary, at the top and side directions of the transducer were measured. The purpose of measuring two orthogonal directions is that the purity of the axial can be determined by the scanning results. For a pure axial mode, the displacement profile from the two directions should be identical. If the vibration profile of the two directions is different, it is an indication of mode coupling with other flexural or bending modes. From the scanning results, it is observed that both directions have almost identical displacement profile. Therefore, both resonances have a very pure axial vibration. The original barrel is attached at the location 18 mm where it is a common nodal point for both resonances. It has a good agreement with the FEM simulation results. Moreover,

both show that the axial vibration is amplified toward the horn tip which matches well with the FEM prediction.

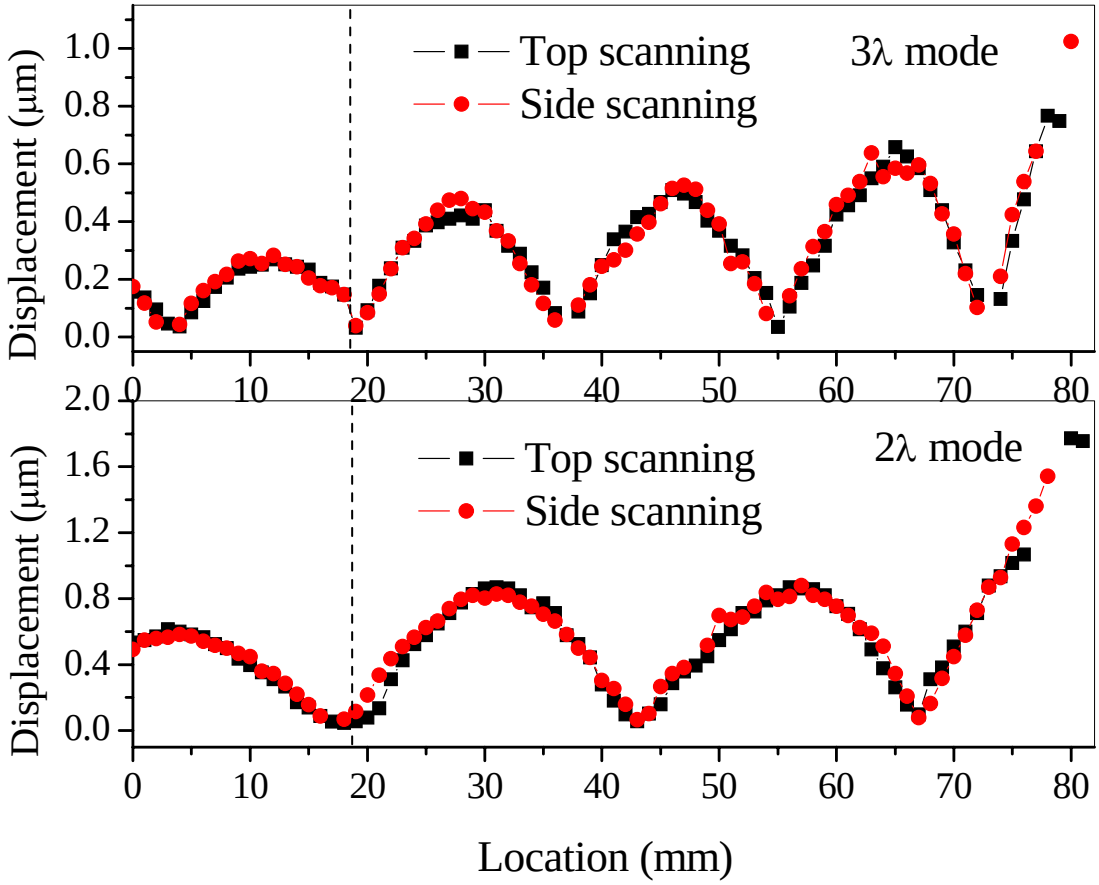

Fig. 4.9 In plane laser vibrometer scanning along the transducer horn.

As the transducer has to be mounted on the bonder during the operation, the effect of clamping on the ultrasonic properties is also an important issue. The electrical impedance responses of the transducer were tested under the clamped condition. As the barrel was attached at the nodal location for both resonances, the transducer characteristics should not be altered after clamping. The electrical impedance spectrum of the transducer at the free condition is compared to that under the clamped condition. The results are plotted in Fig.

4.10. For the 2λ mode at 97 kHz, the spectrum is unaffected even though the transducer is clamped. It is seen that the barrel structure provides a mounting support for the transducer and the ultrasonic signature under the clamped and free conditions are almost identical. For the designated operation mode, although the spectrum has been distorted at around 142 kHz, there is no other change of the spectrum near the frequency of 136 kHz. With the ability of the phase lock loop (PLL) control system of the bonder machine, the transducer will not encounter any problem in working at both resonance modes.

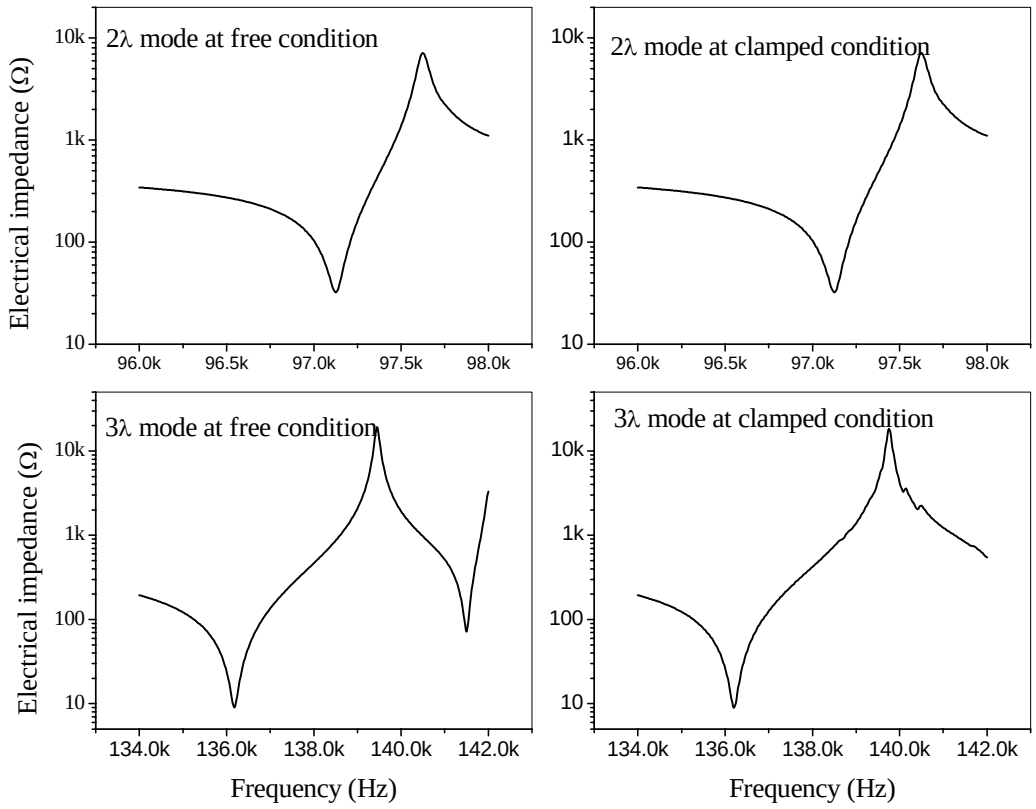

Fig. 4.10 Electrical impedance spectra under both free and clamped conditions.

The vibration amplitudes of the transducer at both resonances have been measured by another out plane vibrometer OFV-505 from Polytec. The vibration is measured at the

transducer horn tip at both 97 kHz and 136 kHz. The measurement results are shown in Fig. 4.11. When compared with the designated 136 kHz mode, the 97 kHz resonance has even higher vibration amplitudes. It can be explained by the general phenomena that the vibration amplitude reduces as the frequency increases. In Fig. 4.11, the vibration amplitudes for both resonance modes are high enough for use in the wire bonding process.

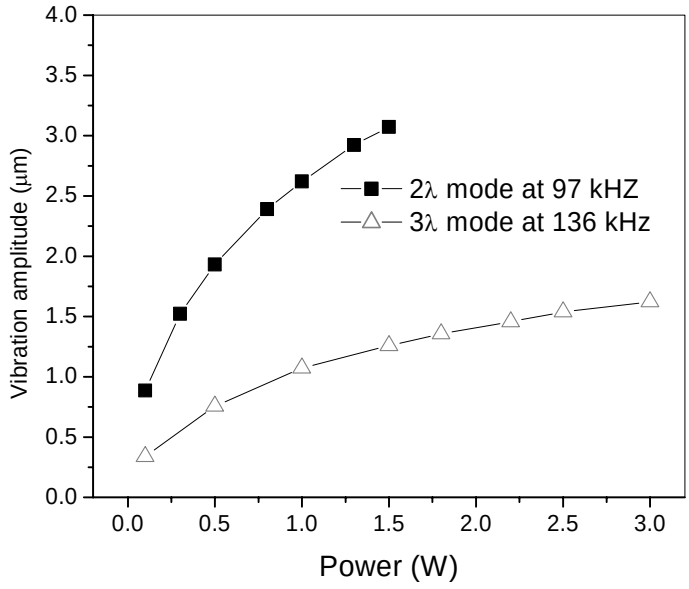

Fig. 4.11 Horn tip vibrations of the transducer operated at 97 kHz and 136 kHz.

4.2.4 Summary

By using the nodal position matching approach, a bundle of resonances from the transducer can be analyzed by a numerical method such as FEM. It is possible to identify more than one resonances that have a common nodal location for the mounting structure either in the form of barrel or flange. The FEM results can be verified by laser vibrometer measurements. The transducer has proven to have more than one resonances that meet the ultrasonic properties required for wire bonding operation.

4.3 Balanced Wavelength Transducers

Although it is possible to have a conventional transducer with multi-frequency nature, not every transducer design can have two or more resonances that share the same nodal location. Therefore, the nodal position matching method can only be applied in some particular case which is not universal. In this Chapter, a novel transducer concept is proposed on the design of wire bonding transducers with multi-frequency features. The design concept is referred to as the balanced wavelength method. A diagram of the transducer design for the ball bonding process with flange support is shown in Fig. 4.12. The transducer consists of two metal masses sandwiched with 4 pieces of PZT rings. A mounting flange is located in middle of the PZT stack. The two metal masses were designed to have similar shape to balance the axial wave profile of the transducer. With such configuration, the transducer can operate in its fundamental resonance having a nodal displacement point at its driving and clamping location. Due to the balanced nature, the nodal position will not shift away at its higher order harmonic resonance. Therefore, the transducer can operate at two or more frequencies in a wire bonding system.

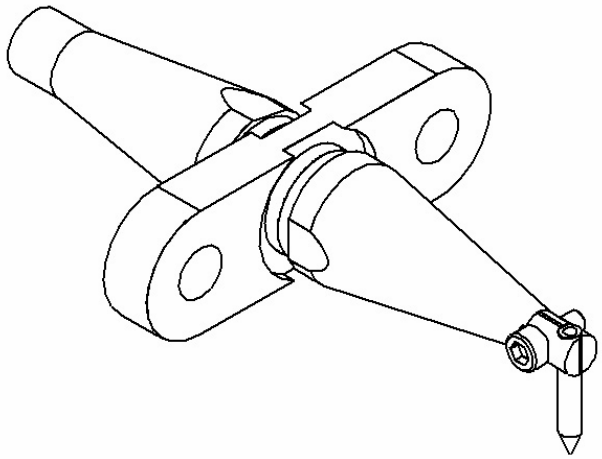

Fig. 4.12 Multi-frequency transducer based on the balanced wavelength method.

4.3.1 Structure of Transducer

The design concept utilized the fact that the transducer requires both the mounting and driving point at an axial displacement nodal location. It combines the two nodal requirements in a single location with the PZT stack placed in the middle of the transducer structure. Fig. 4.13 shows the assembly structure of the novel transducer concept. The transducer consists of 4 pieces of PZT rings, or any other even number of pairs, sandwiched by two metal bodies. One of them calls the amplifying horn with tapered shape that magnifies the vibration amplitude. On the other side of the PZT stack, there is a balance body with a geometry similar to the horn. The amplifying horn and the balance body compress the PZT stack by bolt tightening similar to a Langevin driver. A mounting structure, either in form of a flange or barrel, is placed in the middle of the PZT stack. At the free end of the amplifying horn where there is a maximum vibration amplitude, a capillary is attached.

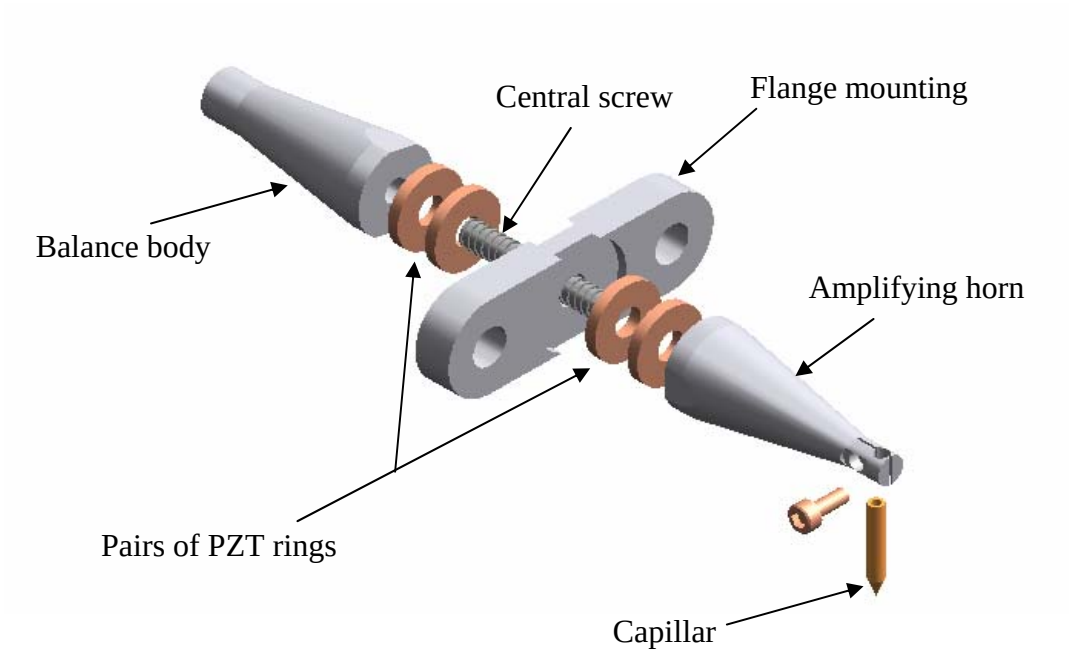

Fig. 4.13 Assembly structure of the balanced wavelength multi-frequency transducer.

Fig. 4.14 shows a photograph of the transducer prototype with the balanced wavelength design concept. Unlike the previous illustration, the prototype has a total number of 8 PZT rings with 4 pieces at each side of the flange. The dimensions of the PZT ring is 8 mm and 3 mm for the outer and inner diameters, respectively. The ring as a thickness is 1.2 mm. Similar to conventional Langevin devices, the PZT rings are connected electrically in parallel and mechanically in series. The amplifying horn and the balanced body are made by titanium (Ti) alloy. The use of Ti alloy gives the transducer better rigidity and thermal stability. The light weight of Ti alloy has reduced the mass of transducer to 15 grams. The transducer can be barrel-mounted if the central flange structure is replaced by a barrel.

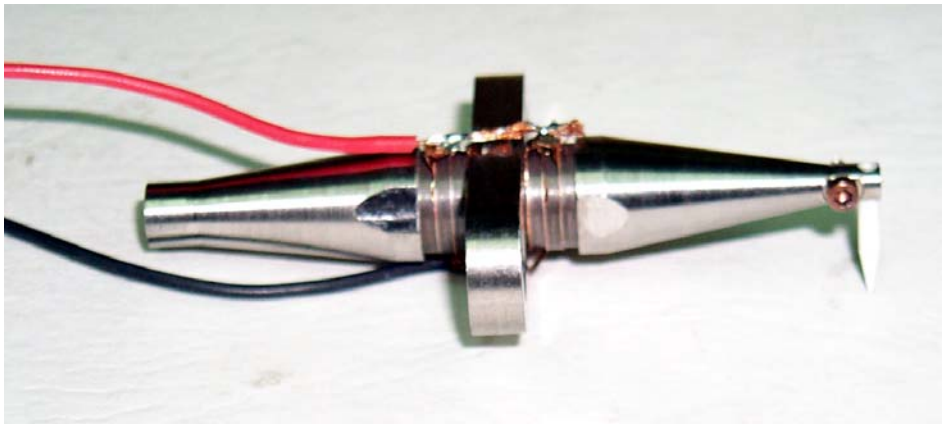

Fig. 4.14 Photograph of the multi-frequency transducer.

4.3.2 Finite Element Analysis

To understand the working principal of the novel multi-frequency design, it will be best to explain using the modal analysis results of the transducer. A FEM model, by ANSYS, was constructed with three dimensional elements similar to all the previous models. The three dimension FEM model of the multi-frequency transducer is shown in Fig. 4.15.

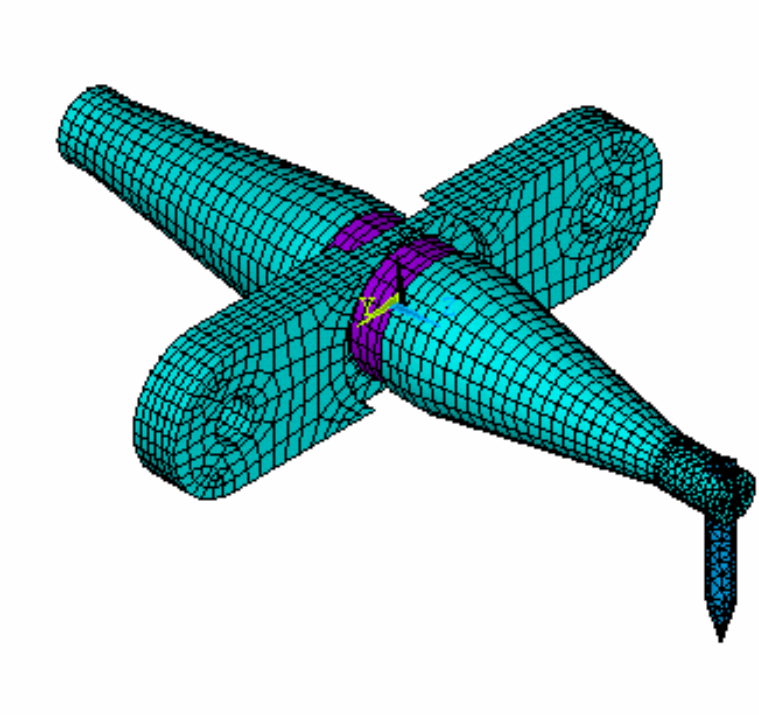

Fig. 4.15 FEM model of the new multi-frequency transducer.

A modal analysis was performed to identify its axial resonance modes. The working principle of the balanced wavelength design can be illustrated by the axial displacement profile of the fundamental resonance and its higher frequency harmonics as shown in Fig. 4.16. The resonance frequency of the fundamental axial mode, with the length of transducer equal to half wavelength, is found at 50.1 kHz. The structure of the transducer is designed to balance the acoustical wavelength with respect to the centre of the mounting flange. Therefore, a nodal point is located in the middle of the transducer such that both the mounting and driving locations fall into the same zero displacement point. For a higher frequency harmonic axial mode, such as the second harmonics at 127.2 kHz, the transducer vibrates at a 1.5 λ mode. Due to the symmetric and balanced nature of the acoustical wavelength, the transducer has an identical nodal location as that of the fundamental mode. Similarly, at the nodal location remains unchanged even

at higher harmonics of 0.5 + nλ modes, where n is an integer. Hence, the new balanced wavelength transducer has multi-frequency capabilities and can be operated at the fundamental mode and its higher frequency harmonics.

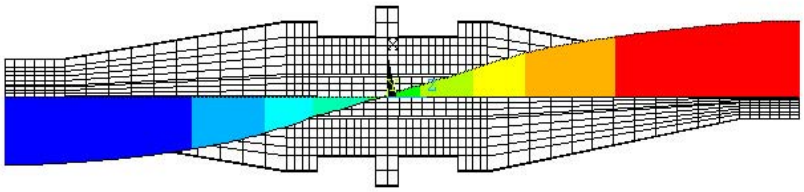

Fr = 50.1 kHz
Fundamental mode (0.5λ)

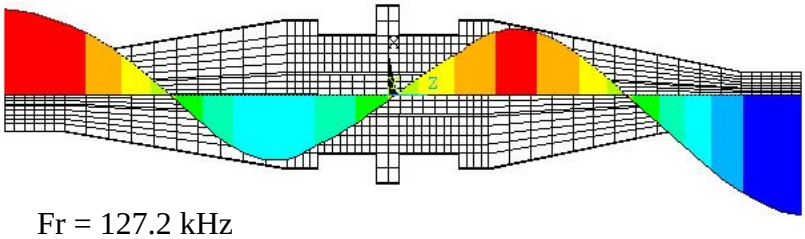

Fr = 127.2 kHz
Second harmonic mode (1.5λ)

Fig. 4.16 FEM axial displacement profiles showing the multi-frequency transducer design concept.

4.3.3 Transducer Characteristics

The electrical properties and vibration amplitude of the transducer have been characterized. The electrical impedance spectrum of the prototype measured by the HP impedance analyzer has been plotted in Fig. 4.17. The measurement data is compared with a harmonic analysis from FEM. The coupled field element (SOLID5) in ANSYS allows the electrical impedance signature to be simulated. Good agreements have been obtained between the measurement and FEM prediction. From the results of Fig. 4.17, it is noticed

that the transducer exhibits a clean spectrum from 40 kHz to 160 kHz. Only two prominent resonances, the fundamental mode and the 2nd harmonics, can be identified. It does not have any mode coupling in this frequency range. This is a highly desirable property of a transducer. A summary of the electrical properties of the transducer and its FEM results are listed in Table 4.3. It is found that the transducer has more than one resonances with good ultrasonic properties for use in wire bonding operation.

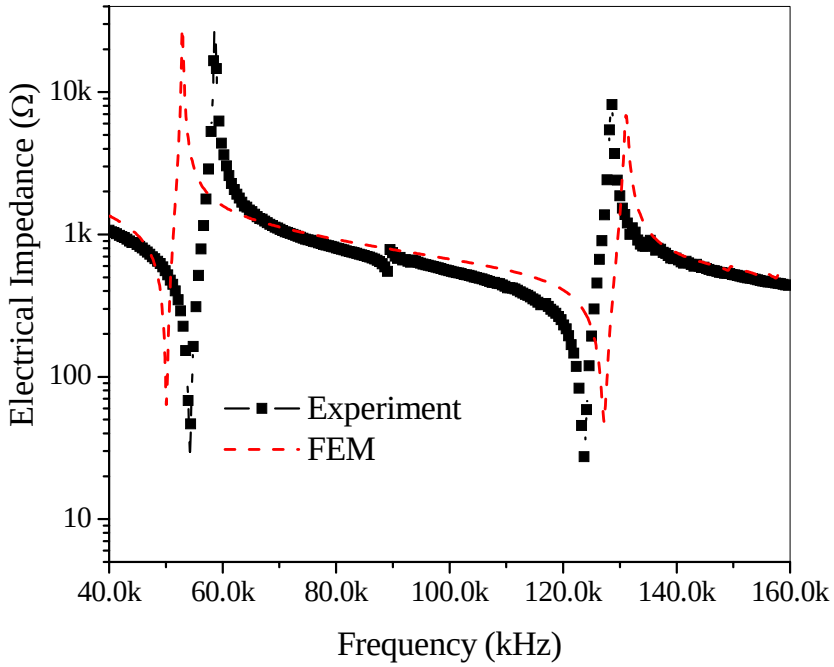

Fig. 4.17 Electrical impedance spectrum for the novel multi-frequency transducer.

TABLE 4.3 SUMMARY ON THE ELECTRICAL CHARACTERISTICS OF THE MULTI-FREQUENCY TRANSDUCER.

	Measurement			FEM	
Mode	F_r (kHz)	k_{eff}	Z (Ω)	F_r (kHz)	k_{eff}
0.5 λ	54.3	0.38	22.5	50.1	0.33
1.5 λ	123.7	0.27	21.3	127.2	0.24

The vibration amplitude of the transducer is measured in the frequency domain at an ultrasonic power of 1 W. The results are shown in Fig. 4.18 together with a comparison with the FEM prediction. As there are only two prominent modes in this frequency domain, the transducer vibration amplitude exhibits two peaks from 40 kHz to 160 kHz. No other adjacent modes are excited in this novel design.

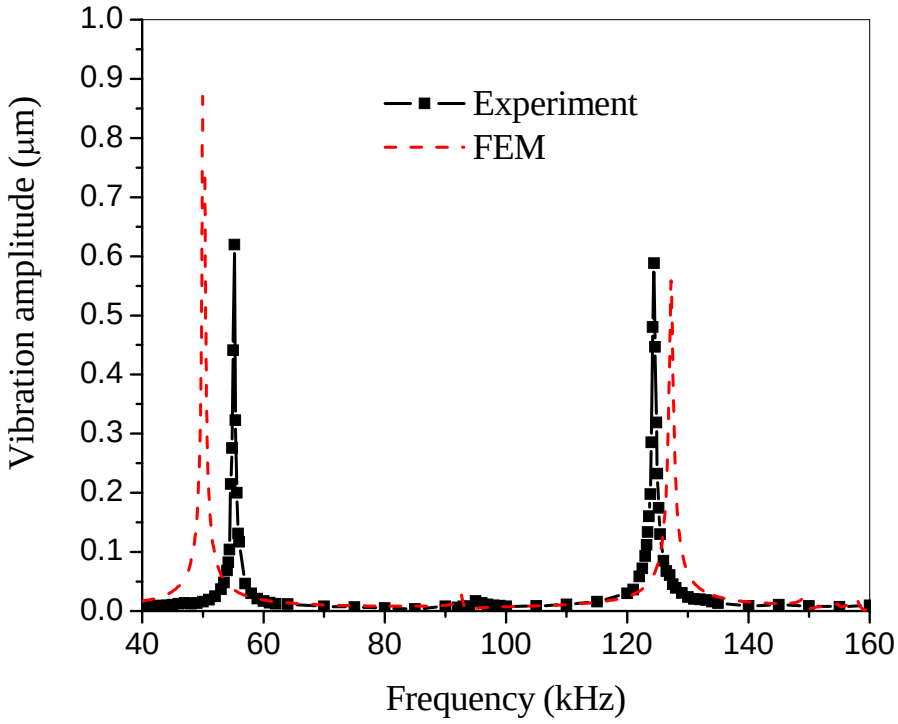

Fig. 4.18 Vibration amplitude in the frequency domain.

By making use of the new transducer design concept, it is possible to make transducers with multi-frequency nature. Unlike the nodal position matching method, all the transducer with symmetric balanced acoustical wavelength will possess multi-frequency functions.

4.4 Comparison of the Two Methods

Both nodal position matching method and balanced wavelength design can give rise to a transducer with a multi-frequency function. For the nodal position matching approach, the concept is to identify a bundle of axial modes in the frequency domain, and by using FEM, or other numerical techniques, together with experimental verifications to find out if there are any other axial modes which have a common nodal point with the designated operation mode. Not every transducer has the nodal position matching properties. Therefore, the balanced wavelength design concept has been proposed. The transducer is designed to have balanced acoustical wavelength with respect to the centre of the transducer. The centre location is the common nodal location for both mounting and driving purposes. Due to the symmetric nature, a zero nodal displacement will always exist and coincide with the fundamental mode and its higher frequency odd harmonics. Fig. 4.19 shows a comparison of the transducers fabricated with the two multi-frequency concept. The size of the balanced wavelength transducer is much smaller than a conventional one. The mass has been reduced from 38 g to 15 g (60% reduction). A lighter transducer is a bonus for high speed wire bonder.

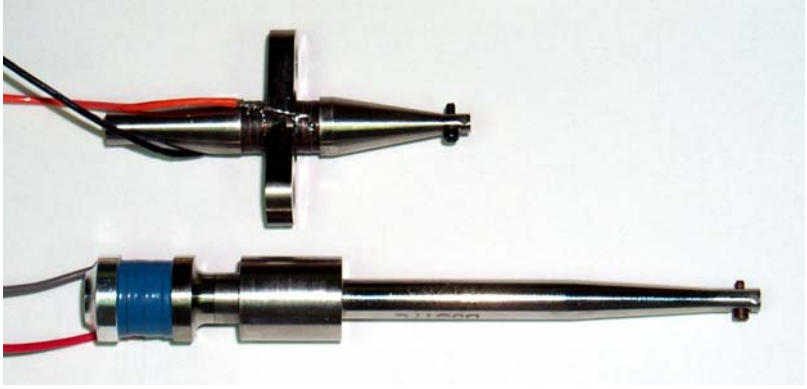

Fig. 4.19 The two multi-frequency transducers.

Apart from the mechanical point of view, the novel design also offers advantages over the conventional transducer in its electrical properties. Consider the electrical impedance spectra of the two transducers as shown in Fig. 4.20, the balanced wavelength method allows the multi-modes to be used at low order modes (0.5λ and 1.5λ), at which the electrical spectrum is usually free from other spurious vibrations. Therefore, the mode coupling problem can be solved. In the conventional design, the modes to be used is of higher order, where there are more adjacent modes or spurious peaks. Such feature will make the mode coupling to happen more easily.

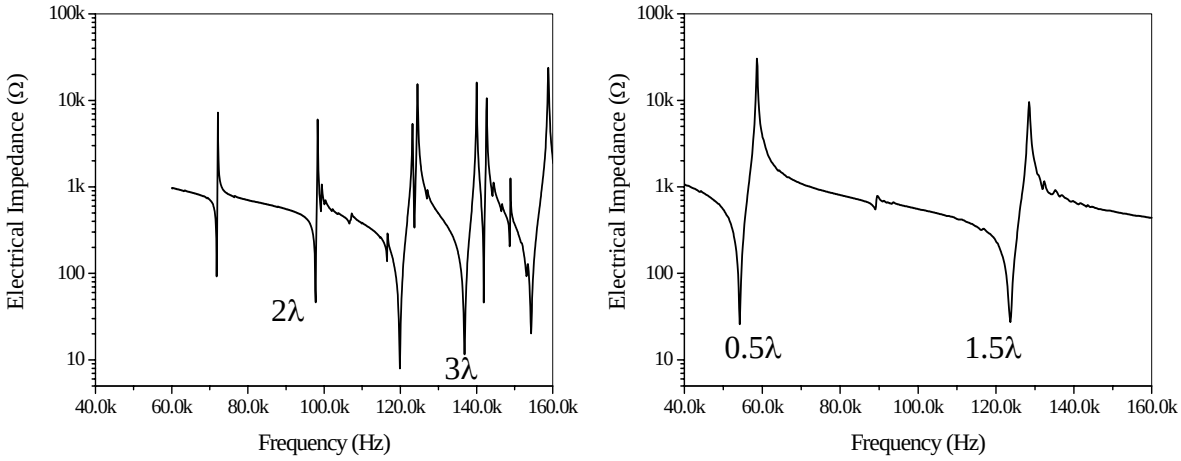

(a) **(b)**

Fig. 4.20 Electrical impedance spectra of the two multi-frequency transducer fabricated by (a) nodal position matching method and (b) balanced wavelength design.

4.5 Summary

Two methods in making multi-frequency transducers are proposed in this Chapter. They are the nodal position matching method and the balanced wavelength design. A methodology to use the multi-frequency function by the nodal position matching approach is demonstrated by a case study of a commercial ball bonding transducer. By using FEM and experimental results, the commercial transducer can have more than one resonances that can be used to perform the wire bonding operation. The transducer is able to work in its 3 λ mode at 136.8 kHz and at a 2 λ mode at 97 kHz. For the two modes, there is a common nodal location to mount the transducer without disturbing the ultrasonic properties of these two modes. However, not all transducer has the nodal position matching feature. A novel balanced wavelength design concept has been proposed. Due to the symmetry of acoustical wavelength, the new transducer is able to operate at its fundamental resonance frequency of 54 kHz and its 2^{nd} harmonics 124 kHz. The proposed design concept has been verified by both FEM and characterization of real prototype. Apart from its multi-frequency nature, the new design also has superior mechanical and electrical properties over the conventional transducer. The new design will lead to a breakthrough in the new generation advanced wire bonder machine.

CHAPTER FIVE

CONCLUSIONS AND SUGGESTIONS FOR FUTURE WORK

5.1 Conclusions

The ultrasonic transducer is the heart of a thermosonic wire or flip chip bonder machine and its performance can make critical impacts to the process capability. Novel transducer designs with unique advantages can therefore lead to a breakthrough in the current wire bonding or thermosonic flip chip technology. According to the course of research presented in this thesis, several advanced transducer technologies for microelectronic packaging have been proposed. It includes 1-3 composite transducer technology for fine pitch and reliable wire bonding, novel push-pull transducer design for high performance thermosonic flip chip bonding and new balanced wavelength transducer with multi-frequency feature.

5.1.1 1-3 Piezocomposite Transducer

The 1-3 composite technology concept is to replace the conventional full PZT rings with 1-3 composite piezoceramic rings. Design guidelines have been given on how to optimize the performance of the 1-3 composite transducers. The vibration characteristics

of a full PZT ring were first studied by using FEM. The dynamic behaviours were simulated and compared to experimental results. Vibration mode shapes from FEM were further verified by laser vibrometer measurements. The dimensions of the PZT ring were optimized to have 12.7 mm outer diameter, 5.1 mm inner diameter and 2.3 mm ring thickness, based on a 62 kHz transducer using commercial hard PZT (ASM PZT8) from ASM. With the optimized dimensions, the PZT ring has a maximum electromechanical coupling factor for its thickness mode which maximizes the axial excitation of a Langevin driver. The optimized rings were fabricated into 1-3 composite by using a dice-and-fill technique. The minimum number of cuts in each perpendicular direction was determined to be 7 cuts per direction (cpd) in order to obtain as a homogenous composite material. The ceramic volume fraction of the composite was optimized to be 0.91. Both FEM and experiments provided evidences that the 7 cpd composite transducer has been optimized in consideration of function and cost.

The optimized composite rings were installed into a conventional wedge bonding transducer of 64 kHz. The dynamic behaviours were analyzed by FEM. The modal analysis results showed good agreement to the measurement data. The 1-3 composite transducer was fully characterized and some unique features were identified, including:

- Pure axial vibration mode and reduced sideway wedge motion by 80% which can facilitate the fine pitch applications.
- Suppress spurious modes and reduce the chance of mode coupling.
- Comparable axial vibration displacement amplitude without losing in bonding efficiency.

The 1-3 composite transducer has been installed into a commercial wedge wire bonder

for detailed process studies. Benchmarking with a conventional transducer including the operation windows, fine pitch capability, pull and shear performance and bonding stability have been reported. The 1-3 composite transducer shows very promising bonding performances which cannot be achieved using a conventional transducer. The use of 1-3 composite transducer has the follows benefit:

1. It widens the process windows of the bonder machine in both first and second bonds. By using the 1-3 composite transducer, the size of the process windows could be enlarged by 7% and 48% at the 1st and 2nd bond, respectively. Such improvements can increase the process capability and the machine can also be more easily tuned up and operated.
2. It reduces the minimum allowable bond width at the 1st bond from 1.9 mil to 1.78 mil, which is around 6.3% smaller. Therefore, it facilitates process capability to achieve fine pitch bonding.
3. The purer vibration loci of the 1-3 composite also reduces the heel damage of the bonded wire. Not only can it enhance the pull strength of the wire, but it can also improve the bonding yield by inducing lesser bonding defects.
4. The stability and consistency of the bonding can also be improved by using a 1-3 composite transducer. By statistical estimation, the standard deviation of the bond width can be reduced by 17.6% and 46% at the 1st and 2nd bond, respectively. The 1-3 composite transducer therefore offers more robust and stable bondings.

The 1-3 composite transducer technology therefore has great commercial potential in the future generation wire bonder which requires high speed, fine pitch and high bonding yield.

5. 1.2 Thermosonic Flip Chip Transducers

Both transverse and longitudinal types of transducers for thermosonic flip chip bonding have been designed. An analysis has been performed to understand the relationship between the transducer characteristics and the two common bonding defects: die tilting and silicon cratering. Both FEM and experimental methods have been shown that the longitudinal design has a better mechanical rigidity. A perfect bonding co-planarity can be maintained despite the value of bond force applied. In contrast, the transverse transducer has a cantilever bending action at high bond force. In the current design, the transverse transducer suffers serious die tilting problem when the bond force is higher than 2 kg. However, the hammering motion of the longitudinal transducer makes it more susceptible to silicon cratering. From a FEM prediction of the principal stresses generated during both transverse and longitudinal bondings, it was found that the hammering effect of longitudinal transducer induced a 20% higher stress. Silicon cratering during longitudinal bonding has also been observed experimentally. However, under the same condition, no cratering has been found in transverse bonding.

A new push-pull transducer has been developed to tackle the thermosonic flip chip bonding for high pin count devices. The novel idea makes use of two Langevin stacks that has been synchronized to create the push-pull motion. FEM has been used to model the new transducer design and prototypes have been fabricated to prove the design concept. The transducer prototypes have found to have good ultrasonic properties. In addition, the pull and push motion has a summation effect on the vibration output and therefore the vibration amplitude is double compared to that of the conventional flip chip transducers. By taking advantage of the symmetric design in the transducer geometry, the bonding co-

planarity can be perfectly maintained even the transducer is deformed. These features make the push-pull transducer design particularly suitable for high IOs flip chip bonding. Maximum shear strength of 62 g/bump can be achieved at an ultrasonic power of 3 W and a bond force of 125 g/bump. The bonding temperature is 120 °C. The average die titling is 2.38 mdeg on a 1 mm x 1 mm die. No silicon cratering has been observed. Therefore, this transducer can be used to achieve stable and high yield flip chip bondings. This new transducer concept has been adopted in a commercial flip chip bonder.

5.1.3 Multi-frequency Transducers

Multi-frequency transducer is a transducer that can perform bonding at more than one frequencies, preferably one at a low frequency of under 100 kHz and at least one at a higher frequency of over 120 kHz. The purpose of multi-frequency bonding is that it can use high frequency bonding to achieve fine pitch, faster and lower temperature bonding at the 1^{st} bond. At the same time, it can perform stable and high yield bonding at the 2^{nd} bond using lower ultrasonic frequency. Methodologies for designing the multi-frequency transducer were developed. The multi-frequency design concept has been first demonstrated by a commercial transducer using the nodal position matching method. By using FEM and experimental results, a bundle of axial modes of this transducer have been analyzed showing their electrical properties and mode shapes. The transducer can be operated at multi-frequency if there exists a common axial zero displacement point for two or more axial modes. Furthermore, the vibration displacement has to be amplified at the horn tip where the capillary is located. Supported by both FEM simulation and experimental verification, it has been demonstrated that the transducer can be operated at both 3 λ and 2 λ modes which corresponds to 138 kHz and 97 kHz, respectively.

A new transducer design concept based on a balanced acoustical wavelength has been proposed. The transducer makes use of a common nodal point for mounting and driving that is located in the middle of the structure. This special design could allow the new transducer to work at its fundamental mode (0.5 λ) as well as its second harmonics (1.5λ). Prototypes have been fabricated to prove the design concept. Both FEM and prototyping show that the transducer has good ultrasonic properties at more than one frequencies. This novel multi-frequency features can widen the application of the current wire bonder.

5.2 Suggested Future Work

I. Process Studies on Thermosonic Flip Chip and Multi-frequency Transducers

Although novel transducers have been developed in this work, detail process studies are essential to turn them into commercial products. The thermosonic flip chip and multi-frequency bonding processes are two innovative areas that need considerable research efforts. For the thermosonic flip chip bonding, the challenge ahead will be on the bonding of high IOs (> 100) devices. The huge bond force and large ultrasonic power requirement may demand new features on the transducer design. Thermosonic bonding using different frequencies should also be assessed in detail. The use of different frequencies at the first and second bonds can improve the fine pitch capability and bonding yield. In addition, the use of different frequencies at different periods in a single bond is an interesting research topic. As an example, the use of lower frequency may help to initialize the bond formation

due to higher vibration amplitude. Higher frequency vibration can be applied at the later stage to facilitate better bondability.

II. 1-3 Composite Multi-frequency Flip Chip Transducers

The 1-3 composite and multi-frequency technologies can be merged to produce a transducer that can offer stable bondings at both high and low frequencies. To apply this hybrid concept in the push-pull transducer is challenging. The transducer needs to have two common nodal positions for both high and low frequency modes. However, the multi-frequency feature in the TS flip chip process requires a lot of new research work. As the bonding time for the flip chip process is much longer than wire bonding, the complicated bonding mechanism during the whole bonding period is still unknown. Different frequencies can be applied at different stages of the process to improve the bonding performance. For example, one can start with a low frequency using the large vibration to initialize bonding and then apply higher frequency at a later stage. The prerequisite of this research work counts on using a multi-frequency flip chip transducer. It will be an additional advantage to implement the 1-3 composite technology to increase the bonding stability.

III. Multi-directional Transducers

The push-pull transducer can be treated as two conventional transducers joined at its horn tip. The two transducers are then synchronized with opposite phases giving the same vibration direction. However, with similar approaches, more transducers can be joined together. Two push-pull transducers can be joined at two orthogonal directions. In doing so, more PZT stacks can be added to give even high vibration amplitudes. In addition, one

can make use of the phase between the two orthogonal vibrations to control the loci of collet tip vibration. It is expected that this concept can induce interesting research projects for both transducer design and process studies.

REFERENCES

[1] J.H. Lau, *Low Cost Flip Chip Technology for DCA, WLCSP, and PBGA Assemblies*, McGraw-Hill, New York, 2000.

[2] O.L. Anderson and H. Christianson, "Technique for Attaching Electrical Leads to Semiconductors", *Journal of Applied Physics*, Vol. 28, pp. 923-924, 1957.

[3] A. Coucoulas, "Hot Work Ultrasonic Boning – A Method of Facilitating Metal Flow by Restorations Process", *Proceedings of the 20th Electrical Components Conference*, pp. 549-556, 1970.

[4] G.G. Harman, *Wire Bonding in Microelectronics – Materials, Processes, Reliability, and Yield*, McGraw-Hill, New York, 1997.

[5] *Bonding Capillary Catalogue*, Small Precision Tools Ltd, 2000.

[6] *Ultrasonic Bonding Wedge Catalogue*, Small Precision Tools Ltd, 2000.

[7] A. Boland, "*Wire Bonding*", The Swedish Institute of Production Engineering Research and The Nordic Electronic Packaging Guide, University of Essex Nanofab. at http://privatewww.essex.ac.uk/~bolat.

[8] F.N. Sinnadurai, *Handbook of Microelectronics Packaging and Interconnection Technologies*, Electrochemical Publication, Ayr Scotland, 1985.

[9] J.H. Lau, C.P. Wong, J.L Pince and W. Nakayama, *Electronic Packaging Design, Materials, Process, and Reliability*, McGraw-Hill, New York, 1998.

[10] J.H. Lau, *Flip Chip Technologies*, McGraw-Hill, New York, 1996.

[11] R. Furukawa, *High Pin-count Ultrasonic Flip-chip Bonding and Plasma Cleaning Technology*, Technical Publications at http://www.panasonic.co.jp , 2002.

[12] *Bonding Capillaries*, Technical Publications at http://www.smallprecisiontools.com.

[13] M. Hizukuri, N. Watanabe and T. Asano, "Dynamic Strain and Chip Damage During Ultrasonic Flip Chip Bonding", *Japanese Journal of Applied Physics*, Vol. 40, pp. 3044-3088, 2001.

[14] C.C.H. Pang, M.L Sham and K.Y. Hung, "Investigation on the High Frequency Thermosonic Flip Chip Bonding under Low Temperature", *Proceedings IEEE 5th Electronics Packaging Technology Conference (EPTC)*, pp. 376 – 379, 2003.

[15] P. Langevin, *French Patent*, No. 502913, May 1920.

[16] S.W. Or, "Performance Study of the Ultrasonic Wire Bonder used in Microelectronic Packaging", *MPhil. Thesis*, The Hong Kong Polytechnic University, 1997.

[17] B. Jaffe, W.R. Cook Jr and H. Jaffe, *Piezoelectric Ceramics*, Academic Press, New York, 1971.

[18] D. Stansfield, "Hydrophones", *Underwater Electroacoustic Transducers*, Chapter 10, Bath University Press, Great Britain, 1991.

[19] T.R. Gururaja, A. Safari, R.E. Newnham and L.E. Cross, *Electronic Ceramics*, Levinson L.M. (Ed.), Dekker, New York, 1988.

[20] C.P. Chong, H.L.W. Chan and P.C.K. Liu, "Vibration and Resonance Characteristics of PZT/Epoxy 1-3 Composite Ultrasonic Wire Bonding Transducers", *Proceedings of the Fourth Pacific Rim International Conference on Advanced Materials and Processing (PRICM4)*, Vol. 2, pp. 1579-1582, 2001.

[21] C.P. Chong, H.L.W. Chan, M.W. Ng and P.C.K. Liu, "Effect of Hybrid Structure (1-3 Composite and Ceramic) on the Performance of Sandwich Transducers", *Materials Science and Engineering B*, Vol. 99, pp. 6-10, 2003.

[22] C.P. Chong, H.L.W. Chan, M.H. Chan and P.C.K. Liu, "Analysis of the Resonance Modes of PZT/Epoxy 1-3 Composite Rings", *Proceedings IEEE 13th International Symposium on the Applications of Ferroelectrics (XIII ISAF 2002)*, Nara, Japan, pp. 295-299, 2002.

[23] Q. Tan, W.G. Zhang, B. Schaible, L.J Bond, T. H. Ju and Y.C. Lee, "Thermosonic Flip-Chip Bonding Using Longitudinal Ultrasonic Vibration", *IEEE Transactions on Components, Packaging, and Manufacturing Technology – Part B*, Vol. 21, No. 1, pp. 53-58, 1998.

[24] B. Gonzalez, S. Knecht, H. Handy and J. Ramirez, "The Effect of Ultrasonic Frequency on Fine Pitch Aluminum Wedge Wirebond", *Proceedings IEEE Electronic Components and Technology Conference (ECTC)*, pp. 1078-1087, 1996.

[25] H.K. Charles Jr, K.J. Mach, S.J. Lehtonen, A.S. Francomacaro, J.S. DeBoy and R.L. Edwards, "Wirebonding at Higher Ultrasonic Frequencies: Reliability and Process Implications", *Microelectronics Reliability*, Vol. 43, pp 141-153, 2003.

[26] R.E. Newnham, D.P. Skinner and L.E. Cross, "Connectivity and Piezoelectric-Pyroelectric Composites", *Materials Research Bullets*, Vol. 13, pp. 523-536, 1978.

[27] M.J. Haun and R.E. Newnham, "An Experimental and Theoretical Study of 1-3 and 1-3-0 Piezoelectric PZT-polymer Composites for Hydrophone Applications", *Ferroelectrics*, Vol. 68, pp. 123-139, 1986.

[28] D. Stansfield, *Underwater Electroacoustic Transducers*, Bath University Press, Great Britain, 1991.

[29] W.A. Smith, "The Role of Piezocomposites in Ultrasonic Transducers", *Proceedings IEEE Ultrasonics Symposium*, pp. 755-766, 1989.

[30] W.A. Smith, "The Application of 1-3 Piezocomposites in Acoustic Transducers", *Proceedings IEEE International Symposium on Application Ferroelectric*, pp. 145-152, 1990.

[31] W.A. Smith, A. Shaulov and B.A. Auld, "Tailoring the Properties of Composite Piezoelectric Materials for Medical Ultrasonic Transducers", *Proceedings IEEE Ultrasonics Symposium*, pp. 642-647, 1985.

[32] J. Poguet, G. Fleury, J.L. Guey and P. Conche, "Piezocomposite Technology: An Innovative Approach to the Improvement of N.D.T Performance Using Ultrasounds", *The E-Journal of Nondestructive Testing (* http://www.NDT.net. *)*, Vol. 7, No.5, 2002.

[33] R.E. Newnham, "Composite Sensors and Actuators", *Proceedings of the SPIE on Structures and Materials*, Vol. 2716, pp. 347-352, 1996.

[34] J.G. Wan and B.Q Tao, "Design and Study on a 1-3 Anisotropy Piezocomposite Sensor", *5th IUMRS International Conference on Intelligent Materials*, Vol. 21, pp. 533-542, 2000.

[35] R. Gentilman, D. Fiore, P.N. Hong, W. Serwatka, B. Pazol, C. Near, P. McGuire and L. Bowen, "1-3 Piezocomposite Smart Panels for Active Surface Control", *Proceedings of the SPIE on Industrial and Commercial Applications of Smart Structures Technologies*, Vol. 2721, pp. 234 - 239, 1996.

[36] S.W. Or, "High Frequency Transducer for Ultrasonic Bonding", *Ph.D. Thesis*, The Hong Kong Polytechnic University, 2000.

[37] C.P. Chong, "1-3 Composite Transducer for Ultrasonic Bonding", *MPhil. Thesis*, The Hong Kong Polytechnic University, 2002.

[38] D.A. Berlincourt, D. R. Curran and H. Jaffe, "Piezoelectric and Piezomagnetic Materials and Their Function in Transducers", *Physical Acoustics*, Vol. IA, 1964.

[39] A. Iula, N. Lamberti and M, Pappalardo, "A Model For The Theoretical Characterization of Thin Piezoceramic Rings", *IEEE Transactions on Ultrasonics, Ferroelectrics and Frequency Control*, Vol. 43, No. 3, 1996.

[40] W. Pajewski, P. Kielczynski and M. Szalewski, "Ring Vibrations in an Acoustic Medium As a Source of Ultrasonic Radiation", *IEEE Transactions on Ultrasonics, Ferroelectrics and Frequency Control*, Vol. 41, No. 6, 1994.

[41] H.L.W. Chan and J. Unsworth, "Simple Model for Piezoelectric Ceramic/Polymer 1-3 Composites Used in Ultrasonic Transducer Application", *IEEE Transactions on Ultrasonics, Ferroelectrics and Frequency Control*, Vol. 36, pp. 434-441, 1989.

[42] W.A. Smith and B.A. Auld, "Modeling 1-3 Composite Piezoelectric: Thickness-Mode Oscillation", *IEEE Transactions on Ultrasonics, Ferroelectrics and Frequency Control*, Vol. 38, pp. 40-47, 1991.

[43] G. Hayward and J.A. Hossack, "Unidimensional Modeling of 1-3 Composite Transducers", *Journal of Acoustical Society of Americ*a, Vol. 8, pp. 99-608, 1990.

[44] J.A. Hossack and G. Hayward, "Finite Element Analysis of 1-3 Composite Transducers", *IEEE Transactions on Ultrasonics, Ferroelectrics and Frequency Control*, Vol. 38, pp. 618-629, 2001.

[45] R. Steinhausen, T. Hauke, W. Seifert, H. Beige, W. Watzka, S. Seifert, D. Sporn, S. Starke and A. Schonecker, "Finescaled Piezoelectric 1-3 Composite: Properties and Modeling", *Journal of the European Ceramic Society*, Vol. 19, pp. 1289-1293, 1999.

[46] H.E. Pettermann and S. Suresh, "A Comprehensive Unit Cell Model: A Study of Coupled Effects in Piezoelectric 1-3 Composites", *International Journal of Solids and Structures*, Vol. 37, pp. 5447-5464, 2000.

[47] S.W. Or and H.L.W. Chan, "Mode Coupling in Lead Zirconate Titanate/Epoxy 1-3 Piezocomposite Rings", *Journal of Applied Physics*, Vol. 90, pp. 4122-4219, 2001.

[48] *ANSI/IEEE Std. 176-1987: IEEE Standard on Piezoelectricity*, The Institution of Electrical and Electronics Engineers, Inc., 1987.

[49] P.C. Kohnke, *ANSYS 5.2 User's Manual — Vol.ume IV Theory*, ANSYS, Inc., 1995.

[50] H.L Li, H.L.W. Chan and C.L. Choy, "Vibration Characteristics of Piezoceramic Rings", *Ferroelectrics*, Vol. 263, pp. 211-216, 2001.

[51] P. Elenius, "Flip Chip Bumping for IC Packaging Contractors", *Prismark Partners Flip Chip Report*, 1997.

[52] J.H. Lau and S.W.R. Lee, *Microvias for Low Cost High Density Interconnects*, McGraw-Hill, New York, 2001.

[53] S.Y. Kang, P.M. Williams and Y.C. Lee, "Modeling and Experimental Studies on Thermosonic Flip-Chip Bonding", *IEEE Transactions on Components, Packaging, and Manufacturing Technology – Part B*, Vol. 18, No. 4, pp. 728-733, 1995.

[54] T.S. McLaren, S.Y. Kang, W.G. Zhang, T.H. Ju and Y.C. Lee, "Thermosonic Bonding of an Optical Transceiver Based on an 8 x 8 Vertical Cavity Surface Emitting Laser Array", *IEEE Transactions on Components, Packaging, and Manufacturing Technology – Part B*, Vol. 20, No. 2, 1997.

[55] Q. Tan, B. Schaible, L.J. Bond and Y.C. Lee, "Thermosonic Flip-Chip Bonding System with a self-Planarization Feature using Polymer", *IEEE Transactions on Advanced Packaging*, Vol. 22, No.2, pp. 468-475, 1999.

[56] T. Sattel and M. Brokelmann, "A Simple Transducer Model for Longitudinal Flip-Chip Bonding", *Proceedings IEEE Ultrasonics Symposium*, pp. 695-69, 2002.

[57] T. Tomioka, T. Iguchi and I. Mori, "Thermosonic Flip-Chip Bonding for SAW Filter", Microelectronic Reliability, Vol. 44, pp. 149-154, 2004.

[58] S.Y. Kang, K. Chuang and Y.C. Lee, "Random Change of Vibration Modes in Thermosonic Bonding", *Journal of Electronic Packaging*, Vol. 120, pp. 253-258, 1998.

[59] C.M. Tan and Z. Gan, "Failure Mechanisms of Aluminum Bondpad Peeling During Thermosonic Bonding", *IEEE Transactions on Device and Materials Reliability*, Vol. 3, No 2, pp. 44-50, 2003.

[60] M. Hizukuri, N. Watanabe and T. Asano, "Dynamic Strain and Chip Damage during Ultrasonic Flip Chip Bonding", *Japanese Journal of Applied Physics,* Vol. 40, pp. 3044-3048, 2001.

[61] N. Willems, *Strength of Materials*, McGraw-Hill, New York, pp. 310-319, 1991.

[62] P. Stepin, *Strength of Materials*, Gordon and Breach, New York ,1963.

[63] K.C. Joshi, "Formation of Ultrasonic Bonds Between Metals", *Welding Journal,* Vol. 50, pp. 840-848, 1971.

[64] G.K.C. Chen, "The Roll of Micro-Slip in Ultrasonic Bonding of Microelectronic Dimensions", *International Microelectronic Symposium (ISHM),* pp. 5-9, 1972.

[65] G.G. Harman and J. Albers, "The Ultrasonic Welding Mechanism as Applied to Aluminum and Gold Wire-Bonding in Microelectronics", *IEEE Transactions on Parts, Hybrids, and Packaging*, Vol. 13, pp. 406-412, 1977.

[66] J. Tsujino, T. Mori, T. Onozato and K. Hasegawa, "Welding Characteristics of Ultrasonic Wire Bonding Using High Frequency Vibration System", *Japanese Journal of Applied Physics,* Vol. 32, No. 5B, pp. 2435-2440, 1993.

[67] J. Tsujino, K. Hasegawa, Y. Sone and K. Nozaki, "Frequency Characteristics of Ultrasonic Wire Bonding Systems of 40 kHz to 780 kHz", *Proceedings of IEEE International Ultrasonics Symposium,* pp. 1021-1026, 1996.

[68] J. Tsujino, H. Yoshihara, T. Itoh, K. Inujima and Y. Hirano, "Transmission Rise and Welding Characteristics of Ultrasonic Wire Bonding Using 190 kHz Linear, Circular and Square Vibration Loci and 600 kHz Linear Vibration Locus Welding Tips", *Japanese Journal of Applied Physics*, Vol. 37, No. 5B, pp. 3009-3012, 1998.

[69] T.H. Ramsey and C. Alfaro, "The Effect of Ultrasonic Frequency on Intermetallic Reactivity of Au-Al Bonds", *Solid State Technology*, Vol. 34, pp. 37- 38, 1991.

[70] B. Gonzalez, S. Knecht and H. Handy, "The Effect of Ultrasonic Frequency on Fine Pitch Al Wedge Wirebond", *Proceedings on the 46th Electronic Components and Technology Conference*, pp. 1078-1087, 1996.

[71] T.H. Ramsey and C. Alfaro, "High-Frequency Enhancement for Ambient Temperature Ball Bonding", *Semiconductor International*, Vol. 20, pp. 93-96, 1997.

[72] " *Room Temperature Bonding Using Higher Frequencies*", ESEC Asia Pacific Pte. Ltd, Wirebond Process Research and Development Team, http://www.aprova.com.

[73] V.P. Jaecklin "Room Temperature Ball Bonding Using High Ultrasonic Frequencies", *Proceedings of Semicon – Test, Assembly and Packaging*, pp. 208-214, 1995.

[74] Y.M. Cheung, S.W. Or, and S. Ching, "Low Temperature Gold Wire Bonding", *Proceedings IEEE 24th International Electronics Manufacturing Technology (IEMT) Symposium at SEMICON® Southwest*, pp. 196-202, 1999.